Characterization of proteins involved in lipid homeostasis of *Pseudomonas aeruginosa* and *Agrobacterium tumefaciens*

Von der Fakultät für Lebenswissenschaften
der Technischen Universität Carolo-Wilhelmina zu Braunschweig
zur Erlangung des Grades
einer Doktorin der Naturwissenschaften
(Dr. rer. nat.)
genehmigte
D i s s e r t a t i o n

von Maike Kathrin Groenewold
aus Leer (Ostfriesland)

1. Referent: Professor Dr. Dirk Heinz
2. Referent: Professor Dr. Dieter Jahn
eingereicht am: 09.06.2017
mündliche Prüfung (Disputation) am: 21.08.2017

Druckjahr 2017

Vorveröffentlichungen der Dissertation

Teilergebnisse aus dieser Arbeit wurden mit Genehmigung der Fakultät für Lebenswissenschaften, vertreten durch den Mentor der Arbeit, in folgenden Beiträgen vorab veröffentlicht:

Publikationen

Hebecker, S., Krausze, J., Hasenkampf, T., Schneider, J., Groenewold, M., Reichelt, J., Jahn, D., Heinz, D. W. and Moser, J. Structures of two bacterial resistance factors mediating tRNA-dependent aminoacylation of phosphatidylglycerol with lysine or alanine. Proc Natl Acad Sci U S A 112(34): 10691-10696 (2015).

Groenewold, M. K., Massmig, M., Hebecker, S., Magnowska, Z., Nimtz, M., Jahn, D., Heinz, D. W., Jänsch, J. and Moser, J. Identification of a Phosphatidic Acid Binding Protein Responsible for the Adaptation of *Pseudomonas aeruginosa* to Anaerobic Biofilm Conditions. *In revision.*

Tagungsbeiträge

Groenewold, M., Krüger, S. and Zegenhagen, L.: Attack and defense – All against one. 6. Public Retreat of the Helmholtz International Graduate School for Infection Research, Braunschweig (2015).

Groenewold, M. and Moser, J.: Lipid modification in *Pseudomonas aeruginosa*. Protein Crystallography Summer School, St. Andrews, Scotland (2015).

Groenewold, M. and Moser, J.: Lipid homeostasis in *Pseudomonas aeruginosa*. Lehrstuhl für Biologie der Mikroorganismen, Prof. Dr. Narberhaus, Bochum (2016).

Groenewold, M., Krüger, S. and Schinner, S.: Lung pathogens: Think big, because they do. 7. Public Retreat of the Helmholtz International Graduate School for Infection Research, Goslar-Hahnenklee (2016).

Posterbeiträge

Groenewold, M., Moser, J. and Heinz, D. W.: PA3911 – a potential lipid carrier protein in *Pseudomonas aeruginosa* PAO1. 5. Public Retreat of the Helmholtz International Graduate School for Infection Research, Goslar-Hahnenklee (2014)

Groenewold, M., Wolf, A.-K., Magnowska, Z., Jänsch, L., Heinz, D. W. and Moser, J.: PA3911 – a potential lipid carrier protein in *Pseudomonas aeruginosa*. VAAM und DGHM Jahrestagung, Dresden (2014)

Groenewold, M., Massmig, M., Wolf, A.-K., Jänsch, L., Heinz, D. W. and Moser, J.: Characterization of a putative lipid binding protein from *Pseudomonas aeruginosa*. 8. PhD Symposium of the Helmholtz Centre for Infection Research, Braunschweig (2014)

Groenewold, M., Massmig, M., Wolf, A.-K., Jänsch, L., Heinz, D. W. and Moser, J.: Characterization of a putative lipid binding protein from *Pseudomonas aeruginosa*. VAAM Jahrestagung, Marburg (2015)

Groenewold, M., Massmig, M., Wolf, A.-K., Jänsch, L., Heinz, D. W. and Moser, J.: Towards the function of the lipid binding protein PA3911 from *Pseudomonas aeruginosa*. 9. PhD Symposium of the Helmholtz Centre for Infection Research, Braunschweig (2015)

Groenewold, M., Massmig, M., Wolf, A.-K., Jänsch, L., Heinz, D. W. and Moser, J.: Towards the function of the lipid binding protein PA3911 from *Pseudomonas aeruginosa*. VAAM Jahrestagung, Jena (2016)

Table of contents

Abbreviations

A	ampere
A-PG	alanyl-phosphatidylglycerol
A-PGH	alanyl-phosphatidylglycerol hydrolase
A-PGS	alanyl-phosphatidylglycerol synthase
aa	amino acid(s)
aaPG	aminoacyl-phosphatidylglycerol
aaPGS	aminoacyl-phosphatidylglycerol synthase(s)
ACP	acyl carrier protein
ALA	5-aminolevulinic acid
Anr	anaerobic regulation of arginine deiminase and nitrate reduction
Ap	ampicillin
Ap^r	ampicillin resistance
AP	alkaline phosphatase
APS	ammonium persulfate
AS	acetosyringone
ATP	adenosine triphosphate
BCIP	5-bromo-4-chloro-3-indolyl phosphate
BLAST	basic local alignment search tool
bp	base pair(s)
BSA	bovine serum albumin
CAI	Codon Adaptation Index
CAMP	cationic antimicrobial peptide
Cb	carbenicillin
CDC	Centers for Disease Control and Prevention
CDNB	1-chloro-2,4-dinitrobenzene
CDP-DAG	cytidine diphosphate-diacylglycerol
CF	cystic fibrosis
CFTR	cystic fibrosis transmembrane conductance regulator
Cm	chloramphenicol
CMP	cytidine monophosphate
CoA	coenzyme A
CTP	cytidine triphosphate
CV	column volume(s)
DAG	diacylglycerol
DESY	Deutsches Elektronen-Synchrotron
DMPE	dimethyl-phosphatidylethanolamine
dNTP	deoxynucleotide triphosphate
$DOOR^2$	Database of prOkaryotic OpeRons[2]
DPG	diphosphatidylglycerol
ESI-MS	electrospray ionization mass spectrometry
ESRF	European Synchrotron Radiation Facility
FRT	Flp recombinase target
G3P	glycerol-3-phosphate
Gm	gentamicin
GPC	gel permeation chromatography
GST	glutathione S-transferase
GUS	β-glucuronidase
HEPES	4-(2-hydroxyethyl)-1-piperazineethanesulfonic acid
IPTG	isopropyl-β-D-galactopyranoside

iTRAQ	isobaric Tags for Relative and Absolute Quantitation
Kan	kanamycin
L-PG	lysyl-phosphatidylglycerol
L-PGS	lysyl-phosphatidylglycerol synthase
LB	Luria Bertani
LBP	lipid binding protein(s)
LC	liquid chromatography
LPA	lysophosphatidic acid
MALDI-TOF	matrix-assisted laser desorption ionization-time of flight
MD	malate dehydrogenase
MES	2-(*N*-morpholino)ethanesulfonic acid
MIC	minimal inhibitory concentration
MMPE	monomethyl-phosphatidylethanolamine
MPD	2-methyl-2,4-pentanediol
MS	mass spectrometry
MWCO	molecular weight cut-off
NaOH	sodium hydroxide
NBT	nitrotetrazolium blue
No.	number
OD_{xxx}	optical density at a wavelength of xxx nm
orf	open reading frame
ori	origin of replication
PA	phosphatidic acid
PBS	Phosphate Buffered Saline
PC	phosphatidylcholine
PCR	polymerase chain reaction
PDB	Protein Data Bank
PE	phosphatidylethanolamine
PEG	polyethylene glycol
PG	phosphatidylglycerol
PGP	phosphatidylglycerol phosphate
PI	phosphatidylinositol
PLD	phospholipase D
Pmt	phospholipid *N*-methyltransferase(s)
PS	phosphatidylserine
psi	pounds per square inch
PVDF	polyvinylidene difluoride
rmsd	root-mean-square deviation
RNase A	ribonuclease A
rpm	rounds per minute
RT	room temperature
SAD	single-wavelength anomalous dispersion
SAH	*S*-adenosylhomocysteine
SAM	*S*-adenosylmethionine
SAXS	small-angle X-ray scattering
SCP	sterol carrier protein
SD	standard deviation
SDS	sodium dodecyl sulfate
SDS-PAGE	sodium dodecyl sulfate polyacrylamide gel electrophoresis
SeMet	L(+)-selenomethionine
SER	Surface Entropy Reduction

SLS	Swiss Light Source
Spc	spectinomycin
Str	streptomycin
T4SS	type IV secretion system
TAE	Tris-acetate-EDTA
T-DNA	transfer-DNA
TEMED	N,N,N',N'-tetramethylethylene diamine
Tet	tetracycline
Ti	Tumor inducing
Tic	ticarcillin
TLC	thin-layer chromatography
T_M	melting temperature(s)
tRNA	transfer RNA
V	volt
(v/v)	volume per volume
(w/v)	weight per volume
x g	gravity
X-Gluc	5-bromo-4-chloro-3-indolyl-β-D-glucuronide
YEB	Yeast Extract Broth

1. Introduction

1.1 Composition of bacterial cell envelopes

The bacterial cytoplasmic membrane is composed of a glycerophospholipid bilayer containing embedded or associated proteins. On the one hand this membrane separates the cytoplasm from the surroundings, on the other hand it allows the exchange of compounds and signals with the environment, thereby functioning as a permeability barrier (1).

The cell envelope is different in Gram-positive and Gram-negative bacteria (2). In Gram-positives the cytoplasmic membrane is surrounded by a thick peptidoglycan layer containing teichoic acids. By contrast, a thin peptidoglycan layer covered by an additional outer membrane is present in Gram-negatives. This outer membrane is composed of glycerophospholipids in the inner leaflet and of lipopolysaccharides in the outer leaflet (3, 4). The cytoplasmic membrane and the outer membrane enclose a concentrated gel-like matrix, the periplasm (5).

Continuous adaptation to changing environmental conditions is essential for bacterial survival. One mechanism is to adjust the glycerophospholipid composition which significantly influences the biophysical properties of membranes (1). Therefore, the types of fatty acids in glycerophospholipids are modified or the ratio of unsaturated to saturated fatty acids is altered, influencing the membrane fluidity and permeability. Furthermore, the glycerophospholipid head groups can be modified to modulate the membrane surface charge leading e.g. to an increase in the bacterial resistance to antimicrobial peptides (6).

1.1.1 Glycerophospholipid biosynthesis

The biosynthesis of glycerophospholipids proceeds by a common biosynthetic pathway that takes place on/within the inner leaflet of the cytoplasmic membrane (7). To initiate this pathway in bacteria the central precursor molecule phosphatidic acid (PA) has to be generated. Therefore, glycerol-3-phosphate (G3P) is acylated at the *sn*1- and *sn*2-position by acyltransferases. Initially one fatty acid is transferred from a thioester of either acyl-coenzyme A (acyl-CoA) or acyl-acyl carrier protein (acyl-ACP) to the

*sn*1-position of G3P by PlsB (8) or PlsX and PlsY (9) yielding lysophosphatidic acid (LPA). Afterwards the *sn*2-position is acylated by PlsC resulting in PA, a universal glycerophospholipid precursor (6). Glycerophospholipids mostly possess saturated fatty acids at the *sn*1-position and unsaturated fatty acids at the *sn*2-position due to the substrate specificities of the acyltransferases (10).

Besides the *de novo* synthesis, PA can be generated by the recycling of already existing phospholipids. One possibility is the phosphorylation of the *sn*3-position of diacylglycerol (DAG) by DAG kinases like the integral membrane kinase DgkA (11) in Gram-negative bacteria or the soluble kinase DgkB (12) in Gram-positive bacteria. Furthermore, PA can be formed by the hydrolysis of a glycerophospholipid headgroup by phospholipase D (PLD) (13).

PA is coupled to diverse headgroup moieties which results in a diversity of different glycerophospholipids. An overview is presented in figure 1.

At first, PA is converted by the cytidine diphosphate diglyceride-synthase CdsA with cytidine triphosphate (CTP) to the activated intermediate cytidine diphosphate-diacylglycerol (CDP-DAG) (14). CDP-DAG represents the branching point in the biosynthetic pathways to either anionic glycerophospholipids like phosphatidylglycerol (PG), diphosphatidylglycerol (DPG, also named cardiolipin), phosphatidylinositol (PI) and phosphatidylserine (PS) or zwitterionic glycerophospholipids like phosphatidylethanolamine (PE) and phosphatidylcholine (PC) (15).

The formation of the zwitterionic glycerophospholipids PE and PC starts with the condensation of L-serine and CDP-DAG coupled to the release of cytidine monophosphate (CMP) by the PS synthase PssA which results in the formation of PS (16). The decarboxylation of the serine headgroup of PS by the PS decarboxylase Psd leads to the formation of PE (17). Finally, PE can be converted to PC by phospholipid *N*-methyltransferases (Pmt) catalyzing the successive methylation using *S*-adenosylmethionine (SAM) as a methyl donor (18). PC can also be obtained by a reaction catalyzed by the PC synthase Pcs condensing CDP-DAG with choline (19). In the literature the presence of PC in at least 15% of the organisms from the domain *Bacteria* was estimated (20).

In prokaryotes like actinomycetes, myxobacteria and *Treponema* PI is present and comprises up to 25% of the total membrane lipids. For PI formation CDP-DAG and *myo*-inositol are condensed by a PI synthase (21).

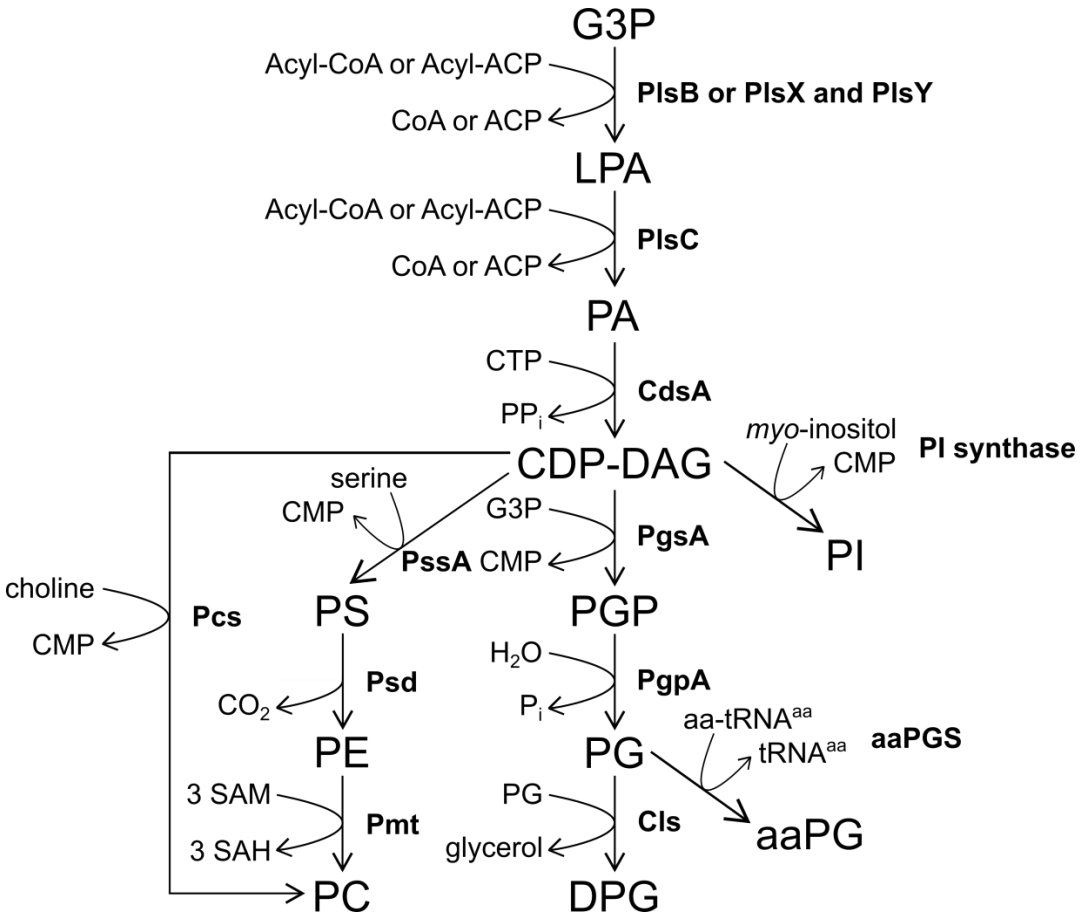

Figure 1: Overview of glycerophospholipid biosynthesis pathways in bacteria according to Geiger *et al*. (2010) (22)
The basis for glycerophospholipid biosynthesis is the molecule glycerol-3-phosphate (G3P). G3P is coupled to two fatty acids resulting in phosphatidic acid (PA). PA is the precursor for cytidine diphosphate-diacylglycerol (CDP-DAG), an important branching point for the synthesis of the zwitterionic glycerophospholipids phosphatidylcholine (PC) and phosphatidylethanolamine (PE) or the anionic glycerophospholipids phosphatidylserine (PS), phosphatidylglycerol (PG), diphosphatidylglycerol (DPG) and phosphatidylinositol (PI). Glycerophospholipid synthesizing or modifying enzymes are depicted in bold font. aa: amino acid, aaPG: aminoacyl-phosphatidylglycerol, ACP: acyl carrier protein, CMP: cytidine monophosphate, CoA: coenzyme A, CTP: cytidine triphosphate, LPA: lysophosphatidic acid, PGP: phosphatidylglycerol phosphate, P_i: inorganic phosphate, PP_i: inorganic pyrophosphate, SAH: *S*-adenosylhomocysteine, SAM: *S*-adenosylmethionine, tRNA: transfer RNA

The anionic glycerophospholipid PG is formed in a two-step reaction. Initially, the CMP moiety of CDP-DAG is substituted by G3P by the phosphatidylglycerol phosphate synthase PgsA. Then, the obtained phosphatidylglycerol phosphate (PGP) is dephosphorylated to PG by the PGP phosphatase PgpA (23). The condensation of two PG molecules by the cardiolipin synthase Cls results in DPG formation (24). Apart from being a precursor for DPG, PG can be modified in certain bacteria by aminoacyl-phosphatidylglycerol synthases (aaPGS).

These enzymes transfer an amino acid (e.g. alanine, arginine or lysine) in a transfer RNA (tRNA)-dependent reaction to PG yielding aminoacyl-phosphatidylglycerol (aaPG) (25).

Most bacterial membranes are comprised of PE, PG and DPG as the major constituents. For *Escherichia coli* the following membrane composition was described: 70-80% PE, 15-20% PG and up to 5% DPG (26).

Pseudomonas aeruginosa membranes contain similar amounts of the major constituents (~73% PE, ~17% PG, ~5% DPG) but additionally the zwitterionic glycerophospholipid PC (~4%) (27). PC is present in high amounts in *Agrobacterium tumefaciens* membranes (~22%) and also the DPG content (~15%) is significantly increased when compared to *E. coli* or *P. aeruginosa* membranes. PE together with PG accounts for ~45% of the total glycerophospholipid content. Additionally, *A. tumefaciens* membranes contain ~15% of monomethyl-PE (MMPE) and 4% of dimethyl-PE (DMPE) (28).

1.1.2 Structure and function of bacterial glycerophospholipids

Glycerophospholipids represent the major component of bacterial cell membranes and consist of a glycerol backbone coupled to a modifiable phosphate group (head) and two fatty acids (tails). Due to the hydrophilic head and the hydrophobic tail region glycerophospholipids possess an amphipathic character resulting in spontaneous bilayer or micelle formation in aqueous environments (29).

Anionic (e.g. PS, PG, DPG and PI) or zwitterionic (e.g. PE and PC) glycerophospholipids are able to significantly influence the surface charge of the cell membrane. Therefore, the lipid composition has to be balanced in an optimal way to maintain the integrity of the cell membrane and the correct topology of integral membrane proteins (15). Within bilayers a rapid lateral diffusion of glycerophospholipids occurs which allows the formation of lipid domains, e.g. DPG-rich domains in the septal and on the polar membrane regions of *E. coli* cells (30). In recent years, it was shown that this lipid domain formation can recruit proteins with specific functions to their place of action, e.g. enzymes involved in the glycerophospholipid biosynthesis are septally localized (31). Additionally, glycerophospholipids are involved in several other cellular processes. Anionic glycerophospholipids for instance can stimulate continuous

rounds of DNA replication initiation (32), are necessary for protein membrane translocation (33) or play an important role in ice nucleation (34). For zwitterionic glycerophospholipids the involvement in several solute transport systems was described (35). Furthermore, they play a role in proper membrane protein folding (36), in the bacterial symbiosis with host plants (37) and in virulence (38).

1.2 Modification of phosphatidylglycerol by aminoacylation

Lipid composition analyses revealed the presence of aminoacylated PG derivatives in some bacteria. This modification of PG with different amino acids was first described for certain Gram-positives in the 1960s (39–41). In the last decades several bacteria containing aaPG were identified and the physiological relevance of this lipid modification was explored (42).

The most abundant aminoacylated PG variants contain a lysine or alanine moiety but also the modification with arginine, glycine or ornithine was described (42). The structures of lysyl-phosphatidylglycerol (L-PG) and alanyl-phosphatidylglycerol (A-PG) are presented in figure 2.

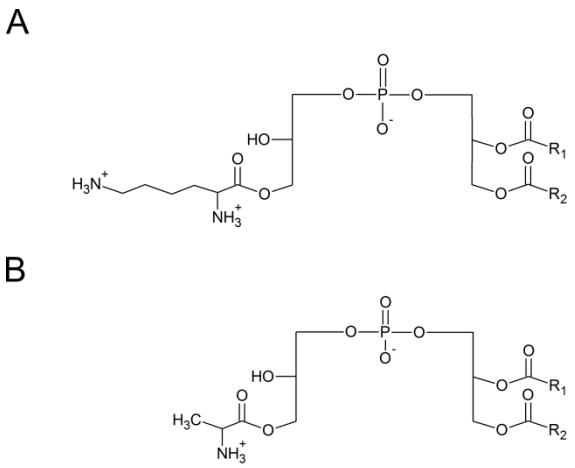

Figure 2: Structures of the PG derivatives lysyl-phosphatidylglycerol (A) and alanyl-phosphatidylglycerol (B)
The PG derivatives L-PG and A-PG are depicted. R_1 and R_2 represent fatty acid side chains.

The general mechanism for the aminoacylation of PG is the transfer of a specific amino acid from the corresponding tRNA onto the 2’ or 3’ hydroxyl group of PG by an aaPGS (43, 44). Depending on the utilized amino acid glycerophospholipids with zwitterionic (e.g. A-PG) or positive (e.g. L-PG) net charges are generated (figure 2). It was proposed that membrane properties

like surface charge, fluidity, molecular packing and permeability or intermolecular lipid-lipid interactions are modulated by the presence of aaPG (45, 46, 43).

1.2.1 Synthesis of aminoacylated phosphatidylglycerol in *P. aeruginosa*

Several bacteria that are associated with eukaryotes as pathogens, symbionts or commensals contain aaPG in their cell membrane(s) (22). In our laboratory a PG-modifying system in the opportunistic pathogen *P. aeruginosa* was discovered and characterized (43, 47–49). The aminoacylation of PG with L-alanine is catalyzed under acidic pH conditions by the alanyl-phosphatidylglycerol synthase (A-PGS) that is encoded by the open reading frame (orf) PA0920 in *P. aeruginosa*. The N-terminal domain anchors the A-PGS in the cytoplasmic membrane, whereas the C-terminal domain faces the cytoplasm and catalyzes the transfer of L-alanine from the corresponding tRNA to a hydroxyl group of PG resulting in A-PG (47).

In other aaPGS a flippase function was ascribed to the N-terminal domain resulting in the translocation of the respective aaPG into the outer leaflet of the cytoplasmic membrane (50, 51). A similar mechanism was proposed for *P. aeruginosa*.

A-PG synthesis results in an increased resistance of *P. aeruginosa* in the presence of the heavy metal $CrCl_3$, the β-lactam antibiotic cefsulodin, the cationic antimicrobial peptide (CAMP) protamine sulphate and the osmolyte sodium lactate (43).

1.2.2 Biochemical characterization of protein PA0919

In a recent study performed in our laboratory the gene product of orf PA0919, adjacent to orf PA0920 which encodes for the A-PGS, was biochemically characterized. The results of Arendt *et al.* (2013) (49) are summarized in the following chapter.

Growth analyses revealed a significant phenotype of the *P. aeruginosa* ΔPA0919 deletion mutant in the stationary growth phase under acidic cultivation conditions (pH 5.3) when compared to the *P. aeruginosa* wild type. Moreover, the deletion mutant and the wild type strain were cultivated under acidic conditions and their lipid composition was analyzed by two-dimensional

thin-layer chromatography (TLC). The deletion mutant contains twice as much A-PG as the wild type. Wild type growth and lipid composition were restored by a chromosomal complementation of the ΔPA0919 mutant. Accordingly, a functional role of protein PA0919 in the regulation of the cellular A-PG content in *P. aeruginosa* was proposed.

A hypothetical promoter region was identified within 430 base pairs (bp) upstream of orf PA0919. It is located within orf PA0920. Several promoter fragment-reporter gene fusions (430, 206 or 140 bp upstream of orf PA0919 fused to the reporter gene *lacZ*) were constructed and the respective promoter activity was determined under neutral and acidic growth conditions. The analyses revealed that only the activity of the 430 bp promoter fragment was significantly induced under acidic growth conditions in the stationary phase indicating the presence of a pH-controlled promoter in this region.

Sequence analyses revealed that protein PA0919 contains a characteristic LIPASE_SER motif that is typically found in lipases (52). Based on a sequence alignment of PA0919 homologs conserved serine and histidine residues (Ser240, Ser307 and His401) were identified and a functional role of protein PA0919 in A-PG hydrolysis was proposed.

To get insight into a potential catalytic function, protein PA0919 and mutant variants were heterologously produced in *E. coli* cells and purified by affinity chromatography. Gel permeation chromatography (GPC) analyses revealed that purified PA0919 is a monomer and spectroscopic analyses did not indicate the presence of a cofactor. Artificial *p*-nitrophenol derivatives, mostly *p*-nitrophenol esters of amino acid derivatives or aliphatic acid compounds, were employed in an *in vitro* activity assay to monitor the potential hydrolysis activity of purified PA0919. Only 4-nitrophenyl esters containing an amino acid moiety e.g. alanine, glycine or lysine were accepted by PA0919. The determined specific activities were in the same magnitude for all the employed amino acid *p*-nitrophenyl esters suggesting that the amino acid side chain is of minor importance for substrate recognition. In contrast, artificial substrates lacking an amino group were not hydrolyzed by PA0919 which highlights the importance of the amino group for substrate recognition. Based on these findings a specific cleavage of the aminoacyl bond in the putative native substrate A-PG was proposed.

The purified PA0919 mutant proteins S240A, S307A and H401A were also analyzed in the *in vitro* activity assay using the L-alanine 4-nitrophenyl ester (similar to the putative natural substrate A-PG) as a substrate. The S240A protein variant showed a significantly reduced specific activity of 45% when related to the wild type protein. However, no substrate hydrolysis was detected for the mutant proteins S307A and H401A which implies that the amino acids Ser307 and His401 are of prime importance for PA0919 catalysis.

To proof whether protein PA0919 is able to hydrolyze the putative natural substrate A-PG an *in vitro* activity assay using radioactively labeled A-PG was employed. Therefore, [1-^{14}C]-A-PG was synthesized by the purified A-PGS in an *in vitro* system (47). The polar lipids were extracted, solubilized by Triton™ X-100 and incubated with the purified PA0919 protein variants. The reaction products were separated by one-dimensional TLC and detected by autoradiography. For the wild type protein and the S240A variant the hydrolysis product [1-^{14}C]-L-alanine (identical migration to a L-alanine reference sample) was observed, whereas it was absent in the experiments using the S307A or H401A mutant protein. These results emphasize that protein PA0919 is able to hydrolyze A-PG *in vitro* and functions as an alanyl-phosphatidylglycerol hydrolase (A-PGH). Moreover, the amino acids Ser307 and His401 were clearly identified as the key residues of A-PGH catalysis.

To corroborate the physiological relevance of protein A-PGH a localization study was performed. *P. aeruginosa* ΔPA0919 cells containing a plasmid-encoded PA0919 gene fused to a *Strep*-tag® II sequence were separated into their soluble (periplasm and cytoplasm) and insoluble (inner and outer membrane) fractions. The analyses of the respective cellular fractions clearly indicated the presence of A-PGH in the inner membrane of *P. aeruginosa* and it was concluded that the protein is anchored by an N-terminal transmembrane helix. The C-terminal protein domain was proposed to be directed towards the periplasm based on a previous localization study using an alkaline phosphatase (AP) fusion screen (53). This localization permits the specific interaction of protein A-PGH with A-PG molecules in the inner membrane of *P. aeruginosa*.

In recent studies it was shown that the presence of aaPG molecules in the cell membrane(s) of different organisms reduces their susceptibility against several

antimicrobial agents (54, 43, 55). For *Staphylococcus aureus* a ‘charge repulsion’ mechanism for the interaction with CAMPs was proposed (54, 56). Anionic glycerophospholipids like PG cause a negatively charged membrane surface and their anionic head groups interact with the positively charged CAMPs which disorders the membrane structure. In contrast, the presence of L-PG results in a more positively charged membrane surface which leads to the repulsion of CAMPs and causes resistance.

The deletion of orf PA0919 resulted in artificially elevated A-PG levels in *P. aeruginosa*. Accordingly, the susceptibility of this strain was analyzed in the presence of selected antimicrobial compounds. However, for all the tested compounds a reduction instead of the expected increase of the minimal inhibitory concentration (MIC) compared to the wild type strain was determined indicating the importance of a fine-tuned cellular membrane composition for *P. aeruginosa* resistance.

1.2.3 Model for phosphatidylglycerol modification in *P. aeruginosa*

In recent years, research in our laboratory contributed to a comprehensive understanding of PG modification in *P. aeruginosa* (43, 47–49, 57).

The two enzymes A-PGS and A-PGH responsible for A-PG synthesis and hydrolysis, respectively, were discovered and biochemically characterized. From the obtained results a model for PG modification under acidic conditions in *P. aeruginosa* was proposed (58) which is presented in figure 3.

The transmembrane protein A-PGS catalyzes the transfer of the amino acid alanine from its Ala-tRNA^{Ala} to a hydroxyl group of PG by its C-terminal, catalytic domain which is located in the cytoplasm (47). It was proposed, in analogy to other aaPGS (50, 51), that A-PG is transferred from the inner to the outer leaflet of the cytoplasmic membrane by a flippase function of the N-terminal domain. A-PG is subsequently translocated into the inner leaflet of the outer membrane by a so far unknown mechanism. The A-PGH protein is anchored in the cytoplasmic membrane by one transmembrane helix and is localized in the periplasm (49). For A-PG hydrolysis an enzymatic mechanism according to lipases was postulated (58). The ester bond between PG and alanine is attacked by the hydroxyl group of Ser307 and a covalent enzyme-substrate intermediate is formed. The PG moiety is liberated and

alanine is released into the periplasm. The participation of key amino acid His401 was proposed.

Biochemical studies highlighted the relevance of an accurately fine-tuned cellular A-PG level for the resistance of *P. aeruginosa* against several antimicrobial compounds (43, 58). Dysbalancing the lipid homeostasis increased the susceptibility of *P. aeruginosa* against CAMPs and antimicrobials. Based on these findings, the A-PGS/A-PGH system was proposed as a promising target for the development of specific inhibitors in order to overcome the high antibiotic resistance of *P. aeruginosa*.

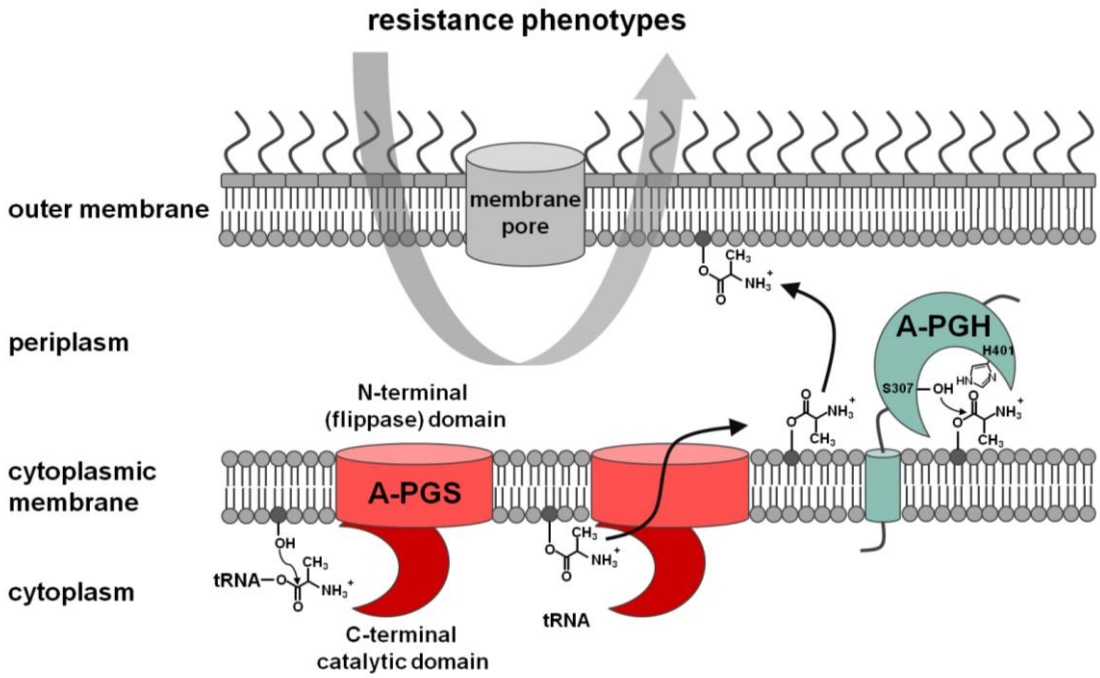

Figure 3: Proposed model for PG modification in *P. aeruginosa* (modified according to Arendt (2013) (58))
The amino acid alanine is transferred from the corresponding tRNA to a hydroxyl group of the glycerophospholipid PG (dark grey-colored lipid). This reaction is catalyzed by the C-terminal, catalytic domain of the A-PGS. The N-terminal transmembrane domain was shown to be responsible for aaPG flipping across the cytoplasmic membrane in several organisms (50, 51). An analogous mechanism was proposed for *P. aeruginosa*. The alanine moiety of A-PG is hydrolyzed by the N-terminally anchored A-PGH containing the key residues Ser307 and His401.

1.2.4 Homologous A-PGH proteins in bacteria

The A-PGH encoding orf PA0919 is located downstream of orf PA0920 which encodes for the A-PGS. Sequence alignments revealed that this sequential arrangement is conserved in several Gram-negatives (e.g. *Agrobacterium tumefaciens*, *Burkholderia phymatum*, *Ralstonia pickettii* and *Rhizobium tropici*)

and A-PGH homologous sequences were identified in α-, β- and γ-proteobacteria as well as enterobacteria (49). By contrast, no A-PGH homologous sequences were detected in Gram-positives which is in agreement with the presence of an N-terminal signal peptide and a previous localization study which indicated that the C-terminal part of protein A-PGH faces the periplasm (53).

Some A-PGH homologous proteins are already described in the literature like AtvA (acid tolerance and virulence protein A) of *R. tropici* as well as AcvB (*Agrobacterium* chromosomal virulence protein B) and VirJ of *A. tumefaciens*. For an *atvA* transposon mutant in *R. tropici* prolonged generation times under acidic cultivation conditions were observed and it was demonstrated that AtvA is required for nodulation competitiveness (52). Moreover, a LIPASE_SER motif was detected within the AtvA protein sequence. An exchange of the active site serine against alanine in the wild type strain resulted in a growth phenotype as observed for the *atvA* transposon mutant. Accordingly, amino acid Ser313 was proposed as a key residue for the so far unknown protein function and AtvA was proposed to belong to a new family of lipolytic enzymes (52) that might down-modulate the L-PG amounts in *R. tropici* membranes (59).

A transposon insertion in the *acvB* gene resulted in an avirulent *A. tumefaciens* strain, but virulence could be restored by a plasmid-encoded *acvB* gene (60). In addition, a paralogous *acvB* version with a sequence identity of 52% was identified in *A. tumefaciens* strains containing an octopine-type Tumor inducing (Ti)-plasmid (61). The VirJ protein corresponds to the C-terminal part of AcvB and a plasmid-encoded *virJ* gene was also able to restore wild type virulence for the *A. tumefaciens acvB* transposon mutant (61). Localization studies indicated a periplasmic localization of AcvB and VirJ (62, 63) and a potential function as periplasmic chaperones involved in the translocation of transfer-DNA (T-DNA) and effector proteins into the plant cell was postulated (64, 65).

1.2.5 Introduction to two model organisms containing modified glycerophospholipids – characteristics and impact

In the following chapter two bacterial species containing modified glycerophospholipids in their cell membranes will be introduced: *A. tumefaciens* as a plant pathogen and *P. aeruginosa* as an opportunistic human pathogen.

A. tumefaciens: A model organism for the investigation of the type IV secretion system

A. tumefaciens is a ubiquitous rod-shaped, Gram-negative bacterium belonging to the class of α-proteobacteria and is present in the soil microflora (66). Several *Agrobacterium* strains cause neoplastic diseases on plants like 'hairy root' by *A. rhizogenes*, 'cane gall' by *A. rubi* or 'crown gall' by *A. tumefaciens* (67). The broad-host-range phytopathogenic bacterium *A. tumefaciens* is able to initiate tumors on dicotylic and some monocotylic plant species (68). The formation of crown galls was first described in 1853 (69) and was connected to *A. tumefaciens* as the causal agent in 1907 (70).

Researchers became interested in the 'tumor inducing principle' (71) altering normal host cells into tumor cells. In the 1970s, it was demonstrated that the transfer and subsequent genomic integration of the T-DNA region from the Ti-plasmid of virulent *Agrobacterium* species is responsible for the formation of crown gall tumors in plants (72). The mechanism of *Agrobacterium*-mediated transformation of host cells was intensively studied in the last decades and so *Agrobacterium* was established as an important model system to study host-pathogen interaction.

Initially, *A. tumefaciens* cells sense signal molecules (e.g. phenolic or sugar compounds) in the soil which were released by wounded plants (73). Upon these stimuli the two-component regulatory system VirA/VirG activates the transcription of the Ti plasmid-encoded virulence operons (*vir* genes) (74). The respective Vir proteins form the VirB complex, a prototypical type IV secretion system (T4SS), which is responsible for the translocation of the T-strand in complex with several Vir proteins (referred to as T-complex) and other effector proteins from an attached *Agrobacterium* cell into the plant cell (75). The formation of a super-T-complex, additionally containing plant proteins, in the plant cytoplasm was postulated by Gelvin (2010) (76). After the

super-T-complex is targeted into the nucleus, associated proteins are removed from the T-strand prior to its genomic integration (76). Subsequently, the infected plant cells produce enzymes which are involved in the syntheses of the plant hormones auxin and cytokinin whose activity leads to tumor formation (77). Moreover, enzymes involved in opine syntheses are produced. Opines are amino acid and sugar phosphate derivatives and serve as a nutrient source for *A. tumefaciens* (78).

P. aeruginosa: A model organism for the investigation of antimicrobial resistance

P. aeruginosa is a ubiquitous, facultative anaerobic Gram-negative bacterium belonging to the class γ-proteobacteria. It is highly abundant worldwide but especially found in soil, marshes, coastal areas and on tissues of plants and animals (79). *P. aeruginosa* can grow or survive under anaerobic conditions using nitrate or nitrite as a terminal electron acceptor or by the fermentation of arginine or pyruvate, respectively, and is thus well adapted for the survival under microaerobic and anaerobic conditions (80).

As an opportunistic human pathogen *P. aeruginosa* can cause serious infections e.g. in burn wounds and the urinary or respiratory tract (79). It is one of the major nosocomial pathogens and primarily infects immunocompromised and cystic fibrosis (CF) patients (81).

In 2013, the Centers for Disease Control and Prevention (CDC) of the United States classified multidrug resistant *P. aeruginosa* strains as a serious threat. From the estimated 51’000 healthcare-associated infections reported to the CDC per year about 8% are caused by *P. aeruginosa*. From the estimated total number of *P. aeruginosa* infections 13% were attributed to multidrug resistant strains. Multidrug resistance is one of the major problems in the treatment of *P. aeruginosa* infections and leads to a threefold higher in-hospital mortality rate of ~27% when compared to the infection with susceptible organisms (82).

Besides a high intrinsic resistance against several structurally diverse antibiotics, *P. aeruginosa* is capable of acquiring and developing additional resistance mechanisms (83). *P. aeruginosa* resistance is caused by, *inter alia*, the low permeability of the outer membrane, very efficient and constitutively active multidrug efflux systems or/and the enzymatic inactivation or degradation

of antibiotics (84, 83).

Furthermore, *P. aeruginosa* is able to form biofilms on various surfaces in the environment, tissues and medical devices such as catheters (79, 85). Several factors were demonstrated to be important for the establishment and differentiation of such *P. aeruginosa* biofilms, e.g. bacterial motility provided by functional type IV pili (86), signaling molecules like the second messenger cyclic diguanosine-5'-monophosphate (87) or the quorum sensing molecule *N*-(3-oxododecanoyl)-L-homoserine lactone (88) and the production of exopolysaccharides (89).

The existing concentration gradients (e.g. nutrients, oxygen and signaling molecules) within a biofilm lead to bacterial cells in different physiological states that are adapted to the respective local microenvironment (90, 91). *P. aeruginosa* cells growing in biofilms are protected from diverse environmental factors and are up to 1'000 times more resistant against antimicrobials than planktonic bacteria (92, 93). Therefore, this lifestyle allows for a long-term colonization of surfaces and additionally impedes the eradication of *P. aeruginosa* infections (94).

1.3 Relevance of *P. aeruginosa* infection in cystic fibrosis patients

The human genetic disorder CF is caused by mutations in the gene encoding for the CF transmembrane conductance regulator (CFTR) which result in a defective chloride channel in epithelial cells (95). This defect affects the function of different organs like the pancreas, the liver, the gastrointestinal tract and in particular the respiratory system (96). In the latter case the airway mucus dehydrates and becomes viscous because of an impaired CFTR-mediated chloride secretion into the airways and the excessive reabsorption of sodium and water at the same time (97). Furthermore, goblet cells hypersecrete mucins to the apical surface which leads to plaque generation (98). Plaque accumulation results in a reduced mucociliary transport, an important innate defense mechanism to clear bacteria, viruses and foreign substances (95).

If bacteria invade a CF lung they will be trapped in a thick viscous mucus layer with a dramatically reduced oxygen tension forming a 'steep hypoxic gradient' (99). It was demonstrated that infected CF lungs are colonized by a diverse bacterial community comprised of more than 15 species, also including

facultative and obligate anaerobic species (100). *P. aeruginosa* is well adapted for such microaerophilic to anaerobic conditions (80) and represents the main pathogen leading to chronic infections in CF patients (101).

During the colonization of a CF lung *P. aeruginosa* undergoes diverse genetic, morphological and physiological changes. For instance, the bacterial cells switch from the non-mucoid to a mucoid cell type during the progression from an intermittent to a chronic infection (99). Mucoid strains produce a matrix (biofilm) containing the exopolysaccharide alginate that protects against antibiotics, reactive oxygen species and phagocytosis (101, 96). Furthermore, the mutation rate is increased resulting in a partial or complete loss of function of genes encoding for e.g. virulence factors or multidrug efflux pumps (102, 103). Besides this the production of virulence factors by *P. aeruginosa* is decreased or stopped resulting in a reduced immune recognition by the host and serving as a survival strategy in chronic infections (104).

Such chronic infections lead to a bacterial bronchitis that evolves into a syndrome of bronchiectasis, bronchiolectasis and finally respiratory failure and the death of the patient (98).

The current therapies (mainly antibiotic treatment) only alleviate the symptoms of a chronic infection, thereby improving the quality of life and the life expectancy of the patients but until today an eradication of the colonizing organisms is almost impossible (101).

1.4 Proteomics studies

The gene expression under defined conditions can be easily analyzed by microarray approaches. However, on the translational level further regulation mechanisms are involved and so the transcription profile does not directly reflect the proteomic pattern (105). Therefore, proteomics studies provide complementary information allowing for a detailed understanding of bacterial adaptation.

In the last decades, most proteomics studies focused on the analyses of cytoplasmic proteins, primarily due to technical difficulties. However, up to 30% of all bacterial genes are encoding for membrane proteins (106). Proteins embedded or associated with membranes play important roles in energy and signal transduction, metabolism, motility, growth and transport (105). Especially

for pathogenic bacteria the cell envelope represents the initial contact point to host cells which contains several virulence factors and mediates antibiotic resistance (107). Therefore, it is of great interest to also explore bacterial pathogenicity by membrane proteomics studies to discover potential biomarkers or to develop antimicrobial drugs and vaccines (108).

For proteomic approaches either gel-based (one- or two-dimensional) or non-gel based techniques are employed. Two-dimensional gel-based techniques are frequently used to separate mainly soluble proteins by isoelectric focusing in the first dimension and a sodium dodecyl sulfate (SDS) gel separation in the second dimension (109, 110). After gel staining, the respective spots are picked and digested before the peptides are identified by mass spectrometry (MS) analyses.

Since gel-based techniques are not suitable to analyze the membrane proteome, non-gel based techniques are used. For this, the entire protein mixture is digested and peptides are analyzed by one- or two-dimensional liquid chromatography (LC) coupled to MS analyses (105).

Bioinformatical analyses revealed that the *P. aeruginosa* genome encodes for ~2'000 known or putative proteins containing at least one transmembrane domain (111). The large-scale proteomics study of Blonder *et al.* (2004) (111) focused on the analysis of the *P. aeruginosa* PAO1 membrane subproteome by using a LC-MS/MS approach. This study was able to detect ~17% of the estimated *P. aeruginosa* membrane proteins involved in e.g. susceptibility, adaptation processes or antibiotic resistance. Further development of non-gel based techniques will facilitate the identification of more membrane proteins and the analyses of post-translational modifications, topology and orientation of membrane proteins in membranes (112).

1.4.1 Comparative *P. aeruginosa* membrane proteomics study

A recent proteomics study focused on the comparative analysis of the *P. aeruginosa* PAO1 membrane proteome under aerobic and anaerobic biofilm conditions which mimic the metabolic changes during CF infection progression (113).

In the study *P. aeruginosa* biofilms were grown on artificial sputum medium agar plates under aerobic and anaerobic conditions. Cells were disrupted by a

French Press® and membrane proteins were enriched and separated into the inner and outer membrane fraction by an isopycnic gradient centrifugation. Integral or strongly associated proteins were precipitated from the two membrane fractions and proteolytically digested. The obtained peptides were labeled with isobaric Tags for Relative and Absolute Quantitation (iTRAQ), a method that allows a simultaneous and relative quantification of peptides in a pooled sample *via* MS analyses (114, 115). The samples were fractionated by strong cation exchange chromatography and analyzed by LC-MS/MS. Protein identification was performed *via* Mascot database search and protein regulation (aerobic vs. anaerobic biofilm growth) was validated using the in-house bioinformatics tool iTRAQassist (116). Approximately 1'000 robustly regulated proteins were identified and ranked according to their regulation reliability.

This proteomics study identified 3'043 proteins which are associated with the membrane of *P. aeruginosa* PAO1. During biofilm cultivation 695 membrane proteins (571 and 124 identified proteins in the inner and outer membrane fraction) were detected which corresponds to ~35% of the estimated number (111) of proteins containing at least one transmembrane domain.

In general, *P. aeruginosa* adapted to anaerobic CF lung-like conditions *via* the upregulation of proteins involved in the denitrification pathway, for example Nar, Nir, Nor and Nos proteins which are necessary for the assembly of the nitrate, nitrite, nitric oxide or nitrous oxide reductase, respectively. Furthermore, proteins embedded in the outer membrane functioning as virulence factors, receptors or transporters were downregulated. Similar findings were described in the literature as a survival strategy of *P. aeruginosa* during chronic CF infections (104).

The conserved hypothetical proteins PA3913, PA3912 and PA3911 were detected among the top 20 upregulated proteins in the inner membrane fraction under anaerobic biofilm conditions and are encoded by a putative operon as described by Filiatrault *et al.* (2006) (117).

The gene expression of operon PA3913-PA3912-PA3911 is upregulated under reduced oxygen concentrations of 2% or 0.4% (118) and under anaerobic conditions in the presence of nitrate as a terminal electron acceptor (119, 118). Gene expression of PA3912 or PA3913 was induced under oxygen limited conditions in response to nitrate and nitrite (120) or under anaerobic conditions

with nitrate (121), respectively. Furthermore, gene expression was upregulated for all three genes during the cultivation in enhanced synthetic sputum medium (122).

Growth of PA3912 and PA3913 transposon mutants was significantly impaired or abolished under anaerobic conditions with nitrate as the electron acceptor. Also the presence of nitrite or arginine did not allow for anaerobic growth of both transposon mutants which indicates the general requirement of PA3912 and PA3913 for anaerobic growth (117). These findings are supported by the identification of a binding site for the major anaerobic transcriptional regulator Anr (anaerobic regulation of arginine deiminase and nitrate reduction) in the promoter region of PA3913 (119, 117).

The genes PA3913 and PA3912 encode for potential proteases with a peptidase family U32 signature, whereas gene PA3911 encodes for a conserved hypothetical protein with homology to lipid carrier proteins of the sterol carrier protein (SCP)-2 sterol transfer family (117). A transposon mutant of PA3912 revealed impaired swarming and swimming motility, whereas the biofilm formation was increased compared to the PAO1 wild type (123). By contrast, no functional role for proteins PA3913 and PA3911 is described in the literature to date.

1.5 Lipid carrier proteins

The comparative proteomics study described in chapter 1.4.1 identified protein PA3911 as the second-most significantly upregulated protein under anaerobic biofilm conditions mimicking the situation during a CF infection (113). In the literature PA3911 is described as a conserved hypothetical protein which shares homology with lipid carrier proteins of the SCP-2 family (117).

Research in the field of soluble fatty acid binding proteins and lipid binding proteins (LBP) facilitating the intracellular transport, metabolism and storage of these poorly soluble ligands started in the early 1970s with the investigation of the mammalian fatty acid binding protein (124). Since then a variety of soluble LBP was studied which led to the discovery of a very prominent domain in LBP, the SCP-2 domain. This domain can be found in stand-alone form or fused with other domains in bacteria, archaea and eukaryotes. Due to diverse architectures in multidomain proteins SCP-2 might have multiple functions in

various cellular contexts (125).

Although the sequence homology of LBP is very low nearly all possess a hydrophobic cavity to accommodate specific ligands (126). In case of the mammalian SCP-2 *in vitro* binding studies revealed a broad ligand spectrum (e.g. fatty acids, fatty acyl CoA esters, cholesterol and phospholipids) and the protein is, therefore, also known as the non-specific lipid transfer protein (127). The 58 kDa multidomain protein SCP-X is composed of an N-terminal 3-ketoacyl CoA thiolase and a C-terminal SCP-2 domain which can be cleaved off post-translationally (128). Cytosolic SCP-2 plays a role in the cellular uptake of cholesterol and fatty acids as well as in the intracellular cholesterol transport to the plasma membrane, whereas peroxisomal SCP-2 takes part in the β-oxidation of fatty acids (127).

From all branches of life three-dimensional structures of proteins containing a SCP-2 domain are available. SCP-2 domains have an α/β fold consisting of a five-stranded β-sheet surrounded by five α-helices (126). The secondary structure elements and their spatial orientation are highly conserved as demonstrated by the superposition of 22 three-dimensional structures containing SCP-2 domains (125). Most SCP-2 domains contain an internal cavity which is large enough to accommodate bulky hydrophobic ligands, but their size and shape can differ widely (126, 129, 130). Another characteristic of SCP-2 domains is a surface patch with a positive electrostatic potential which is predominantly located at the opening for ligand access/exit (125). This patch is proposed to interact with membranes *via* electrostatic interactions (125).

Despite several decades of research the functional diversity of proteins containing SCP-2 domains still has to be discovered, particularly for SCP-2 proteins from bacteria or plants.

1.6 Aim of this study

In bacteria, aminoacylation of the glycerophospholipid PG represents an adaptation strategy to various stress conditions and was demonstrated to increase the resistance against several antimicrobials. In the opportunistic pathogen *P. aeruginosa* PG is modified with L-alanine, yielding A-PG, under acidic conditions (43). In recent studies the enzymes A-PGS and A-PGH responsible for A-PG synthesis and hydrolysis were biochemically characterized

(43, 47–49). It was demonstrated that a fine-tuned cellular A-PG content is critical for the bacterial susceptibility in the presence of antimicrobials. To get insight into the underlying molecular principle of A-PG hydrolysis in *P. aeruginosa* it was intended to elucidate the three-dimensional structure of protein A-PGH by X-ray crystallography.

The sequential arrangement of orthologous A-PGS and A-PGH genes is conserved in several Gram-negatives (49). The proteins LpiA or AcvB and VirJ of *A. tumefaciens* were identified as homologous A-PGS and A-PGH proteins, respectively, and a functional role in L-PG synthesis or hydrolysis was proposed. To elucidate the biochemical function of these proteins *in vitro* activity assays using purified wild type protein or active site mutants had to be performed. Furthermore, the localization of AcvB and VirJ in *A. tumefaciens* had to be analyzed. In cooperation with Prof. Franz Narberhaus and Dr. Meriyem Aktas from Ruhr-University Bochum *A. tumefaciens* Δ*lpiA* or Δ*acvB* mutants had to be characterized concerning their growth behavior and lipid composition. Besides this, the physiological relevance of LpiA and AcvB in tumorigenesis of the phytopathogenic bacterium *A. tumefaciens* had to be investigated.

A comparative proteomics study identified the conserved hypothetical protein PA3911 as the second-most significantly upregulated protein under anaerobic CF lung-like conditions (113). For phenotypical characterization a *P. aeruginosa* PA3911 transposon mutant had to be analyzed with respect to growth, lipid composition, motility, biofilm formation and antimicrobial susceptibility. Furthermore, the cellular localization of PA3911 in *P. aeruginosa* PAO1 had to be studied. Protein PA3911 shares homology with lipid carrier proteins of the SCP-2 family (117). Accordingly, the lipid binding capability of the purified wild type protein and of protein variants had to be explored.

2. Materials and methods

2.1 Instruments, chemicals and materials

2.1.1 Instruments

Table 1: List of instruments used in this study

instrument	model	manufacturer
agarose gel electrophoresis chamber	Mini-Sub® Cell GT	Bio-Rad
agarose gel documentation	DeVision G system	Science Tec
autoclave	LVSA 50/70	Zirbus
blot machine	Trans-Blot® Turbo™	Bio-Rad
blue-light transilluminator	Flu-O-Blu	Biozym Scientific GmbH
centrifuge	Avanti® J-30I	Beckman Coulter GmbH
	Avanti® J-E	Beckman Coulter GmbH
	Megafuge® 1.0R	Heraeus®
	MiniSpin®	Eppendorf
	Optima™ L-90K ultracentrifuge	Beckman Coulter GmbH
	Biofuge® fresco	Heraeus®
cell disruptor	FastPrep®-24	MP Biomedicals
clean bench	HERAsafe®	Heraeus®
FPLC	ÄKTAexplorer™	GE Healthcare
	ÄKTApurifier™	GE Healthcare
French Press®	French® Pressure Cell Press	Polytec
French Press® cell	French® Pressure Cell	Thermo Electron Corporation
gel scanner	BIO-5000 Plus VIS gel scanner	Serva
magnetic stirrer	IKAMAG® KMO-1	IKA®
	VARIOMAG® Multipoint HP15	Thermo Scientific
mass spectrometer	Orbitrap Fusion™	Thermo Scientific
microplate incubator	OmniLog®	Biolog
microplate reader	Model 680	Bio-Rad
	Varioskan® Flash	Thermo Scientific
pH determination	CG 842	Schott
photometer	Ultrospec 2000	Amersham Pharmacia Biotech
	Libra S22	Biochrom
pipettes	0.5-10 µl Research®	Eppendorf
	10-100 µl Research®	Eppendorf
	100-1'000 µl Research®	Eppendorf
	10 ml Research plus	ABI Med
	5-100 µl Xplorer®, 8 channels	Eppendorf
	50-1'200 µl Xplorer®, 8 channels	Eppendorf
power supply electrophoresis	PowerPac™ Basic 300 V	Bio-Rad
real-time PCR	C1000™ Thermal Cycler with CFX96™ real-time system	Bio-Rad
rocker	PMR-30	Grant
roller mixer	RM5	Assistent
scales	BL1500	Sartorius
	BP61S	Sartorius
	SBA52	Scaltec
scintillation counter	Tri-Carb® 2900TR	PerkinElmer
SDS-PAGE system	Mini-PROTEAN® Tetra Cell	Bio-Rad
shakers	305/3020	GFL®
	CH-4103	Infors HT

instrument	model	manufacturer
spectrophotometer	NanoDrop™ ND-1000	PEQLAB Biotechnologie GmbH
Speed Vac®	SPD101B	Savant
thermocycler	Tpersonal	Biometra
	C1000™ Thermal Cycler	Bio-Rad
thermomixer	Thermomixer compact	Eppendorf
TLC plate heater	TLC plate heater III	CAMAG®
UV-VIS spectrophotometer	V-650	Jasco
vortex	Vortex-Genie® 2	Scientific Industries™
water purification system	Milli-Q® system	Merck Millipore
X-ray generator	MicroMax™-007 HF	Rigaku

2.1.2 Chemicals and materials

Table 2 summarizes the chemicals and materials used in this study. Chemicals not specifically listed were purchased from the following manufacturers: Fluka®, Merck, Riedel-de Haën®, Roche, Roth® and Sigma-Aldrich® (quality grade p.a.).

Table 2: List of utilized chemicals and materials

application	product	manufacturer
antibodies and detection reagents	5-bromo-4-chloro-3-indolyl phosphate	Roth®
	Anti-mouse IgG (Fc-specific)-alkaline phosphatase antibody produced in goat	Sigma-Aldrich®
	nitrotetrazolium blue	Roth®
	Penta-His mouse monoclonal IgG antibody BSA-free	QIAGEN
	Strep-Tactin® AP conjugate	iba
blotting	Immobilon-P membrane, polyvinylidene difluoride, pore size 0.45 µm	Merck Millipore
	blotting paper, 150 x 150 mm, 550 g/m²	neoLab®
chemicals	avidin	Calbiochem®
	Bradford reagent	Sigma-Aldrich®
	[1-^{14}C]-L-alanine	Moravec Biochemicals
	1-chloro-2,4-dinitrobenzene	Sigma-Aldrich®
	chloramphenicol	Roth®
	crystal violet	Merck
	D-desthiobiotin	iba
	deoxynucleotide triphosphate mixture	New England BioLabs®
	GelStar® Nucleic Acid Gel Stain	Lonza
	InstantBlue™	Expedeon
	isopropyl-β-D-galactopyranoside	GERBU Biotechnik
	minocycline hydrochloride	Sigma-Aldrich®
	Nafcillin sodium salt	Sigma-Aldrich®
	oligodeoxynucleotides	Biomers, Invitrogen, Eurofins Genomics
	OptiPhase HighSafe 2	PerkinElmer
	oxacillin sodium salt monohydrate	Sigma-Aldrich®
	polymyxin B	Sigma-Aldrich®
	L(+)-selenomethionine	ACROS Organics™
	Sodium chloride (NaCl)	Fisher Chemical
	Strep-Tactin® regeneration buffer	iba
	SYPRO® Orange Protein Gel Stain	Thermo Fisher Scientific
	thiamphenicol	Sigma-Aldrich®
crystallization	CrystalCap-T™ Cap/Vial HR 8-116 with loops	Hampton Research
	CrystalClear	Manco® Inc.

application	product	manufacturer
	Crystalgen 24 Well SuperClear™ Plate (REF 23-252)	Jena Bioscience
	INTELLI-PLATE®, 96-well (REF 102-0001-03)	Art Robbins Instruments
	NeXtal crystallization screens	QIAGEN
enzymes	Antarctic Phosphatase	New England BioLabs®
	Benzonase®	Merck Millipore
	Phusion® High-Fidelity DNA Polymerase	New England BioLabs®
	restriction endonucleases	New England BioLabs®
	T4 DNA Ligase	New England BioLabs®
kits	In-Fusion® HD Cloning Kit	Clontech® Laboratories
	QIAprep Spin Miniprep Kit	QIAGEN
	QIAquick Gel Extraction Kit	QIAGEN
	QIAquick PCR Purification Kit	QIAGEN
	QuikChange Site-Directed Mutagenesis Kit	Agilent Technologies
markers	Gel Filtration Markers Kit for Protein Molecular Weights 12'000-200'000 Da	Sigma-Aldrich®
	GeneRuler™ DNA Ladder Mix	Thermo Fisher Scientific
	MassRuler™ DNA Ladder Mix	MBI Fermentas
	PageRuler™ Prestained Protein Ladder	Thermo Fisher Scientific
	Unstained Protein Molecular Weight Marker	Thermo Fisher Scientific
microplate appliance	Breathe-Easy™ sealing membrane	Diversified Biotech
	microplate, 96-well flat bottom (REF 82.1581.001)	Sarstedt
	microplate, 96-well round bottom, polypropylene	Nunc™
Phenotype microarray™	IF-0 medium	Biolog
	IF-10 medium	Biolog
	MicroPlates™ PM9 to PM20	Biolog
	Redox Dye Mix A	Biolog
protein purification, concentration and dialysis	Amicon® Ultra-0.5 device (molecular weight cut-off (MWCO): 10 kDa)	Merck Millipore
	Chelating Sepharose™ Fast Flow	GE Healthcare
	dialysis tubing membrane visking (MWCO: 14 kDa)	Roth®
	illustra NAP-5	GE Healthcare
	Poly-Prep® Chromatography Column (0.8 x 4 cm)	Bio-Rad
	Protino® Glutathione Agarose 4B	Macherey-Nagel
	Strep-Tactin® Superflow®	iba
	Strep-Tactin® Superflow® high capacity	iba
	Superdex™ 200 Increase 5/150 GL	GE Healthcare
	Superdex™ 200 HR 10/30	GE Healthcare
	TALON® metal affinity resin	Clontech® Laboratories
	Vivaspin® Turbo 4	Sartorius stedim biotech
others	cuvette (REF 67.742)	Sarstedt
	pH indicator test stripes (pH Fix 4.5-10.0)	Macherey-Nagel
	silica glass cuvette type 115F-QS	Hellma®
	sterile filters Filtropur S (Ø 0.2 or 0.45 µm) or Filtropur BT50 (Ø 0.22 µm), 500 ml	Sarstedt
	Membrane Lipid Strips™ P-6002	Echelon Biosciences
thermal shift assay	Microseal® 'B' seal	Bio-Rad
	Multiplate™ PCR plates 96-well, clear	Bio-Rad
thin-layer chromatography	TLC plate Alugram® SIL G/UV254	Macherey-Nagel
	molybdatophosphoric acid	Roth®
	Molybdenum Blue spray reagent	Sigma-Aldrich®
	ninhydrin spray solution	Merck

2.2 Bacterial strains, plasmids and oligodeoxynucleotides

2.2.1 Bacterial strains

The bacterial strains used in this work are listed in table 3.

Table 3: Overview of the bacterial strains used in this study

strain	genotype	reference
Agrobacterium tumefaciens		
C58	wild type	C. Baron (Montreal, Canada)
C58 Δ*acvB*	markerless deletion mutant of orf Atu2522 from *A. tumefaciens* C58	M. Aktas, Ruhr-University Bochum, unpublished
C58 Δ*lpiA*	markerless deletion mutant of orf Atu2521 from *A. tumefaciens* C58	M. Aktas, Ruhr-University Bochum, unpublished
Escherichia coli		
BL21(λDE3)	B F^- *dcm ompT hsdS*(r_B^- m_B^-) *gal* λ(DE3)	Stratagene, (131)
DH10B	F^- *araD*139 Δ(*ara*, *leu*)7697 Δ*lacX*74 *galU galK rpsL deoR* Φ80d*lacZ*ΔM15 *endA1 nupG recA1 mcrA* Δ(*mrr hsdRMS mcrBC*), Str^r	Invitrogen, (132)
Rosetta™ (DE3) pLysS	F^- *ompT hsdS*$_B$(r_B^- m_B^-) *gal dcm* (DE3) pLysSRARE, Cm^r	Novagen
ST18	S17 λ*pir* Δ*hemA*	(133)
Stellar™	F^-, *endA1, supE44, thi-1, recA1, relA1, Φ80d lacZ*Δ *M15, ΔmcrA,* Δ*(lacZYA-argF) U169, λ–, phoA,* Δ*(mrr hsdRMS mcrBC), gyrA96*	Clontech® Laboratories
Pseudomonas aeruginosa		
PAO1	wild type	(79)
PAO1 pUCP20T-P_{PA3911}-PA3911	PAO1 containing vector pUCP20T-P_{PA3911}-PA3911, Cb^r	this work
MPAO1	wild type of transposon mutant bank	(134)
PW7609	PA3911-C03::IS*phoA*/hah, Tet^r	(134)

2.2.2 Plasmids

The plasmids used in this work are listed in table 4. Correct integration of the insert sequence into the respective vector was verified by sequencing.

Table 4: List of plasmids used in this study

plasmid	description	reference
pET22b(+)	vector for recombinant protein production in *E. coli*, provides a T7 promoter, an N-terminal *pelB* secretion signal sequence and a C-terminal His_6-tag, Ap^r	Novagen, Merck
pET22b(+)Strep	pET22b(+) derivative providing a C-terminal *Strep*-tag® II, cloned into *Hin*dIII/*Xho*I sites, Ap^r	(49)
pET22b(+)PA0919-Strep	pET22b(+)Strep derivative encoding amino acids 34-427 of orf PA0919 from *P. aeruginosa* cloned into *Nco*I/*Hin*dIII sites, employed for production of A-PGH fused to an N-terminal *pelB* sequence and a C-terminal *Strep*-tag® II, Ap^r	(49)

plasmid	description	reference
pET22b(+)PA0919$_{trunc}$-Strep	pET22b(+)Strep derivative encoding amino acids 203-427 of orf PA0919 from *P. aeruginosa* cloned into *Nco*I/*Hin*dIII sites, employed for production of A-PGH$_{trunc}$ fused to an N-terminal *pelB* sequence and a C-terminal *Strep*-tag® II, Ap^r	(135)
pET22b(+)PA0919$_{trunc}$-Strep/AAK	pET22b(+)PA0919$_{trunc}$-Strep derivative, amino acids E_{176}EK were changed to AAK, Ap^r	this work
pET22b(+)PA0919$_{trunc}$-Strep/AAA	pET22b(+)PA0919$_{trunc}$-Strep derivative, amino acids E_{176}EK were changed to AAA, Ap^r	this work
pET22b(+)Strep_*pelB_acvB* ΔAS1-24	pET22b(+)Strep derivative encoding amino acids 25-456 of orf Atu2522 from *A. tumefaciens*, employed for production of AcvB fused to an N-terminal *pelB* sequence and a C-terminal *Strep*-tag® II, Ap^r	(136)
pET22b(+)Strep_*pelB_acvB* ΔAS1-24-S269A	pET22b(+)Strep_*pelB_acvB*ΔAS1-24 derivative, amino acid serine 269 of AcvB was changed to alanine, Ap^r	(137)
pET22b(+)Strep_*pelB_acvB* ΔAS1-24-S336A	pET22b(+)Strep_*pelB_acvB*ΔAS1-24 derivative, amino acid serine 336 of AcvB was changed to alanine, Ap^r	(137)
pET22b(+)Strep_*pelB_acvB* ΔAS1-24 H433A	pET22b(+)Strep_*pelB_acvB*ΔAS1-24 derivative, amino acid histidine 433 of AcvB was changed to alanine, Ap^r	(137)
pET22b(+)Strep_*pelB_acvB* ΔAS1-24-H433N	pET22b(+)Strep_*pelB_acvB*ΔAS1-24 derivative, amino acid histidine 433 of AcvB was changed to asparagine, Ap^r	(137)
pET22b(+)Strep_*pelB_virJ* ΔAS1-21	pET22b(+)Strep derivative containing the codon-optimized sequence of *virJ* (amino acids 22-255) from *A. tumefaciens*, employed for production of VirJ fused to an N-terminal *pelB* sequence and a C-terminal *Strep*-tag® II, Ap^r	(136)
pET28b(+)	vector for recombinant protein production, P_{T7}, ori$_{pBR322}$, *lacI*, N-terminal His_6-tag, Kan^r	Novagen
pET28b(+)PA0903	derivative of pET28b(+) encoding orf PA0903 (alanyl-tRNA synthetase) from *P. aeruginosa* inserted into the *Nde*I/*Bam*HI sites; production of protein PA0903 fused to an N-terminal His_6-tag, Kan^r	(47)
pET28b(+)-PA3911	derivative of pET28b(+) containing the codon-optimized sequence of orf PA3911 from *P. aeruginosa* inserted into the *Nco*I/*Xho*I sites; production of protein PA3911 fused to an N-terminal His_6-tag, Kan^r	this work
pET32a(+)	vector for recombinant protein production, P_{T7}, ori$_{pBR322}$, *lacI*, N-terminal thioredoxin-His_6-S-tag, C-terminal His_6-tag, Ap^r	Novagen
pET32a(+)/PA3911$_{opt}$ ΔAS1-19	derivative of pET32a(+) encoding amino acids 20-171 of orf PA3911 (codon-optimized sequence) from *P. aeruginosa* inserted into the *Sac*I/*Not*I sites; production of protein PA3911 fused to an N-terminal thioredoxin-His_6-S-tag, PreScission™ protease specific cleavage site, Ap^r	(138)

plasmid	description	reference
pET32a(+)-PA3911	derivative of pET32a(+)/PA3911$_{opt}$ ΔAS 1-19 containing the codon-optimized sequence of orf PA3911 from *P. aeruginosa* (synthetic fragment) inserted into the *EcoR*I/*Not*I sites; production of protein PA3911 fused to an N-terminal thioredoxin-His$_6$-S-tag, Ap^r	this work
pET32a(+)-PA3911-L56R	derivative of pET32a(+)-PA3911, amino acid leucine 56 of PA3911 was changed to arginine, Ap^r	(139)
pET32a(+)-PA3911-L56W	derivative of pET32a(+)-PA3911, amino acid leucine 56 of PA3911 was changed to tryptophan, Ap^r	(139)
pET32a(+)-PA3911-L58R	derivative of pET32a(+)-PA3911, amino acid leucine 58 of PA3911 was changed to arginine, Ap^r	(139)
pET32a(+)-PA3911-L58W	derivative of pET32a(+)-PA3911, amino acid leucine 58 of PA3911 was changed to tryptophan, Ap^r	(139)
pET32a(+)-PA3911-V69R	derivative of pET32a(+)-PA3911, amino acid valine 69 of PA3911 was changed to arginine, Ap^r	(139)
pET32a(+)-PA3911-V69W	derivative of pET32a(+)-PA3911, amino acid valine 69 of PA3911 was changed to tryptophan, Ap^r	(139)
pET32a(+)-PA3911-F95R	derivative of pET32a(+)-PA3911, amino acid phenylalanine 95 of PA3911 was changed to arginine, Ap^r	(139)
pET32a(+)-PA3911-F95W	derivative of pET32a(+)-PA3911, amino acid phenylalanine 95 of PA3911 was changed to tryptophan, Ap^r	(139)
pET32a(+)-PA3911-L114R	derivative of pET32a(+)-PA3911, amino acid leucine 114 of PA3911 was changed to arginine, Ap^r	(139)
pET32a(+)-PA3911-L114W	derivative of pET32a(+)-PA3911, amino acid leucine 114 of PA3911 was changed to tryptophan, Ap^r	(139)
pEX18Ap	gene replacement vector, *oriT*$^+$, *sacB*$^+$, Ap^r	(140)
pEX18Ap-ΔPA3911	pEX18Ap derivative with 460 bp upstream sequence of orf PA3911, gentamicin resistance cassette of pPS858 (flanked by *Bam*HI sites) and 649 bp downstream of orf PA3911, inserted into *Kpn*I/*Hin*dIII sites, Ap^r, Gm^r	this work
pFLP2	source of Flp recombinase, Ap^r	(140)
pFU84	pSC101* vector backbone with *phoA* gene from *E. coli* inserted into *Sal*I/*Not*I sites, Ap^r	(141)
pFU84_QC	pFU84 derivative with silent mutation in the codon of amino acid 298 of the *phoA* gene to eliminate the *Nco*I restriction site, Ap^r	(142)
pGEX-6P-1	vector for recombinant protein production, P$_{tac}$, ori$_{pBR322}$, N-terminal glutathione S-transferase (GST)-tag, PreScission™ protease specific cleavage site, Ap^r	GE Healthcare

plasmid	description	reference
pGEX-6P-1/PA3911$_{opt}$ ΔAS1-19	derivative of pGEX-6P-1 encoding amino acids 20-171 of orf PA3911 (codon-optimized sequence) from *P. aeruginosa* inserted into the *Eco*RI/*Not*I sites; production of protein PA3911 fused to an N-terminal GST-tag, PreScission™ protease specific cleavage site, Ap^r	(138)
pGEX-6P-1-PA3911	derivative of pGEX-6P-1/PA3911$_{opt}$ ΔAS 1-19 containing the codon-optimized sequence of orf PA3911 from *P. aeruginosa* inserted into the *Eco*RI/*Not*I sites; production of protein PA3911 fused to an N-terminal GST-tag, Ap^r	this work
pPS858	source of gentamicin resistance cassette, Ap^r, Gm^r	(140)
pTrc200	*trc* promoter production vector, *lacI*^{q}, Spc^r, Str^r	(143)
pTrc200 '*phoA*	pTrc200 derivative encoding amino acids 34-471 of *phoA* gene (signal sequence removed, silent mutation in the codon of amino acid 298 to eliminate the *Nco*I restriction site) from *E. coli* cloned into *Nco*I/*Hin*dIII sites, Spc^r, Str^r	(142)
pTrc200 *phoA*	pTrc200 derivative containing the *phoA* gene (silent mutation in the codon of amino acid 298 to eliminate the *Nco*I restriction site) from *E. coli* cloned into *Nco*I/*Hin*dIII sites, Spc^r, Str^r	(142)
pTrc200 leader *acvB* '*phoA*	pTrc200 derivative containing a synthetic fragment encoding for the *acvB* leader sequence (amino acids 1-24) and amino acids 34-471 of *phoA* gene (signal sequence removed), cloned *via* In-Fusion® HD Cloning, Spc^r, Str^r	(142)
pTrc200 leader *virJ* '*phoA*	pTrc200 derivative containing a synthetic fragment encoding for *virJ* leader sequence (amino acids 1-22) and amino acids 34-471 of *phoA* gene (signal sequence removed), cloned *via* In-Fusion® HD Cloning, Spc^r, Str^r	(142)
pTrc200_*acvB*_Strep	pTrc200 derivative encoding for orf Atu2522 from *A. tumefaciens*, employed for production of AcvB fused to a C-terminal *Strep*-tag® II, Spc^r, Str^r	S. Hebecker, unpublished
pTrc200_*acvB*_Strep-S269A	pTrc200_*acvB*_Strep derivative, amino acid serine 269 of AcvB was changed to alanine, Spc^r, Str^r	this work
pTrc200_*acvB*_Strep-S336A	pTrc200_*acvB*_Strep derivative, amino acid serine 336 of AcvB was changed to alanine, Spc^r, Str^r	this work
pTrc200_*acvB*_Strep-H433A	pTrc200_*acvB*_Strep derivative, amino acid histidine 433 of AcvB was changed to alanine, Spc^r, Str^r	this work
pTrc200_*acvB*_Strep-H433N	pTrc200_*acvB*_Strep derivative, amino acid histidine 433 of AcvB was changed to asparagine, Spc^r, Str^r	this work
pTrc200_*virJ*_Strep	pTrc200 derivative containing a synthetic fragment encoding for the *virJ* gene from *A. tumefaciens*, employed for production of VirJ fused to a C-terminal *Strep*-tag® II, cloned *via* In-Fusion® HD Cloning, Spc^r, Str^r	S. Hebecker, unpublished

plasmid	description	reference
pUCP20T	*E. coli-P. aeruginosa* shuttle vector, Cb^r	(144)
pUCP20T-P_{PA3911}-PA3911	pUCP20T derivative containing the putative promoter (500 bp upstream of orf PA3911), orf PA3911 and the *Strep*-tag® II sequence, cloned into *Xba*I/*Bam*HI sites, Cb^r	this work

2.2.3 Oligodeoxynucleotides

In table 5 oligodeoxynucleotides are listed that were used for cloning purposes in this work. They were purchased from Biomers (Ulm, Germany), Invitrogen (Carlsbad, CA, USA) or Eurofins Genomics (Ebersberg, Germany).

Table 5: Oligodeoxynucleotides utilized for cloning
Restriction sites are underlined and exchanged nucleotides for site-directed mutagenesis are highlighted in bold font. Oligodeoxynucleotides highlighted superscript derived from: [1](135), [2](142), [3](145), [4](139), [5](134). No., number.

No.	name	sequence (5' – 3')
1[1]	$APGH_{trunc}$_fw	CCGGCGATGGCCATGGACGTGCTCGCCCATCAGTTG
2[1]	$APGH_{trunc}$_rv	AAGCGCTGAGAAGCTTGGCGTCGGGAGCGTTCTC
3	A-PGH EEK-AAK fw	GCATCTATGGCGCC**GCAGCAAAG**GACGAAAGCGGCT G
4	A-PGH EEK-AAK rv	CAGCCGCTTTCGTC**CTTTGCTGC**GGCGCCATAGATGC
5	A-PGH EEK-AAA fw_2	GCATCTATGGCGCC**GCAGCAGCG**GACGAAAGCGCTG
6	A-PGH EEK-AAA rv_2	CAGCCGCTTTCGTC**CGCTGCTGC**GGCGCCATAGATGC
7[2]	CAT zu CAC-fw	CCGAAAGCAACGTACCA**C**GGCAATATCGATAAG
8[2]	GTA zu GTG-rv	CTTATCGATATTGCCGT**G**GTACGTTGCTTTCGG
9[2]	*Nco*I *phoA* fw	AGGAAACAGACCATGGTGAAACAAAGCACTATTGCACT GGC
10[2]	*Nco*I '*phoA* fw	AGGAAACAGACCATGGCTCAGGGCGATATTACTGCAC C
11[2]	'*phoAHin*dIII-rv	CAAAACAGCCAAGCTTTTATTTCAGCCCCAGAGCGGCT TTC
12[3]	pTrc200_*acvB* fw	GTAGCCATGGCGGTGATCTAT
13[3]	pTrc200_*acvB* rv_*Xma*I	GTTACCCGGGTTATTTTTCGAACTGCG
14[4]	L56R_fw	GCTGGAAGGTCGTTGGC**GC**CGTCTGGAAGTTCGTGAT CTGGG
15[4]	L56R_rv	GATCACGAACTTCCAGACG**GC**GCCAACGACCTTCCAG CAG
16[4]	L56W_fw	GCTGGAAGGTCGTTGG**TG**GCGTCTGGAAGTTCGTGAT CTGGG
17[4]	L56W_rv	GATCACGAACTTCCAGACGC**CA**CCAACGACCTTCCAG CAG
18[4]	L58R_fw	GGAAGGTCGTTGGCTGCGTC**GC**GAAGTTCGTGATCTG GG
19[4]	L58R_rv	CCCAGATCACGAACTTC**GC**GACGCAGCCAACGACCTT CC
20[4]	L58W_fw	GGAAGGTCGTTGGCTGCGT**T**GGGAAGTTCGTGATCTG GG
21[4]	L58W_rv	CCCAGATCACGAACTTCCC**A**ACGCAGCCAACGACCTT CC
22[4]	V69R_fw	GGGTGTGGGTTGGTGT**CGC**ACCCGTGTTCCGGGTGG
23[4]	V69R_rv	CCACCCGGAACACGGGT**GCG**ACACCAACCCACACCC
24[4]	V69W_fw	GGGTGTGGGTTGGTGT**TGG**ACCCGTGTTCCGGGTGG
25[4]	V69W_rv	CCACCCGGAACACGGGT**CCA**ACACCAACCCACACCC

No.	name	sequence (5' – 3')
26[4]	F95R_fw	CGTGGTGATTGGCGTGAT**CGC**CTGCTGCTGGCAAGCCG
27[4]	F95R_rv	GACGGCTTGCCAGCAGCAG**GCG**ATCACGCCAATCACCACGAATGG
28[4]	F95W_fw	CGTGGTGATTGGCGTGATT**GG**CTGCTGCTGGCAAGCCG
29[4]	F95W_rv	GACGGCTTGCCAGCAGCAG**CC**AATCACGCCAATCACCACGAATGG
30[4]	L114R_fw	CCCTGTTTTTTCGTCGTCGTC**GC**GTTATTGAAGGTGATACCGAAC
31[4]	L114R_rv	GTTCGGTATCACCTTCAATAAC**GC**GACGACGACGAAAAAACAGGG
32[4]	L114W_fw	CCCTGTTTTTTCGTCGTCGT**TG**GGTTATTGAAGGTGATACCGAAC
33[4]	L114W_rv	GTTCGGTATCACCTTCAATAACC**CA**ACGACGACGAAAAAACAGGG
34	pPA3911_fw *Xba*I	CACTCTAGAGTATTCCTGGGGCATGCGCCGCTGGATTC
35	PA3911_nativ rev compl. *Bam*HI	ATACGGATCCTCAGTCGACCTTTTCGAACTGCGGGTGGCTCCAGAGCTCGCCGCCCCGCGCGCCCTGGACCGGC
36	P1 fw 3911 *Kpn*I	CGTCAAGGTACCTCTCCGGCAAGCTGC
37	P2 rv 3911 *Bam*HI	GCATTCGGATCCAGCCCTGCCTCCTC
38	P3 fw 3911 *Bam*HI	CGTCAAGGATCCGGTCGGTGGAAAGGG
39	P4 rv 3911 *Hin*dIII	GCATATAAGCTTGGCGCACTGCGCAGG
40[5]	PAO1 PA3911 fw	GCTTCAGGGAATACACCCAA
41[5]	PAO1 PA3911 rv	CCAGCAGTATCCCGAAGGTA
42[5]	Hah-138	CGGGTGCAGTAATATCGCCCT

Oligodeoxynucleotides used for sequencing are listed in table 6.

Table 6: Oligodeoxynucleotides applied for sequencing reactions
If not stated otherwise, standard oligodeoxynucleotides from GATC Biotech (Konstanz, Germany) were used for sequencing. Oligodeoxynucleotides highlighted superscript were taken from: [1](142). No., number.

No.	name	sequence (5' – 3')
A	pET-RP	CTAGTTATTGCTCAGCGG
B[1]	pFU84 *phoA* fw	CAGTTGGTGAGCGATGCTGC
C	pBR1	CGAAAAGTGCCACCTGAC
D	pTI2-1-1	GGCAAATATTCTGAAATGAGC
E	pTI2-1-2	GCGTTTCACTTCTGAGTTCG
F	pTrcHis-RP	CTGATTTAATCTGTATCAGG
G	T7	TAATACGACTCACTATAGGG
H	pGEX3-RP	TCAAGAATTATACACTCCG
I	pET30er-FP	TCATCATTCTTCTGGTCTG
J	PAO1 PA3911 rv	CCAGCAGTATCCCGAAGGTA

2.2.4 Synthetic genes

Synthetic genes used in this study were purchased as GeneArt® Strings™ DNA fragments from Life Technologies GmbH (Carlsbad, CA, USA) and are listed in table 7.

Table 7: Synthetic gene sequences

Restriction sites are underlined and leader sequences are highlighted in bold font. Specifically labeled sequences derived from: [1](142), [2]S. Hebecker, unpublished.

name	codon usage	sequence (5' – 3')
AcvB_leader_*phoA*[1]	native	AGGAAACAGACC**ATGGTGAAACGCAATCTGATAGGGGCATTCATTG** **CCGCTTCGACGCTACTCTCCTCGTCTGTCGCCTTTTCC**GCTCAGGGC GATATTACTGCACCCGGCGGTGCTCGCCGTTTAACGGGTGATCAGAC TGCCGCTCTGCGTGATTCTCTTAGCGATAAACCTGCAAAAAATATTAT TTTGCTGATTGGCGATGGGATGGGGGACTCGGAAATTACTGCCGCAC GTAATTATGCCGAAGGTGCGGGCGGCTTTTTTAAAGGTATAGATGCC TTACCGCTTACCGGGCAATACACTCACTATGCGCTGAATAAAAAAACC GGCAAACCGGACTACGTCACCGACTCGGCTGCATCAGCAACCGCCT GGTCAACCGGTGTCAAAACCTATAACGGCGCGCTGGGCGTCGATATT CACGAAAAAGATCACCCAACGATTCTGGAAATGGCAAAAGCCGCAGG TCTGGCGACCGGTAACGTTTCTACCGCAGAGTTGCAGGATGCCACGC CCGCTGCGCTGGTGGCACATGTGACCTCGCGCAAATGCTACGGTCC GAGCGCGACCAGTGAAAAATGTCCGGGTAACGCTCTGGAAAAAGGC GGAAAAGGATCGATTACCGAACAGCTGCTTAACGCTCGTGCCGACGT TACGCTTGGCGGCGGCGCAAAAACCTTTGCTGAAACGGCAACCGCT GGTGAATGGCAGGGAAAAACGCTGCGTGAACAGGCACAGGCGCGTG GTTATCAGTTGGTGAGCGATGCTGCCTCACTGAATTCGGTGACGGAA GCGAATCAGCAAAAACCCCTGCTTGGCCTGTTTGCTGACGGCAATAT GCCAGTGCGCTGGCTAGGACCGAAAGCAACGTACCACGGCAATATC GATAAGCCCGCAGTCACCTGTACGCCAAATCCGCAACGTAATGACAG TGTACCAACCCTGGCGCAGATGACCGACAAAGCCATTGAATTGTTGA GTAAAAATGAGAAAGGCTTTTTCCTGCAAGTTGAAGGTGCGTCAATCG ATAAACAGGATCATGCTGCGAATCCTTGTGGGCAAATTGGCGAGACG GTCGATCTCGATGAAGCCGTACAACGGGCGCTGGAATTCGCTAAAAA GGAGGGTAACACGCTGGTCATAGTCACCGCTGATCACGCCCACGCC AGCCAGATTGTTGCGCCGGATACCAAAGCTCCGGGCCTCACCCAGG CGCTAAATACCAAAGATGGCGCAGTGATGGTGATGAGTTACGGGAAC TCCGAAGAGGATTCACAAGAACATACCGGCAGTCAGTTGCGTATTGC GGCGTATGGCCCGCATGCCGCCAATGTTGTTGGACTGACCGACCAG ACCGATCTCTTCTACACCATGAAAGCCGCTCTGGGGCTGAAATAAAA GCTTGGCTGTTTTG
PA3911_full-length	*E. coli*	GAATTCATGCTGAATCGTCAGCGTCTGCTGCTGGGTGTTGCAGGTCG CCTGCTGCCGCTGGCAGCCAAAGTTCCGCGTGGTCTGCAGCATCTG GTTCTGCAGCGTGTTGCAAATCGTCTGTTTGCACAGCCGCTGGAAGA AGGTGCATTTGATCTGCTGGAAGGTCGTTGGCTGCGTCTGGAAGTTC GTGATCTGGGTGTGGGTTGGTGTGTTACCCGTGTTCCGGGTGGCCT GCGCCTGGTTGAACGTCCGCGTGCAAGCGTTACCATTCGTGGTGATT GGCGTGATTTCCTGCTGCTGGCAAGCCGTCATGAAGATCCGGATACC CTGTTTTTTCGTCGTCGTCTGGTTATTGAAGGTGATACCGAACTGGGT CTGGCAGTTAAAAACCTGCTGGATAGCCTGGACCCTGAACATCTGCC TCCGTGGCTGTGGAATGCAGTTGAACGTGCAGGTCGTGCAGTTCAAG AGGAACGTGGTGAAGCACCGCAGGGTCCGGTTCAGGGTGCACGTGG TGGTTAAGCGGCCGC
VirJ_Strep[2]	*E. coli*	AGGAAACAGACC**ATGGCCATTAAACTGGTTCTGATCCTGGTTTTTAC** **CCTGTTTCTGGCAGCAGATGCAGCCTAT**GCAAATGATCGTGCAAATG GTGTTATGTGGTCAAATGGTGGTGAAGCCGGTGTTCGTCTGCCGCTG CGTGTTTTTAATGCAAAACCGGCAAAAAATACCGTGGCCATTATCTAT AGCGGTGATGCAGGTTGGCAGAATATTGATGAAGTTATTGGCACCTA TCTGCAGACCGAAGGTATTCCGGTTATTGGTGTTAGCAGCCTGCGTT ATTTTTGGAGCGAACGTAGCCCGAGCGAAACCGCAAAAGATCTGGGT CATATTATTGACGTGTACACCAAACATTTTGGCGTTCAGAATGTTCTG CTGATCGGTTATAGCTTTGGTGCAGATGTTATGCCTGCCAGCTTTAAT CGTCTGACCCTGGAACAGAAAAATCGCGTTAAACAAATTAGCCTGCT GGCACTGAGCCATCAGGTTGATTATGTTGTTAGCTTTCGTGGTTGGCT GCAGCTGGAAACCGAAGGCAAAGGTGGTAATCCGCTGGATGATCTG CGTTTTATTGATCCGGCAATTGTTCAGTGTATGTATGGTCGTGAAGAT CGTAATAATGCATGTCCGAGCCTGCGTCAGACCGGTGCAGAAGTGAT TGGTTTTAGCGGTGGTCATCATTTTGGCAACGATTTCAAAAAACTGAG CACCCGTGTTGTGAGCGGTCTGGTTGCACGTCTGAGTCATCAGTATA GCAGCGGTCCGGCTCCGCTGAAGCTTCTCAGCGCTTGGAGCCACCC GCAGTTCGAAAAATAACCCGGGGATCCTCTAG

name	codon usage	sequence (5' – 3')
VirJ_leader_*phoA*[1]	native	AGGAAACAGACC**ATGG**CGATAAAATTGGTATTGATACTCGTATTTAC **ACTGTTTCTCGCGGCAGACGCTGCCTATGCG**GCTCAGGGCGATATTA CTGCACCCGGCGGTGCTCGCCGTTTAACGGGTGATCAGACTGCCGC TCTGCGTGATTCTCTTAGCGATAAACCTGCAAAAAATATTATTTTGCTG ATTGGCGATGGGATGGGGGACTCGGAAATTACTGCCGCACGTAATTA TGCCGAAGGTGCGGGCGGCTTTTTTAAAGGTATAGATGCCTTACCGC TTACCGGGCAATACACTCACTATGCGCTGAATAAAAAAACCGGCAAAC CGGACTACGTCACCGACTCGGCTGCATCAGCAACCGCCTGGTCAAC CGGTGTCAAAACCTATAACGGCGCGCTGGGCGTCGATATTCACGAAA AAGATCACCCAACGATTCTGGAAATGGCAAAAGCCGCAGGTCTGGCG ACCGGTAACGTTTCTACCGCAGAGTTGCAGGATGCCACGCCCGCTGC GCTGGTGGCACATGTGACCTCGCGCAAATGCTACGGTCCGAGCGCG ACCAGTGAAAAATGTCCGGGTAACGCTCTGGAAAAAGGCGGAAAAGG ATCGATTACCGAACAGCTGCTTAACGCTCGTGCCGACGTTACGCTTG GCGGCGGCGCAAAAACCTTTGCTGAAACGGCAACCGCTGGTGAATG GCAGGGAAAAACGCTGCGTGAACAGGCACAGGCGCGTGGTTATCAG TTGGTGAGCGATGCTGCCTCACTGAATTCGGTGACGGAAGCGAATCA GCAAAAACCCCTGCTTGGCCTGTTTGCTGACGGCAATATGCCAGTGC GCTGGCTAGGACCGAAAGCAACGTACCACGGCAATATCGATAAGCCC GCAGTCACCTGTACGCCAAATCCGCAACGTAATGACAGTGTACCAAC CCTGGCGCAGATGACCGACAAAGCCATTGAATTGTTGAGTAAAAATG AGAAAGGCTTTTTCCTGCAAGTTGAAGGTGCGTCAATCGATAAACAG GATCATGCTGCGAATCCTTGTGGGCAAATTGGCGAGACGGTCGATCT CGATGAAGCCGTACAACGGGCGCTGGAATTCGCTAAAAAGGAGGGT AACACGCTGGTCATAGTCACCGCTGATCACGCCCACGCCAGCCAGAT TGTTGCGCCGGATACCAAAGCTCCGGGCCTCACCCAGGCGCTAAATA CCAAAGATGGCGCAGTGATGGTGATGAGTTACGGGAACTCCGAAGA GGATTCACAAGAACATACCGGCAGTCAGTTGCGTATTGCGGCGTATG GCCCGCATGCCGCCAATGTTGTTGGACTGACCGACCAGACCGATCTC TTCTACACCATGAAAGCCGCTCTGGGGCTGAAATAA**AAGCTT**GGCTG TTTTG

2.3 Sterilization, growth media and media additives

2.3.1 Sterilization

Heat-resistant media and items were steam pressure sterilized at 121 °C and 1 bar excess pressure for 20 min. Sterilization of temperature sensitive solutions was performed by filtration (pore size 0.2 µm).

2.3.2 Media

2.3.2.1 Luria Bertani medium

Luria Bertani (LB) medium (146) was used as a standard medium to cultivate the bacterial strains unless indicated otherwise. To obtain solid medium 1.5% (w/v) agar-agar was added before sterilization.

LB medium	tryptone	10 g/l
	yeast extract	5 g/l
	NaCl	5 g/l

2.3.2.2 AB medium

Modified AB medium was used as a minimal medium for the cultivation of *P. aeruginosa* PAO1 strains. Therefore, AB medium (147) was prepared without sodium citrate and supplemented with glucose and $FeSO_4$. The pH of the modified AB medium was adjusted by varying the ratio of phosphate buffer components. Depending on the utilized A10 solution (e.g. pH 5.0 or 7.0) the pH

value of the resulting AB medium is increased by 0.3 units (e.g. pH 5.3 or 7.3) (43).
All media components were prepared as stock solutions. Sterilization of A10, $MgCl_2$ and $CaCl_2$ solution was performed by autoclaving and glucose, $FeSO_4$ and trace element solution by filtration (pore size 0.2 µm).

AB medium	A10 solution	100 ml/l
	1 M D(+)-glucose	20 ml/l
	trace elements	1 ml/l
	1 M $MgCl_2$	1 ml/l
	$FeSO_4 \cdot 7\ H_2O$ (14 mg/ml)	0.5 ml/l
	1 M $CaCl_2$	0.1 ml/l
trace elements	$CaSO_4 \cdot 2\ H_2O$	200 mg/l
	$FeSO_4 \cdot 7\ H_2O$	200 mg/l
	$MnSO_4 \cdot H_2O$	20 mg/l
	$CuSO_4 \cdot 5\ H_2O$	20 mg/l
	$ZnSO_4 \cdot 7\ H_2O$	20 mg/l
	$NaMoO_4 \cdot H_2O$	10 mg/l
	H_3BO_3	5 mg/l
A10 solution pH 5.0	$(NH_4)_2SO_4$	20 g/l
	Na_2HPO_4	20 mM
	KH_2PO_4	430 mM
A10 solution pH 7.0	$(NH_4)_2SO_4$	20 g/l
	Na_2HPO_4	300 mM
	KH_2PO_4	150 mM

2.3.2.3 Yeast Extract Broth

A. tumefaciens was cultivated in Yeast Extract Broth (YEB) (148). Solid medium was obtained by the addition of 2% (w/v) agar-agar previous to sterilization.

YEB medium	beef extract	5 g/l
	yeast extract	1 g/l
	peptone	5 g/l
	D(+)-sucrose	5 g/l
	$MgSO_4$	2 mM

2.3.2.4 Media for *Arabidopsis* seedling infection

Arabidopsis thaliana seedlings were infected with different *A. tumefaciens* strains according to the AGROBEST method (149).

MS medium	Murashige & Skoog salt	2.17 g/l
	D(+)-sucrose	5 g/l

adjusted to pH 5.7 with potassium hydroxide, but pH 5.5 after autoclaving

For AB-MES pH 5.5 medium all media components were prepared as stock solutions. Sterilization was performed by autoclaving, except for glucose and

$FeSO_4$ solution which were sterilized by filtration (pore size 0.2 µm).

AB-MES pH 5.5 medium	K_2HPO_4	17.2 mM
	NaH_2PO_4	8.3 mM
	NH_4Cl	18.7 mM
	KCl	2 mM
	$MgSO_4$	1.25 mM
	$CaCl_2$	100 µM
	$FeSO_4$	10 µM
	MES	50 mM
	D(+)-glucose	2% (w/v)
	adjusted to pH 5.5 with HCl	
Infection medium	MS medium	500 ml/l
	AB-MES pH 5.5 medium	500 ml/l
	acetosyringone (AS)	200 µM

2.3.2.5 Medium for protein labeling with L(+)-selenomethionine

For incorporation of L(+)-selenomethionine (SeMet; ACROS Organics™, Geel, Belgium) into proteins during heterologous production in *E. coli* cells a minimal medium supplemented with SeMet and the respective antibiotic(s) was used for the cultivation (150).

SeMet minimal medium	NH_4Cl	20.8 mM
	KH_2PO_4 pH 7.0	24.5 mM
	Na_2HPO_4 pH 7.0	24.9 mM
SeMet nutrients	D(+)-glucose	1.11 M
	$MgSO_4$	24.7 mM
	thiamine HCl	332 µM
	$Fe_2(SO_4)_3$	260 µM
amino acids with SeMet	L-lysine	100 mg/l
	L-phenylalanine	100 mg/l
	L-threonine	100 mg/l
	L-isoleucine	50 mg/l
	L-leucine	50 mg/l
	L-valine	50 mg/l
	SeMet	60 mg/l

The components for the minimal medium and the nutrients were prepared as stock solutions whereof all solutions were autoclaved except from D(+)-glucose, thiamine HCl and $Fe_2(SO_4)_3$ which were sterilized by filtration (pore size 0.2 µm). The amino acid mixture containing SeMet was dissolved in 14 ml sterile dH_2O before use.

2.3.3 Additives

Concentrated stock solutions of antibiotics and media additives dissolved in water, unless indicated otherwise, were sterilized by filtration (pore size 0.2 µm).

Table 8 shows an overview of the utilized additives with the corresponding concentrations for usage.

Table 8: Antibiotics and media additives

Additive	Stock solution (solvent)	Final concentration		
		E. coli	***A. tumefaciens***	***P. aeruginosa***
5-aminolevulinic acid (ALA)	50 mg/ml	50 µg/ml	-	-
acetosyringone (AS)	39.24 mg/ml (DMSO)	-	200 µM	-
ampicillin (Ap)	100 mg/ml	100 µg/ml	-	-
carbenicillin (Cb)	50 mg/ml	-	-	250 µg/ml
chloramphenicol (Cm)	34 mg/ml (100% EtOH)	34 µg/ml	-	-
gentamicin (Gm)	10 mg/ml	10 µg/ml	-	50 µg/ml
isopropyl-β-D-galacto-pyranoside (IPTG)	1 M	25-300 µM	15 µM	-
kanamycin (Kan)	100 mg/ml	100 µg/ml	-	-
potassium nitrate	2 M	-	-	50 mM
spectinomycin (Spc)	50 mg/ml	50 µg/ml	300 µg/ml	-
streptomycin (Str)	75 mg/ml	-	100 µg/ml	-
tetracycline (Tet)	10 mg/ml (70% EtOH)	-	-	60 µg/ml
ticarcillin (Tic)	100 mg/ml	-	100 µg/ml	-
D(+)-sucrose	50% (w/v)	-	-	5% (w/v)

2.4 Microbiological techniques

2.4.1 Cultivation of bacterial cells

Bacterial cells were cultivated at 37 °C (*E. coli* and *P. aeruginosa*) or 30 °C (*A. tumefaciens*) under vigorous shaking (200 rpm).
To generate pre-cultures, 5-50 ml of the desired medium containing the respective antibiotic(s) in test tubes or baffled flasks was inoculated with a single colony from a plate culture or with cell material from a glycerol stock and was cultivated overnight.
For plate cultures a bacterial cell suspension (5-250 µl) was plated with a Drigalski spatula or cell material was streaked with an inoculating loop on sterile agar plates and incubated at the respective temperature overnight.

2.4.2 Determination of cell density

To determine cell densities of liquid bacterial cultures the optical density (OD) at a wavelength of 578 nm was measured photometrically. An OD_{578} of 1 corresponds to a cell density of ~$1 \cdot 10^9$ cells/ml (146).

2.4.3 Storage of bacteria

Glycerol stocks were prepared for long-term storage of bacteria. Bacterial overnight cultures were, therefore, mixed with sterile glycerol to result in a final concentration of 20% (w/v) and stored at -80 °C (146).

2.4.4 Cultivation of *E. coli* for recombinant protein production

For the heterologous production of recombinant proteins in *E. coli* 500 ml LB medium supplemented with the respective antibiotic in baffled flasks was inoculated in a ratio of 1:100 (v/v) with an overnight pre-culture. Cultivation was performed at 37 °C and 200 rpm until an OD_{578} of 0.5-0.6 was reached. After the induction of protein production by IPTG addition the cultivation was preceded at 17 °C overnight.

2.4.5 Monitoring of *P. aeruginosa* growth behavior

To determine the growth behavior of *P. aeruginosa* strains, pre-cultures in LB medium were inoculated with a single colony from a plate culture (2.4.1) and were incubated at 37 °C and 200 rpm overnight.
For aerobic main cultures LB medium (2.3.2.1) or AB medium pH 5.3 or 7.3 (2.3.2.2) in baffled flasks was inoculated with the respective pre-culture to an OD_{578} of 0.05. Cultivation was performed at 37 °C and 200 rpm for 24 h, meanwhile measuring the OD_{578} at certain time points.
For anaerobic main cultures LB medium or AB medium pH 7.3 supplemented with 50 mM potassium nitrate in anaerobic culture flasks was inoculated to an OD_{578} of 0.3 using a pre-culture of the respective *P. aeruginosa* strain. During cultivation at 37 °C and 100 rpm for 24 h the optical densities were monitored on a regular basis.

2.5 Molecular biological techniques

2.5.1 Preparation of competent cells

2.5.1.1 $CaCl_2$ method for competent *E. coli* cells

100 ml LB medium in a 500 ml baffled flask was inoculated 1:100 (v/v) with an overnight pre-culture of the desired *E. coli* strain and incubated at 37 °C and 200 rpm until an OD_{578} of 0.6-0.8 was reached. Cells were sedimented by centrifugation (3'000 x g, 4 °C, 10 min), washed with 10 ml ice-cold $CaCl_2$ solution, gently resuspended in 1 ml ice-cold $CaCl_2$ solution and stored in aliquots at -80 °C (146).

$CaCl_2$ solution	$CaCl_2$	100 mM
	Glycerol	10% (w/v)

2.5.1.2 RbCl method for competent *E. coli* cells

Overnight pre-cultures of the desired *E. coli* strain were used to inoculate 500 ml LB medium in a 1 l baffled flask in a ratio of 1:100 (v/v). After cultivation at 37 °C and 200 rpm to an OD_{578} of 0.5-0.6 the cells were harvested by centrifugation (3'000 x g, 4 °C, 10 min). The received cell sediment was suspended in 100 ml of ice-cold TFB-I buffer and incubated on ice for 5 min. Cells were centrifuged (4'500 x g, 4 °C, 10 min) and subsequently resuspended in twice as much ice-cold TFB-II buffer referring to the cell sediment volume (~2-3 ml). After incubation on ice for 1 h cells were divided into aliquots and stored at -80 °C (151).

TFB-I	$CaCl_2$	10 mM
	potassium acetate	30 mM
	$MnCl_2$	50 mM
	RbCl	100 mM
	glycerol	15% (w/v)
	adjusted to pH 5.8 with acetic acid, sterilized by filtration	
TFB-II	piperazine-N,N'-bis(2-ethanesulfonic acid)-HCl pH 6.5	10 mM
	RbCl	10 mM
	$CaCl_2$	75 mM
	glycerol	15% (w/v)
	adjusted to pH 6.5 with KOH, sterilized by filtration	

2.5.1.3 $CaCl_2$ method for competent *A. tumefaciens* cells

50 ml YEB medium in a baffled flask was inoculated 1:25 (v/v) with an overnight pre-culture of the desired *A. tumefaciens* strain and incubated at 30 °C and 250 rpm until an OD_{578} of 0.5-1.0 was reached. The cell suspension was chilled on ice for 5 min. The cells were sedimented by centrifugation (3'000 x g, 4 °C, 5 min), washed with 10 ml of an ice-cold 20 mM $CaCl_2$ solution, gently resuspended on ice in 1 ml of 20 mM ice-cold $CaCl_2$ solution and stored in aliquots at -80 °C (152).

2.5.2 Transformation of competent cells

2.5.2.1 *E. coli* cells

For transformation purposes 25-100 µl of $CaCl_2$ or RbCl competent *E. coli* cells (2.5.1.1 and 2.5.1.2) were mixed with 1-10 µl plasmid DNA solution (50 µg/ml). The mixture was incubated on ice for 20 min and afterwards a heat shock of the cells at 42 °C for 45 sec was performed. Following another incubation step on ice for 2 min, the cells were gently resuspended in 500 µl LB medium and incubated for 1 h at 37 °C and 300 rpm in a thermomixer. To select transformed clones 10-250 µl of the cell suspension was plated on LB agar plates supplemented with the respective antibiotic(s) and incubated overnight at 37 °C (146).

2.5.2.2 *A. tumefaciens* cells

To transform *A. tumefaciens* cells 1-1.5 µg of plasmid DNA was mixed with 100 µl $CaCl_2$ competent *A. tumefaciens* cells (2.5.1.3). The reaction tube containing the cell suspension was incubated for 5 min in warm water (37 °C) and subsequently 150 µl of YEB medium were added. The mixture was incubated for 3 h at 28 °C and 300 rpm in a thermomixer. Afterwards transformed clones were selected by plating 250 µl of the cell suspension on YEB agar plates containing the appropriate antibiotic(s) and incubated for 1-3 days at 30 °C (152).

2.5.3 Preparation of plasmid DNA

To isolate high amounts of plasmid DNA from *E. coli* cells (e.g. for cloning

purposes) 4 ml of an overnight culture were sedimented (12'100 x g, room temperature (RT), 2 min) in a reaction tube. The cell pellet was resuspended in 300 µl buffer P1 (ribonuclease A (RNase A) was added shortly before use). 300 µl buffer P2 were added, the reaction tube was inverted several times and the suspension was incubated (RT, 2 min). After the addition of 300 µl buffer P3 cell debris and denatured proteins were separated by centrifugation (12'100 x g, RT, 20 min). The resulting supernatant was mixed with 600 µl isopropanol to precipitate the plasmid DNA. The plasmid DNA was sedimented by centrifugation (12'100 x g, RT, 20 min) and washed with 400 µl 70% (v/v) ethanol. Following a final centrifugation step (12'100 x g, RT, 5 min) the sedimented plasmid DNA was dried at 37 °C in a thermomixer, dissolved in 35 µl dH_2O and subsequently stored at -20 °C (146).
Plasmid DNA that was intended for subsequent sequencing was isolated from *E. coli* cells using the QIAprep Spin Miniprep Kit according to the manufacturer's instructions (QIAGEN, Hilden, Germany).

buffer P1	ethylenediaminetetraacetic acid (EDTA)	10 mM
	Tris-HCl pH 8.0	50 mM
	RNase A	100 µg/ml
RNase A solution	RNase A dissolved in 50% (w/v) glycerol	10 mg/ml
buffer P2	sodium hydroxide (NaOH)	200 mM
	SDS	1% (w/v)
buffer P3	potassium acetate pH 5.5	3 M

2.5.4 Determination of DNA concentration

To determine the concentration and purity of a DNA solution the absorbance at 260 nm and 280 nm was measured with a spectrophotometer (NanoDrop™ ND-1000, PEQLAB Biotechnologie GmbH, Erlangen, Germany). An absorbance value of 1 measured at 260 nm represents a concentration of 50 ng/µl of double-stranded DNA. Protein impurities in the sample result in high absorbance values at 280 nm. That is why the quotient A_{260}/A_{280} provides information about the DNA purity. A DNA sample with a value of A_{260}/A_{280} = 1.8-2.0 is considered to be pure (146).

2.5.5 Amplification of DNA by polymerase chain reaction

To amplify DNA fragments the method polymerase chain reaction (PCR) (153) was applied. Therefore, specific oligodeoxynucleotides (2.2.3) were designed that bind to a specific region of the template DNA and depending on purpose provide recognition sites for endonucleases or homologous regions necessary for the In-Fusion® HD cloning method.
The reaction mixtures contain the template DNA, the respective primers, a deoxynucleotide triphosphate (dNTP) mixture, the Phusion® High-Fidelity DNA Polymerase and its corresponding GC buffer. Polymerase, buffer and dNTP mixture were purchased from New England BioLabs® (Ipswich, MA, USA).

Plasmid DNA or a bacterial colony served as a template for the PCR reaction. For colony PCR the respective *P. aeruginosa* colony was suspended in 50 µl dH_2O and incubated at 95 °C for 10 min. 1 µl of this mixture was used as a template for PCR.

compound	**amount**
template DNA	1 µl colony suspension or 1-10 ng plasmid DNA
5x GC buffer	4 µl
10 mM dNTPs	0.4 µl
10 µM forward primer	1 µl
10 µM reverse primer	1 µl
Phusion® polymerase	0.2 µl
dH_2O	filled up to 20 µl

The PCR reaction is subdivided into several steps. At first single-stranded DNA was created by denaturation (98 °C, 30-60 sec). Afterwards 30 cycles consisting of denaturation (98 °C, 10 sec), primer annealing (55-75 °C, 15-30 sec) and elongation (72 °C, 15-30 sec per kilobase of target DNA fragment for Phusion® High-Fidelity DNA Polymerase) were performed. The PCR reaction was finished by a final elongation step (72 °C, 10 min). PCR samples were stored at 4 °C or -20 °C (146).

2.5.6 Agarose gel electrophoresis

Agarose gel electrophoresis was used to separate DNA fragments in terms of their size. Therefore, DNA samples were mixed with the appropriate amount of loading dye and filled into the slots of an agarose gel (1% (w/v) in 1x Tris-acetate-EDTA (TAE) buffer). Additionally the size marker GeneRuler™ DNA Ladder Mix (Thermo Fisher Scientific, Waltham, MA, USA) containing defined DNA fragments was applied to allow for DNA fragment size determination in the sample. For electrophoresis a voltage of 90-110 V was applied. Afterwards the agarose gels were incubated in 0.1% (w/v) ethidium bromide solution for 15 min or in GelStar® Nucleic Acid Gel Stain (Lonza, Basel, Switzerland) for 30 min. DNA visualization was performed using UV or blue light sources, respectively (146).

6x loading dye	bromophenol blue	350 µM
	xylene cyanol FF	450 µM
	glycerol	50% (w/v)
1x TAE buffer	Tris-acetate pH 8.0	40 mM
	EDTA	1 mM

2.5.7 Restriction of DNA

Plasmid DNA (vectors) or PCR amplified DNA fragments (inserts) were digested by restriction endonucleases according to the manufacturer's instructions (New England BioLabs®, Ipswich, MA, USA). Following restriction digest of vector DNA the sample was subjected to agarose gel electrophoresis to separate residual restriction enzymes. The agarose gel was stained with GelStar® Nucleic Acid Gel Stain (2.5.6) and target DNA was visualized on a

blue light detector (Biozym Scientific GmbH, Hessisch Oldendorf, Germany). After the excision with a scalpel the target DNA was purified by the QIAquick Gel Extraction Kit according to the manufacturer's instructions (QIAGEN, Hilden, Germany).

2.5.8 Dephosphorylation of vector DNA

The 5' ends of linearized vector DNA were dephosphorylated to prohibit self-ligation using Antarctic Phosphatase according to the manufacturer's instructions (New England BioLabs®, Ipswich, MA, USA).

2.5.9 Purification of PCR products

DNA fragments obtained by PCR were purified by the QIAquick PCR Purification Kit according to the manufacturer's instructions (QIAGEN, Hilden, Germany).

2.5.10 Ligation of DNA

DNA fragments were ligated using the T4 DNA ligase according to the manufacturer's instructions (New England BioLabs®, Ipswich, MA, USA). In general, a molar ratio of 1:4 for vector to insert DNA was used. Reaction mixtures were incubated at 17 °C overnight and transformed into competent *E. coli* cells (2.5.2.1).

2.5.11 In-Fusion® HD cloning

In addition to traditional cloning procedures in which insert and vector DNA are digested by restriction endonucleases and subsequently ligated to yield the desired vector construct the 'almost' restriction-free In-Fusion® HD cloning method (154) was used in this study.
Therefore, the vector DNA was linearized by a restriction endonuclease. Specific oligodeoxynucleotides (2.2.3) were designed which contain a 15 bp homologous overlap to the vector DNA on both sites of the insert. After amplification of the desired insert DNA fragment with respective oligodeoxynucleotides by PCR (2.5.5) the In-Fusion® HD cloning reaction was set up according to the manufacturer's instructions (Clontech® Laboratories, Mountain View, CA, USA). The resulting reaction mixtures were transformed into competent *E. coli* Stellar™ cells according to the manufacturer's instructions (Clontech® Laboratories, Mountain View, CA, USA).

2.5.12 Site-directed mutagenesis

Plasmid DNA vectors can be modified by a method called site-directed mutagenesis. Thereby specific primers are designed that allow for the mutation of one or several bp at the desired position of the nucleotide sequence. In a PCR reaction the specific primers anneal to the target DNA and synthesis of a mutated plasmid takes place. In this work the QuikChange Site-Directed Mutagenesis Kit (Agilent Technologies, Santa Clara, CA, USA) was used according to the manufacturer's instructions. Plasmid DNA which wasn't modified during PCR was eliminated by restriction digest with *Dpn*I.

The mutated plasmid DNA was transformed into competent *E. coli* cells (2.5.1.2). If no transformed colonies were obtained, the protocol was modified in the following way: increase of the primer concentration by 20%, duplication of the DNA template amount and addition of 4% (v/v) DMSO to the reaction mixture as well as an increase of the annealing temperature to 68 °C.

2.5.13 Construction of vectors

Several vectors were generated in this study by the insertion of DNA fragments into existing vector backbones or by modification of present vector constructs. The used oligodeoxynucleotides are listed in table 5. Methods for vector construction are presented in the sections 2.5.1 to 2.5.12 and resulting plasmids are summarized in table 4.

Plasmid for the recombinant production of A-PGH$_{trunc}$ in *E. coli*

To recombinantly produce A-PGH$_{trunc}$ in *E. coli* BL21(λDE3) cells the gene sequence encoding for the amino acids 203-427 of orf PA0919 was amplified by PCR from pET22b(+)PA0919-Strep using primers 1 and 2. The PCR fragment was inserted into the vector pET22b(+)Strep (2.2.2) by the In-Fusion® HD cloning method (2.5.11) resulting in vector pET22b(+)PA0919$_{trunc}$-Strep (135). The correct integration of the DNA fragment into the vector was verified by sequencing with primer A. The resulting construct allows for the recombinant production of protein A-PGH$_{trunc}$ fused to an N-terminal *E. coli pelB* signal sequence for periplasmic export and a C-terminal *Strep*-tag® II (155). Protein production in *E. coli* BL21(λDE3) cells was induced with IPTG *via* the provided T7 promoter (131).

Plasmids for the recombinant production of A-PGH$_{trunc}$ mutant proteins

For crystallization attempts protein variants of A-PGH$_{trunc}$ were generated based on the Surface Entropy Reduction (SER) approach (156).
Therefore, the vector pET22b(+)PA0919$_{trunc}$-Strep (135) was modified by site-directed mutagenesis (2.5.12) with primers 3 and 4 resulting in plasmid pET22b(+)PA0919$_{trunc}$-Strep/AAK. The obtained vector was further modified in a second mutagenesis reaction with primers 5 and 6 resulting in plasmid pET22b(+)PA0919$_{trunc}$-Strep/AAA. The successful mutagenesis was verified by sequencing with primer A.

Plasmids for AcvB and VirJ localization in *A. tumefaciens*

To analyze the putative export of the proteins AcvB and VirJ into the periplasm of *A. tumefaciens* several localization plasmids based on the IPTG inducible pTrc200 vector backbone were constructed. To monitor the export the reporter gene alkaline phosphatase (*phoA*) was used (157).
For cloning of the insert fragments into the pTrc200 vector the restriction sites *Nco*I and *Hin*dIII were chosen. Therefore, the *Nco*I restriction site within the *phoA* gene on plasmid pFU84 had to be eliminated by QuikChange Site-Directed Mutagenesis (2.5.12) using primers 7 and 8. Successful mutagenesis was verified by sequencing with primers B and C. The resulting plasmid pFU84_QC was used as a template to amplify the *phoA* gene

sequence with or without its own signal sequence by PCR (2.5.5) with the primers 9 and 11 or 10 and 11. The DNA fragments were ligated into the *Nco*I/*Hin*dIII sites of vector pTrc200 resulting in the plasmids pTrc200 *phoA* (positive control) and pTrc200 '*phoA* (negative control). For the localization vectors of AcvB and VirJ synthetic DNA insert fragments (table 7) were obtained commercially (Life Technologies GmbH, Carlsbad, CA, USA) which were customized for the In-Fusion® HD cloning method (2.5.11). These DNA fragments contained a 15 bp homologous sequence (5' and 3' end) to the pTrc200 vector and the signal sequence of the *acvB* or *virJ* gene fused to the *phoA* gene lacking its own signal sequence. The synthetic fragments were inserted into the linearized pTrc200 vector *via* In-Fusion® HD cloning (2.5.11) resulting in plasmids pTrc200 leader *acvB* '*phoA* and pTrc200 leader *virJ* '*phoA*. The four vector constructs (142) were verified by sequencing with primers D and E.

Plasmids for the recombinant production of AcvB mutant proteins

To study the function of AcvB protein in T-DNA transfer in *A. tumefaciens* point mutations of conserved amino acids of the potential active site were generated. DNA fragments containing the desired point mutation were amplified by PCR using primers 12 and 13 from plasmids pET22b(+)Strep_*pelB*_*acvB* ΔAS1-24-S269A, pET22b(+)Strep_*pelB*_*acvB* ΔAS1-24-S336A, pET22b(+)Strep_*pelB*_*acvB* ΔAS1-24-H433A and pET22b(+)Strep_*pelB*_*acvB* ΔAS1-24-H433N (137). The PCR fragments were ligated (2.5.10) into the *Nco*I/*Xma*I sites of vector pTrc200_*acvB*_Strep (S. Hebecker, unpublished) resulting in vectors pTrc200_*acvB*_Strep-S269A, pTrc200_*acvB*_Strep-S336A, pTrc200_*acvB*_Strep-H433A and pTrc200_*acvB*_Strep-H433N. Correct integration of the respective DNA fragment into the vector was verified by sequencing with primers D and F.

Plasmids for the recombinant production of PA3911 in *E. coli*

For recombinant production of the PA3911 protein in *E. coli* BL21(λDE3) cells the gene sequence was initially codon-optimized for *E. coli* and commercially obtained as a GeneArt® Strings™ DNA fragment (table 7; Life Technologies GmbH, Carlsbad, CA, USA). The DNA fragment was ligated into several vector systems to produce PA3911 fusion proteins with different tags.

original plasmid	**restriction sites**	**resulting plasmid (table 4)**
pET28b(+)	*Nco*I/*Xho*I	pET28b(+)-PA3911
pET32a(+)/PA3911$_{opt}$ ΔAS 1-19	*EcoR*I/*Not*I	pET32a(+)-PA3911
pGEX-6P-1/PA3911$_{opt}$ ΔAS 1-19	*EcoR*I/*Not*I	pGEX-6P-1-PA3911

The correct insertion of the PA3911 DNA fragment into the respective vector was checked by sequencing with primers G and A (pET28b(+)-PA3911), primer A (pET32a(+)-PA3911) or primer H (pGEX-6P-1-PA3911). Protein production was performed in *E. coli* BL21(λDE3) cells induced by IPTG addition.

Plasmids for the recombinant production of PA3911 mutant proteins

To study the influence of several amino acid residues on the lipid binding

capacity of protein PA3911 a total of ten plasmid variants was generated by site-directed mutagenesis (2.5.12) on the basis of plasmid pET32a(+)-PA3911. The success of mutagenesis was analyzed by sequencing with primer I (139).

mutation	primer (table 5)	resulting plasmid (table 4)
L56R	14, 15	pET32a(+)-PA3911-L56R
L56W	16, 17	pET32a(+)-PA3911-L56W
L58R	18, 19	pET32a(+)-PA3911-L58R
L58W	20, 21	pET32a(+)-PA3911-L58W
V69R	22, 23	pET32a(+)-PA3911-V69R
V69W	24, 25	pET32a(+)-PA3911-V69W
F95R	26, 27	pET32a(+)-PA3911-F95R
F95W	28, 29	pET32a(+)-PA3911-F95W
L114R	30, 31	pET32a(+)-PA3911-L114R
L114W	32, 33	pET32a(+)-PA3911-L114W

Plasmid for PA3911 localization in *P. aeruginosa*

For localization of PA3911 in *P. aeruginosa* a vector construct consisting of the putative promoter sequence (500 bp upstream of PA3911 gene), orf PA3911 and a C-terminal *Strep*-tag® II sequence was cloned. PA3911 gene sequence and the putative promoter region were amplified by colony PCR (2.5.5) of *P. aeruginosa* PAO1 (primers 34 and 35). During PCR primer 35 coded for the *Strep*-tag® II sequence at the 3' end of the fragment. The resulting fragment was cloned into the *Xba*I/*Bam*HI sites of vector pUCP20T resulting in plasmid pUCP20T-P_{PA3911}-PA3911. Plasmid transfer into *P. aeruginosa* PAO1 was performed *via* diparental mating with *E. coli* ST18 cells.

Plasmid for gene replacement in *P. aeruginosa*

To delete the complete orf PA3911 from the PAO1 chromosome the gene replacement vector pEX18Ap-ΔPA3911 was constructed. This vector contains the Gm resistance cassette from vector pPS858 flanked by two genomic sequences homologous to the upstream and downstream region of the target gene PA3911. Genomic sequences allow for the homologous recombination and subsequently the replacement of orf PA3911 by the Gm resistance cassette (140).

PCR (2.5.5) was employed to amplify the genomic sequences upstream (460 bp) and downstream (649 bp) of orf PA3911 with primers 36 and 37 or 38 and 39. Vector pPS858 was digested (2.5.7) with *Bam*HI to isolate the Gm resistance cassette. The two resulting PCR fragments and the Gm resistance cassette fragment were ligated into the *Kpn*I/*Hin*dIII sites of vector pEX18Ap yielding vector pEX18Ap-ΔPA3911.

2.5.14 Sequencing

Sequence determination of plasmids or PCR products was performed by the company GATC Biotech (Konstanz, Germany) based on the Sanger method (158) with oligodeoxynucleotides listed in table 6. Analyses of resulting sequence files were performed with the Lasergene® software package

(DNASTAR, Madison, WI, USA).

2.5.15 Diparental mating with *P. aeruginosa*

Shuttle vectors can be transferred from *E. coli* to *P. aeruginosa* cells by conjugation. In this study, the shuttle vector derivatives pEX18Ap-ΔPA3911 and pUCP20T-P_{PA3911}-PA3911 (2.2.2) were transferred from *E. coli* ST18 to *P. aeruginosa* PAO1 *via* diparental mating.
The respective plasmid was transformed into $CaCl_2$ competent *E. coli* ST18 cells (2.2.1). Overnight pre-cultures of the *E. coli* ST18 donor strain carrying the desired plasmid and the recipient strain *P. aeruginosa* PAO1 were prepared. 1 ml of *E. coli* ST18 pre-culture was mixed with 100 µl *P. aeruginosa* PAO1 pre-culture, sedimented (2'400 x g, RT, 2 min) and the resulting pellet was gently resuspended in 100 µl LB medium containing 50 µg ALA. The complete cell suspension was pipetted onto a LB agar plate and was dried for 30 min in a clean bench. After incubation at 37 °C for 6 h the cell material was scraped from the LB agar plate with an inoculating loop, resuspended in 1 ml LB medium and plated onto LB agar plates containing the respective antibiotic(s) and additives to select for transformants (133).

2.5.16 Construction of a markerless *P. aeruginosa* deletion mutant

For chromosomal deletion of orf PA3911 from *P. aeruginosa* PAO1 a well-established protocol (two step procedure) was used. In the first step the chromosomal orf is replaced by a Gm resistance cassette, which will be excised in the second step to generate a markerless deletion mutant (140).

The constructed gene replacement vector pEX18Ap-ΔPA3911 (2.5.13) was transferred into *P. aeruginosa* PAO1 *via* diparental mating (2.5.15). Cells were selected for integration of the Gm resistance cassette by homologous recombination (double crossover event) by resistance against Gm and their ability to grow on D(+)-sucrose. The pEX18Ap-ΔPA3911 vector encodes for the enzyme levansucrase (*sacB* gene) which converts sucrose to the toxic product levan and thereby prevents growth in the case of a single crossover event (vector still present). The chromosomal Gm resistance cassette is flanked by Flp recombinase target (FRT) sites allowing for the excision by the Flp recombinase. Therefore, the vector pFLP2 encoding for Flp recombinase has to be transferred into the generated *P. aeruginosa* strain by diparental mating resulting in a markerless deletion mutant.

2.6 Protein biochemical methods

2.6.1 Recombinant protein production

2.6.1.1 Production of A-PGH protein variants

A-PGH protein, the truncated version A-PGH_{trunc} and its mutant variants A-PGH_{trunc}/AAK and A-PGH_{trunc}/AAA were recombinantly produced in *E. coli* BL21(λDE3) cells containing the respective plasmid pET22b(+)PA0919-Strep, pET22b(+)$PA0919_{trunc}$-Strep, pET22b(+)$PA0919_{trunc}$-Strep/AAK or pET22b(+)$PA0919_{trunc}$-Strep/AAA (table 4). The resulting proteins were

secreted into the periplasm of *E. coli via* an N-terminal *pelB* signal sequence and fused to a C-terminal *Strep*-tag® II (2.5.13).

For protein production in baffled flasks 500 ml LB medium was supplemented with Ap and inoculated with the respective overnight pre-culture in a ratio of 1:100 (v/v). Cells were cultivated at 37 °C and 200 rpm to an OD_{578} of 0.5. Then protein production was induced with 25 µM IPTG and cultivation was preceded at 17 °C and 180 rpm for 24 h. Cells were sedimented by centrifugation (3'000 x g, 4 °C, 20 min) and afterwards resuspended in harvesting buffer A. The cell pellets obtained after a second centrifugation step (4'000 x g, 4 °C, 30 min) were stored at -20 °C (49).

harvesting buffer A	HEPES-NaOH pH 8.0	50 mM
	NaCl	150 mM
	D(+)-sucrose	20% (w/v)

2.6.1.2 Production of L(+)-selenomethionine labeled A-PGH protein

To determine the phase information by anomalous dispersion SeMet can be incorporated into the protein during heterologous production.
Therefore, a pre-culture was generated by inoculation of 50 ml LB-Ap-medium (in a baffled flask) with *E. coli* BL21(λDE3) cells carrying the plasmid pET22b(+)PA0919-Strep (table 4). The pre-culture was cultivated at 37 °C and 130 rpm for ~36 h. 50 ml of this pre-culture was mixed with 50 ml LB-Ap-medium and cultivated for 3 h at the same conditions. After the addition of 400 ml LB-Ap-medium to the pre-culture cultivation was preceded as previously for 2 h. Cells were harvested by centrifugation (6'000 x g, RT, 10 min), resuspended in 25 ml sterile dH_2O and sedimented again (6'000 x g, RT, 10 min). This washing step was repeated three times in total. Then cells were split up and transferred into 2x 500 ml SeMet minimal medium containing SeMet nutrients (2.3.2.5) supplemented with Ap in a 1 l baffled flask and cultivated for 30 min at 37 °C and 180 rpm. Following the addition of the amino acid mix supplemented with SeMet (2.3.2.4) to the culture cultivation was continued at 17 °C and 180 rpm for 15 min. Protein production was induced with 250 µM IPTG and the cultivation was preceded overnight (~21 h) at 17 °C and 180 rpm. Cells were harvested as described in chapter 2.6.1.1.

2.6.1.3 Production of AcvB protein and derivatives

The protein AcvB and its variants were produced in *E. coli* BL21(λDE3) cells containing the plasmid pET22b(+)Strep_*pelB_acvB* ΔAS1-24 or the respective derivatives of it (table 4). Similarly to the construct for recombinant production of protein A-PGH (2.6.1.1) these plasmids encode for the AcvB protein or mutant variants fused to a C-terminal *Strep*-tag® II. Periplasmic export of the protein is facilitated by an N-terminal *pelB* signal sequence.
Recombinant protein production was performed exactly as for proteins A-PGH and $A\text{-}PGH_{trunc}$ as described in section 2.6.1.1 with a modified inductor concentration of 50 µM IPTG (136, 137).

2.6.1.4 Production of PA3911 protein and mutant variants

E. coli BL21(λDE3) cells containing the plasmid pET32a(+)-PA3911 or plasmid variants (table 4) were used for the recombinant production of PA3911 protein or mutant variants fused to an N-terminal thioredoxin-His_6-S-tag (2.5.13). The sole thioredoxin-His_6-S-tag protein was analogously produced in *E. coli* BL21(λDE3) cells containing the plasmid pET32a(+). Further PA3911 fusion proteins (2.5.13) were also produced in *E. coli* BL21(λDE3) cells containing the plasmid pET28b(+)-PA3911 (PA3911 fused to an N-terminal His_6-tag) or plasmid pGEX-6P-1-PA3911 (PA3911 fused to an N-terminal GST-tag).

E. coli BL21(λDE3) cells carrying the desired plasmid were cultivated in 500 ml of LB medium containing the respective antibiotic in baffled flasks at 37 °C and 200 rpm to an OD_{578} of 0.5-0.6. Protein production was induced by the addition of 50 µM IPTG. Further cultivation was performed at 17 °C and 180 rpm overnight. The cells were harvested by centrifugation (3'000 x g, 4 °C, 15 min), resuspended in harvesting buffer B (His_6-tag and thioredoxin-His_6-S-tag) or harvesting buffer C (GST-tag), sedimented again (3'000 x g, 4 °C, 20 min) and stored at -20 °C.

harvesting buffer B	sodium phosphate pH 7.0	50 mM
	NaCl	300 mM
harvesting buffer C	Tris-HCl pH 8.0	50 mM
	NaCl	150 mM

2.6.2 Cell disruption

2.6.2.1 Isolation of the periplasmic fraction (A-PGH and AcvB protein)

A-PGH and AcvB protein variants are exported to the periplasm of *E. coli via* their *pelB* signal sequence. This allows for the specific protein isolation from the periplasmic fraction. Therefore, the cells were incubated with polymyxin B leading to a permeable cell envelope. The resulting spheroblasts were stabilized in the presence of sucrose (159).

The pellet obtained during recombinant protein production (2.6.1.1 or 2.6.1.2) was thawed on ice overnight. The cells were gently resuspended in disruption buffer A (2 ml buffer for 1 ml pellet volume) and incubated on a roller mixer for 90 min at 4 °C. To separate the cell debris from the soluble periplasmic fraction the cell suspension was centrifuged (12'100 x g, 4 °C, 30 min).

disruption buffer A	HEPES-NaOH pH 8.0	50 mM
	NaCl	150 mM
	D(+)-sucrose	20% (w/v)
	polymyxin B	2 mg/ml

2.6.2.2 PA3911 protein variants

E. coli BL21(λDE3) cell pellets (2.6.1.4) containing recombinantly produced PA3911 protein variants with an N-terminal His_6-tag, an N-terminal

thioredoxin-His_6-S-tag or an N-terminal GST-tag or the sole thioredoxin-His_6-S-tag were thawed on ice overnight and suspended in harvesting buffer B (His_6-tag and thioredoxin-His_6-S-tag) or harvesting buffer C (GST-tag) supplemented with Benzonase® (Merck Millipore, Darmstadt, Germany). Cells were disrupted by a single passage through a French Press® (Thermo Fisher Scientific, Waltham, MA) at 14'500 psi and were subjected to ultracentrifugation (84'000 x g, 4 °C, 1 h) to separate the soluble fraction from insoluble cell components.

harvesting buffer B	sodium phosphate pH 7.0	50 mM
	NaCl	300 mM
harvesting buffer C	Tris-HCl pH 8.0	50 mM
	NaCl	150 mM

2.6.3 Protein purification by affinity chromatography

2.6.3.1 Purification of A-PGH and AcvB protein variants

A-PGH and AcvB protein variants fused to a *Strep*-tag® II were purified using *Strep*-Tactin® resin according to the manufacturer's instructions (iba, Göttingen, Germany). Therefore, the isolated periplasmic fraction (2.6.2.1) was initially incubated with 0.4 µM avidin (Calbiochem® by Merck, Darmstadt, Germany) for 15 min at 4 °C on a roller mixer to mask biotinylated proteins. Then the fraction was loaded into a Poly-Prep® Chromatography Column (Bio-Rad, Hercules, CA, USA) containing 1 ml *Strep*-Tactin® Superflow® or *Strep*-Tactin® Superflow® high capacity resin which was previously equilibrated with 2x 5 column volumes (CV) washing buffer A. The resin was washed twice with 5 CV washing buffer A and then the protein of interest was eluted with 4x 1 CV elution buffer A. The obtained protein was stored at 4 °C. To regenerate the *Strep*-Tactin® resin it was washed with 3x 5 CV regeneration buffer (iba, Göttingen, Germany) according to the manufacturer's instructions and the columns were stored at 4 °C. Before further use the resin was washed extensively with washing buffer B until the orange color of the resin disappeared completely. To equilibrate the pH value of the resin it was washed with washing buffer C.

washing buffer A	HEPES-NaOH pH 8.0	50 mM
	NaCl	100 mM
washing buffer B	Tris-HCl pH 10.5	100 mM
	NaCl	150 mM
	EDTA	1 mM
washing buffer C	Tris-HCl pH 8.0	100 mM
	NaCl	150 mM
	EDTA	1 mM
elution buffer A	HEPES-NaOH pH 8.0	50 mM
	NaCl	100 mM
	D-desthiobiotin	2.5 mM

regeneration buffer	Tris-HCl pH 8.0	100 mM
	NaCl	150 mM
	EDTA	1 mM
	2-(4'-hydroxyl-benzeneazo)-benzoic acid	1 mM

2.6.3.2 Purification of GST-tagged PA3911 protein

The cell free extract containing PA3911 protein with an N-terminal GST-tag (2.6.2.2) was loaded onto 2 ml Protino® Glutathione Agarose 4 B (Macherey-Nagel, Düren, Germany) which was equilibrated with 10 CV of dH_2O and 10 CV of harvesting buffer C. The supernatant was incubated with the resin for 2 h at RT on a roller mixer. The obtained flow-through was loaded onto the resin again, followed by four washing steps with 5 CV of harvesting buffer C, respectively. The protein of interest was eluted with 4x 1 CV of elution buffer B. Alternatively, protein elution was performed by on-column cleavage with PreScission™ Protease (GE Healthcare, Chalfont St Giles, UK). Therefore, protein PA3911 bound to glutathione agarose resin was incubated with 200 U PreScission™ Protease in 1 CV harvesting buffer C for 20 h at 4 °C on a roller mixer.

harvesting buffer C	Tris-HCl pH 8.0	50 mM
	NaCl	150 mM
elution buffer B	Tris-HCl pH 8.0	50 mM
	NaCl	150 mM
	glutathione	10 mM

2.6.3.3 Purification of His_6- or thioredoxin-His_6-S-tagged PA3911 protein

To purify PA3911 protein variants with an N-terminal His_6-tag, an N-terminal thioredoxin-His_6-S-tag or the sole thioredoxin-His_6-S-tag the soluble supernatant obtained after ultracentrifugation (2.6.2.2) was loaded onto 1 ml TALON® metal affinity resin (Clontech® Laboratories, Mountain View, CA, USA) which was equilibrated with 5 CV dH_2O and 2x 5 CV of harvesting buffer B. The supernatant was incubated with the resin for 20 min at RT on a roller mixer. The resin was washed once with 5 CV of harvesting buffer B and then four pre-elution steps with 5 CV of harvesting buffer B supplemented with 10, 20, 40 or 60 mM imidazole were performed. For protein elution 10x 0.5 CV of elution buffer C were applied to the column and elution fractions were stored at 4 °C.

harvesting buffer B	sodium phosphate pH 7.0	50 mM
	NaCl	300 mM
elution buffer C	sodium phosphate pH 7.0	50 mM
	NaCl	300 mM
	imidazole	150 mM

2.6.4 Dialysis

2.6.4.1 A-PGH protein variants

Elution fractions of protein A-PGH and A-PGH$_{trunc}$ were pooled and dialyzed in a dialysis membrane (dialysis tubing membrane visking, molecular weight cut-off (MWCO) of 14 kDa; Roth®, Karlsruhe, Germany) against at least 250 volumes of dialysis buffer A, dialysis buffer B or washing buffer A. Dialysis was performed in two steps at 4 °C for at least 2 h each with exchange of the dialysis buffer in between. The obtained protein solution was stored at 4 °C.

dialysis buffer A	HEPES-NaOH pH 6.8	20 mM
dialysis buffer B	sodium citrate pH 5.4	40 mM
	NaCl	80 mM
washing buffer A	HEPES-NaOH pH 8.0	50 mM
	NaCl	100 mM

2.6.4.2 AcvB protein variants

Dialysis of elution fractions of AcvB protein variants was performed in a dialysis membrane (dialysis tubing membrane visking, MWCO of 14 kDa; Roth®, Karlsruhe, Germany) against at least 250 volumes of washing buffer A. Dialysis was performed in two steps at 4 °C for at least 2 h each with exchange of the dialysis buffer in between. The dialyzed protein solution was stored at 4 °C.

washing buffer A	HEPES-NaOH pH 8.0	50 mM
	NaCl	100 mM

2.6.4.3 PA3911 protein variants

Buffer exchange in PA3911 elution fractions against dialysis buffer C was performed with illustra NAP-5 columns according to the manufacturer's instructions (GE Healthcare, Chalfont St Giles, UK).

dialysis buffer C	ammonium acetate	5 mM

2.6.5 Protein concentration

Fractions containing purified protein were concentrated up to the desired protein concentration (2-15 mg/ml) in centrifugal concentrators with a MWCO of 10 kDa (Amicon® Ultra-0.5 or Vivaspin® Turbo 4) according to the manufacturer's instructions (Merck Millipore, Darmstadt, Germany or Sartorius, Göttingen, Germany).

2.7 Protein characterization

2.7.1 Determination of protein concentration

Concentrations of purified proteins were determined photometrically using the method developed by Bradford (1976) (160). Underlying principle of this method is a shift in the absorption maximum of the dye Coomassie Brilliant Blue G-250 from 470 to 595 nm upon complex formation with proteins. Measurement of the absorption at 595 nm allows for the determination of the protein concentration in the sample compared to a calibration curve.

Protein concentrations were determined using Bradford reagent (Sigma-Aldrich®, St. Louis, MO, USA). Therefore, 30 µl protein solution was mixed with 1 ml Bradford reagent and incubated for 10 min. Absorption was measured at 595 nm and protein concentration was determined using a calibration curve of bovine serum albumin (BSA) dissolved in the respective buffer. Samples containing a high protein concentration were diluted with the respective buffer before measurement.
Furthermore, protein concentrations were measured spectrophotometrically (NanoDrop™ ND-1000, PEQLAB Biotechnologie GmbH, Erlangen, Germany) according to the manufacturer's instructions considering the molecular weight and the extinction coefficient of the respective protein.

2.7.2 Discontinuous sodium dodecyl sulfate polyacrylamide gel electrophoresis

Protein samples were analyzed under denaturing conditions *via* discontinuous sodium dodecyl sulfate polyacrylamide gel electrophoresis (SDS-PAGE). Therefore, the samples are incubated with the anionic detergent SDS to denature the proteins and to apply a negative charge to them. Furthermore, the addition of 2-mercaptoethanol reduces disulfide linkages in the protein sample. This sample preparation allows for the separation of proteins in a polyacrylamide gel according to their molecular weights (161). In addition to that the use of discontinuous SDS-PAGE sharpens the resulting protein bands and increases the separating capacity (162).

Protein samples were mixed with 2x SDS loading dye and incubated at 95 °C for 10 min. Afterwards samples were centrifuged (12'100 x g, RT, 5 min) and loaded onto a SDS polyacrylamide gel. Two size standards were used: the Unstained Protein Molecular Weight Marker and the PageRuler™ Prestained Protein Ladder (Thermo Fisher Scientific, Waltham, MA, USA). The latter one was employed for polyacrylamide gels subsequently used for blotting. Electrophoresis was performed at 45 mA per polyacrylamide gel and Coomassie Brilliant Blue R-250 or InstantBlue™ (Expedeon Inc., San Diego, CA, USA) were utilized to stain the gels. Protein bands were visualized by destaining the background and the polyacrylamide gels were documented on a BIO-5000 Plus VIS gel scanner (Serva, Heidelberg, Germany) (146).

running gel, 12% (w/v)	Rotiphorese® Gel 30	2 ml
	1.5 M Tris-HCl pH 8.8 with 0.4% (w/v) SDS	1.25 ml
	dH_2O	1.75 ml
	10% (w/v) ammonium persulfate (APS)	50 µl
	N,N,N',N'-tetramethylethylene diamine (TEMED)	5 µl
running gel, 15% (w/v)	Rotiphorese® Gel 30	2.5 ml
	1.5 M Tris-HCl pH 8.8 with 0.4% (w/v) SDS	1.25 ml
	dH_2O	1.25 ml
	10% (w/v) APS	50 µl
	TEMED	5 µl
stacking gel, 6% (w/v)	Rotiphorese® Gel 30	0.5 ml
	0.5 M Tris-HCl pH 6.8 with 0.4% (w/v) SDS	625 µl
	dH_2O	1.375 ml
	10% (w/v) APS	25 µl
	TEMED	2.5 µl
2x SDS loading dye	Tris-HCl pH 6.8	50 mM
	2-mercaptoethanol	2 mM
	glycerol	10% (v/v)
	SDS	2% (w/v)
	bromophenol blue	0.1% (w/v)
electrophoresis buffer	Tris-HCl pH 8.8	50 mM
	glycine	385 mM
	SDS	0.1% (w/v)
staining solution	acetic acid	10% (v/v)
	ethanol	30% (v/v)
	Coomassie Brilliant Blue R-250	0.25% (w/v)
destaining solution	acetic acid	10% (v/v)
	ethanol	30% (v/v)

2.7.3 Protein transfer *via* blotting

Protein samples destined for N-terminal sequence determination (2.7.5) or immunochemical detection of specific proteins were separated by discontinuous SDS-PAGE (2.7.2). The resulting unstained polyacrylamide gel and two pieces of blotting paper (neoLab®, Heidelberg, Germany) were equilibrated in Towbin buffer for 10 min. The proteins were transferred onto a methanol-activated and in Towbin buffer equilibrated polyvinylidene difluoride (PVDF) membrane (Immobilon-P Transfer Membrane with a pore size of 0.45 µm, Merck Millipore, Darmstadt, Germany) using the semi-dry Trans-Blot® Turbo™ system (Bio-Rad,

Hercules, CA, USA). The transfer was performed at 25 V and the transfer time was adjusted based on the molecular weight of the protein of interest.

sample	**transfer time (per mini gel)**
AcvB (localization, chapter 2.12.2)	13 min
PA3911 (localization, chapter 2.11)	6 min
VirJ (localization, chapter 2.12.2)	7 min

PVDF membranes intended for N-terminal sequence determination (2.7.5) were stained with Ponceau S solution to visualize the protein bands and the desired bands were excised with a scalpel for further analysis.

Towbin buffer	Tris-HCl pH 9.5	25 mM
	glycine	192 mM
	methanol	20% (v/v)
Ponceau S solution	Ponceau S	0.2% (w/v)
	trichloroacetic acid	3% (w/v)
	sulfosalicylic acid	3% (w/v)

2.7.4 Immunochemical detection of *Strep*II-tagged® proteins

For immunochemical detection of *Strep*II-tagged® proteins the *Strep*-Tactin® AP conjugate was used according to the manufacturer's instructions (iba, Göttingen, Germany) with slight modifications. All incubation steps were performed on a roller mixer at RT.
After protein transfer the PVDF membrane was incubated in 20 ml blocking buffer A for 1 h. Following three washing steps with Phosphate Buffered Saline (PBS)-Tween® buffer (20 ml buffer, 5 min) biotinylated proteins were masked with avidin (Calbiochem® by Merck, Darmstadt, Germany). Therefore, the membrane was incubated for 10 min with 10 ml PBS-Tween® buffer containing 10 µl of a 2 mg/ml avidin stock solution. The antibody *Strep*-Tactin® AP conjugate (iba, Göttingen, Germany) was added to the membrane in a 1:4'000 dilution in 10 ml PBS-Tween® buffer and incubation took place for 1 h. Subsequently, several washing steps were performed: 2x with PBS-Tween® buffer (20 ml, 1 min) and 2x with PBS buffer (20 ml, 1 min). For immunochemical detection the membrane was initially equilibrated with 15 ml reaction buffer for 10 min. This buffer was exchanged against 15 ml reaction buffer supplemented with 49.5 µl of nitrotetrazolium blue (NBT) and 49.5 µl of 5-bromo-4-chloro-3-indolyl phosphate (BCIP) and incubated until optimal visualization of protein bands. Dye formation by AP was stopped by several washing steps of the membrane with dH_2O.

1x PBS buffer	KH_2PO_4	2 mM
	KCl	2.7 mM
	Na_2HPO_4	10 mM
	NaCl	137 mM
PBS-Tween® buffer	Tween® 20 in 1x PBS buffer	0.1% (v/v)

blocking buffer A	BSA	3% (w/v)
	Tween® 20	0.5% (v/v)
	in 1x PBS buffer	
reaction buffer	Tris-HCl pH 9.5	100 mM
	NaCl	100 mM
	$MgCl_2$	5 mM
BCIP stock solution	BCIP	50 mg/ml
	in 100% (v/v) dimethylformamide	
NBT stock solution	NBT	100 mg/ml
	in 70% (v/v) dimethylformamide	

2.7.5 Amino acid sequence determination

Protein identity was verified by determination of the N-terminal amino acid sequence. Therefore, a method according to Edman *et al.* (1950) (163) was applied. This work was kindly performed by Beate Jaschok-Kentner (Helmholtz Centre for Infection Research, Braunschweig, Germany).

2.7.6 Native molecular mass determination by gel permeation chromatography

The native molecular masses of purified proteins were determined by analytical GPC using a Superdex™ 200 Increase 5/150 GL or a Superdex™ 200 HR 10/30 chromatography column (GE Healthcare, Chalfont St Giles, UK). For proteins A-PGH, A-PGH_{trunc} and AcvB the chromatography column was equilibrated with washing buffer A.
Sample volumes from 50-150 µl with a protein concentration of 5-10 mg/ml were loaded onto the respective column and elution was performed with a flow rate of 0.45 ml/min. During the chromatography run the absorptions at 260 nm and 280 nm were detected to monitor DNA and protein elution, respectively. Several protein standards from the Gel Filtration Markers Kit for Protein Molecular Weights 12’000-200’000 Da (Sigma-Aldrich®, St. Louis, MO, USA) were processed analogously to generate a calibration curve which allows for the determination of the native molecular mass of the sample.

washing buffer A	HEPES-NaOH pH 8.0	50 mM
	NaCl	100 mM

2.7.7 Determination of molecular mass by electrospray ionization mass spectrometry

The molecular mass of the purified thioredoxin-His_6-S-tagged PA3911 protein (2.6.3.2) was determined by electrospray ionization mass spectrometry (ESI-MS). For analysis, 250 µl of a freshly purified protein sample was loaded onto an illustra NAP-5 column (GE Healthcare, Chalfont St Giles, UK) and buffer exchange against dialysis buffer C was performed according to the manufacturer’s instructions. The sample was stored at 4 °C until use and 10% (v/v) formic acid were mixed with the sample immediately before

measurement. Sample measurement on an Orbitrap Fusion™ (Thermo Scientific, San Jose, CA, USA) with a theoretical mass accuracy of ± 10 ppm resulted in an isotope resolved spectrum. Sample measurement and data evaluation were kindly performed by Dr. Manfred Nimtz (Helmholtz Centre for Infection Research, Braunschweig, Germany).

dialysis buffer C	ammonium acetate	5 mM

2.7.8 Thermal Shift Assay

The Thermal Shift Assay was performed to determine the melting temperature (T_M) of proteins. This enables the comparison of wild type with mutant proteins or the determination of protein stability in different conditions (e.g. buffer systems or presence of additives). The underlying principle is the binding of a fluorescent dye to the hydrophobic parts of a protein during denaturation and unfolding. The maximum of the first derivative of the resulting melting curve corresponds to the T_M of the protein under the given conditions (164).

Initially 40 µl protein buffer, 5 µl protein solution (0.5, 1 or 2 mg/ml) and 5 µl SYPRO® Orange Protein Gel Stain (Thermo Fisher Scientific, Waltham, MA, USA) solution (10x, 50x or 100x) were mixed in the wells of a microtiter plate (Bio-Rad, Hercules, CA, USA). The plate was sealed (Microseal® 'B' seal, Bio-Rad, Hercules, CA, USA) air-tight and the measurement was performed in a real-time PCR machine (C1000™ Thermal Cycler with CFX96™ real-time system, Bio-Rad, Hercules, CA, USA). The samples were heated from 10 °C to 90 °C in 0.5 °C steps and the fluorescence intensity at 570 nm was determined every 15 sec. Based on the melting curves and their derivatives the ideal experimental concentrations with respect to protein and fluorescent dye ratio were determined. The following measurements were then performed under these ideal conditions. Either solutions of wild type protein were compared with mutant proteins or the protein of interest was exposed to different buffers or additives. To calculate the T_M the maximum of the first derivative was determined using the software CFX Manager (Bio-Rad, Hercules, CA, USA).

2.7.9 Determination of selenomethionine incorporation by mass spectrometry

The SeMet occupancy for protein A-PGH was analyzed *via* matrix-assisted laser desorption ionization-time of flight mass spectrometry (MALDI-TOF MS). Therefore, elution fractions from affinity purification were separated by discontinuous SDS-PAGE (2.7.2) and the polyacrylamide gel was stained with Coomassie Brilliant Blue. Following extensive treatment with destaining solution and several washing steps with dH_2O the relevant protein bands were excised from the polyacrylamide gel with a scalpel. The fragments were dried under vacuum for 1 h at 30 °C (Speed Vac®, Savant). The sample preparation for MALDI-TOF MS analysis (e.g. tryptic digest) as well as the measurement and data evaluation was kindly performed by Dr. Manfred Nimtz (Helmholtz Centre for Infection Research, Braunschweig, Germany).

2.7.10 Small-angle X-ray scattering

Small-angle X-ray scattering (SAXS) is a versatile solution-based method to study the structure of biological macromolecules of broad size ranges. In a SAXS experiment the sample is exposed to a collimated and focused X-ray beam. The scattered intensity is recorded by a detector as a function of the scattering angle and the obtained scattering curve allows for the determination of a low-resolution model. With this technique the oligomeric state of biological macromolecules or complexes can be determined and flexible systems undergoing conformational changes can be studied (165, 166).

SAXS experiments were performed by Dr. Jörn Krauße (Helmholtz Centre for Infection Research, Braunschweig) at beamline BM29 (167) of the European Synchrotron Radiation Facility (ESRF, Grenoble, France) to elucidate the A-PGH solution structure. Samples of purified A-PGH protein at concentrations ranging from 10-214 µM in dialysis buffer B were loaded to a quartz capillary mounted in vacuum by an automated sample changer and exposed to X-ray energy of 12.5 keV. Scattering images covering a momentum transfer range of 0.0025-5 nm^{-1} were recorded. Ten images per sample with an exposure time of one second per frame were recorded. The scattering functions were determined using PRIMUS. Data were averaged, normalized and corrected for buffer scattering. DAMMIF was used to compute twenty models from SAXS data and a representative *ab initio* model was constructed using DAMAVER and SUPCOMP. Utilized programs are part of the ATSAS program package (168).

2.7.11 Protein-lipid overlay assay

To analyze the ability of PA3911 wild type or mutant proteins to bind membrane lipids a protein-lipid overlay assay was performed. Therefore, a hydrophobic membrane with several lipids spotted onto it was incubated with the purified protein of interest. Following several washing steps protein-lipid interaction was visualized by immunochemical detection.

The lipid binding capability of PA3911 wild type or mutant proteins was investigated using Membrane Lipid Strips™ P-6002 (Echelon Biosciences, Salt Lake City, UT, USA) according to the manufacturer's instructions with slight modifications. All steps were performed on a lab rocker at RT unless indicated otherwise.
The lipid strips were blocked overnight at 4 °C in 10 ml blocking buffer B. Then 0.5 µg/ml purified PA3911 protein or mutant variants (N-terminal thioredoxin-His_6-S-tag, 2.6.3.3) in 10 ml blocking buffer B were added to the lipid strip and incubated for 1 h. Three washing steps with PBS-Tween® buffer (2.7.4) were performed (10 ml, 7 min). Afterwards the lipid strip was incubated for 1 h with a primary Penta-His mouse monoclonal IgG antibody (QIAGEN, Hilden, Germany) diluted 1:2'000 in 10 ml blocking buffer B. The lipid strip was washed again as described before and subsequently incubated for 1 h with the secondary anti-mouse IgG (Fc-specific)-alkaline phosphatase antibody (Sigma-Aldrich®, St. Louis, MO, USA) diluted 1:5'000 in blocking buffer B. Unbound antibodies were washed away as described before and lipid-interacting proteins were detected by AP-dependent substrate conversion of BCIP and NBT. Therefore, the lipid strip was equilibrated in 10 ml reaction

buffer (2.7.4) for 10 min. Then 10 ml reaction buffer supplemented with 49.5 µl BCIP and 49.5 µl NBT (2.7.4) was added and incubated until optimal visualization. The reaction was stopped by extensive washing of the lipid strip in dH_2O.

blocking buffer B	BSA	3% (w/v)
	Tween® 20	0.1% (v/v)
	in 1x PBS (2.7.4)	

2.8 Lipid analysis

2.8.1 Lipid extraction

For lipid analysis, *P. aeruginosa* cells were cultivated for 24 h at 37 °C and 200 rpm in different media (e.g. LB medium, AB medium pH 5.3 or pH 7.3). The bacterial cell suspensions were adjusted to their optical densities (15 ml culture with OD_{578} = 0.6) before harvesting (4'000 x g, 4 °C, 20 min). The cell sediment was stored at -20 °C until further processing. *E. coli* membrane fractions from *in vitro* A-PGS activity assays were harvested by centrifugation (11'000 x g, RT, 30 min) and the cell sediments were stored at -20 °C. Lipids were extracted by a modified method according to Bligh and Dyer (1959) (169). The cell pellet was resuspended in a total volume of 100 µl dH_2O. 375 µl methanol/chloroform (2:1 (v/v)) were added, vigorously mixed with the suspension and incubated for 3 min at RT. After centrifugation (12'100 x g, RT, 3 min), 200 µl chloroform/dH_2O (1:1 (v/v)) were intensively mixed with the resulting supernatant. Following centrifugation (12'100 x g, RT, 3 min) the lower chloroform phase was collected and evaporated at 40 °C in a thermomixer. The dried lipids were stored at -20 °C (170). Lipid fractions extracted from *in vitro* A-PGS activity assays were dried at RT and used for scintillation analyses.

2.8.2 Lipid analysis by thin-layer chromatography

To analyze the polar lipid content, lipid extracts from *P. aeruginosa* cells (2.8.1) were dissolved in 20 µl methanol/chloroform (1:1 (v/v)) and loaded onto a 10x10 cm TLC plate (Alugram® SIL G/UV254, Macherey-Nagel, Düren, Germany) in 5 µl steps. Lipid separation was carried out at 25 °C. To analyze the major lipid classes of *P. aeruginosa* the solvent system for the first dimension consisted of chloroform/methanol/water (65:25:4 (v/v/v)). The TLC plate was dried under a fume hood and was then employed for the second dimension with the following solvent system: chloroform/methanol/acetic acid/water (80:12:15:4 (v/v/v/v)) (171). Furthermore, solvent systems for the specific separation of PA from the major lipid classes were applied with chloroform/ethanol/water/triethylamine (30:35:7:35 (v/v/v/v)) (172) or chloroform/methanol/water (65:25:4 (v/v/v)) in the first dimension and chloroform/methanol/ammonium hydroxide (65:25:4 (v/v/v)) in the second dimension (173).
Reaction mixtures from AcvB/VirJ *in vitro* activity assays were spotted onto TLC plates at defined time points together with L-lysine as a reference. One-dimensional TLC separation using n-butanol, acetic acid and water (4:1:1 (v/v/v)) as solvent system (174) was carried out at 25 °C.
Several staining solutions were used to detect specific lipid classes on TLC

plates. Spraying with 5% (w/v) molybdatophosphoric acid (in ethanol; Roth®, Karlsruhe, Germany) and incubation at 120 °C on a TLC plate heater (CAMAG®, Muttenz, Switzerland) allowed for the detection of reducing compounds like lipids. Ninhydrin spray solution (0.3% (w/v), Merck, Darmstadt, Germany) was used for the identification of compounds containing free amino groups, appearing after incubation at 110 °C on a TLC plate heater. Molybdenum Blue spray reagent (1.3% (w/v), Sigma-Aldrich®, St. Louis, MO, USA) enabled the detection of phospholipids by incubation at RT until spot development.

2.8.3 Liquid scintillation counting

4 ml of OptiPhase HighSafe 2 (PerkinElmer, Waltham, MA, USA) was added to radioactively labeled phospholipids (2.8.1) and scintillation counting was performed in a Tri-Carb® 2900TR liquid scintillation analyzer (PerkinElmer, Waltham, MA, USA).

2.8.4 Quantification of phosphatidic acid in *P. aeruginosa* cells

For quantification of the cellular PA content of *P. aeruginosa* strains MPAO1 and PW7609 the commercially available Total Phosphatidic Acid Assay Kit (Cell Biolabs, San Diego, CA, USA) was used according to the manufacturer's instructions.
The sample preparation had to be adjusted due to the use of bacterial cells instead of mammalian cells. To ensure comparable conditions for PA quantification, *P. aeruginosa* cells were cultivated aerobically and anaerobically to the mid-logarithmic phase defined as the OD_{578} at the midpoint of the linear range of exponential growth. This time point was determined by monitoring the growth behavior over a time period of 10 h.
500 ml AB medium pH 7.3 in baffled flasks (one flask per sample) was inoculated to an OD_{578} of 0.05 using an overnight culture of either strain *P. aeruginosa* MPAO1 or *P. aeruginosa* PW7609. Cells were cultivated aerobically at 37 °C and 200 rpm to the mid-logarithmic phase (~4 h after inoculation). Alternatively, 125 ml AB medium pH 7.3 supplemented with 50 mM potassium nitrate in anaerobic culture flasks (three flasks per sample) was inoculated to an OD_{578} of 0.3 using an overnight culture of *P. aeruginosa* strain MPAO1 or PW7609. Anaerobic cultivation was performed at 37 °C and 100 rpm to the mid-logarithmic phase (~6.5 h after inoculation). Identical amounts of cells (15 ml culture with OD_{578} = 6) were harvested by centrifugation (4'000 x g, 4 °C, 10 min), the cell pellets were washed with cold PBS (2.7.4, containing 1 mM $CaCl_2$ and 0.5 mM $MgCl_2$) and were stored at -20 °C. After resuspending the cell pellet in 1 ml cold PBS, lipids were extracted according to the manufacturer's instructions. The dried samples were dissolved in 30 µl 1x Assay Buffer and stored at -80 °C. PA contents in the samples were determined as means ± standard deviation (SD) of duplicates from three independent experiments.

2.9 Determination of *in vitro* A-PGS activity

To determine the activity of recombinantly produced and purified A-$PGS_{543-881}$ protein variants a well-established *in vitro* activity assay (47) was performed.

The formation of A-PG is catalyzed by the A-PGS which transfers an alanine moiety from the corresponding Ala-tRNA^{Ala} to the hydroxyl group of PG (43). Due to the presence of the alanyl-tRNA synthetase in the assay system the uncharged tRNA^{Ala} is re-charged and alanylated by consumption of two adenosine triphosphate (ATP) molecules. Therefore, the reaction mixture contains an ATP regenerating system to provide sufficient ATP molecules. The catalytic A-PGS domain (containing amino acid residues 543-881) and mutant variants were recombinantly produced in *E. coli*. Purified proteins used in this assay were generously provided by S. Hebecker.
To recombinantly overproduce the alanyl-tRNA synthetase from *P. aeruginosa* 500 ml LB medium (supplemented with 30 µg/ml Kan and Cm) was inoculated with an overnight pre-culture of *E. coli* Rosetta™ (DE3) pLysS pET28b(+)PA0903 in a ratio of 1:100 (v/v). Cells were cultivated at 37 °C and 180 rpm to an OD_{578} of 0.5. Cultures were shifted to 30 °C and 180 rpm for 10 min. Then, 200 µM IPTG were added to induce protein production and cultivation was continued at 30 °C and 180 rpm for 4 h. Cells were sedimented by centrifugation (3'000 x g, 4 °C, 20 min) and washed with 50 mM HEPES-NaOH pH 7.8. Following a second centrifugation step (4'000 x g, 4 °C, 15 min) cells were resuspended in 50 mM HEPES-NaOH pH 7.8 and supplemented with DNase I (Invitrogen, Carlsbad, CA, USA). Cells were disrupted by a single passage through a French Press® (Thermo Fisher Scientific, Waltham, MA, USA) at 19'200 psi. The obtained crude cellular extract provides the substrate molecule PG, tRNA^{Ala} and the alanyl-tRNA synthetase for the *in vitro* assay. The reaction was performed in a total volume of 700 µl. Therefore, 500 µl of this crude cellular extract was supplemented with 2 mM ATP, an ATP regenerating system (35 U/ml creatine phosphokinase and 18 mM creatine phosphate) and 20 µM [1-^{14}C]-L-alanine (Moravec Biochemicals, Brea, CA, USA). The reaction was started by the addition of 10 µM of the respective purified A-PGS$_{543-881}$ protein variant (wild type, K676E, K676S, N683D, N683S, R684E, R684S, R687S) and was incubated at 37 °C and 1'000 rpm for 1 h. Samples were taken at distinct time points, heat inactivated (60 °C, 5 min) and stored at -20 °C for lipid extraction (2.8.1) and scintillation counting (2.8.3).

2.10 *In vitro* activity assay for AcvB and VirJ

The L-PG hydrolyzing activity of AcvB variants and VirJ was determined in an *in vitro* activity assay. Therefore, 1 mg of 18:1 L-PG (Avanti® Polar Lipids, Alabaster, AL, USA) was solubilized in 200 µl dialysis buffer A containing 3 mg/ml Triton™ X-100 at 37 °C for 15 min under vigorous shaking. 80 µl of this L-PG micelle solution was incubated with 80 µl of 20 µM purified AcvB (or mutant variant), VirJ or *Strep*-tag® II protein in dialysis buffer A at 37 °C and 1'000 rpm for 60 min. At defined time points 5 µl of the respective reaction mixture was spotted onto a TLC plate together with 5 µl of a 68 µM L-lysine solution (Fluka, Buchs, Switzerland) as a reference. Subsequent to TLC separation and ninhydrin staining (2.8.2) spot intensities were determined using the software TotalLab Quant (Cleaver Scientific Ltd, Rugby, UK). Comparison with a linear calibration curve (spot intensities plotted against the respective L-lysine concentration) allowed for the quantification of L-lysine formation during *in vitro* activity assays and for the calculation of specific activities for AcvB variants and VirJ.

Phenotypic characterization

The *P. aeruginosa* mutant strain PW7609 was compared with the wild type strain MPAO1 concerning the following phenotypic characteristics: twitching, swimming and swarming motility, biofilm formation and growth in the presence of 1'152 different culture conditions (Phenotype Microarray™).

2.10.1 Confirmation of *P. aeruginosa* mutant strain PW7609

Prior to the phenotypic characterization of *P. aeruginosa* mutant strain PW7609, the correct insertion of the IS*phoA*/hah transposon into orf PA3911 was confirmed according to a procedure described by the library curators (134). Therefore, gene flanking primers 40 and 41 as well as gene flanking primer 41 and transposon specific primer 42 were utilized in a colony PCR (2.5.5) to verify the absence of the gene of interest and the correct insertion of the transposon. The obtained transposon specific fragment was purified with the QIAquick PCR Purification Kit (QIAGEN, Hilden, Germany) and was sequenced (GATC Biotech, Konstanz, Germany) with primer J to verify the transposon insertion site.

2.10.2 Standard phenotype assays

2.10.2.1 Twitching motility

To analyze the twitching motility of *P. aeruginosa* strains the respective inoculum was stabbed down to the agar-plastic interface of a thin 1% (w/v) LB-Lennox agar plate by a sterile toothpick. The agar plates were incubated in a humidified chamber at 37 °C for 24 h. The twitch zones of five independent biological experiments using six replicates each were measured (175). For comparison of the wild type and mutant strain the twitch zone diameter of the wild type strain was set to 100%.

2.10.2.2 Swimming motility

Swimming motility was analyzed on thick M8 agar plates containing 0.3% (w/v) agar. A sterile toothpick was dipped into an overnight culture of the respective strain and stabbed into the middle of the agar layer. The diameter of the motility zone was measured after incubation for 24 h at 37 °C (175). Two independent biological experiments with six replicates were performed.

2.10.2.3 Swarming motility

Swarming motility analysis was performed on thick M8 agar plates containing 0.5% (w/v) agar. The agar plates were inoculated with 2.5 µl of an overnight culture of the respective strain and incubated for 21 h at 37 °C before the motility zone diameter was determined (175). Two independent biological experiments with six replicates were performed.

2.10.2.4 Biofilm assay

The biofilm formation of *P. aeruginosa* strains was analyzed in a static microtiter

plate-based assay in nine independent experiments containing eight replicates. Therefore, overnight cultures of the respective strains were grown to stationary phase, optical density adjusted (OD_{600} = 0.05) and diluted in a ratio of 1:100 (v/v) with fresh LB medium to yield 5x 10^5 cells/ml. 96-well polypropylene round-bottom microtiter plates (Nunc™, Roskilde, Denmark) were inoculated with 100 µl cell suspension per well and incubated at 37 °C for 24 h without shaking. After the removal of planktonic cells the microtiter plates were extensively rinsed with water and surface-attached bacteria were stained with 0.1% (w/v) crystal violet solution for 10 min. The microtiter plates were again extensively rinsed with water and the biofilms were solubilized with 30% (v/v) acetic acid for quantification of A_{595} (175).

2.10.3 Phenotype Microarray™ analyses

Phenotypic differences for the isogenic mutant strain PW7609 were analyzed using a broad range of stress conditions (e.g. salts, pH and antibiotics). For analysis the transposon mutant strain PW7609 and the wild type strain MPAO1 were subjected to an overall of 1'152 growth conditions (MicroPlates™ PM9 to PM20) using a commercially available microarray system from Biolog (Hayward, CA, USA) according to the manufacturer's instructions. The plates were incubated at 37 °C in an OmniLog® incubator and the color change (reduction of a tetrazolium dye as a result of cell respiration) was monitored for 48 h. Growth kinetics were analyzed using OmniLog®-PM software (release OL_PM_FM/Kin 1.20.02 Aug. 12, 2005).
Significant growth phenotypes were independently reproduced in non-commercial microarray experiments which were performed in triplicate. Therefore, the strains were cultivated as described above in the presence of minocycline hydrochloride (0.25-9 µg/ml), nafcillin sodium salt (100-1'000 µg/ml), oxacillin sodium salt monohydrate (200-2'800 µg/ml), chloramphenicol (2-1'200 µg/ml; Roth®, Karlsruhe, Germany), thiamphenicol (2.5-1'000 µg/ml) and 1-chloro-2,4-dinitrobenzene (CDNB) (1-200 µg/ml) in 120 µl IF-10 medium containing tetrazolium dye A (Biolog, Hayward, CA, USA) using 96-well plates (REF 82.1581.001, Sarstedt, Nümbrecht, Germany). Unless noted otherwise, the chemicals were purchased from Sigma-Aldrich® (St. Louis, MO, USA).

2.11 Localization of protein PA3911 in *P. aeruginosa*

Localization studies were performed with *P. aeruginosa* PAO1 strain carrying plasmid pUCP20T-P_{PA3911}-PA3911. This plasmid encodes for the PA3911 protein fused to a C-terminal *Strep*-tag® II sequence. Analysis of subcellular fractions was performed *via* Western blotting with *Strep*-Tactin® AP conjugate (iba, Göttingen, Germany) according to the manufacturer's instructions.

2.11.1 Cultivation for localization studies

The *P. aeruginosa* PAO1 strain carrying the plasmid pUCP20T-P_{PA3911}-PA3911 (2.2.2) was cultivated, harvested and analyzed by subcellular localization experiments.

1 l LB medium supplemented with Cb (in baffled flasks) was inoculated to an OD_{578} of 0.05 using an overnight culture of strain *P. aeruginosa* PAO1 pUCP20T-P_{PA3911}-PA3911 and was incubated at 37 °C and 200 rpm for 4 h (end of the exponential growth phase). Cells were harvested by centrifugation (3‘000 x g, 4 °C, 15 min), resuspended in 50 ml harvesting buffer A (for analysis of the periplasmic and cytoplasmic fraction) or disruption buffer B (for analysis of the total membrane fraction) and sedimented again (4’000 x g, 4 °C, 20 min). The isolation of the periplasmic and cytoplasmic fraction was performed directly after cell harvesting, whereas cell pellets for the isolation of the total membrane fraction were stored at -20 °C until further use.

harvesting buffer A	HEPES-NaOH pH 8.0	50 mM
	NaCl	150 mM
	D(+)-sucrose	20% (w/v)
disruption buffer B	Tris-HCl pH 8.0	50 mM

2.11.2 Isolation of the periplasmic and cytoplasmic fraction

To localize the PA3911 protein in *P. aeruginosa* cells the periplasmic and cytoplasmic fraction were isolated. Therefore, cells were treated with polymyxin B as already described in chapter 2.6.2.1 and the formed spheroblasts were further utilized for the isolation of the cytoplasmic fraction.

The harvested cell pellet (2.11.1) was suspended in the double sediment volume of disruption buffer A and was incubated at 4 °C for 90 min on a roller mixer. Following a centrifugation step (10’000 x g, 4 °C, 15 min) the supernatant contained the periplasmic proteins, whereas the spheroblasts containing cytoplasmic and membrane proteins were sedimented. The spheroblast fraction was stored at -20 °C until further analysis.
The thawed spheroblast fraction was resuspended in four volumes of washing buffer A for one pellet volume. 750 µl of the obtained cell suspension was mixed with 250 mg glass beads and was subjected to cell disruption *via* FastPrep® (3x 45 sec at 5.5 m/s; MP Biomedicals, Santa Ana, CA, USA). After centrifugation (20’000 x g, 4 °C, 1 h) the resulting supernatant contained the cytoplasmic proteins.

disruption buffer A	HEPES-NaOH pH 8.0	50 mM
	NaCl	150 mM
	D(+)-sucrose	20% (w/v)
	polymyxin B	2 mg/ml
washing buffer A	HEPES-NaOH pH 8.0	50 mM
	NaCl	100 mM

2.11.3 Isolation of the total membrane fraction

To isolate the total membrane fraction the cells were lysed, cell debris was separated and the membrane fraction was sedimented from the supernatant by high-speed centrifugation (49).

Harvested cells (2.11.1) were thawed and suspended in a total volume of 10 ml disruption buffer B. Cells were disrupted by a single passage through a French Press® (Thermo Fisher Scientific, Waltham, MA, USA) at 19'200 psi and cell debris was separated by low-speed centrifugation (20'000 x g, 4 °C, 20 min). The obtained supernatant was subjected to ultracentrifugation (100'000 x g, 4 °C, 1 h) to sediment the total membrane fraction. After three washing steps with 500 µl of washing buffer D, respectively, the membrane proteins were solubilized. Therefore, the membrane pellet was overlaid with 5 ml solubilization buffer and was gently stirred for 2 h at 4 °C. In a second ultracentrifugation step (100'000 x g, 4 °C, 1 h), lipids were sedimented and the resulting supernatant contained the solubilized membrane proteins.

disruption buffer B	Tris-HCl pH 8.0	50 mM
washing buffer D	Tris-HCl pH 8.0	50 mM
	$MgCl_2$	20 mM
solubilization buffer	Tris-HCl pH 8.0	50 mM
	$MgCl_2$	20 mM
	Triton™ X-100	2% (v/v)

2.11.4 Sample preparation and analysis

Samples of the cellular fractions (2.11.2 and 2.11.3) were mixed with 2x SDS loading dye in a ratio of 1:1 (v/v), were incubated at 95 °C for 10 min in a thermomixer and were separated by SDS-PAGE (2.7.2). The proteins were blotted onto a membrane according to the procedure described in chapter 2.7.3. Detection of the C-terminal *Strep*-tag® II sequence of protein PA3911 in the cellular fractions was performed as described in section 2.7.4.

2.12 Localization of AcvB and VirJ in *A. tumefaciens*

For the localization of proteins AcvB and VirJ in *A. tumefaciens* two different methods were employed. Therefore, *A. tumefaciens* cells carrying the respective plasmid were cultivated, fractionated into the soluble periplasmic and cytoplasmic part and analyzed either *via* an AP activity assay or *via* a Western Blot with subsequent immunochemical detection.

2.12.1 Localization of AcvB and VirJ *via* alkaline phosphatase fusions

2.12.1.1 Cultivation for localization studies

The *A. tumefaciens* strains carrying plasmids pTrc200 '*phoA*, pTrc200 *phoA*, pTrc200 leader *acvB* '*phoA* or pTrc200 leader *virJ* '*phoA* (2.2.2) were cultivated, harvested and utilized for fractionation experiments.

40 ml YEB medium supplemented with Spc and Str in baffled flasks was inoculated to an OD_{578} of 0.4 using the respective *A. tumefaciens* overnight culture and incubated at 30 °C and 200 rpm for 30 min. Then 15 µM IPTG was added to the bacterial cell culture (OD_{578} = 0.5) and the incubation was

preceded for 3.5 to 4 h (end of exponential phase) at 30 °C and 200 rpm. Cells were adjusted to their optical densities (35 ml culture with OD_{578} = 1.6) and harvested (10‘000 x g, RT, 5 min).

2.12.1.2 Isolation of the periplasmic and cytoplasmic fraction

Fractionation of *A. tumefaciens* cells was performed according to the protocol of Kang *et al.* (1994) (62) with modifications.
The harvested cell pellet (2.12.2) was suspended in 5 ml of disruption buffer C or disruption buffer D. The cell suspension was incubated at 4 °C for 30 min on a roller mixer. Following a centrifugation step (10’000 x g, 4 °C, 5 min) the supernatant contained the periplasmic proteins and the pellet the cytoplasmic and membrane proteins. The cell pellet was resuspended in 7 ml of disruption buffer B and disrupted by French Press® (Thermo Fisher Scientific, Waltham, MA) at 19’200 psi. Undisrupted cells were separated by centrifugation (12’000 x g, RT, 5 min). The supernatant was adjusted to a total volume of 8 ml with disruption buffer B and subsequently subjected to ultracentrifugation (213’000 x g, 4 °C, 60 min). The resulting supernatant contained the cytoplasmic proteins and the pellet contained the membrane proteins.

disruption buffer B	Tris-HCl pH 8.0	50 mM
disruption buffer C	Tris-HCl pH 8.0	50 mM
	D(+)-sucrose	20% (w/v)
	EDTA	2 mM
	lysozyme	0.2 mg/ml
disruption buffer D	Tris-HCl pH 8.0	50 mM
	D(+)-sucrose	20% (w/v)
	EDTA	2 mM
	polymyxin B	2 mg/ml

2.12.1.3 Determination of alkaline phosphatase activity

The AP activity was determined in the soluble fractions (periplasm and cytoplasm) isolated from *A. tumefaciens* cells carrying the respective plasmid (2.2.2). Activity determination was performed as described by De Maagd and Lugtenberg (1986).
The utilized test solution AP contains *p*-nitrophenyl phosphate which can be converted to *p*-nitrophenol by AP. The resulting reaction product is yellow and can be monitored spectrophotometrically at a wavelength of 405 nm.
To analyze the soluble fractions (2.12.1.2) concerning their AP activity 50 µl of the respective fraction was mixed with 500 µl test solution AP and the absorption at 405 nm was monitored with a UV-VIS spectrophotometer (V-650, Jasco, Oklahoma City, Oklahoma, USA) for 180 sec. To analyze the spontaneous conversion of the substrate to *p*-nitrophenol during the reaction control measurements solely with the test solution AP were performed. For data analysis the program Spectra Manager (Jasco, Oklahoma City, Oklahoma, USA) was used.

test solution AP	Tris-HCl pH 8.5	0.1 M
	$MgCl_2$	0.4 M
	p-nitrophenyl phosphate	0.4 mg/ml

2.12.1.4 Plate-based assay for the determination of alkaline phosphatase activity in whole cells

As an alternative method to determine AP activity in *A. tumefaciens* cells a plate-based assay with BCIP as substrate was used. BCIP can be hydrolyzed by AP to 5-bromo-4-chloroindolyl and phosphate. 5-bromo-4-chloroindolyl can then be oxidized with oxygen to the blue dye 5,5'-dibromo-4,4'-dichloroindigo (176). If active AP is present in the *A. tumefaciens* cells carrying the respective plasmid (2.2.2), BCIP supplemented to the YEB agar plates will be converted into the indigo dye and blue-colored *A. tumefaciens* colonies will appear.
For analyses of AP activity YEB agar plates were supplemented with 90 µg/ml of BCIP as a substrate. Furthermore, several concentrations of disodium hydrogen phosphate pH 7.2 (5-100 mM) were added to the YEB agar plates to inhibit the endogenous AP activity (53). Several dilutions of overnight cultures of *A. tumefaciens* cells carrying the respective plasmid (volume 50 µl) were plated on YEB agar plates containing BCIP and disodium hydrogen phosphate, incubated at 30 °C for four days and analyzed concerning the coloration of the colonies (white or blue).

2.12.1.5 Determination of malate dehydrogenase activity

Impurities of the periplasmic fraction with cytoplasmic proteins were detected *via* a malate dehydrogenase (MD) activity assay. MD is a cytoplasmic protein and it can convert oxaloacetate to malate (177). During this reaction $NADH+H^+$ is oxidized to NAD^+ and its decrease can be detected in a UV-VIS spectrophotometer (V-650, Jasco, Oklahoma City, Oklahoma, USA) at a wavelength of 340 nm. The activity assay was performed according to the protocol of De Maagd and Lugtenberg (1986).
For activity analyses 500 µl test solution MD were mixed with 50 µl of the respective periplasmic or cytoplasmic fraction (2.12.1.2). The reaction was started by the addition of 25 µl 10 mM oxaloacetate solution and the absorption at 340 nm was monitored with a UV-VIS spectrophotometer (V-650, Jasco, Oklahoma City, Oklahoma, USA) for 180 sec. For data analyses the program Spectra Manager (Jasco, Oklahoma City, Oklahoma, USA) was used.

test solution MD	HEPES-NaOH pH 7.2	50 mM
	NADH	0.3 mM

2.12.2 Localization of AcvB and VirJ *via* Western Blot

2.12.2.1 Cultivation for localization studies

A. tumefaciens strains carrying plasmid pTrc200_*acvB*_Strep or pTrc200_*virJ*_Strep (2.2.2) were cultivated, harvested and cell pellets were subjected to fractionation experiments.

A pre-culture of the respective *A. tumefaciens* strain was used to inoculate

500 ml YEB medium supplemented with Spc and Str in a baffled flask to an OD_{578} of 0.1. Cultivation was performed at 30 °C and 200 rpm for 4 h to an OD_{578} ~0.5, 15 µM IPTG were added to the main culture and cultivation was preceded for 3 h (OD_{578} ~1.6). Cells from 1 l cell culture were harvested (3'000 x g, 4 °C, 15 min), resuspended in 50 ml harvesting buffer D and sedimented again (4'000 x g, 4 °C, 25 min). Cell pellets were stored at -20 °C until use.

harvesting buffer D	Tris-HCl pH 8.0	50 mM
	NaCl	150 mM
	D(+)-sucrose	20% (w/v)

2.12.2.2 Isolation of the soluble cell fractions

A modified protocol according to Kang *et al.* (1994) (62) was used to fractionate *A. tumefaciens* cells.
Suspension of the respective cell pellet (2.12.2.1) in 5 ml of disruption buffer D was followed by incubation at 4 °C for 30 min on a roller mixer. The periplasmic fraction was separated from the cell pellet containing cytoplasmic and membrane proteins by centrifugation (10'000 x g, RT, 5 min). After resuspending the remaining cell pellet in 7 ml of disruption buffer B, cells were disrupted by French Press® (Thermo Fisher Scientific, Waltham, MA) at 19'200 psi and unbroken cells were removed by centrifugation (12'000 x g, RT, 5 min). Adjusting the final suspension volume to 9 ml was followed by ultracentrifugation (213'000 x g, 4 °C, 60 min) to separate the soluble cytoplasmic proteins from membrane proteins.

disruption buffer B	Tris-HCl pH 8.0	50 mM
disruption buffer D	Tris-HCl pH 8.0	50 mM
	D(+)-sucrose	20% (w/v)
	EDTA	2 mM
	polymyxin B	2 mg/ml

2.12.2.3 Analysis of the fractionation efficiency

To analyze the cross-contamination of the periplasmic fraction with cytoplasmic proteins, the MD activity within the isolated soluble fractions (2.12.2.2) was determined as described in section 2.12.1.5.

2.12.2.4 Isolation of the total membrane fraction

The sedimented pellet after ultracentrifugation (2.12.2.2) containing the membrane proteins was carefully washed with 3x 500 µl of washing buffer D. The membrane pellet was covered with 5 ml solubilization buffer and was stirred for 2 h at 4 °C. Solubilized membrane proteins were transferred into the supernatant by ultracentrifugation (110'000 x g, 4 °C, 60 min).

washing buffer D	Tris-HCl pH 8.0	50 mM
	$MgCl_2$	20 mM

solubilization buffer	Tris-HCl pH 8.0	50 mM
	$MgCl_2$	20 mM
	Triton™ X-100	2% (v/v)

2.12.2.5 Sample preparation and analyses

Samples of the cellular fractions (2.12.2.2 and 2.12.2.4) were mixed with 2x SDS loading dye in a ratio of 1:1 (v/v), were incubated at 95 °C for 10 min in a thermomixer and were separated by SDS-PAGE (2.7.2). Protein transfer onto a membrane was employed according to the procedure described in chapter 2.7.3. The C-terminal *Strep*-tag® II sequence of the proteins AcvB or VirJ within the fractions was detected as described in section 2.7.4.

2.13 *A. tumefaciens* infection assays

The experiments described in the following chapter were performed during an internship in the group of Prof. Franz Narberhaus (Lehrstuhl für Biologie der Mikroorganismen, Ruhr-University Bochum).

2.13.1 Potato disc infection assay

The quantitative determination of *A. tumefaciens*-induced tumorigenesis on potato tuber discs was carried out according to Wu *et al*. (2008) (178).
Pre-cultures of the respective *A. tumefaciens* strains were grown overnight at 30 °C in 5 ml YEB medium supplemented with the appropriate antibiotics. Cell suspensions were diluted to an OD_{600} = 0.1 in 10 ml YEB medium containing the respective antibiotics. Cells were cultivated to an OD_{600} = 0.4, 40 µM IPTG were added and cultivation was preceded to an OD_{600} = 1. Cells were washed once with 1x PBS and resuspended in concentrations of 10^6 or 10^8 cells/ml in 1x PBS for inoculation. The surface of peeled potatoes (type Marabel, new crop) was disinfected by immersion in 0.625% (w/v) sodium hypochlorite for 5 min and subsequently two washing steps in sterile dH_2O were performed for 1 min each. Cylinders were cut out from potato tubers using a cork borer and were cut into discs of ~0.4 cm thickness. For infection, the discs were placed on water agar and 10 µl of the respective bacterial cell suspension (10^6 or 10^8 cells/ml) was applied per disc. The petri dishes were sealed and incubated in a phytochamber (80 µE light energy, 16 h light/8 h dark period, humidity of 30-45%) at 23 °C for two days. Discs were transferred to water agar containing 100 µg/ml Tic to kill the bacteria and incubation was preceded in a phytochamber (conditions see above) at 23 °C for three weeks before tumors were counted.

2.13.2 Infection of *Arabidopsis* seedlings with *Agrobacterium*

To analyze the T-DNA transfer capability of different *A. tumefaciens* strains into plant cells infection assays according to the AGROBEST method (149) were performed.
Arabidopsis thaliana efr-1 seeds were sterilized in 50% (v/v) bleach containing 0.05% (v/v) Triton™ X-100 for 10 min and subsequently rinsed five times with sterile dH_2O. Seeds were incubated at 4 °C for three days. Then, ten seeds were transferred to each well, filled with 1 ml MS medium (2.3.2.4), of a 6-well

plate for germination in a phytochamber (80 µE light energy, 16 h light/8 h dark period) at 23 °C for four days.
Pre-cultures of the respective *A. tumefaciens* strains were pelleted, resuspended to an OD_{600} = 0.2 in AB-MES pH 5.5 medium (2.3.2.4) supplemented by 200 µM AS and 0.4 mM IPTG and cultivation was preceded at 28 °C and 220 rpm for 12-16 h to induce *vir* gene expression. Cells were sedimented and resuspended to an OD_{600} = 0.02 in infection medium (2.3.2.4; if required, supplemented with 40 mM $CaCl_2$ for strain *A. tumefaciens* C58 Δ*acvB*). The MS medium containing the seedlings was replaced by 1 ml of the respective *A. tumefaciens* suspension (in infection medium) and co-cultivation was performed in a phytochamber (conditions see above) at 23 °C for three days.
The seedlings were incubated with 500 µl β-glucuronidase (GUS) staining solution containing 5-bromo-4-chloro-3-indolyl-β-D-glucuronide (X-Gluc) per well at 37 °C for 6 h to visualize GUS activity.

GUS staining solution	sodium phosphate pH 7.0	1 M
	$K_3Fe(CN)_6$	50 mM
	$K_4Fe(CN)_6$	50 mM
	Triton™ X-100	10% (v/v)
	EDTA	0.5 M
	X-Gluc	100 mM

2.14 Protein crystallization

Protein crystallization *via* vapor diffusion is one of the standard techniques in structural biology. The underlying principle is the equilibration of the vapor pressure between the drop of a low concentrated protein-precipitant solution with a large reservoir solution containing the precipitant in a higher concentration. A prerequisite of this method is the air-tight sealing of the crystallization well allowing for the transfer of water from the protein-precipitant drop to the reservoir solution due to differences in the vapor pressure. This leads to an increase of the protein and precipitant concentration within the drop, facilitates nucleation events and thereby the formation of protein crystals (179).
Two common experimental set-ups for the vapor diffusion method are the hanging-drop and the sitting-drop format. In the hanging-drop format the protein-precipitant solution is spotted as a drop on the underside of a cover slip which covers the reservoir well from the environment, additionally sealed with silicone oil at the cover slip-well interface. For the sitting-drop format the crystallization wells have to contain a large cavity for the reservoir solution and a separated small cavity on a pedestal for the protein-precipitant drop. Sealing of the crystallization well (e.g. with an adhesive foil) from the environment is also essential for this format (180).

2.14.1 Preparation of crystals from A-PGH protein or variants

Crystallization attempts were performed to determine the three-dimensional structure of protein A-PGH. In general, the sitting-drop vapor diffusion method in 96-well plates (INTELLI-PLATE®, Art Robbins Instruments, Sunnyvale, CA, USA) was applied and commercially available NeXtal screens from QIAGEN (Cryos Suite, JCSG Core Suite I, JCSG Core Suite II, JCSG+ Suite, PEGs

Suite, PEGs II Suite) served as reservoir solutions (60 µl per well). Solutions of freshly purified A-PGH, selenomethionine-derivatized A-PGH or A-PGH$_{trunc}$ protein (2.6.3.1), dialyzed against washing buffer A or dialysis buffer B, were initially centrifuged (12'100 x g, 4 °C, 10 min) to separate protein aggregates. The resulting supernatant containing a protein concentration range of 5-20 mg/ml was utilized for crystallization attempts. The crystallization plates were either prepared at 4 °C or at RT. For each sitting-drop 1 µl of the reservoir solution was mixed with either 1 µl of the respective protein solution or 1 µl of the respective protein solution containing 5 mM L-alanine or 5 mM L-alanine amide during manual plate set-up. For crystallization plates which were set-up by the crystallization robot OryxNano (Douglas Instruments, Hungerford, UK) only 0.2 µl of reservoir and protein solution were used. The plates were sealed (CrystalClear, Manco® Inc., OH, USA) and incubated either at 4 °C or 17 °C.
The hanging-drop vapor diffusion method was applied to optimize crystallization conditions which were identified in initial screenings. 24-well plates (Crystalgen 24 Well SuperClear™ Plate, Jena Bioscience, Jena, Germany) were filled with self-made reservoir solutions (500 µl per well) with varying pH values or precipitant concentrations compared to the original reservoir solution. For each hanging-drop 2 µl of the reservoir solution was mixed with 2 µl of the respective protein solution or 2 µl of the respective protein solution containing 5 mM L-alanine on the underside of a silanized cover slip. The rim of each well was greased with silicone oil before the cover slip with the drop was carefully placed onto the well. The plates were incubated at 4 °C or 17 °C.
Potential crystal formation within the wells was checked manually with a microscope (SZX9, Olympus, Tokyo, Japan) on a regular basis and was documented by taking pictures with a camera.

washing buffer A	HEPES-NaOH pH 8.0	50 mM
	NaCl	100 mM
dialysis buffer B	sodium citrate pH 5.4	40 mM
	NaCl	100 mM

2.14.2 Crystal soaking

Crystals were cryo-protected in the presence of 2.5-10% (v/v) glycerol or 10% (v/v) (2R,3R)-(-)-2,3-butanediol and flash-cooled in liquid nitrogen. Heavy metal derivatives were produced by soaking A-PGH crystals with 66 mM $Sm(NO_3)_3$ for 20-30 seconds.

2.14.3 Data collection and structure determination

Crystals of adequate size were initially tested in diffraction experiments under a nitrogen cryostream at the home source of the Helmholtz Centre for Infection Research (Braunschweig), consisting of the microfocus rotating anode X-ray generator MicroMax™-007 HF with a Saturn944+ detector (Rigaku, Tokyo, Japan). For promising crystals data was collected at European synchrotrons (e.g. PETRA III, Hamburg, Germany or Swiss Light Source (SLS), Villigen, Switzerland). Data collection, processing and structure determination were performed by Dr. Jörn Kraußе (Helmholtz Centre for Infection Research,

Braunschweig). For structure determination of protein A-PGH X-ray diffraction data of a single crystal (crystallization condition JCSG Core Suite II No. 47, soaked with 10% (v/v) (2R,3R)-(-)-2,3-butanediol and 66 mM $Sm(NO_3)_3$) was collected at the home source (anomalous data set) and at beamline P11 (native data set), jointly operated by Deutsches Elektronen-Synchrotron (DESY), the Max Planck society and the Helmholtz Centre for Infection Research, at PETRA III (181) synchrotron (Hamburg, Germany). Data were processed in space group I222 with *XDS* (182, 183). The phase problem was solved by a single-wavelength anomalous dispersion (SAD) experiment at λ = 1.541 Å. This wavelength is in close proximity to the absorption edges of samarium's L shell (L-I: 1.6025 Å, L-II: 1.6957 Å, L-III: 1.8460 Å) resulting in a data set with Bijvoet differences significantly different from zero and so applicable to solve the phase problem. Localization of the heavy metal sites, the computation of a first electron density map and the building of an initial polyalanine model was performed with ShelxC/D/E (184). The native data set contained information of higher resolution. The high-resolution structure of A-PGH was determined by molecular replacement using the polyalanine model as a search template. Subsequent to iterative cycles of manual model building in COOT (185) and refinement in PHENIX (186) the final structural model contained amino acids 34-215 of protein A-PGH.

2.14.4 Bioinformatical analyses

Surface Entropy Reduction approach

The crystallizability of proteins can considerably depend on their surface properties. Especially long and flexible polar side chains (e.g. lysines and glutamates) with high conformational entropy can interfere with intermolecular contact formation and the assembly of a crystal lattice. Therefore, the selective replacement of these residues against small amino acids (e.g. alanine) with little or no conformational entropy can significantly improve the protein crystallizability and represents the basic principle of the SER approach (156). The prediction of promising surface residues for mutation in protein A-PGH was performed with the SERp web server (187). The respective vectors (2.5.13) were constructed by site-directed mutagenesis of plasmid pET22b(+)$PA0919_{trunc}$-Strep (135).

Protein structure analysis

The overall quality of the A-PGH_{34-215} protein structure was verified by determination of several quality metrics including the R-factors R_{work} and R_{free} and the root-mean-square deviation (rmsd) from ideal geometry. General validation was performed with the MolProbity analysis tool (188). To calculate the Matthews coefficient and the corresponding solvent content the Matthews Probability Calculator (189) was employed. Average *B*-factors were determined using the program baverage from the CCP4 suite (190, 191). Electrostatic surface potentials were computed employing the program APBS v1.4 (192).

Protein structure comparison

For comparison of the 3D protein structure of A-PGH_{34-215} against protein structures submitted in the Protein Data Bank (PDB) the Dali web server DaliLite v. 3 (193) was used. The underlying principle for the structural alignment is the distance alignment matrix method (194).

2.15 Bioinformatic tools

Sequence comparison
Protein sequences homologous to the respective protein of interest were identified using the basic local alignment search tool (BLAST) (195) with the default settings and were aligned by Clustal Omega (196).

Operon prediction
The Database of prOkaryotic OpeRons^2 (DOOR^2) (197) was utilized for operon prediction of the respective protein of interest according to the provider's instructions.

Prediction of signal sequences and transmembrane helices
Potential N-terminal signal sequences or transmembrane helices within the respective protein sequences were analyzed by the following online tools: LipoP 1.0 (198), LocTree 3 (199), Phobius (200), PrediSi (201), Psortb v3.0 (202), SignalP 4.1 (203) and TMHMM v. 2.0 (106).

Protein structure homology modeling
A three-dimensional structural model of protein PA3911 based on the human SCP-2 like domain (PDB code 1IKT) as a template was generated employing the SWISS-MODEL server (204).

Molecular visualization software
PyMOL (205) was used for the molecular visualization of three-dimensional protein structures and their structural superposition for the purpose of comparison.

3. Results and Discussion

3.1 Identification of A-PGS amino acids involved in tRNA interaction

The aminoacylation of PG by aaPGS enzymes represents a bacterial adaptation strategy to various stress conditions (42). For *P. aeruginosa* it was demonstrated that the transmembrane protein A-PGS catalyzes the transfer of alanine from the corresponding Ala-tRNA^{Ala} to a hydroxyl group of PG (1.2.1). Synthesis of the aminoacylated glycerophospholipid A-PG results in increased resistance of *P. aeruginosa* against e.g. antimicrobials and CAMPs (43, 48). Accordingly, the design of a specific A-PGS inhibitor was proposed as a promising strategy to disbalance lipid homeostasis and consequently to render *P. aeruginosa* more susceptible to antimicrobial compounds. To develop specific enzyme inhibitors, it is important to understand the molecular reaction mechanism in detail.

In the framework of a paper revision the question has been raised which surface-located A-PGS amino acids are involved in the interaction with the tRNA-cosubstrate. The subsequent part of this chapter solely refers to this isolated question to support the A-PGS investigation of Dr. S. Hebecker during her parental leave.

Based on an *in silico* model (figure 4) of the C-terminal catalytic domain of the A-PGS (including amino acids 543-881) and a tRNA molecule (PDB code 1TN1) amino acids Lys676, Asn683, Arg684 and Arg687 were proposed as key residues for the A-PGS/tRNA interaction. These amino acids are all located on α-helix 5 in van der Waals distance (except Asn683) from the already identified recognition elements of the tRNA^{Ala} acceptor stem (47).

In a site-directed mutagenesis approach these mainly positively charged amino acids were either exchanged against the small polar amino acid serine or a negatively charged amino acid (e.g. aspartic acid or glutamic acid). A-PGS$_{543-881}$ wild type and mutant proteins K676E, K676S, N683D, N683S, R684E, R684S and R687S were recombinantly produced in *E. coli*, purified *via* affinity chromatography and analyzed in a well-established *in vitro* A-PGS activity assay (47).

Therefore, the respective A-PGS protein variant was mixed with ATP, an ATP regenerating system, [1-^{14}C]-L-alanine and the crude cellular extract from *E. coli*

cells overproducing the alanyl-tRNA synthetase (2.9). This synthetase transfers ^{14}C-labeled alanine to the corresponding tRNA^{Ala} which is provided by the *E. coli* extract. The [1-^{14}C]-L-alanine moiety is subsequently transferred from the [1-^{14}C]-L-Ala-tRNA^{Ala} to a hydroxyl group of PG catalyzed by the purified A-PGS$_{543\text{-}881}$ protein variant. At distinct time points samples were taken from the reaction mixture, heat inactivated and subjected to lipid extraction (2.8.1). The incorporation of [1-^{14}C]-L-alanine into the lipid fraction by the formation of radioactively labeled A-PG was analyzed by scintillation counting (2.8.3). The *in vitro* activity of the wild type enzyme was set to 100% and all other activities were related to that.

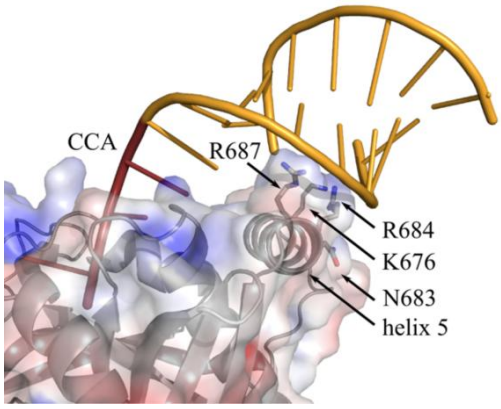

Figure 4: Model for the interaction of the catalytic domain of the A-PGS and a tRNA molecule (according to Hebecker *et al.* (2015) (57))
Based on the A-PGS/tRNA model potential amino acids involved in tRNA interaction were proposed. Amino acid substitution on positions Lys676, Arg684 and Arg687, which are located on helix 5 in van der Waals distance from the already identified recognition elements of the tRNA^{Ala} acceptor stem (47), resulted in impaired or abolished *in vitro* A-PGS activity.

The mutant proteins K676S, N683D, R684S and R687S resulted in impaired *in vitro* activities of 29 ± 8%, 11 ± 1%, 21 ± 1% and 13 ± 1%, respectively. A rather slight reduction of the *in vitro* activity to 71 ± 2% was determined for the N683S variant. By contrast, for K676E and R684E *in vitro* A-PGS activity was no longer detectable. These results indicate a potential tRNA interaction with amino acids Lys676, Arg684 and Arg687 of protein A-PGS$_{543\text{-}881}$. The outcome of the overall investigation is summarized in Hebecker *et al.* (2015) (57).

3.2 Towards the structure of protein A-PGH from *P. aeruginosa*

In a previous study protein PA0919 was identified as an A-PGH involved in the regulatory circuit of A-PG dependent lipid homeostasis in the membrane of *P. aeruginosa* (49). It was shown that the fine-tuning of the A-PG content plays an important role in the bacterial susceptibility to specific antimicrobial compounds. To gain insight into the underlying molecular principles of A-PG hydrolysis it was intended to elucidate the three-dimensional A-PGH structure by X-ray crystallography.

3.2.1 Production and purification of native A-PGH protein

For crystallization purposes protein A-PGH was recombinantly produced in *E. coli* BL21(λDE3) cells carrying plasmid pET22b(+)PA0919-Strep (2.6.1.1) and purified according to a well-established protocol (2.6.3.1) from Arendt *et al*. (2013) (49). Figure 5 presents the SDS-PAGE analysis of a typical A-PGH protein purification.

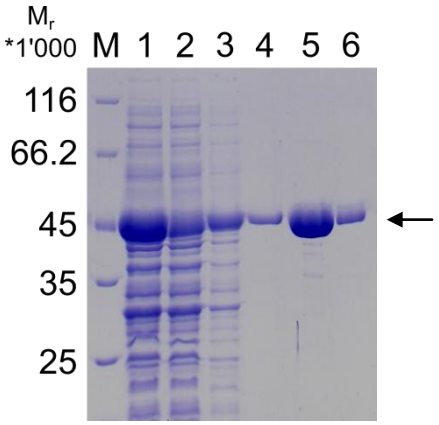

Figure 5: SDS-PAGE analysis of an A-PGH protein purification
Protein A-PGH was recombinantly produced in *E. coli* BL21(λDE3) cells and purified *via Strep*-tag® II affinity chromatography as described previously (49). Sample fractions were denatured with 2x SDS loading dye (95 °C, 10 min), subjected to SDS-PAGE analysis (12% (w/v) running gel) and proteins were visualized by Coomassie Brilliant Blue staining (2.7.2). An arrow indicates protein A-PGH with a calculated molecular weight of 44.6 kDa.
Lane M: Unstained Protein Molecular Weight Marker, relative molecular masses (*1'000) are indicated; Lane 1: 10 µl periplasmic fraction; Lane 2: 10 µl column flow-through; Lane 3: 10 µl washing step 1; Lane 4: 10 µl washing step 2; Lane 5: 2 µl elution fraction 1; Lane 6: 2 µl elution fraction 2.

The periplasmic fraction (lane 1) from *E. coli* cells overproducing protein A-PGH was isolated by polymyxin B treatment (2.6.2.1) and loaded onto *Strep*-Tactin®

resin for affinity chromatography (2.6.3.1). Unbound proteins ran through the column and remained in the flow-through fraction (lane 2). A reduction of the band intensity for the protein of interest in lane 2 compared to lane 1 indicates that a significant amount of the *Strep*II-tagged® protein was immobilized on the resin. Contaminating proteins were removed from the resin by extensive washing (lanes 3 and 4). Homogeneous A-PGH protein fractions (lanes 5 and 6) were eluted from the column by the addition of D-desthiobiotin. A typical purification yielded ~3 mg A-PGH protein from 1 l *E. coli* culture. Elution fractions were dialyzed for buffer exchange (2.6.4.1) and concentrated to 10 mg/ml (2.6.5) for subsequent crystallization experiments.

3.2.2 Production and purification of a selenomethionine derivative

Since no protein structure with sufficient homology to protein A-PGH was available, *de novo* phase determination methods had to be considered.

One possible approach is the derivatization of the protein with SeMet. Therefore, SeMet was incorporated into the protein instead of L(+)-methionine during heterologous protein production. This method is well-established to solve the phase problem and is made possible by selenium functioning as an anomalous scatterer. One major advantage of this technique is to obtain all the data required from one crystal without facing the problem of obtaining non-isomorphic crystals as commonly occurring during subsequent heavy atom incorporation (206). For a successful structure determination based on a multi-wavelength anomalous dispersion experiment approximately one selenomethionine residue is necessary per ~75-100 amino acids (207). The A-PGH protein (without signal sequence) is composed of 395 aa containing eight methionines which represents a promising starting point for the intended SeMet approach.

For the production of protein SeMet-A-PGH a protocol according to Heidler (2015) (150) with minor modifications (2.6.1.2) was used. Therefore, *E. coli* BL21(λDE3) cells carrying plasmid pET22b(+)PA0919-Strep were initially grown in LB medium. Media components of the rich medium were removed by extensive washing and cells were resuspended in minimal medium containing SeMet. Protein production was induced with IPTG and the cultivation was continued overnight. The typical result of a SeMet-A-PGH protein purification,

analyzed by SDS-PAGE, is depicted in figure 6.

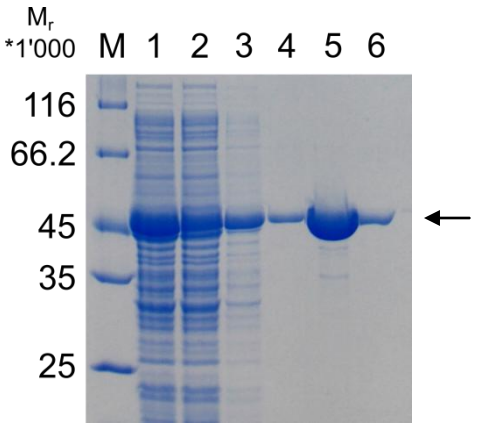

Figure 6: Analysis of the SeMet-A-PGH purification by SDS-PAGE
E. coli BL21(λDE3) cells were employed for the recombinant production of SeMet-A-PGH. The protein of interest was purified *via* its *Strep*-tag® II by affinity chromatography analogously to the native A-PGH protein. Sample fractions were denatured with 2x SDS loading dye (95 °C, 10 min), subjected to SDS-PAGE analysis (12% (w/v) running gel) and proteins were visualized by staining with InstantBlue™ (2.7.2).
Lane M: Unstained Protein Molecular Weight Marker, relative molecular masses (*1'000) are indicated; Lane 1: 10 µl periplasmic fraction; Lane 2: 10 µl column flow-through; Lane 3: 10 µl washing step 1; Lane 4: 10 µl washing step 2; Lane 5: 10 µl elution fraction 1; Lane 6: 10 µl elution fraction 2.

Harvested cells were disrupted by polymyxin B treatment (2.6.2.1) to release the periplasmic fraction (lane 1). *Strep*II-tagged® SeMet-A-PGH was purified from this cellular fraction by affinity chromatography using *Strep*-Tactin® resin (2.6.3.1) analogously to the native A-PGH protein. The flow-through fraction (lane 2) contained proteins that were not able to bind to the column material. The washing steps (lanes 3 and 4) allowed for the efficient removal of unbound proteins from the resin so that the resulting elution fractions (lanes 5 and 6) contained almost homogeneous SeMet-A-PGH protein. Approximately 1 mg protein was obtained from 1 l *E. coli* culture, corresponding to one-third of the yield obtained for the native A-PGH protein. For crystallization experiments the elution fractions were dialyzed (2.6.4.1) and concentrated to 10 mg/ml (2.6.5).
To determine the SeMet incorporation rate MALDI-TOF MS analysis (2.7.9) was performed by Dr. Manfred Nimtz (Helmholtz Centre for Infection Research, Braunschweig). An incorporation rate of ~80% was observed verifying efficient SeMet derivatization and also the successful export of SeMet-A-PGH protein into the periplasm of *E. coli*.

3.3 Thermal Shift Assays

For crystallization experiments protein stability is of great importance. A simple method for the determination of protein stability in different buffer systems and in the presence of additives represents the Thermal Shift Assay also referred to as Thermofluor Assay. In principle, the temperature increases during the measurement, the respective protein denatures and exposes its hydrophobic core to the environment. Thereupon the dye SYPRO® Orange induces an increase in fluorescence due to the binding to these hydrophobic regions. However, protein aggregation finally leads to the quenching of the fluorescence signal. Protein stability is determined in terms of the respective T_M, corresponding to the minimum of the negative first derivative of the melting curve (164).

Starting point for stability determination was the purified native A-PGH protein in dialysis buffer A (20 mM HEPES-NaOH pH 6.8) as utilized for *in vitro* activity assays in previous work (49). At first, different concentrations of protein (0.5, 1 or 2 mg/ml) and fluorescent dye (10x, 50x or 100x) were tested to identify optimal protein to dye ratios. The established conditions (2 mg/ml A-PGH protein and 100x SYPRO® Orange dye, data not shown) were employed for subsequent experiments. Protein stability was determined in several buffer systems containing 40 mM of the respective buffering compound and 0-400 mM NaCl covering a pH range from 4.0 to 9.4. The pH influence of selected buffer systems (40 mM buffering compound and 80 mM NaCl) on the T_M of protein A-PGH is shown exemplarily in figure 7.

The negative first derivatives of the melting curves for A-PGH in diverse buffer systems are plotted against the temperature. To compare protein stability the corresponding T_M values were determined represented by the minimum of each curve. The T_M in the original buffer condition (20 mM HEPES-NaOH pH 6.8) was 31 °C. A prominent decrease in the T_M of A-PGH was detected under acidic (e.g. acetate pH 4.4 / T_M = 26.5 °C) and in (slightly) alkaline (Tris pH 8.4 / T_M = 19 °C; CHES pH 9.4 / T_M = 15.5 °C) buffer systems. HEPES buffer pH 7.4 resulted in an almost similar T_M of 29.5 °C when compared to 31 °C in the original buffer. By contrast, MES buffer pH 6.4 and citrate buffer pH 5.4 significantly increased the T_M to 35 °C and 36 °C, respectively. According to these findings purified A-PGH protein was extensively dialyzed

(2.6.4.1) against dialysis buffer B (40 mM sodium citrate pH 5.4, 80 mM NaCl) prior to further crystallization experiments.

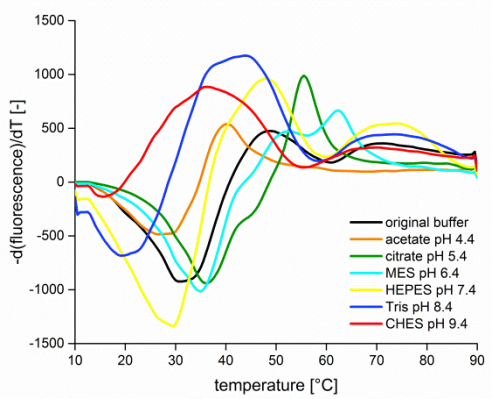

Figure 7: Graph for T_M determination of protein A-PGH in different buffer systems
A-PGH melting curves and the resulting T_M were determined *via* Thermal Shift Assay (2.7.8) with 2 mg/ml purified A-PGH protein in dialysis buffer A and 100x SYPRO® Orange in a temperature range of 10-90 °C. The depicted buffer systems contained 20 mM HEPES-NaOH pH 6.8 (original buffer) or 40 mM of the respective buffering compound and 80 mM NaCl covering a pH range from pH 4.4-9.4. T_M values were calculated using the CFX Manager program and the diagram was generated with the graphing software OriginPro.

3.4 Structure determination of protein A-PGH

3.4.1 Crystallization of native A-PGH

Freshly purified, dialyzed and concentrated A-PGH protein was utilized for initial screenings using commercially available NeXtal screens employing the sitting-drop vapor diffusion method in 96-well plates (2.14.1). For screening purposes different protein concentrations (5-20 mg/ml) as well as A-PGH protein mixtures in the presence of L-alanine or L-alanine amide were used and the experiments were incubated at 4 °C or 17 °C.

An overview of conditions in which protein crystals of native A-PGH were obtained is given in table 9. In general, protein crystals were obtained under conditions containing polyethylene glycol (PEG) with a molecular weight ranging from 3'350-20'000 g/mol. Crystal formation was documented and promising A-PGH crystallization conditions are depicted in figure 8.

Table 9: Crystallization conditions that produced native A-PGH protein crystals
Specifically highlighted (*) crystallization conditions derived from (135). 2,3-BD, (2R,3R)-(-)-2,3-butanediol; HEPES, 4-(2-hydroxyethyl)-1-piperazineethanesulfonic acid; MES, 2-(*N*-morpholino)ethanesulfonic acid; MPD, 2-methyl-2,4-pentanediol; N.D., not determined; PEG, polyethylene glycol; $Sm(NO_3)_3$, samarium nitrate.

NeXtal screen and number, crystallization condition	protein buffer	incubation temperature [°C]	time period for crystal formation, appearance	cryopro-tectant	diffraction limit using Cu Kα radiation	diffraction limit using synchrotron radiation	optimization in 24-well plates, hanging-drop vapor diffusion
JCSG Core Suite I No. 17, 0.1 M HEPES pH 7.5 20% (w/v) PEG 4'000 10% (v/v) isopropanol	dialysis buffer B or washing buffer A	4 (fig. 8 A and B), 17 (fig. 8 C)	2-8 weeks, cluster of rod-shaped crystals	-	~2.6 Å, complete data set collected	N.D.	HEPES pH 6.5-8.0, 4.5-12% isopropanol or 0-10% MPD, 4 °C, no suitable crystals
JCSG Core Suite II No. 51, 1.0 M Lithium chloride 0.1 M MES pH 6.0 20% (w/v) PEG 6'000	dialysis buffer B	4	4 months, lens-shaped	soaked with 10% (v/v) glycerol	~10 Å	N.D.	MES pH 5.5-7.0, 5-25% (w/v) PEG, 4 °C, no crystal improvement
JCSG Core Suite II No. 19, 0.2 M Lithium acetate 20% (w/v) PEG 3'350	dialysis buffer B	17	4 weeks, plate cluster	-	N.D.	N.D.	-
JCSG Core Suite II No. 40, 0.2 M Potassium sulfate 20% (w/v) PEG 3'350	dialysis buffer B	17	4 weeks, needle cluster	-	N.D.	N.D.	-
* JCSG Core Suite II No. 47, 0.1 M MES pH 6.5, 12% (w/v) PEG 20'000	washing buffer A	17	5 weeks, rhombohedral or rod-shaped	soaked with 10% (v/v) 2,3-BD and $Sm(NO_3)_3$	~2.0 Å, complete anomalous data set collected	1.64 Å, (DESY, Hamburg)	-
* JCSG Core Suite II No. 34, 0.1 M HEPES pH 6.5, 10% (w/v) PEG 6'000, final pH 7.0	washing buffer A	17	2 months, rhombohedral	soaked with 10% (v/v) 2,3-BD and $Sm(NO_3)_3$	~2.0 Å	N.D.	-

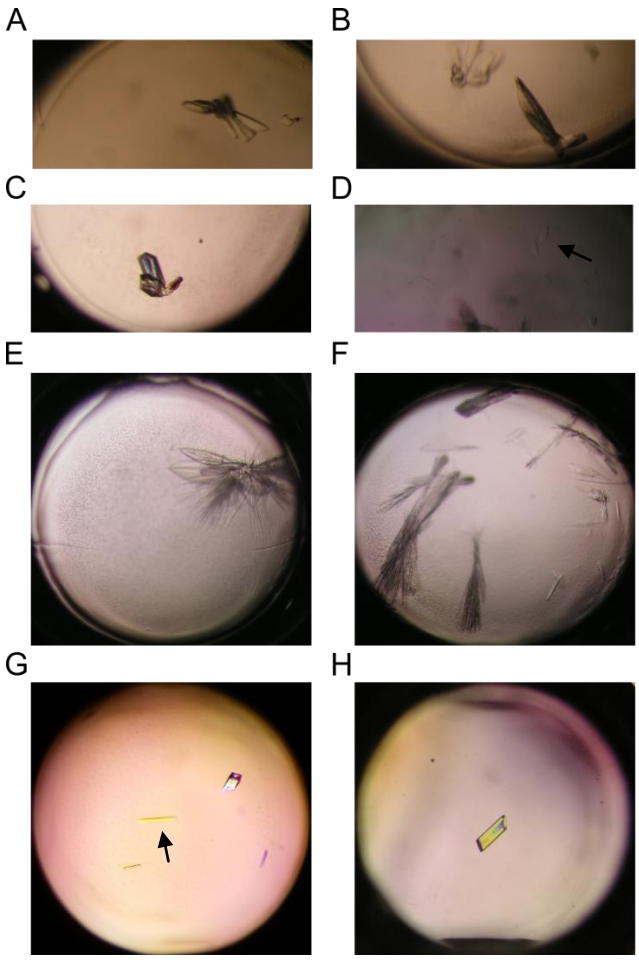

Figure 8: A-PGH crystals obtained under different crystallization conditions
A: Crystal screen JCSG Core Suite I (0.1 M HEPES pH 7.5, 20% (w/v) PEG 4'000, 10% (v/v) isopropanol), 10 mg/ml A-PGH protein in dialysis buffer B, crystals were obtained within 14 days. **B:** Crystal screen JCSG Core Suite I (0.1 M HEPES pH 7.5, 20% (w/v) PEG 4'000, 10% (v/v) isopropanol), 10 mg/ml A-PGH protein in dialysis buffer B containing 5 mM L-alanine, crystals were obtained within 14 days. **C:** Crystal screen JCSG Core Suite I (0.1 M HEPES pH 7.5, 20% (w/v) PEG 4'000, 10% (v/v) isopropanol), 10 mg/ml A-PGH protein in washing buffer A, crystals were obtained within eight weeks (135). **D:** Crystal screen JCSG Core Suite II (1.0 M Lithium chloride, 0.1 MES pH 6.0, 20% (w/v) PEG 6'000), 10 mg/ml A-PGH protein in dialysis buffer B, crystals (indicated by an arrow) were obtained within four months. **E:** Crystal screen JCSG Core Suite II (0.2 M Lithium acetate, 20% (w/v) PEG 3'350), 20 mg/ml A-PGH protein in dialysis buffer B, crystals were obtained within four weeks. **F:** Crystal screen JCSG Core Suite II (0.2 M Potassium sulfate, 20% (w/v) PEG 3'350), 20 mg/ml A-PGH protein in dialysis buffer B, crystals were obtained within four weeks. **G:** Crystal screen JCSG Core Suite II (0.1 M MES pH 6.5, 12% (w/v) PEG 20'000), 10 mg/ml A-PGH protein in washing buffer A containing 5 mM L-alanine amide, crystals were obtained within five weeks (135). **H:** Crystal screen JCSG Core Suite II (0.1 M HEPES pH 6.5, 10% (w/v) PEG 6'000, final pH 7.0), 10 mg/ml A-PGH protein in washing buffer A, crystal was obtained within two months (135).

3.4.2 Crystallization of SeMet-A-PGH

Screenings for crystallization conditions were performed with freshly purified, dialyzed and concentrated SeMet-A-PGH protein as described for the native protein (3.4.1).

Table 10: Crystallization conditions resulting in SeMet-A-PGH crystals
MES, 2-(*N*-morpholino)ethanesulfonic acid; MPD, 2-methyl-2,4-pentanediol; N.D., not determined; PEG, polyethylene glycol; SLS, Swiss Light Source.

NeXtal screen and number, crystallization condition	protein buffer	incubation temperature [°C]	time period for crystal formation, appearance	cryoprotectant	diffraction limit using Cu Kα radiation	diffraction limit using synchrotron radiation
optimization of JCSG Core Suite II, No. 51, 1.0 M Lithium chloride 0.1 M MES pH 6.5 20% (w/v) PEG 6'000	dialysis buffer B	4	2 weeks, needle cluster or lens-shaped	soaked with 5% (v/v) glycerol	~10 Å	N.D.
JCSG Core Suite I, No. 43, 0.2 M di-Ammonium tartrate 20% (w/v) PEG 3'350	dialysis buffer B	17	3 months, cluster of rod-shaped crystals	soaked with 10% (v/v) glycerol	~3.3 Å	~3.0 Å (SLS, Villigen, Switzerland)
Cryos Suite, No. 90, 0.17 M Sodium acetate 0.085 M Tris-HCl pH 8.5 25.5% (w/v) PEG 4'000 15% (v/v) glycerol	dialysis buffer B	4	4 days, plates	-	N.D.	~2.8 Å (SLS, Villigen, Switzerland)

Similar to the native A-PGH protein, crystals were obtained under conditions (table 10) containing different PEG variants (3'350-6'000 g/mol). Conditions were regularly monitored for crystal formation and potential SeMet-A-PGH crystals, shown in figure 9, were documented. For SeMet-A-PGH crystals from conditions JCSG Core Suite I No. 43 and Cryos Suite No. 90 complete data sets were collected at the synchrotron SLS (Villigen, Switzerland) by Dr. Jörn Krauße (Helmholtz Centre for Infection Research, Braunschweig). However, the data quality was not sufficient to solve the phase problem.

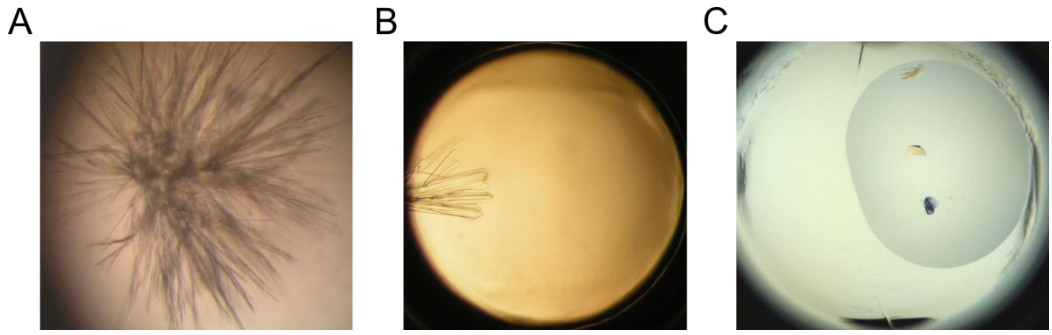

Figure 9: SeMet-A-PGH crystals grown under different crystallization conditions
A: Optimization of No. 51 from crystal screen JCSG Core Suite II (1.0 M Lithium chloride, 0.1 M MES pH 6.5, 20% (w/v) PEG 6'000), 10 mg/ml SeMet-A-PGH protein in dialysis buffer B containing 5 mM L-alanine, crystals were obtained within two weeks. **B:** Crystal screen JCSG Core Suite I (0.2 M di-Ammonium tartrate, 20% (w/v) PEG 3'350), 10 mg/ml SeMet-A-PGH protein in dialysis buffer B containing 5 mM L-alanine amide, crystals were obtained within three months. **C:** Crystal screen Cryos Suite (0.17 M Sodium acetate, 0.085 M Tris-HCl pH 8.5, 25.5% (w/v) PEG 4'000, 15% (v/v) glycerol), 10 mg/ml SeMet-A-PGH protein in dialysis buffer B, crystals were obtained within four days.

3.4.3 Soaking of native A-PGH crystals with heavy metals

Given that structure solution based on SeMet-A-PGH crystals was not successful another *de novo* phase determination method was carried out. For this purpose, native A-PGH crystals were soaked with heavy metals. The binding of heavy metal atoms to specific positions within the protein crystal results in intensity changes in the diffraction pattern which allow for phase determination, for example by using the SAD method.

To generate heavy metal derivatives the rhombohedral A-PGH crystals from conditions No. 34 and 47 from JCSG Core Suite II (3.4.1) were soaked in the respective reservoir solution containing 10% (v/v) (2R,3R)-(-)-2,3-butanediol as a cryoprotectant and 66 mM $Sm(NO_3)_3$ as a heavy metal (2.14.2). The crystals diffracted up to 2.0 Å at the home source and a complete anomalous data set was recorded for one crystal from condition No. 47 (figure 8 G). For the same crystal a complete native data set with a maximal resolution limit of 1.64 Å was recorded by Dr. Jörn Kraußе (Helmholtz Centre for Infection Research, Braunschweig) at beamline P11 at the PETRA III synchrotron (Hamburg, Germany). These data sets (native and anomalous) allowed for the three-dimensional structure elucidation using the SAD approach.

3.4.4 Structure determination, refinement and validation

Processing of collected data and structure determination were performed by Dr. Jörn Krauße (Helmholtz Centre for Infection Research, Braunschweig). The observed reflections (native and anomalous data set) of a crystal from condition No. 47 of the JCSG Core Suite II (3.4.3) were indexed and scaled using the *XDS* package (182, 183). The crystal belonged to the body centered orthorhombic space group I222 (No. 23) with unit cell dimensions a = 67.85 Å, b = 72.76 Å and c = 76.42 Å and according angles α = β = γ = 90° (table 11).

The number of molecules per asymmetric unit was estimated by the determination of the Matthews coefficient (208), ranging from 1.68-3.53 Å³/Da for proteins, using the Matthews Probability Calculator (189). Assuming one A-PGH protein per asymmetric unit an unusual Matthews's coefficient of 1.06 Å³/Da was obtained. Accordingly, it was hypothesized that the full-length A-PGH protein cannot be crystallized within these unit cell dimensions.

The three-dimensional structure of protein A-PGH was determined by SAD phasing. For this purpose, a data set was collected at the home source at λ = 1.541 Å. This wavelength is in close proximity to the absorption edges of samarium's L shell (L-I: 1.6025 Å, L-II: 1.6957 Å, L-III: 1.8460 Å) resulting in a data set with Bijvoet differences significantly different from zero and so applicable to solve the phase problem. The resolution limit of the recorded data set is d_{min} = 2.03 Å. This initial data set was sufficient for the localization of the heavy metal sites, the computation of a first electron density map and the building of an initial polyalanine model with ShelxC/D/E (184). A native data set recorded at beamline P11 (DESY, Hamburg) contained information of higher resolution (d_{min} = 1.64 Å). The high-resolution structure of A-PGH was determined by molecular replacement using the polyalanine model as a search template. Subsequent to iterative cycles of manual model building in COOT (185) and refinement in PHENIX (186) the final structural model contained amino acids 34-215 of protein A-PGH. The data collection statistics are summarized in table 11.

Thorough investigation of the calculated electron density map revealed that the C-terminal part of protein A-PGH is not traceable in the obtained electron density and thus it was concluded that the protein A-PGH was proteolytically degraded prior to the crystallization process. SDS-PAGE analyses confirmed

that crystallization plates were set up with a solution containing the native A-PGH protein, whereas samples of crystal-containing drops from different conditions only revealed the presence of a ~20 kDa protein corresponding to the N-terminal part of protein A-PGH (135). Recalculation of the Matthews coefficient with the N-terminal part of protein A-PGH (amino acids 34-215) resulted in a reasonable Matthews value of 2.38 Å³/Da in the presence of one molecule per asymmetric unit with a solvent content of 48.44%, which is within the expected range of 27-65% for protein crystals (208).

Table 11: Data collection and processing parameters of A-PGH$_{34-215}$

‡R_{merge} = $\frac{\sum_{hkl}\sum_{i=1}^{n}|I_{hkl,i}-\langle I_{hkl}\rangle|}{\sum_{hkl}\sum_{i=1}^{n}I_{hkl,i}}$; n, number of independent measurements; $I_{hkl,i}$, intensity of a reflection; $\langle I_{hkl}\rangle$, average of symmetry-related observations of a unique reflection. *R_{meas} = $\frac{\sum_{hkl}\sqrt{\frac{n}{n-1}}\sum_{i=1}^{n}|I_{hkl,i}-\langle I_{hkl}\rangle|}{\sum_{hkl}\sum_{i=1}^{n}I_{hkl,i}}$. †Fraction of correlation between intensities from random half-datasets (209). Values in parentheses are for the highest-resolution shell. No., number.

Data set A-PGH$_{34-215}$	**anomalous**	**native**
Data collection		
Beamline	MicroMax™-007 HF, HZI (Braunschweig)	PETRA III P11 DESY (Hamburg)
Temperature [K]	100	100
Wavelength [Å]	1.541 Å	1.008 Å
Data processing		
Resolution range, d_{max}-d_{min} [Å]	30.260-2.034 (2.106-2.034)	19.940-1.640 (1.699-1.640)
Space group	I222	
Unit cell dimensions [Å]	a = 67.85, b = 72.76, c = 76.42	
Angles [°]	α = β = γ = 90°	
No. of observed reflections	254’908 (16’716)	287’711 (28’829)
No. of unique reflections	12’368 (1’133)	22’888 (2’313)
Multiplicity	20.6 (14.7)	12.6 (12.5)
Completeness	0.95 (0.93)	0.97 (0.99)
Mean I/σ(I)	35.74 (5.98)	24.96 (2.14)
Wilson *B*-factor [Å²]	23.38	22.60
R_{merge}‡	0.0888 (0.5343)	0.0624 (1.2900)
R_{meas}*	0.0910 (0.5536)	0.0651 (1.3440)
$CC_{(1/2)}$†	0.999 (0.946)	1.000 (0.843)

To validate refined three-dimensional protein structures the crystallographic R-factors R_{work} and R_{free} (210) are determined. R_{work} represents a measure of consistency between the X-ray diffraction data and the constructed crystallographic model. R_{free} is calculated analogously to R_{work} only utilizing a defined amount (usually 5%) of the reflections from the data set for calculation.

This so-called 'test set' is excluded from the refinement process and determination of R_{free} allows for the estimation of over-interpretation of the data. For the refined structure of A-PGH_{34-215} (see table 12 for statistics) R_{work} and R_{free} were determined to be 21.04% and 23.36%, respectively. The rmsd of bond lengths and bond angles of the refined model differ by 0.01 Å and 1.07° from ideal geometry.

The temperature factor, also referred to as Debye-Waller factor or *B*-factor, is a measure to quantify the uncertainty of atom positions within a protein crystal (211, 212). Particularly rigid parts in the protein (e.g. α-helices) exhibit low *B*-factors compared to flexible regions (e.g. loops) with considerably higher *B*-factors. For the refined structure of A-PGH_{34-215} an average *B*-factor of 33.05 Å² was determined.

Table 12: Refinement statistics

*$R_{work} = \frac{\sum_{hkl} ||F_o|-|F_c||}{\sum_{hkl} |F_o|}$; $|F_o|$, structure factor magnitudes observed; $|F_c|$, structure factors calculated. §R_{free} is computed as R_{work} but using 5% randomly assigned reflections excluded from refinement. Values in parentheses are for the highest-resolution shell. No., number; Rmsd, Root-mean-square deviation.

Data set A-PGH_{34-215}	**native**
No. of reflections	
In refinement	22'846 (2'313)
For R_{free}	1'145 (116)
Refinement	
R_{work}* [%]	21.04 (27.52)
R_{free}§ [%]	23.36 (30.37)
No. of non-hydrogen atoms per asymmetric unit	
Total	1'479
Protein	1'391
Ligands	3
No. of molecules per asymmetric unit	
Protein	1
Water	68
Additional molecules (Sm^{3+})	3
Atomic displacement factor *B*	
Average *B* [Å²]	33.05
Rmsd from ideal geometry	
Bond lengths [Å]	0.01
Bond angles [°]	1.07
Ramachandran statistics	
Favored [%]	98.4
Allowed [%]	1.6
Disallowed [%]	0.0

Further validation of the final structure model was performed by calculating the Ramachandran plot (213) with the MolProbity analysis tool (188). In these plots the backbone torsion angles Psi (ψ, C_α-C bond) and Phi (φ, N-C_α bond) are plotted against each other thereby displaying the statistical distribution of combinations from these dihedral angles. The plot visualizes the occurrence of secondary structures which cluster around average φ and ψ torsion angles: -60° and -45° for common right-handed α-helices, +60° and +45° for rare left-handed α-helices and -135° and +135° for β-sheets.

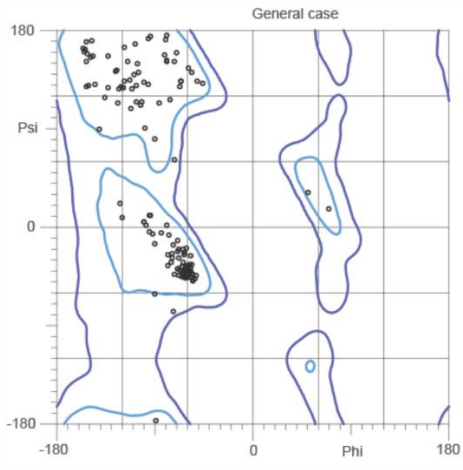

Figure 10: Ramachandran plot of the refined A-PGH$_{34\text{-}215}$ structure
In the Ramachandran plot computed by the MolProbity analysis tool (2.14.4) the torsion angle ψ is plotted against the torsion angle φ. Outer contours in light blue define favored regions, whereas dark blue lines border allowed regions. Residual areas belong to the disallowed regions. The Ramachandran plot of all residues, except proline and glycine, shows that most of the residues (98.4%) are in the favored region and only a minor part (1.6%) is in the allowed region. No outliers were identified.

Glycine residues are an exception from clustering around the α-helix and β-sheet regions. Because of their missing side chain they are highly flexible in the polypeptide chain and can adopt normally forbidden rotation angles.

The Ramachandran plot can be consulted for quality control of the determined structure. In figure 10 the respective Ramachandran plot for the general case (except proline and glycine residues) of the refined A-PGH$_{34\text{-}215}$ structure is presented. 98.4% of the ψ/φ torsion angle combinations are in the favored and 1.6% in the allowed regions. No outliers were identified in the refined structure. Ramachandran statistics taken together with determined R-factors verified the appropriate fitting of the structure into the electron density.

3.4.5 Structure description

The three-dimensional structure of A-PGH$_{34-215}$ consists of a central eight stranded β-sheet in strand order 12435678 with the second β-strand being antiparallel to the others. The topology is depicted in figure 11 and the amino acids of each secondary structural element are indicated.

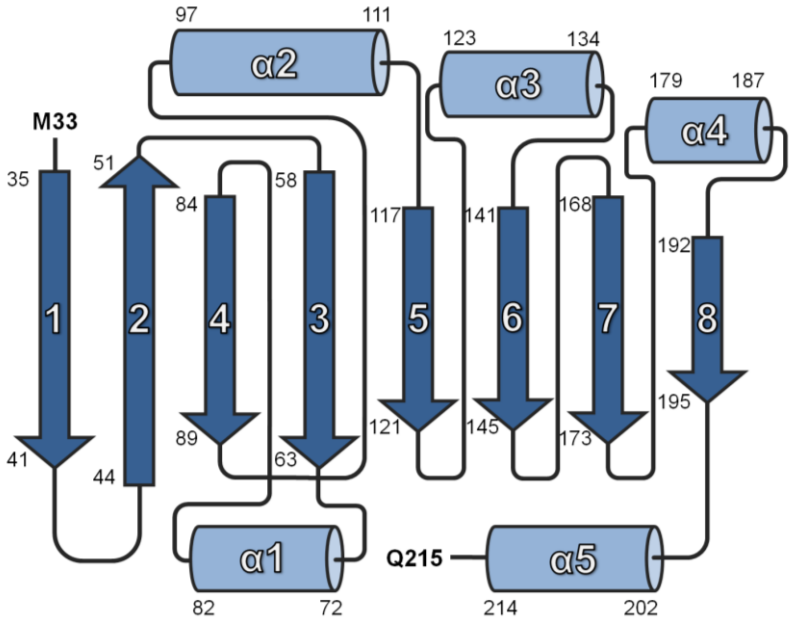

Figure 11: Topology diagram of A-PGH$_{34-215}$
Helices are depicted as cylinders (light blue) and β-strands as arrows (dark blue). The amino acids of each secondary structural element are indicated.

The three-dimensional structure (figure 12) shows a highly twisted β-sheet so that the first and last strands are orthogonal to one another. Furthermore, it is surrounded by five α-helices which connect strands β_3, β_4, β_5 and β_6 as well as β_7 and β_8. Helices α_1 and α_5 are located on one side, whereas helices α_2, α_3 and α_4 are located on the opposite side of the β-sheet. A disulfide bridge is formed by amino acids Cys97 and Cys156, thereby connecting helix α_2 and the loop between strands β_6 and β_7. Three samarium ions of the heavy atom derivative are located in van der Waals distance to the negatively charged amino acids Asp136, Asp148 and Asp197, respectively.

B-factor analysis (figure 13 A) revealed that the majority of protein atoms exhibit low *B*-factors indicating a well-ordered structure. Elevated *B*-factors were determined at the terminal ends (Met33 and Gln215) due to high flexibility.

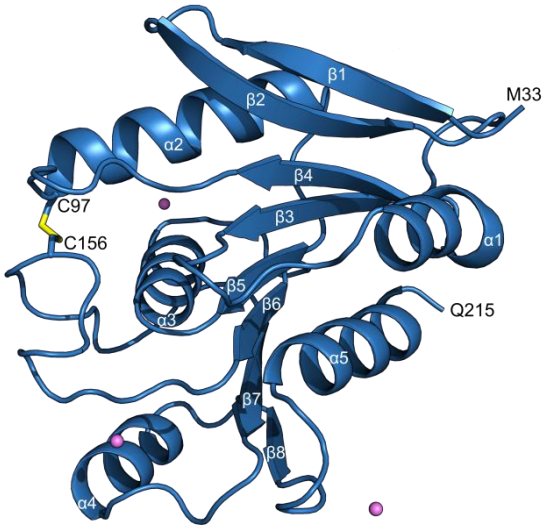

Figure 12: Cartoon model of the N-terminal part of protein A-PGH from *P. aeruginosa*
The N-terminal part of protein A-PGH consisting of amino acids 34-215 (based on the native A-PGH protein sequence) is composed of a central eight stranded β-sheet which is surrounded by five α-helices. Disulfide bridge formation occurs between amino acids Cys97 and Cys156. Samarium ions of the heavy atom derivative are presented as violet spheres.

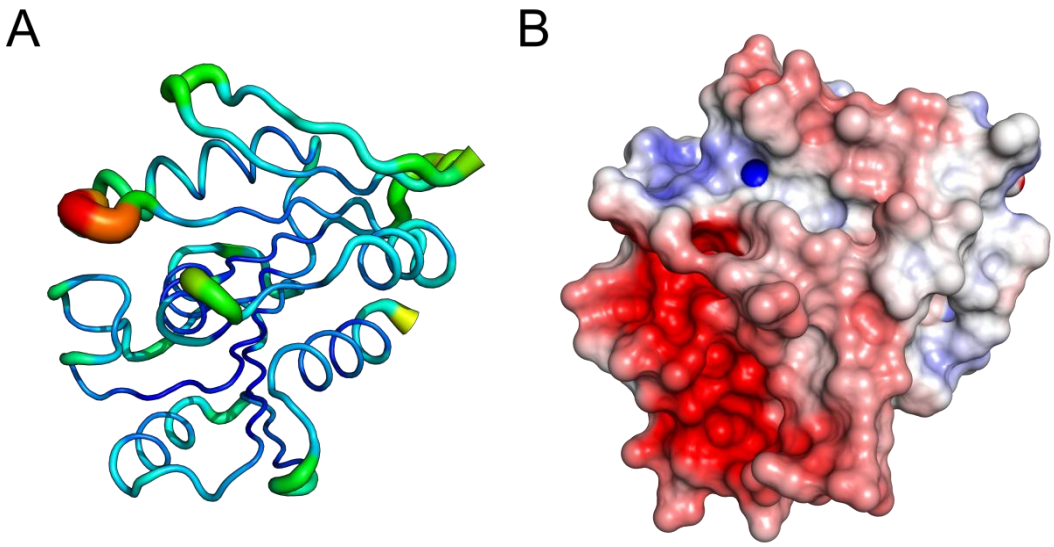

Figure 13: Presentation of the *B*-factor distribution (A) and the electrostatic surface potential (B) of A-PGH$_{34-215}$
A: The *B*-factors are visualized by color, displaying low (blue), medium (green) and high (red) *B*-factor values. Large structure parts exhibit low *B*-factors, especially the α-helices and β-strands, whereas the terminal ends and some loop regions display medium to high *B*-factors. The protein structure orientation is equivalent to figure 12. **B:** The electrostatic surface potential was computed by APBS v1.4 (192). Negatively charged regions of A-PGH$_{34-215}$ are colored in red, whereas positively charged regions are presented in blue (± 6 k_BT). Neutrally charged regions are shown in white. The protein structure is oriented according to figure 12.

Besides this, high *B*-factors were determined for amino acids Glu93, Asn94 and Gly95 in the loop region between the secondary structure elements β_4 and α_2. The electrostatic surface potential was calculated by APBS v1.4 (192) and the corresponding depiction of the surface is presented in figure 13 B. In general, several charged amino acids are distributed within the protein and generate locally positive or negative surface potentials. Remarkably, the protein exhibits one region with a highly negative electrostatic surface potential (colored in red) primarily caused by the amino acids aspartic acid and glutamic acid (mainly Glu93, Asp148, Glu153, Asp175 and Asp178). Although the three-dimensional structure of the C-terminal part of protein A-PGH and its spatial arrangement related to the N-terminal part is not known this region of highly negative electrostatic surface potential might be involved in protein-substrate or protein-protein interaction.

3.5 Dali search

In previous work, the key catalytic residues Ser307 and His401 located on the C-terminal part of protein A-PGH were characterized (49). However, for the N-terminal part no biochemical function is assigned and so a structure-based search for homologs by the Dali web server (193) was conducted. The structural alignment performed with protein structures already deposited in the PDB is based on the distance alignment matrix method (194).

The obtained results allow for the identification of homologous structures based on structural similarity specified *via* Z-scores. A Z-score above two corresponds to ‘significant similarities’ and usually similar folds. ‘Strong matches’ are defined as exhibiting sequence identities above 20% or a Z-score exceeding a specific cut-off based on the protein size (193). Furthermore, key residues or functional sites of a new structure might be identified due to conserved residues that might point towards a potential molecular function (214).

In general, the Dali search resulted in 967 PDB entries exceeding a Z-score of 2.0 and thus implicating a similar fold. The obtained results display low sequence identities (< 20%) to the query structure and the maximum Z-score reached a value of 16.8. Numerous matches are hydrolases or esterases catalyzing reactions with varying substrates. Detailed sequence comparison did not reveal any conservation of key residues in the structure of A-$PGH_{34\text{-}215}$. The

top six results for protein A-PGH are ranked according to Z-scores in table 13.

Table 13: List of Dali search results for the query structure A-PGH$_{34-215}$
Obtained results are ordered by decreasing Z-scores which correlate with the structural similarity between the query and the respective PDB structure. No., number; PDB ID, Protein Data Bank identification code.

No.	PDB ID-Chain	Z-score	total No. of aligned residues	sequence identity [%]	description
1	3QIT-A	16.8	172	14	thioesterase
2	5CML-A	16.6	172	12	OsmC domain carboxyl esterase
3	3F67-A	15.8	173	13	putative dienelactone hydrolase
4	3KXP-I	15.7	167	8	2-(acetamidomethylene) succinate hydrolase
5	3QM1-A	15.7	171	11	cinnamoyl esterase
6	4AO7-A	15.1	173	10	cold-adapted esterase

These structures, deposited under PDB IDs 3QIT (215), 5CML (216), 3F67 (unpublished), 3KXP (217), 3QM1 (218) and 4AO7 (219), all exhibit an α/β hydrolase fold that typically consists of eight β-strands connected by six α-helices (220).

Referring to the conserved structural core presented in Carr and Ollis (2009) (221), α-helix D (between strands β_6 and β_7) is replaced by an extended loop region in protein A-PGH$_{34-215}$. Furthermore, the catalytically active Ser-His-Asp residues of structures 3QIT, 5CML, 3KXP, 3QM1 and 4AO7 or Cys-His-Asp residues of structure 3F67 are not conserved in the structure of the A-PGH fragment. These proteins all contain a subdomain, putatively modulating the accessibility of the active site, which is not present in the structure of A-PGH$_{34-215}$. However, structural alignments show that these subdomains are located in the region of the highly negatively charged patch of A-PGH$_{34-215}$ which also includes several flexible residues showing high *B*-factors (3.4.5).

3.6 Strategies to solve the structure of the C-terminal part of A-PGH

As described in section 3.4 the three-dimensional structure of A-PGH$_{34-215}$ (N-terminal part) was successfully resolved but the obtained crystals from native or SeMet-A-PGH protein did not allow for the structure determination of the full-length protein. Accordingly, alternative strategies had to be pursued. On the

one hand crystallization experiments with a truncated A-PGH variant containing only the C-terminal part were performed; on the other hand the SER approach (156) was applied to improve the crystallizability of the native A-PGH protein.

3.6.1 Production and purification of the C-terminal part of protein A-PGH or mutant variants

To crystallize the sole C-terminal part of protein A-PGH a truncated variant (A-PGH$_{trunc}$) containing amino acids 203-427 was recombinantly produced in *E. coli* BL21(λDE3) cells (2.6.1.1) carrying plasmid pET22b(+)PA0919$_{trunc}$-Strep (135).

Protein sequence analysis using the SERp web server (156) indicated that replacing amino acid residues Glu378, Glu379 and Lys380 (numbered according to the native A-PGH sequence) by alanine could significantly improve the crystallizability of protein A-PGH. Based on this theoretical analysis the proposed cluster was mutated for A-PGH$_{trunc}$ either into Glu176Ala and Glu177Ala or into Glu176Ala, Glu177Ala and Lys178Ala (numbered according to the A-PGH$_{trunc}$ sequence).

The two variants were produced analogously to protein A-PGH$_{trunc}$ in *E. coli* BL21(λDE3) cells carrying the plasmid pET22b(+)PA0919$_{trunc}$-Strep/AAK or pET22b(+)PA0919$_{trunc}$-Strep/AAA (2.6.1.1), respectively. The purification procedure (2.6.3.1) was adopted from Arendt *et al*. (2013) (49). A representative SDS-PAGE analysis of an A-PGH$_{trunc}$ protein purification is shown in figure 14.

The A-PGH$_{trunc}$ protein or mutant variants were isolated from the periplasmic fraction (lane 1) of the respective *E. coli* strain which was obtained by polymyxin B treatment (2.6.2.1). This fraction was utilized for affinity chromatography using *Strep*-Tactin® resin (2.6.3.1). Significant amounts of A-PGH$_{trunc}$ protein were immobilized as indicated by an obvious intensity reduction of the respective protein band in the column flow-through (lane 2). Extensive washing steps (lanes 3 and 4) efficiently removed unbound proteins so that almost homogeneous A-PGH$_{trunc}$ protein fractions (lanes 5 and 6) were eluted using D-desthiobiotin. Approximately 3 mg A-PGH$_{trunc}$ protein or 2 mg A-PGH$_{trunc}$-AAK or A-PGH$_{trunc}$-AAA protein were obtained from 1 l *E. coli* culture. Elution fractions were dialyzed (2.6.4.1), concentrated to 10 mg/ml

(2.6.5) and applied for crystallization experiments. For protein purifications of A-PGH$_{trunc}$-AAK and A-PGH$_{trunc}$-AAA similar SDS-PAGE results were obtained, however the protein yields were slightly decreased when compared to protein A-PGH$_{trunc.}$

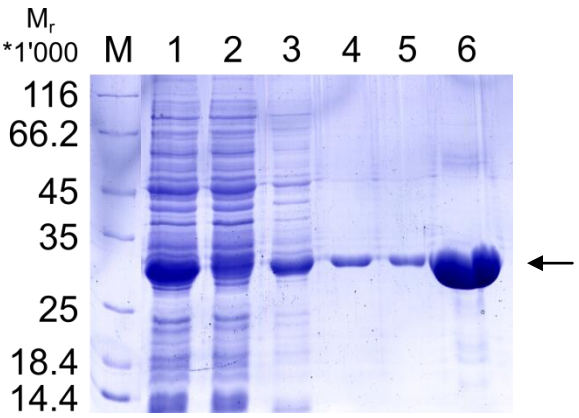

Figure 14: SDS-PAGE analysis of an A-PGH$_{trunc}$ protein purification
Protein A-PGH$_{trunc}$ was recombinantly produced in *E. coli* BL21(λDE3) cells and purified *via Strep*-tag® II affinity chromatography analogously to the native A-PGH protein. Sample fractions were denatured with 2x SDS loading dye (95 °C, 10 min), subjected to SDS-PAGE analysis (12% (w/v) running gel) and proteins were visualized by staining with InstantBlue™ (2.7.2) (135). An arrow indicates protein A-PGH$_{trunc}$ with a calculated molecular weight of 26.4 kDa.
Lane M: Unstained Protein Molecular Weight Marker, relative molecular masses (*1'000) are indicated; Lane 1: 10 µl periplasmic fraction; Lane 2: 10 µl column flow-through; Lane 3: 10 µl washing step 1; Lane 4: 10 µl washing step 2; Lane 5: 10 µl elution fraction 1; Lane 6: 10 µl elution fraction 2.

The truncated A-PGH protein version was initially characterized by the determination of the relative molecular mass and the oligomeric state by analytical GPC (2.7.6) using a Superdex™ 200 Increase 5/150 GL chromatography column (135). Considering the elution volumes of A-PGH$_{trunc}$ and standard proteins employed for calibration a relative molecular mass of 28'000 was determined (see appendix figure 31). Comparison of the experimental result with the calculated molecular mass of 26.4 kDa indicated that A-PGH$_{trunc}$ exhibits a monomeric architecture under the employed conditions. Additionally, the elution profile indicated an almost homogeneous protein fraction which is a good prerequisite for subsequent crystallization attempts.

3.6.2 Crystallization experiments for protein A-PGH$_{trunc}$ or mutant variants

Initial screenings for crystal formation employing the sitting-drop vapor diffusion method in 96-well plates (2.14.1) were performed with freshly purified, dialyzed (against washing buffer A) and concentrated A-PGH$_{trunc}$, A-PGH$_{trunc}$-AAK or A-PGH$_{trunc}$-AAA protein. Therefore, the commercially available NeXtal screens were utilized and protein concentrations ranging from 5-10 mg/ml were employed for A-PGH$_{trunc}$, A-PGH$_{trunc}$-AAK and A-PGH$_{trunc}$-AAA. Crystal plates were set up manually and incubated at 17 °C.

For protein A-PGH$_{trunc}$ either pyramid- or rod-shaped crystals were obtained after 4 days in the Cryos Suite in condition No. 23 (0.085 M Tris pH 8.5, 21.25% (v/v) tert-butanol, 15% (v/v) glycerol) and No. 35 (0.85 M imidazole pH 7.0, 15% (v/v) glycerol) using a protein concentration of 10 mg/ml. However, initial X-ray diffraction analyses at the home source clearly indicated the presence of salt crystals (135). By contrast, protein solutions of A-PGH$_{trunc}$-AAK and A-PGH$_{trunc}$-AAA tended to precipitate at concentrations above 7.5 mg/ml and yielded no crystals in the employed NeXtal screens PEGs Suite and JCSG+ Suite. Within the framework of this study no crystallization condition(s) for protein A-PGH$_{trunc}$ or mutant variants were identified.

3.7 Determination of the A-PGH solution structure by small-angle X-ray scattering

Since the three-dimensional structure of the full-length A-PGH protein could not be obtained by X-ray crystallography in the present study a low-resolution model for protein A-PGH was determined by SAXS. This method can provide complementary information to high-resolution techniques concerning the shape, conformation and interaction of biological macromolecules in solution (222).

For SAXS experiments protein A-PGH was purified (2.6.3.1), dialyzed (2.6.4.1) and dilute solutions in a defined concentration range were prepared (2.7.10). Sample measurement at the ESRF in Grenoble, data analysis and building of the low-resolution model were performed by Dr. Jörn Kraußе (Helmholtz Centre for Infection Research, Braunschweig).

The obtained low-resolution envelope possesses an elongated shape with a protrusion which is visible in the right half of figure 15. Furthermore, a potential arrangement of the N- and C-terminal part of protein A-PGH is indicated. If the

three-dimensional structure of the C-terminal part of A-PGH is obtained by X-ray crystallography, this A-PGH solution structure will provide information about how the N- and C-terminal part are spatially arranged within the protein.

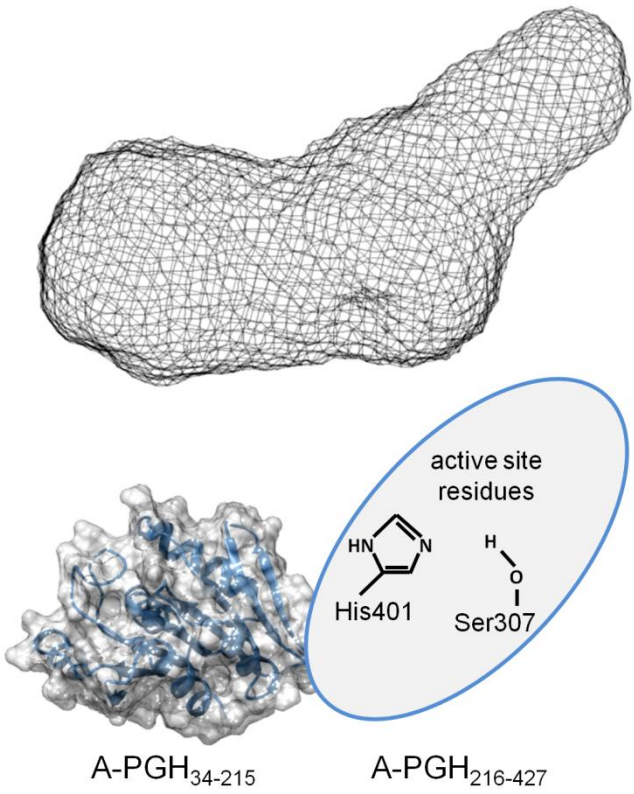

Figure 15: Solution structure of protein A-PGH
Experimental SAXS data obtained from a soluble A-PGH sample was used to generate a representative *ab initio* model using the ATSAS program package (168). A potential arrangement of the N- and C-terminal part of protein A-PGH is indicated.

3.8 Role of AcvB and VirJ in the lipid homeostasis of *A. tumefaciens*

3.8.1 AcvB and VirJ are A-PGH homologs

Only recently, the fine-tuning of cellular A-PG concentrations in *P. aeruginosa* by an A-PGS (PA0920)/A-PGH (PA0919) system (43, 47, 57, 49) was investigated in our laboratory. Sequence comparison, operon prediction and cluster analysis identified homologous PA0920 and PA0919 orfs for several Gram-negative bacteria, e.g. *A. tumefaciens*, *B. phymatum*, *R. pickettii* and *R. tropici* (49).

In *A. tumefaciens* orfs Atu2521 (*lpiA*) and Atu2522 (*acvB*) were identified as PA0920 and PA0919 homologs, respectively. Strains containing an octopine-type Ti-plasmid possess with *virJ* a non-chromosomal, paralogous version of *acvB*. VirJ equates the C-terminal part of AcvB and shows a sequence identity of 52% (61). In the literature a potential function of VirJ and AcvB as periplasmic chaperones involved in the translocation of T-DNA and effector proteins into the plant cell (64, 65) was proposed. Furthermore, it was demonstrated that AcvB is essential for *A. tumefaciens* virulence (60). However, a direct function of AcvB and VirJ has not been elucidated to date.

Comparison of the AcvB and VirJ protein sequences with protein A-PGH (see appendix figure 33) clearly indicates that the catalytically relevant active site residues Ser307 and His401 of protein A-PGH (49) are conserved, pointing towards a potential role of AcvB and VirJ in L-PG hydrolysis and thus in lipid homeostasis of *A. tumefaciens*.

3.8.2 Production and purification of AcvB variants and VirJ

To investigate the biochemical function of AcvB and VirJ from *A. tumefaciens* protein production and purification procedures for the wild type and mutant proteins were established (136, 137, 223). All proteins were isolated from the periplasmic fraction of *E. coli* cells carrying the respective plasmid and purified by affinity chromatography using *Strep*-Tactin® resin (2.6.3.1) as described in detail in sections 3.2.1, 3.2.2 and 3.6.1. Almost homogeneous elution fractions were obtained, dialyzed and concentrated for subsequent use in *in vitro* activity assays. Typically 3 mg of purified AcvB protein (or mutant variants) and 0.05 mg of purified VirJ protein were obtained from 1 l *E. coli* culture.

3.8.3 *In vitro* activity assays with AcvB variants and VirJ

Based on the biochemically characterized A-PGS/A-PGH system from *P. aeruginosa* a hydrolase function of AcvB and VirJ was assumed. Instead of A-PG present in *P. aeruginosa* membranes, *A. tumefaciens* contains L-PG (224) which is synthesized in a tRNA-dependent reaction by the lysyl-phosphatidylglycerol synthase (L-PGS) enzyme termed LpiA (25). Accordingly, L-PG was tested as a potential substrate for AcvB and VirJ.

To analyze a potential L-PG hydrolyzing activity of AcvB and VirJ an *in vitro* activity assay was established (2.10). For this purpose commercially available L-PG was solubilized in buffer containing Triton™ X-100 under vigorous shaking. The resulting L-PG containing micelles were incubated with purified $AcvB_{25-456}$ protein (or mutant variants) or the employed *Strep*-tag® II protein (negative control). During incubation samples were taken at defined time points and spotted onto a TLC plate together with L-lysine as a reference. The reaction mixture was separated by TLC and compounds containing free amino groups were identified by subsequent ninhydrin staining (2.8.2). Representative experimental results using proteins $AcvB_{25-456}$ and *Strep*-tag® II are shown in figure 16 (137).

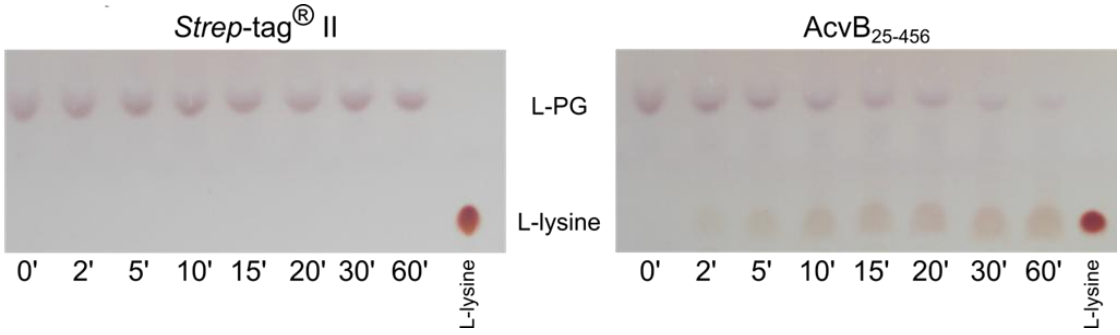

Figure 16: Lipid analyses of reaction products from *in vitro* activity assays
Purified $AcvB_{25-456}$ protein and the employed *Strep*-tag® II protein (negative control) were used for *in vitro* activity assays (2.10). 80 µl of a 5.13 mM L-PG micelle solution was incubated with 80 µl of 20 µM purified $AcvB_{25-456}$ protein or the *Strep*-tag® II at 37 °C and 1'000 rpm for 60 min. At defined time points (0-60 min), 5 µl of the respective reaction mixture was spotted onto a thin-layer chromatography (TLC) plate together with 5 µl of a 68 µM L-lysine solution as a reference and were separated using n-butanol, acetic acid and water (4:1:1 (v/v/v)) as solvent system (174). TLC plates were sprayed with ninhydrin solution and incubated at 110 °C until spot development (2.8.2).

The employed solvent system allows for a distinct separation of the substrate L-PG and the potential reaction products PG and lysine. Under the employed

reaction conditions constant amounts of the substrate L-PG were detected over time for *in vitro* assays that contained either buffer (not shown) or the *Strep*-tag® II protein (figure 16) indicating that no spontaneous L-PG hydrolysis occurs. By contrast, a significant reduction of the L-PG amount goes along with an increase of the lysine amount over time for *in vitro* assays containing protein $AcvB_{25\text{-}456}$. These results clearly indicate that protein $AcvB_{25\text{-}456}$ is able to hydrolyze its potential natural substrate L-PG *in vitro*.

To calculate the specific activity of protein $AcvB_{25\text{-}456}$ a L-lysine calibration curve was prepared. Therefore, L-lysine solutions of different concentrations were spotted onto a TLC plate and subsequently separated and stained as carried out for the *in vitro* activity assay. Spot intensities were determined using the software TotalLab Quant (Cleaver Scientific Ltd, Rugby, UK). By plotting the spot intensities (background intensity subtracted) against the respective L-lysine concentration a linear calibration curve was obtained which enabled the quantification of L-lysine formation during the *in vitro* activity assay. According to this procedure a specific activity of 0.44 $\mu mol \cdot mg_{enzyme}^{-1} \cdot min^{-1}$ was calculated for protein $AcvB_{25\text{-}456}$ (137). For comparison a specific activity of 11 ± 3 $nmol \cdot mg_{enzyme}^{-1} \cdot min^{-1}$ was determined for the hydrolysis of the artificial substrate L-alanine 4-nitrophenyl ester by the homologous A-PGH protein (49). However, a direct comparison of the specific activities is not feasible due to the significantly different employed reaction conditions (e.g. natural vs. artificial substrate or temperature).

Based on a sequence alignment of the homologous proteins A-PGH and AcvB conserved serine and histidine residues (Ser269, Ser336 and His433) of AcvB were identified (see appendix figure 33). These potential active site residues were exchanged by site-directed mutagenesis and mutant proteins were produced and purified according to the AcvB wild type protein (2.6.1.3, 2.6.2.1, 2.6.3.1). Stability of the purified mutant proteins was analyzed by Thermal Shift Assays (2.7.8). T_M values between 54.5 and 55 °C were determined for the wild type protein and the mutant variants AcvB S269A, AcvB S336A, AcvB H433A and AcvB H433N indicating the integrity of the mutant proteins (145).

Purified AcvB mutant proteins were subsequently analyzed in the *in vitro* activity assay. For protein AcvB S269A significantly reduced L-PG hydrolyzing activity was detected as further substantiated by a specific activity of

0.07 µmol·mg_{enzyme}^{-1}·min^{-1}, whereas AcvB variants S336A, H433A and H433N completely lost their ability to hydrolyze L-PG *in vitro* (137). These results highlight the key function of amino acids Ser336 and His433 of AcvB in the enzymatic reaction and are in full agreement with the findings obtained for mutagenesis of residues Ser307 and His401 of protein A-PGH from *P. aeruginosa* (49).

Existence of VirJ, a truncated AcvB version devoid of the ~200 N-terminal amino acids, raised the question if the hydrolyzing activity is inherent to the C-terminal region. Purified $VirJ_{22-255}$ protein and the N-terminally truncated variant $AcvB_{232-456}$ were used for *in vitro* activity assays (223). Both proteins showed comparable L-PG hydrolyzing activity to the wild type AcvB protein. These results reveal that VirJ functions as an L-PG hydrolase *in vitro* and that the C-terminal region of AcvB contains all key catalytic residues, *inter alia* Ser336 and His433, for L-PG hydrolysis.

3.8.4 Membrane alterations in *A. tumefaciens* Δ*lpiA* and Δ*acvB* strains

A typical *A. tumefaciens* membrane contains the main phospholipid components PE, PG, PC, DPG and MMPE as well as minor amounts of DMPE (28). MMPE and DMPE are precursors for the biosynthesis of PC from PE (225). In addition, *A. tumefaciens* possesses the *lpiA* gene. The related gene product allows for the formation of L-PG in a tRNA-dependent reaction (25).

In cooperation with the group of Prof. Franz Narberhaus from the Ruhr-University Bochum *lpiA* and *acvB* deletion mutants in the nopaline-type *A. tumefaciens* strain C58 were generated. Subsequently, the membrane composition and growth behavior of these strains was analyzed.

In the wild type strain the common phospholipids were identified by two-dimensional TLC and subsequent cupric sulfate staining. Furthermore, small amounts of L-PG were present under neutral and acidic growth conditions. Similar observations were recently described for *Bacillus licheniformis* and *Bacillus thuringiensis* and it was postulated that L-PG formation in the bacterial membrane is not only a specific adaptation mechanism to acidic conditions but rather a general adaptation mechanism to diverse environmental surroundings (58).

The Δ*lpiA* mutant strain did not reveal the presence of L-PG within its

membrane which verifies the proposed function of LpiA as a L-PGS in *A. tumefaciens*. By contrast, the Δ*acvB* mutant strain contained increased L-PG amounts when compared to the wild type under neutral and acidic growth conditions pointing towards the *in vivo* function of AcvB as a L-PG hydrolase. Normal L-PG levels were observed for Δ*lpiA* and Δ*acvB* strains complemented by a plasmid-encoded *lpiA* or *acvB* gene, respectively.

In accordance with the *P. aeruginosa* ΔPA0919 strain (49) and an *atvA* transposon mutant of *R. tropici* (52), a growth phenotype of the Δ*acvB* strain was observed under acidic conditions (pH 5.5), but not under neutral conditions (pH 7.5). This growth defect under acidic conditions was restored by providing a plasmid-encoded *acvB* gene. Alternatively, supplementation of the cultivation medium with 40 mM calcium chloride which functions as a membrane stabilizing agent (226) resulted in wild type-like growth. The obtained results imply that AcvB is important for *A. tumefaciens* growth under acidic conditions.

A similar growth defect was observed for a *R. tropici* point mutant where the serine residue of the characteristic LIPASE_SER motif was chromosomally exchanged against alanine, resulting in a strain that synthesizes nonfunctional AtvA protein (52). Taking these observations into consideration, one might speculate that the function of aa-PG hydrolyzing enzymes (e.g. AtvA, AcvB, A-PGH) is of key importance under acidic conditions and that the respective protein is not relevant as a structural component. Dysbalancing the membrane composition by elevated L-PG or A-PG levels appears to have a negative impact on bacterial growth under acidic, but not under neutral conditions.

3.9 Localization of AcvB and VirJ in *A. tumefaciens*

3.9.1 Prediction of signal sequences and transmembrane helices

An important aspect in understanding protein function is the subcellular localization of the protein of interest. Initial evidence can be obtained using bioinformatic tools predicting e.g. signal sequences and/or transmembrane helices. Several prediction tools (2.15) were used to analyze the localization of AcvB and VirJ in *A. tumefaciens*.

For protein AcvB a signal sequence with a cleavage site after amino acid 24 was predicted by LipoP 1.0, Phobius, PrediSi and SignalP 4.1. Localization of AcvB in the periplasmic space was also predicted by LocTree 3 and

TMHMM v. 2.0 detected no transmembrane helix.

Presence of a signal sequence with a cleavage site after amino acid 19 (Phobius and PrediSi) or 22 (LipoP 1.0 and SignalP 4.1) was also predicted for VirJ. Furthermore, TMHMM v. 2.0 postulated one helical segment from amino acid positions 5-22 and LocTree 3 predicted VirJ to be localized in the inner membrane.

These theoretical results point towards a periplasmic localization of AcvB and VirJ due to the identification of N-terminal signal sequences. However, VirJ might be also anchored in the inner membrane of *A. tumefaciens* by a helical segment.

3.9.2 Localization studies using cellular fractions of *A. tumefaciens*

AcvB and VirJ localization experiments were performed using the wild type strain *A. tumefaciens* C58 carrying either plasmid pTrc200_*acvB*_Strep or pTrc200_*virJ*_Strep. Therefore, cells were cultivated to the early log-phase, induced with IPTG and cultivation was continued to the mid-log phase. After harvesting, cells were treated with polymyxin B to release periplasmic proteins which were subsequently separated from cytoplasmic and membrane proteins by centrifugation. The remaining spheroblasts were lysed and unbroken cells were sedimented by low-speed centrifugation. The soluble fraction was subjected to ultracentrifugation to separate cytoplasmic from membrane proteins (2.12.2.2). The obtained pellet was washed, the membrane proteins were solubilized by Triton™ X-100 treatment and the soluble fraction was obtained by ultracentrifugation (2.12.2.4). Protein fractions were separated by SDS-PAGE (2.7.2) and transferred onto a PVDF membrane (2.7.3) for subsequent immunochemical detection of the C-terminal *Strep*-tag® II of AcvB or VirJ (2.7.4). The corresponding PVDF membrane for AcvB localization is presented in figure 17.

AcvB was clearly detectable in the fractions containing disrupted cells (lane 2) or soluble cytoplasmic proteins (lane 3). In contrast, neither the soluble periplasmic fraction (lane 1) nor the fraction containing solubilized membrane proteins (lane 4) reveal the presence of AcvB in this type of analysis. In previous work the same experimental approach was employed and revealed that the homologous protein A-PGH is localized in the cytoplasmic membrane of

P. aeruginosa where it is anchored by one transmembrane helix (227).

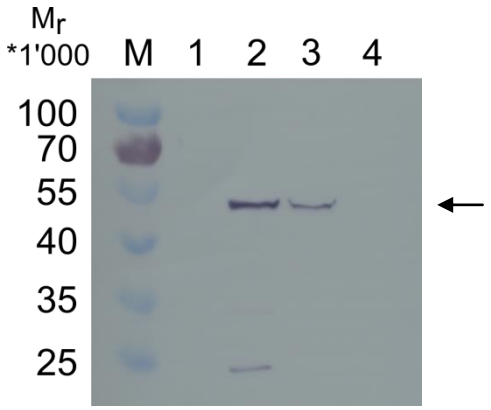

Figure 17: Localization of AcvB in *A. tumefaciens* C58
A. tumefaciens strain C58 carrying plasmid pTrc200_*acvB*_Strep was cultivated to the early log-phase, IPTG was added and cultivation was continued until the mid-log phase was reached. Cells were harvested and fractionated into the periplasmic, cytoplasmic and membrane fraction as described in chapters 2.12.2.2 and 2.12.2.4. Samples were separated by SDS-PAGE, transferred onto a PVDF membrane and AcvB was immunochemically detected *via* its C-terminal *Strep*-tag® II (2.12.2.5). An arrow indicates protein AcvB with a calculated molecular weight of 50.3 kDa.
Lane M: PageRuler™ Prestained Protein Ladder, relative molecular masses (*1'000) are indicated; Lane 1: soluble periplasmic fraction; Lane 2: cells disrupted by French Press®; Lane 3: soluble cytoplasmic fraction; Lane 4: membrane proteins solubilized by Triton™ X-100.

Based on theoretical analyses a periplasmic localization of AcvB was proposed (3.9.1). However, the obtained results of this fractionation experiment do not confirm this. One possible reason might be that the utilized immunochemical detection method is not sensitive enough to detect low protein amounts of AcvB in the periplasmic fraction. Besides this, the employed *Strep*-Tactin® AP conjugate recognizes an innate *A. tumefaciens* protein with a relative molecular mass of ~25'000 (see lane 2). Therefore, this antibody is not applicable to unambiguously detect the VirJ protein with a relative molecular mass of ~27'000 in cellular fractions. Based on these results an alternative experimental approach was employed to analyze the localization of AcvB and VirJ in *A. tumefaciens*.

3.9.3 Protein localization analyses *via* alkaline phosphatase fusions

A second experimental approach was pursued to localize AcvB and VirJ in soluble cellular fractions of *A. tumefaciens* (142). For this purpose the periplasmic protein AP was used as a reporter protein that can easily be

detected in the respective cellular fractions by activity measurements (157).
Two localization vectors containing the putative signal sequences of *acvB* or *virJ* fused to the AP gene *phoA* without its own signal sequence were generated. As a control, two localization vectors for PhoA were constructed; one containing the full-length *phoA* gene (positive control) and one carrying the truncated *phoA* gene lacking its own signal sequence (negative control).

A. tumefaciens C58 cells carrying either plasmid pTrc200 '*phoA*, pTrc200 *phoA*, pTrc200 leader *acvB* '*phoA* or pTrc200 leader *virJ* '*phoA* were cultivated to the early log-phase, induced with IPTG and cultivation was continued to the end of the exponential phase (2.12.1.1). Identical amounts of cells were harvested and the periplasmic proteins were released by polymyxin B treatment. Following separation of the periplasmic proteins from cytoplasmic and membrane proteins by centrifugation the obtained spheroblasts were disrupted by French Press®. Cell debris was separated by low-speed centrifugation and the supernatant was subjected to ultracentrifugation to sediment the total membrane fraction (2.12.1.2). The isolated soluble periplasmic and cytoplasmic fractions were utilized for the determination of AP activity (2.12.1.3) as well as MD activity (2.12.1.5) according to De Maagd and Lugtenberg (1986) (177).
To investigate the quality of the cell fractionation procedure the MD activity assay was performed. The cytoplasmic protein MD can convert oxaloacetate to malate while $NADH+H^+$ is oxidized to NAD^+. The decrease of $NADH+H^+$ in the reaction mixture can be monitored spectrophotometrically at a wavelength of 340 nm.
The measurements clearly revealed MD activity in the isolated cytoplasmic fractions of all four localization strains, whereas it was nearly absent in the periplasmic fractions (see appendix figure 32). The determined MD activity in the periplasmic fraction was related to the one of the cytoplasmic fraction (set to 100%). The following activity ratios for the localization strains were calculated: pTrc200 '*phoA* (negative control): 0.29%, pTrc200 *phoA* (positive control): 0.08%, pTrc200 leader *acvB* '*phoA*: 0.16% and pTrc200 leader *virJ* '*phoA*: 0.20%. These findings demonstrate that the periplasmic fractions contained only minor cytoplasmic contaminants.

Furthermore, the soluble fractions were subjected to an activity assay using the substrate *p*-nitrophenyl phosphate which is converted to the yellow reaction product *p*-nitrophenol by the periplasmic enzyme AP. The formation of *p*-nitrophenol was monitored spectrophotometrically at a wavelength of 405 nm. One AP activity determination, as a representative of four independent experiments, is presented in figure 18.

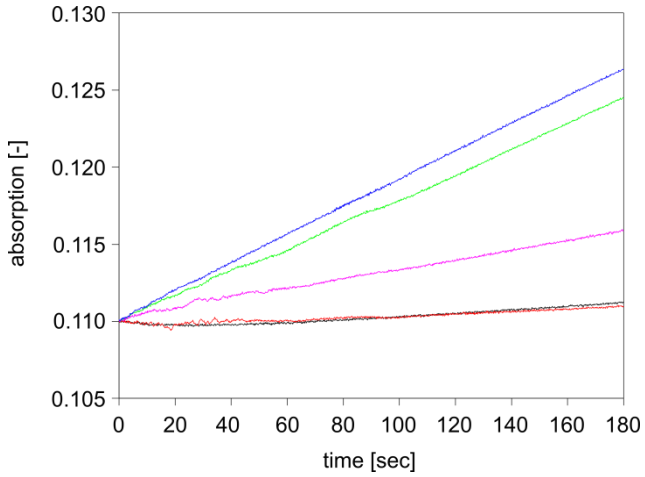

Figure 18: Determination of AP activity in the soluble periplasmic fractions isolated from four different localization strains.
The spectrophotometrically monitored absorption at 405 nm, representing the formation of *p*-nitrophenol due to AP activity, is plotted against time. The graphs depicted correspond to the blank (black), the negative control (red), the positive control (green), the strain pTrc200 leader *acvB* '*phoA* containing the *acvB* signal sequence (pink) and the strain pTrc200 leader *virJ* '*phoA* containing the *virJ* signal sequence (blue).

The determined AP activity resulted in graphs of different steepness based on the formation of *p*-nitrophenol over a time period of 180 sec (figure 18). The graph for the blank (sole test solution) only slightly increases over time which represents the spontaneous conversion of the substrate to *p*-nitrophenol in the test solution. The graph for the negative control (PhoA without its own signal sequence) exhibits a similar curve. This indicates that the PhoA protein without its signal sequence remained in the cytoplasmic fraction and thus no AP activity was detected in the periplasmic fraction. The slight increase in the absorption value over time can be ascribed to the spontaneous substrate hydrolysis as already mentioned above.

By contrast, the graph for the positive control (PhoA with its own signal sequence) shows a constant increase of the absorption over time representing the formation of *p*-nitrophenol by AP activity. This result confirms the successful

export of PhoA into the periplasm of *A. tumefaciens*.

PhoA enzyme activity in the periplasmic fraction was calculated as units (one unit corresponds to an absorption change of 0.001 per minute (62)) considering the time interval ranging from 100 to 160 sec. On the basis of four independent experiments the following activities for the blank and the localization strains were calculated: blank: 0.3-0.8 U, pTrc200 '*phoA*: 0.2-0.7 U, pTrc200 *phoA*: 5.1-29.4 U, pTrc200 leader *acvB* '*phoA*: 1.9-7.2 U and pTrc200 leader *virJ* '*phoA*: 5.3-45.6 U. For all strains significantly increased PhoA enzyme activities were detected in comparison to strain pTrc200 '*phoA* representing the negative control. These results clearly indicate the export of the reporter protein PhoA into the periplasm of *A. tumefaciens* facilitated by the native signal sequences of the genes *acvB* and *virJ*.

3.9.4 Determination of alkaline phosphatase activity in whole cells

The folding of PhoA is dependent upon disulfide bond formation in the bacterial periplasm (228). Accordingly, the export of the PhoA enzyme into the periplasm is essential for its activity. Active PhoA can hydrolyze BCIP which leads to the formation of an indigo dye (176) and thus a blue appearance of the bacterial colonies. In white-colored colonies the substrate BCIP is not hydrolyzed which indicates that the enzyme remained in the cytoplasm and thus is not active. This system was used to study PhoA localization in whole *A. tumefaciens* cells depending on the respective signal sequence (142).

Initial experiments revealed a high endogenous PhoA activity in the *A. tumefaciens* wild type strain C58. For further experiments BCIP agar plates were thus supplemented with 25 mM disodium hydrogen phosphate which efficiently suppresses this undesirable activity.

The obtained results for the four localization strains are presented in figure 19. After four days of cultivation the color of the *A. tumefaciens* colonies was evaluated. For the negative control (figure 19 A) white-colored colonies appeared, whereas for the positive control (figure 19 B) blue-colored colonies were observed indicating that PhoA remained in the cytoplasm or was exported into the periplasm, respectively. For the localization strains containing the *acvB* or *virJ* signal sequence colonies with a light blue (figure 19 C) or a dark blue color (figure 19 D) were observed. So in both cases PhoA was exported into the

periplasm, folded into its active form and hydrolyzed the substrate BCIP.

In summary, the export of the reporter protein PhoA into the periplasm of *A. tumefaciens* is facilitated by the *acvB* and *virJ* signal sequences as demonstrated in cellular fractions (3.9.3) and whole cells (3.9.4). These results clearly indicate a periplasmic localization of proteins AcvB and VirJ in the *A. tumefaciens* C58 strain.

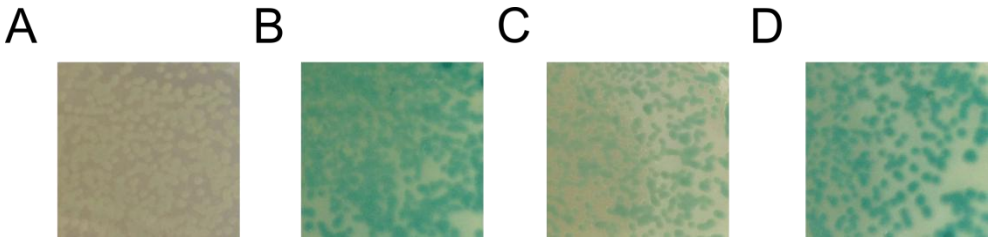

Figure 19: Determination of AP activity in whole cells of the respective localization strains
The generated *A. tumefaciens* localization strains were cultivated for four days at 30 °C on YEB agar plates supplemented with 90 µg/ml BCIP and 25 mM disodium hydrogen phosphate pH 7.2 as described in chapter 2.12.1.4. The AP activity was evaluated based on the colony color from white (no AP activity) to blue (high AP activity). The results of the following localization strains are depicted: (A) pTrc200 '*phoA* (negative control), (B) pTrc200 *phoA* (positive control), (C) pTrc200 leader *acvB* '*phoA* (signal sequence of *acvB*), (D) pTrc200 leader *virJ* '*phoA* (signal sequence of *virJ*).

3.10 *A. tumefaciens* infection assays

3.10.1 Tumorigenesis studies on potato discs

The phytopathogenic bacterium *A. tumefaciens* is able to induce crown gall tumor formation at wound sites of several dicotylic and some monocotylic plant species (70, 68). Therefore, the attached *Agrobacterium* cell translocates its T-DNA and effector proteins *via* the T4SS into the plant cell where the T-DNA is integrated into the genome (229). Infected plant cells thereupon synthesize opines as well as the phytohormones auxin (230) and cytokinin (231) which induce unlimited cell proliferation and thus crown gall formation.

To analyze the potential role of proteins LpiA and AcvB in *A. tumefaciens* tumorigenesis the deletion mutant strains *A. tumefaciens* C58 Δ*lpiA* and Δ*acvB* were employed for potato tuber disc assays (2.13.1) which were performed during an internship in the group of Prof. Franz Narberhaus (Ruhr-University Bochum). The analyses revealed that deleting *lpiA* does not influence tumor formation on potato discs compared to the wild type, whereas no tumors formed

after the infection with the Δ*acvB* mutant. In addition, plasmid-based complementation experiments were performed. Therefore, the *A. tumefaciens* strain Δ*acvB* carrying plasmid pTrc200_*acvB*_Strep was used for the potato tuber disc assay. The complemented strain formed the same amount of tumors on potato discs when compared to the wild type strain carrying the empty pTrc200 vector. This indicates that the plasmid-based *acvB* gene restored tumor formation and virulence. The obtained results for the Δ*acvB* mutant and the complemented strain are in agreement with the observations made by Wirawan *et al*. (1993) (60). These findings point out that the *lpiA* gene product is not relevant for *A. tumefaciens* tumorigenesis, whereas the *acvB* gene product is essential. Interpreted in terms of membrane lipid composition these results might imply that the absence of L-PG in the Δ*lpiA* mutant strain is not crucial for tumor formation. By contrast, an artificially elevated L-PG amount in the Δ*acvB* mutant strain might interfere with the infection process.

3.10.2 T-DNA transfer from *A. tumefaciens* into plant cells

Upon external stimuli (e.g. phenolic compounds, monosaccharides or an acidic extracellular pH (73)) the transcription of the Ti plasmid-encoded virulence operons (*vir* genes) is induced and the respective Vir proteins form the T4SS (232). This system is responsible for the transfer of the T-strand in complex with several Vir proteins (T-complex) into the plant cell (75). Therefore, the T-DNA is recognized for processing and transfer by its flanking regions (left and right T-DNA border) composed of 25 bp direct repeats (233). The T-complex is targeted into the nucleus of the plant cell and subsequently the T-strand is integrated into the genome (76).

3.10.2.1 T-DNA transfer assay using β-glucuronidase as a reporter

Due to the loss of tumor formation ability of the Δ*acvB* mutant strain on potato discs (3.10), it was of interest whether the T-DNA transfer into the plant cell is affected for this mutant strain. The corresponding experiments were performed during an internship in the group of Prof. Franz Narberhaus (Ruhr-University Bochum).

For analyses the T-DNA binary vector pBISN1 (234), containing *inter alia* the β-glucuronidase gene (*gusA*) delimited by the left and right T-DNA border, was

employed. Transformation of this plasmid into the respective *A. tumefaciens* strains, subsequent infection of *A. thaliana efr-1* seedlings according to the AGROBEST method (149) and the determination of GUS activity in the seedlings (2.13.2) allowed to analyze the T-DNA transfer capability of the different strains. GUS staining of the seedlings was performed three days post-infection with the respective *A. tumefaciens* strain. For staining, the seedlings were incubated with X-Gluc which is an artificial substrate of the GUS enzyme (235). Dark blue-colored cotyledons imply a strong GUS activity and so a successful transfer of the T-DNA into plant cells, whereas no GUS activity is detected in unstained cotyledons indicating that the T-DNA is not transferred.

For stained seedlings infected with the *A. tumefaciens* C58 wild type, the wild type containing the empty pTrc200 vector or the Δ*lpiA* mutant blue-colored cotyledons were observed as shown in figure 20 A. These results suggest that the T-DNA transfer is not affected in the wild type and the Δ*lpiA* mutant which is in compliance with their ability to form tumors on potato discs (3.10.1).

By contrast, infection with the Δ*acvB* strain and subsequent GUS staining resulted in unstained cotyledons (figure 20 A). The seedling infection takes place in an acidic cultivation medium. Under these conditions the Δ*acvB* strain exhibits a growth defect that can be restored by the supplementation of 40 mM calcium chloride to the cultivation medium (3.8.4). To rule out an impaired T-DNA transfer of the Δ*acvB* mutant due to a growth defect, infection assays supplemented with 40 mM calcium chloride were performed. However, GUS staining of the respective seedlings revealed again unstained cotyledons (figure 20 A) indicating that the *A. tumefaciens* growth phenotype is not related to the impaired T-DNA transfer. Infection of the seedlings with the *A. tumefaciens* Δ*acvB* pTrc200_*acvB*_Strep strain resulted in blue-colored cotyledons (figure 20 A) after GUS staining. This implies that the T-DNA transfer ability was restored by the plasmid-encoded *acvB* gene.

These results point towards an essential role of protein AcvB and/or its L-PG hydrolyzing activity for the T-DNA transfer process. The impaired T-DNA transfer ability of the Δ*acvB* strain might also account for the absence of tumors on infected potato discs (3.10.1).

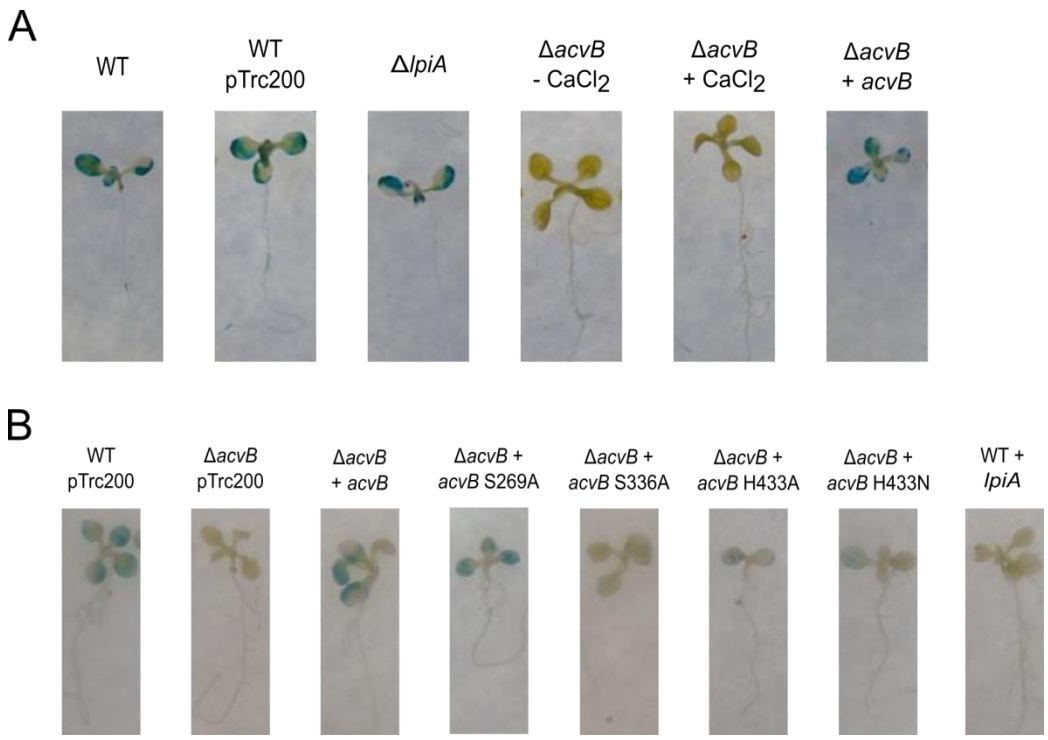

Figure 20: *A. thaliana efr-1* seedlings infected by different *A. tumefaciens* strains and subsequently stained to determine GUS activity
The different *A. tumefaciens* strains containing the pBISN1 plasmid were cultivated in AB-MES pH 5.5 medium containing 200 µM AS to induce *vir* gene expression. Four-day-old *A. thaliana efr-1* seedlings were infected with the respective strain and co-cultivated in infection medium (MS medium and AB-MES pH 5.5 medium in a ratio of 1:1 (v/v) containing 200 µM AS). Three days post-infection the seedlings were stained to determine GUS activity (2.13.2). Two independent experiments are depicted in figure parts A and B. The following *A. tumefaciens* strains were employed: wild type (WT), wild type carrying plasmid pTrc200 (WT pTrc200), Δ*lpiA* mutant (Δ*lpiA*), Δ*acvB* mutant with or without 40 mM calcium chloride supplementation to the cultivation medium (Δ*acvB* + $CaCl_2$ or Δ*acvB* - $CaCl_2$), Δ*acvB* mutant carrying plasmid pTrc200_*acvB*_Strep (Δ*acvB* + *acvB*), Δ*acvB* mutant carrying plasmid pTrc200 (Δ*acvB* pTrc200), Δ*acvB* mutant carrying either plasmid pTrc200_*acvB*_Strep-S269A, pTrc200_*acvB*_Strep-S336A, pTrc200_*acvB*_Strep-H433A or pTrc200_*acvB*_Strep-H433N (Δ*acvB* + *acvB* S269A, Δ*acvB* + *acvB* S336A, Δ*acvB* + *acvB* H433A, Δ*acvB* + *acvB* H433N) and the wild type carrying plasmid pTrc200_*lpiA* (WT + *lpiA*).

To get further insight into the role of AcvB in T-DNA transfer, several plasmids based on the pTrc200 vector encoding for AcvB variants S269A, S336A, H433A and H433N were constructed (2.5.13). These AcvB proteins were previously analyzed in *in vitro* activity assays revealing residual L-PG hydrolyzing activity for protein AcvB S269A, whereas the AcvB mutant proteins S336A, H433A and H433N completely lost their ability to hydrolyze L-PG (3.8.3).
For T-DNA transfer assays the Δ*acvB* strains carrying the respective plasmids containing *acvB* mutant genes were used. These plasmids restore the deleted

acvB gene by the respective gene variant. The infected *A. thaliana* seedlings were stained to determine GUS activity and the obtained results are shown in figure 20 B. Cotyledons of seedlings infected by the wild type or the complemented Δ*acvB* strain containing plasmid pTrc200_*acvB*_Strep were blue-colored after GUS staining which demonstrates a successful T-DNA transfer, whereas infection with the Δ*acvB* mutant strain containing the empty pTrc200 vector resulted in unstained cotyledons as described above.

Following seedling infection with the Δ*acvB* strain containing plasmid pTrc200_*acvB*_Strep-S269A and GUS staining the cotyledons obtained a blue color indicating an effective T-DNA transfer. By contrast, plasmid-based complementation of the Δ*acvB* strain with the AcvB point mutant S336A resulted in unstained cotyledons after seedling infection and staining which means that the T-DNA was not transferred into the plant cells. Cotyledons infected with Δ*acvB* strains complemented by AcvB point mutants H433A or H433N showed isolated blue dots which imply an impaired T-DNA transfer compared to the wild type strain. Furthermore, the wild type strain overexpressing the *lpiA* gene was analyzed and showed a defective T-DNA transfer comparable to the Δ*acvB* mutant and the complemented variant Δ*acvB* + *acvB* S336A.

L-PG amounts in the different *A. tumefaciens* strains were analyzed by two-dimensional TLC and subsequent cupric sulfate staining to estimate the *in vivo* activity of the AcvB protein variants or LpiA. The following L-PG contents were estimated: WT pTrc200: ~1%, Δ*acvB* pTrc200: ~12%, Δ*acvB* + *acvB*: ~2%, Δ*acvB* + *acvB* S269A: ~2%, Δ*acvB* + *acvB* S336A: ~9%, Δ*acvB* + *acvB* H433A: ~5%, Δ*acvB* + *acvB* H433N: ~4%, WT + *lpiA*: ~7%. The *in vivo* activities are in good agreement with the *in vitro* activities (3.8.3) except for the Δ*acvB* strains complemented by AcvB point mutants H433A and H433N. These mutant proteins were not able to hydrolyze L-PG *in vitro*, but show residual *in vivo* activity. Overproduction of LpiA in the wild type strain resulted in comparable L-PG amounts to the Δ*acvB* strain complemented by AcvB point mutant S336A.

The results might indicate that elevated L-PG amounts in the *A. tumefaciens* membrane impair or completely prevent the T-DNA transfer. This implies that a fine-tuned cellular L-PG amount on the basis of a functional AcvB protein is

essential for *A. tumefaciens* T-DNA transfer by the T4SS.

In the present study it was shown that complete lack of L-PG in the Δ*lpiA* mutant strain did not influence tumor formation when compared to the wild type strain (3.10.1). Similar findings were recently described for the DPG-deficient *A. tumefaciens* double mutant Δ*cls1*/Δ*cls2* (170). In contrast, it was demonstrated that reduced PC amounts in a Δ*pmtA* mutant or complete lack of PC in a Δ*pmtA*/Δ*pcs* double mutant resulted in delayed or even abolished tumor formation on *Kalanchoë* leaves, respectively (38). These effects were ascribed to a reduced or complete lack of *vir* gene expression in the particular *A. tumefaciens* strains resulting in an impaired or defective T4SS.

A. tumefaciens also synthesizes phosphorus-free ornithine lipids. Mutant strains of the respective biosynthetic genes *olsB* and *olsE* were either deficient of ornithine lipids or they only synthesized unmodified ornithine lipids. For these strains accelerated tumor formation on potato tuber discs was observed when compared to the wild type strain (236). It was proposed that ornithine lipids are detected by the plant which then induces defense mechanisms that might be hampered or absent during infection with the Δ*olsB* and Δ*olsE* mutant strains. These related studies clearly illustrate that membrane lipids can play a critical role at diverse stages of *A. tumefaciens* tumorigenesis.

In the present study the relevance of a functional AcvB protein in the context of T-DNA transfer and tumorigenesis was demonstrated (3.10.1, 3.10.2). For crown gall tumor formation in plant cells a coordinated infection process takes place which includes, *inter alia*, the attachment of *A. tumefaciens* to the host cell, T-DNA processing and transfer into the host cell by the T4SS, T-DNA transport to the nucleus as well as nuclear import and genomic integration (237).

In different studies the initial infection processes of an *acvB* mutant strain and the wild type strain were analyzed. No differences were observed concerning the signal molecule sensing and subsequent activation of the two-component regulatory system VirA/VirG (63), *vir* gene expression (62, 61, 63), the attachment to plant cells (60, 63) and T-strand formation (62). By contrast, related investigations described a significantly impaired T-DNA transfer ability of the *acvB* mutant strain to maize or tobacco plant cells (63, 238, 239) and it was proposed that AcvB and VirJ might be involved in T-DNA transfer. However,

within all these investigations the observed phenotypes were not related to an L-PG hydrolyzing activity of AcvB. The present investigation for the first time links the cellular L-PG level to the related infection phenotypes of the investigated *acvB* mutant strains. Accordingly, lipid homeostasis might play a critical role during the individual stages of the infection process.

To get further insight into the detailed role of L-PG in *A. tumefaciens* T-DNA transfer further analyses concerning the T4SS maturation are required. Furthermore, an altered membrane composition might influence the recognition of *A. tumefaciens* by plant cells. This might also result in the activation of plant defense mechanisms which could prevent T-DNA transfer.

3.11 Protein PA3911 is upregulated under anaerobic biofilm conditions

In a recent proteomics study performed by Magnowska and co-workers (113, 175) the iTRAQ labeling technique in combination with liquid chromatography and mass spectrometry (2D-LC-MS/MS) was employed to assess the adaptation of *P. aeruginosa* to anaerobic biofilm conditions of the CF lung (1.4.1). Therefore, *P. aeruginosa* biofilms were grown on artificial sputum medium agar plates under aerobic and anaerobic conditions to mimic the metabolic changes during infection progression. The obtained iTRAQ-MS data from three independent experiments revealed that protein PA3911 was the second-most significantly upregulated protein under anaerobic biofilm conditions. This result was statistically evaluated (116) and indicated a 5- to 10-fold induction as judged from 12 unique peptides with a sequence coverage of 43%.

So far, this 19 kDa protein is solely described in the literature as a conserved hypothetical protein that is encoded at the 3' end of a proposed operon including orfs PA3913, PA3912 and PA3911 (117). Several experimental approaches revealed a significant upregulation of these orfs under low oxygen and anaerobic conditions (121, 119, 117, 118, 120) as described in chapter 1.4.1 which is in agreement with the findings described by Magnowska (2010) (113).

3.12 Orthologous PA3911 sequences and operon prediction

Protein homologs of PA3911 from *P. aeruginosa* were identified using the blastp tool (195). Orthologous proteins are present in α-, β- and γ-proteobacteria, whereas related proteins are not conserved in Gram-positives, archaea, fungi, plants and mammals.

Among eukarya, moderate sequence homology of PA3911 to one part of the 58 kDa SCP-X was determined. This protein is composed of an N-terminal 3-ketoacyl CoA thiolase and a C-terminal 13 kDa SCP-2 domain that can be cleaved off post-translationally (128). SCP-2 domain-containing proteins have been described in the literature as non-specific LBP which are associated with many proposed functions in cholesterol transport and lipid metabolism in vertebrates and insects (127, 240, 241).

The PA3913, PA3912 and PA3911 operon of *P. aeruginosa* was also predicted

by the DOOR² database (197). The hypothetical proteins PA3913 and PA3912 were predicted to be members of the peptidase family U32 and PA3911 to belong to the SCP-2 sterol transfer family by the Pfam database (242). Theoretical analyses using the DOOR^2 database revealed similar operon structures for several α-, β- and γ-proteobacteria. In β- and γ-proteobacteria an operon encoding for PA3913, PA3912 and PA3911 orthologous genes is conserved, whereas in α-proteobacteria the genes are rearranged to PA3911, PA3913 and PA3912. Moreover, in several species belonging to the class of α- or β-proteobacteria (e.g. *A. tumefaciens*, *Paracoccus denitrificans* or *Laribacter hongkongensis*) this operon structure is expanded by a fourth gene at the 5' or 3' end, encoding for a hypothetical protein, an oxidoreductase or a regulatory protein.

3.13 Phenotypic characterization

To analyze the physiological role of PA3911 in *P. aeruginosa* a mutant strain was analyzed concerning its growth behavior under various conditions and its motility in comparison to the wild type strain.

3.13.1 *P. aeruginosa* PA3911 mutant strain

For phenotypical analyses the deletion of orf PA3911 from the wild type strain *P. aeruginosa* PAO1 was intended. For mutant generation the method described by Hoang *et al.* (1998) (140) was employed (2.5.16). However, the genomic integration of the gentamicin resistance cassette only occurred as a single crossover instead of a double crossover event. Accordingly, no markerless PA3911 deletion strain was obtained for further experiments.

Therefore, *P. aeruginosa* strain PW7609 (kindly provided by Prof. Susanne Häußler from the Helmholtz Centre for Infection Research, Braunschweig) carrying a transposon insertion in orf PA3911 was employed for subsequent phenotypical characterizations. The integrity of the PA3911 mutant strain was confirmed by PCR analyses and subsequent sequence determination (2.10.1) as recommended by the transposon mutant library curators (134). The sequenced PCR fragment (431 bp) clearly revealed the integration of the transposon IS*phoA*/hah at base position 5 of gene PA3911 which is fully consistent with the information provided by the library curators.

3.13.2 Growth behavior in complex and minimal medium

The growth behavior of the *P. aeruginosa* strains MPAO1 (parental strain) and PW7609 (PA3911 mutant) was analyzed in LB complex and AB pH 7.3 minimal medium under aerobic and anaerobic conditions as described in chapter 2.4.5. Under all conditions identical growth curves for both strains were obtained.

3.13.3 Phenotype Microarray™ analyses

A commercially available Phenotype Microarray™ system from Biolog (Hayward, CA, USA) was applied for comparative analyses of the wild type strain MPAO1 and the mutant strain PW7609 (2.10.3). An overall of 1'152 growth conditions covering a broad range of stressors (e.g. salts, pH and antibiotics) were tested. The cell respiration in the different growth conditions was visualized by a tetrazolium dye functioning as a redox indicator.

Similar growth of both strains was observed in the utilized IF-10 minimal medium which is a good prerequisite to perform comparative studies (figure 21 C). The commercial experiment revealed an increased susceptibility of strain PW7609 compared to the wild type in nine different conditions.

Due to the fact that the manufacturer Biolog does not provide the respective compound concentrations, significant growth phenotypes were independently reproduced in non-commercial microarray experiments. Therefore, 96-well plates were filled with defined concentrations of the respective compounds in IF-10 minimal medium containing the tetrazolium dye, inoculated with the particular *P. aeruginosa* strain and cultivated as described for the commercial experiment (2.10.3).

The observed trends were independently reproduced in three experiments of which one is exemplarily depicted in figure 21. An increased susceptibility of strain PW7609 against the compounds initially identified in the commercial experiment was successfully confirmed in the non-commercial experiments. The respective MICs were determined for selected antimicrobials by serial experiments in the presence of linearly increasing compound concentrations.

Figure 21 A shows the observed susceptibility differences for the wild type and the PA3911 mutant strain PW7609 using sub-inhibitory or inhibitory compound concentrations (for details see the caption of figure 21). Strain PW7609 was more susceptible to the semisynthetic tetracycline derivative minocycline, the

β-lactames nafcillin and oxacillin as well as chloramphenicol and its derivative thiamphenicol. The following MIC values for the mutant versus the wild type strain were determined: 3 or 8 µg/ml for minocycline, 275 or 750 µg/ml for nafcillin, 800 or 2'600 µg/ml for oxacillin, 25 or 1'000 µg/ml for chloramphenicol and 50 or 700 µg/ml for thiamphenicol.

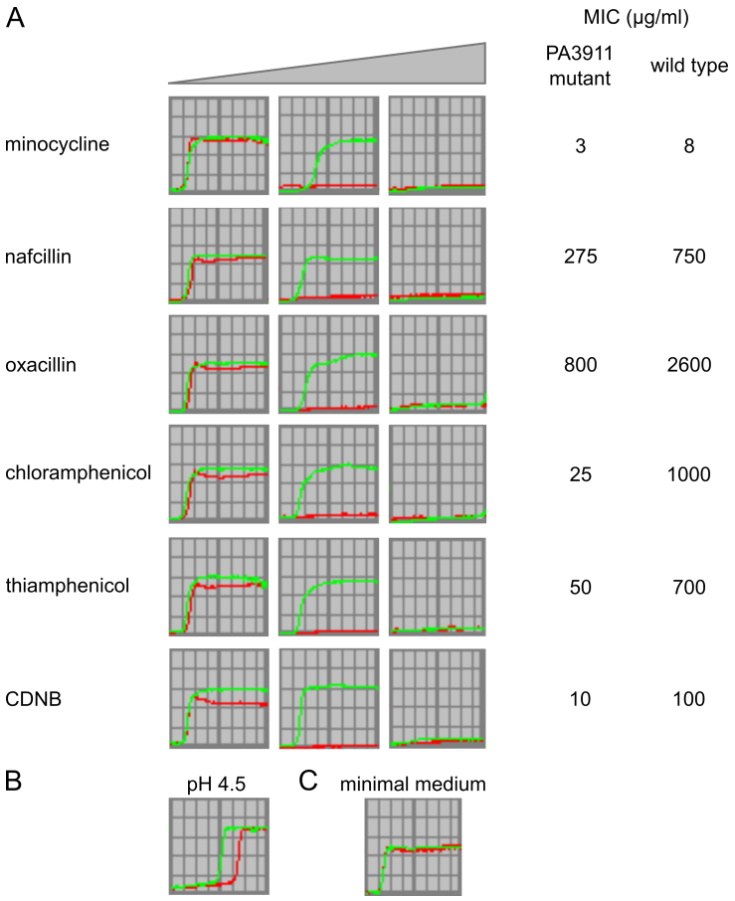

Figure 21: Characterization of strain PW7609 using Phenotype Microarrays™
The cell respiration value (arbitrary OmniLog units 0-500) of the *P. aeruginosa* wild type strain (green line) and the PA3911 mutant strain PW7609 (red line) was plotted against the time (48 h). **A:** Strains were cultivated at 37 °C in 120 µl IF-10 medium supplemented with tetrazolium dye A and inhibitory concentrations of the following substances: 0.25, 3 or 8 µg/ml minocycline; 100, 275 or 750 µg/ml nafcillin; 200, 800 or 2'600 µg/ml oxacillin; 2, 25 or 1'000 µg/ml chloramphenicol; 2.5, 50 or 700 µg/ml thiamphenicol; 1, 10 or 100 µg/ml 1-chloro-2,4-dinitrobenzene (CDNB). Serial experiments in the presence of linearly increasing compound concentrations allowed for the accurate determination of the respective MIC values. **B:** Identical growth experiment as described in part A using IF-10 medium pH 4.5. **C:** Control experiment in the presence of IF-10 minimal medium.

A 1- to 5-fold reduction of MICs in the presence of diverse antimicrobials has recently been described for *P. aeruginosa* mutant strains impaired in lipid homeostasis, e.g. the A-PGS mutant strain ΔPA0920, when compared to the

wild type (48, 49). MIC values were similarly reduced for strain PW7609 in the presence of minocycline (2.6-fold), nafcillin (2.7-fold) and oxacillin (3.3-fold). For comparison, a 1.2-fold reduced MIC value for oxacillin was observed for strain *P. aeruginosa* ΔPA0920 when related to the wild type (48). However, pronounced MIC reductions of 14-fold and 40-fold were observed for strain PW7609 in the presence of thiamphenicol and chloramphenicol, respectively. These findings indicate that the PA3911 gene product contributes to the high intrinsic antibiotic resistance of *P. aeruginosa* and understanding the underlying molecular principles is of central importance for the future development of new antimicrobial strategies.

For the compound CDNB, an artificial substrate of the glutathione S-transferase (243), an increased susceptibility of the mutant strain compared to the wild type was observed which is reflected in MIC values of 10 versus 100 µg/ml (figure 21 A). With respect to the PA3911 mutant, CDNB might influence the glutathione homeostasis and thus the related redox state of the cell.

Furthermore, the commercial Phenotype Microarray™ experiment revealed a growth phenotype of strain PW7609 under an overall of three acidic conditions, as exemplified in figure 21 B. These results might indicate that PA3911 is also involved in the adaptation of *P. aeruginosa* to acidic environmental conditions. Under these conditions similar effects were observed for *P. aeruginosa* strains with an unbalanced cellular lipid composition (43, 49).

3.13.4 Motility and biofilm formation assays

Several properties influence the virulence of *P. aeruginosa*, *inter alia*, different types of motility like swimming, swarming and twitching as well as the ability to form biofilms.

3.13.4.1 Motility assays

P. aeruginosa is highly motile which enables the colonization of several environmental habitats and it was demonstrated that motility is to some extent required for *P. aeruginosa* virulence (86, 244, 245). Accordingly, strain PW7609 was tested for swarming, swimming and twitching motility in comparison to the wild type strain (2.10.2).

Concerning swarming and swimming motility no phenotypical differences were

observed between the two strains (data not shown). To analyze twitching motility the well-established stab-inoculation method was employed in five independent experiments. Twitching zones were stained with crystal violet and measured for comparison (2.10.2.1). The average twitch zone of the wild type strain was set as 100% and the value of strain PW7609 was related to that.

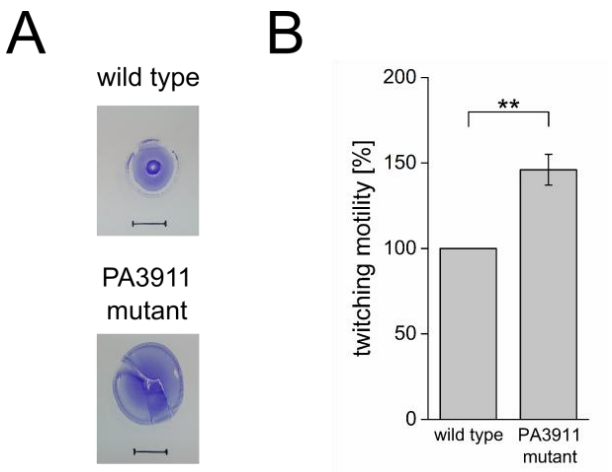

Figure 22: Twitching motility assay
1% LB-Lennox agar plates were stab-inoculated with a toothpick to the plate bottom and incubated in a humidified chamber at 37 °C for 24 h (2.10.2.1). **A:** For visualization purposes the twitching motility zones were stained with 1% (w/v) crystal violet solution for 10 min. Scale bars = 1 cm. **B:** The average twitch zone of the wild type strain was set as 100% and the value of the PA3911 mutant strain was related to that. The data from five independent experiments performed in at least sextuplicate is shown (**, significance with $p < 0.01$).

As depicted in figure 22, strain PW7609 showed clearly enhanced twitching motility with an average twitch zone of 146% (significance with $p < 0.01$). This type of motility is mediated *via* type IV pili and is necessary for the active expansion of *P. aeruginosa* colonies on semisolid or solid surfaces (246). Furthermore, it is required for the spatial organization of mushroom-shaped structures within a biofilm (247–249). Accordingly, biofilm formation of strain PW7609 was subsequently investigated.

3.13.4.2 Biofilm formation

Based on the finding that strain PW7609 shows significantly enhanced twitching motility compared to the wild type (3.13.4.1), both strains were subjected to a well-established static biofilm formation assay in 96-well microtiter plates (2.10.2.4). After 24 h incubation, the surface-attached bacteria were stained with crystal violet, solubilized and the absorbance at 595 nm was determined.

The data from nine independent experiments revealed that the biofilm formation in the PA3911 mutant strain is significantly impaired when compared to the wild type strain (65% versus 100%, significance with $p < 0.001$). These findings might indicate that orf PA3911 is relevant for *P. aeruginosa* biofilm formation under the employed conditions.

3.14 Localization of the PA3911 protein in *P. aeruginosa*

3.14.1 Prediction of signal sequences and transmembrane helices

To gain further insight into the physiological function of protein PA3911 its subcellular localization is of central importance. The employed prediction tools (2.15) LipoP 1.0, LocTree3 and SignalP 4.1 detected no signal peptide and thus proposed a cytoplasmic localization. This finding is supported by the absence of transmembrane helices in PA3911 as predicted by TMHMM v. 2.0. Solely the online tool Phobius detected a signal sequence with a cleavage site after amino acid position 20. However, a genome-wide study to identify *P. aeruginosa* exported proteins using the PhoA fusion method revealed an unclear picture with regard to the cellular localization of PA3911 (53).

3.14.2 Localization of protein PA3911 in cellular fractions

The *P. aeruginosa* strain PAO1 pUCP20T-P_{PA3911}-PA3911 was employed for localization studies. This strain was cultivated to the end of the exponential growth phase. Subsequently, the cells were harvested and subjected to different fractionation techniques. Protein PA3911 was detected within the cellular fractions by its C-terminal *Strep*-tag® II using the *Strep*-Tactin® AP conjugate.

The soluble periplasmic fraction was isolated from harvested cells of the respective strain by polymyxin B treatment and subsequent centrifugation to sediment the spheroblasts. The obtained spheroblasts were homogenized, cell debris was separated by centrifugation and the soluble cytoplasmic fraction was received (2.11.2).

To isolate the total membrane fraction, harvested cells were disrupted by a French Press® and cell debris was sedimented by low-speed centrifugation. The obtained supernatant was subjected to high-speed centrifugation to sediment

the total membrane fraction. Membrane proteins were solubilized out of it using Triton™ X-100 (2.11.3).

Samples of the isolated fractions were separated by SDS-PAGE (2.7.2) and transferred onto a PVDF membrane (2.7.3) for subsequent immunochemical detection of the employed *Strep*-tag® II (2.7.4). The obtained PVDF membrane for PA3911 localization is presented in figure 23.

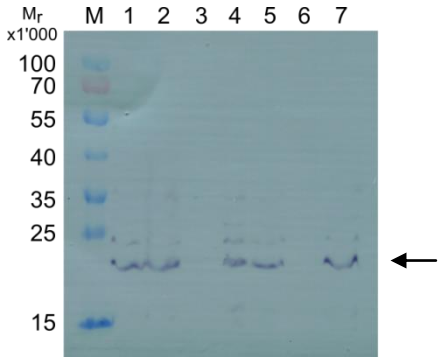

Figure 23: Localization of protein PA3911 in *P. aeruginosa*
Subcellular fractions of the *P. aeruginosa* strain PAO1 carrying plasmid pUCP20T-P_{PA3911}-PA3911 were separated by SDS-PAGE, transferred onto a PVDF membrane by Western blotting and the PA3911 protein was detected by its *Strep*-tag® II (relative molar mass of ~21'000) using the *Strep*-Tactin® AP conjugate (2.11). Lane M: PageRuler™ Prestained Protein Ladder, relative molecular masses (*1'000) are indicated; Lane 1: whole cells; Lane 2: supernatant after cell disruption by a French Press® and low-speed centrifugation; Lane 3: total membrane fraction; Lane 4: supernatant after high-speed centrifugation; Lane 5: whole cells; Lane 6: soluble periplasmic fraction; Lane 7: soluble cytoplasmic fraction.

Protein PA3911 was detected in intact cells of the respective *P. aeruginosa* strain (lane 1). After cell disruption and the removal of unbroken cells by low-speed centrifugation PA3911 was present in the membrane containing supernatant (lane 2). However, in the isolated total membrane fraction (lane 3) protein PA3911 was no longer detectable. By contrast, the supernatant from the high-speed centrifugation step, containing soluble cytoplasmic and periplasmic proteins, revealed a dominant PA3911 band (lane 4).

In an independent experiment intact *P. aeruginosa* cells (lane 5) were incubated with polymyxin B to release the soluble periplasmic fraction (lane 6) which did not indicate the presence of protein PA3911. In the fraction containing soluble cytoplasmic proteins (lane 7) protein PA3911 was clearly detected. The obtained results imply that PA3911 is a soluble protein located in the cytoplasm of *P. aeruginosa* PAO1.

3.15 Production and purification of protein PA3911

For functional *in vitro* studies purified PA3911 protein was required. Initially, the Codon Adaptation Index (CAI) as a measure of codon usage bias was determined. The codon usage of the heterologous expression system (e.g. *E. coli*) is compared with the codons present in the gene of interest (e.g. PA3911) and a frequency score, the CAI, is calculated (250). This score ranges from zero to one and a high value indicates a high proportion of the most abundant codons in the gene of interest. For the PA3911 gene from *P. aeruginosa* a CAI of 0.273 was calculated for the heterologous expression in *E. coli* cells. Thereupon a synthetic fragment containing the codon-optimized PA3911 gene sequence (table 7) was used for vector construction.

Several vector constructs for PA3911 with different N-terminal tags (GST-tag, His_6-tag, thioredoxin-His_6-S-tag) were generated (2.5.13) and recombinant protein production was performed in *E. coli* BL21(λDE3) cells (2.6.1.4). Harvested cells were disrupted by French Press® passage and insoluble components were separated by high-speed centrifugation. His_6-tagged PA3911 protein was purified using TALON® metal affinity resin (2.6.3.3), whereas for the GST-tagged variant Protino® Glutathione Agarose 4 B resin (2.6.3.2) was employed. The purifications of the His_6- and GST-tagged variant yielded only negligible protein amounts (data not shown).

Purification of protein PA3911 with an N-terminal thioredoxin-His_6-S-tag using TALON® metal affinity resin (2.6.3.3) resulted in protein amounts sufficient for subsequent *in vitro* studies. In an identical procedure, the pET32a(+) vector was used for the heterologous overproduction and purification of the sole thioredoxin-His_6-S-tag protein. This protein was used as an appropriate control for *in vitro* studies.

The corresponding SDS-PAGE analysis is depicted in figure 24. Lanes 1 and 2 show the total protein content of *E. coli* BL21(λDE3) cells containing plasmid pET32a(+)-PA3911 before and after IPTG induction, indicating high cellular PA3911 concentrations after induction. A representative elution fraction of purified PA3911 protein is depicted in lane 3. Comparison of lanes 2 and 3 clearly illustrates that large amounts of the produced protein appear in the insoluble fraction. Nevertheless, 1 mg almost homogeneous PA3911 protein per liter *E. coli* culture was obtained.

The major contaminant in the elution fraction with a relative molar mass of ~57'300 was identified as the *E. coli* chaperone GroEL by N-terminal amino acid sequence determination (2.7.5; kindly performed by Beate Jaschok-Kentner, Helmholtz Centre for Infection Research, Braunschweig). Several techniques (e.g. ATP washing steps and anion or cation exchange chromatography) were tested to remove GroEL during protein purification. However, none of the employed methods resulted in the successful separation of GroEL and PA3911.

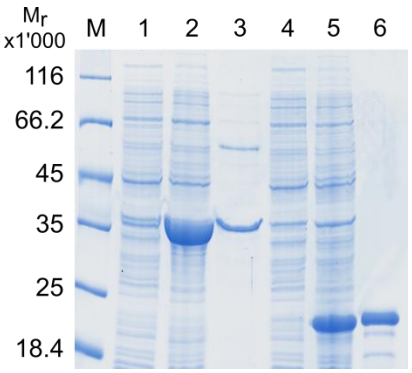

Figure 24: SDS-PAGE analysis of a PA3911 and thioredoxin-His$_6$-S-tag protein purification
Protein PA3911 was recombinantly produced in *E. coli* BL21(λDE3) cells and purified *via* its N-terminal thioredoxin-His$_6$-S-tag using TALON® metal affinity resin (2.6.3.3). Sample fractions were denatured with 2x SDS loading dye (95 °C, 10 min), subjected to SDS-PAGE analysis (12% (w/v) running gel) and proteins were visualized by InstantBlue™ staining (2.7.2).
Lane M: Unstained Protein Molecular Weight Marker, relative molecular masses (*1'000) are indicated; total protein of *E. coli* cells carrying plasmid pET32a(+)-PA3911 before (lane 1) and after (lane 2) IPTG induction; Lane 3: purified PA3911 protein with a relative molar mass of ~37'000; total protein of *E. coli* cells carrying plasmid pET32a(+) before (lane 4) and after (lane 5) IPTG induction; Lane 6: purified thioredoxin-His$_6$-S-tag protein with a relative molar mass of ~20'000.

The integrity of the target protein with a relative molar mass of ~37'000 (as judged from SDS-PAGE) was confirmed to be 37'048.3 Da by ESI-MS measurements (2.7.7) which were kindly performed by Dr. Manfred Nimtz (Helmholtz Centre for Infection Research, Braunschweig).

For control experiments the sole thioredoxin-His$_6$-S-tag protein was produced and purified analogously from *E. coli* BL21(λDE3) cells containing plasmid pET32a(+). After IPTG induction high amounts of the tag protein are visible in the total protein fraction (compare lanes 4 and 5) and after purification almost homogenous protein (lane 6) with a relative molar mass of ~20'000 was obtained.

3.16 Protein-lipid overlay assays

Sequence analyses revealed that protein PA3911 shares homology with LBP (3.12). Accordingly, the lipid binding capability of protein PA3911 was explored in *in vitro* studies. Therefore, the thioredoxin-His_6-S-tagged PA3911 protein as well as the thioredoxin-His_6-S-tag as a control protein were recombinantly produced in *E. coli* cells (2.6.1.4) and purified using TALON® metal affinity resin (2.6.3.3).

Protein-lipid overlay experiments were performed with commercially available Membrane Lipid Strips™ (Echelon® Biosciences, Salt Lake City, UT, USA), hydrophobic membranes whereon 15 different lipids are spotted. After incubating the membranes with equimolar amounts of either protein PA3911 or the tag protein, several washing steps followed and the respective lipid bound protein was detected immunochemically by its His_6-tag (2.7.11). The obtained Membrane Lipid Strips™ are presented in figure 25.

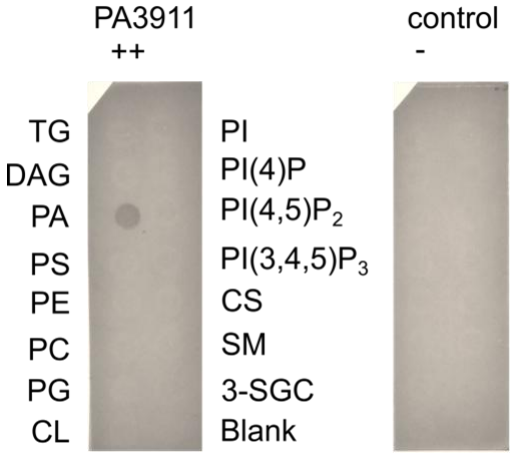

Figure 25: Protein-lipid overlay assays using Membrane Lipid Strips™
The PA3911 protein and the sole thioredoxin-His_6-S-tag protein (control) were purified from the cytoplasm of *E. coli* by His_6-tag chromatography using TALON® metal affinity resin. Subsequently, the lipid binding capability was analyzed with Membrane Lipid Strips™ (Echelon® Biosciences) according to the manufacturer's instructions. The detected spot intensities were classified in the following way: strong PA binding (++), no PA binding (-). TG, triglyceride; DAG, diacylglycerol; PA, phosphatidic acid; PS, phosphatidylserine; PE, phosphatidylethanolamine; PC, phosphatidylcholine; PG, phosphatidylglycerol; CL, cardiolipin; PI, phosphatidylinositol; PI(4)P, phosphatidylinositol (4)-phosphate; $PI(4,5)P_2$, phosphatidylinositol (4,5)-bisphosphate; $PI(3,4,5)P_3$, phosphatidylinositol (3,4,5)-trisphosphate; CS, cholesterol; SM, sphingomyelin; 3-SGC, 3-sulfogalactosylceramide.

Referring to the set of lipids spotted onto the Membrane Lipid Strips™, protein PA3911 specifically binds to PA under the employed conditions. PA is a simple

diacyl-glycerophospholipid which acts as an essential precursor for glycerophospholipid biosynthesis as described in chapter 1.1.1. By contrast, the sole thioredoxin-His_6-S-tag protein did not bind to the spotted lipids at all indicating that lipid binding of protein PA3911 is not mediated by the employed protein tag.

In contrast to PA, the following structurally related phospholipids did not reveal the binding of protein PA3911: (I) the PA derivative DAG which lacks the phosphate 'headgroup' that appears to be a relevant determinant for the binding of PA3911; (II) PS, PE, PC, PG, PI, PI (4)-phosphate, PI (4,5)-bisphosphate, PI (3,4,5)-trisphosphate and sphingomyelin containing, *inter alia*, an 'increased polar headgroup' which might indicate that a more bulky phosphodiester group is not accepted by protein PA3911; (III) CL/DPG contains a modified polar head group and two additional fatty acids when compared to PA which might hamper the binding of PA3911; (IV) the molecules triglyceride, cholesterol and 3-sulfogalactosylceramide are devoid of a phosphate group which might prevent the binding of PA3911. According to these results protein PA3911 is proposed to be a specific PA binding protein under the employed conditions.

3.17 Characterization of the potential lipid binding pocket of PA3911

Due to the homology of protein PA3911 to members of the SCP-2 sterol transfer family (3.12), the existence of a lipid binding pocket was proposed. For SCP-2 protein variants from different origins it was described that they contain tunnel-like cavities or binding pockets, mainly lined by hydrophobic residues (240).

To initially characterize this potential lipid binding pocket of PA3911 a structural modeling approach was used. Therefore, the SWISS-MODEL server (204) was employed to identify suitable templates for modeling. The search revealed 33 potential templates with low to moderate sequence identities ranging from 10-27%. Considering the sequence identity and sequence coverage the structure of the human SCP-2-like domain in complex with Triton™ X-100 (PDB code 1IKT, 19.8% sequence identity) was employed as a template for the modeling of PA3911. A structure-based sequence alignment is presented in figure 26.

```
PA3911  MLNRQRLLLGVAGRLLPLAAKVPRGLQHLVLQRVANRLFAQ-PLEEGAFDLLEGRWLRLEV  60
1IKT    ------------------------------VFEEIGRRLKDIGPE---VVKKVNAVFEWHI  38
4UEI    ----------------------PEDFKVFKYMKILEEAMEN-DTE-NLIEK-VRGIYGFKV  55

PA3911  RD----LGVGWCVTRVPGGLRLVERP---RASVTIRGDWRDFLLLASRHEDPDTLFFRRRL 114
1IKT    TKGGN-IGAKWTIDLKSGSGKVYQGPAKGAADTTIILSDEDFMEVVLGKLDPQKAFFSGRL  98
4UEI    RNGPNGAEGYWVINAKEGKGKVTYNGGE-KPDVTFTISDEDVVDLISGKLNPQKAFFQGKI 115

PA3911  VIEGDTELGLAVKNLLDSLDPEHLPPWLWNAVERAGRAVQEERGEAPQGPVQGARGG 171
1IKT    KARGNIMLSQKLQMILKDYA---------------------------------------- 118
4UEI    KIQGNMGLAMKLTDLQRQAA---------------------------------------- 135
```

Figure 26: Structure-based sequence alignment of PA3911, 1IKT and 4UEI
Alignment of protein sequences PA3911 from *P. aeruginosa* PAO1, SCP-2-like domain of human multifunctional enzyme type 2 (PDB code 1IKT) and SCP-2 domain of *Helicoverpa armigera* (PDB code 4UEI) was generated using the SWISS-MODEL server. Residues proposed to be involved in PA binding by PA3911 and spatially related residues in 1IKT or 4UEI are depicted in bold letters. Amino acids mutagenized by site-directed mutagenesis are highlighted.

Based on the obtained three-dimensional model of protein PA3911 (figure 27) several amino acids, located in the potential hydrophobic lipid binding pocket, were proposed to be involved in PA binding: Leu56 (Phe34), Leu58 (Trp36), Val69 (Ile50), Phe95 (Phe79) and Leu114 (Leu98); spatially related residues in the hydrophobic binding pocket of the human SCP-2 like domain structure (PDB code 1IKT) are specified in brackets.

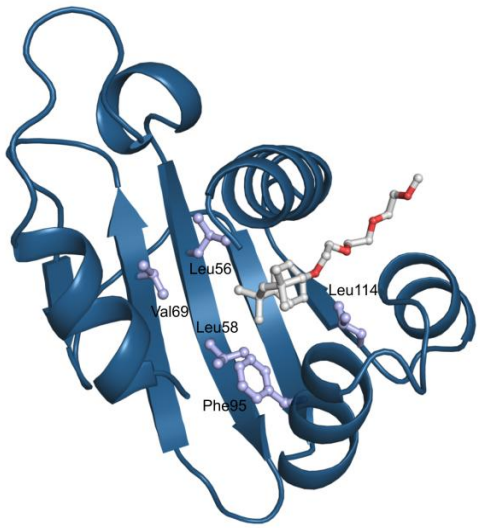

Figure 27: Three-dimensional model of protein PA3911
The three-dimensional model of PA3911 was generated by the SWISS-MODEL server using the human SCP-2-like domain in complex with Triton™ X-100 (PDB code 1IKT) as a template. The proposed amino acids for PA binding are located in the putative lipid binding pocket and are shown as sticks. The depicted ligand was adopted from the structure of 1IKT to illustrate the location of the putative lipid binding pocket.

For amino acids Leu56, Leu58, Val69 and Phe95 a potential interaction with the hydrophobic part of PA was assumed, whereas Leu114 is positioned at the

potential binding pocket entry site and might modulate its accessibility. These amino acids were mutagenized by either a hydrophobic, bulky tryptophan residue or by a positively charged arginine residue. The resulting ten site-directed PA3911 mutant proteins were produced and purified analogously to the wild type protein (2.6.1.4, 2.6.3.3) and the integrity was tested by Thermal Shift Assays as described in chapter 2.7.8 (139). T_M values between 67.5 and 69 °C were determined for the wild type protein and the mutant variants and confirm their integrity.

To study the lipid binding capability of all PA3911 mutant proteins in comparison to the wild type protein, they were simultaneously employed in protein-lipid overlay experiments using Membrane Lipid Strips™. In general, none of the analyzed mutant proteins showed a broadened lipid binding capacity under the tested conditions (data not shown).

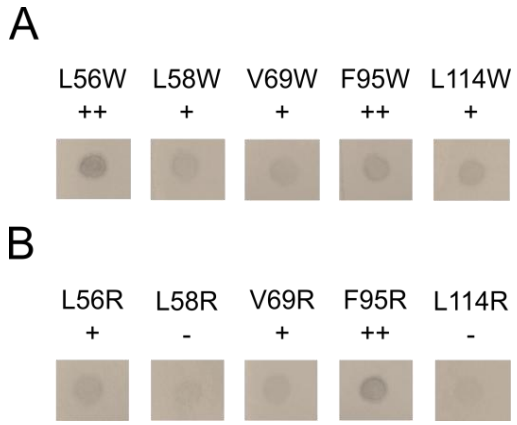

Figure 28: Excerpts of protein-lipid overlay assays depicting the PA binding of PA3911 mutant proteins
Ten PA3911 mutant proteins were produced, purified and analyzed concerning their lipid binding capability analogously as the wild type protein (139). The classified spot intensities for PA binding (strong PA binding (++), reduced PA binding (+), no PA binding (-)) are indicated in the panels A and B for the tryptophan and arginine mutants, respectively. The brightness of all images was adjusted to obtain an identical background level as for the PA3911 wild type experiment (figure 25) using the Inkscape software.

The analyses, depicted in figure 28, revealed the following differences for PA3911 mutant proteins with respect to the binding of PA: binding was not influenced for mutant proteins L56W, F95W and F95R when compared to the wild type protein. This might indicate that amino acid residue Phe95 is not involved in PA binding. For mutant proteins L58W, V69W and L114W reduced PA binding related to spot intensities was observed (figure 28 A). To some

extent, tryptophan might act as a substitute for the respective leucine or valine residues in the proposed binding pocket of PA3911.

Substitution of the respective amino acids with arginine resulted in more pronounced effects. Significantly reduced PA binding for mutant proteins L56R and V69R was detected, whereas it was completely prevented for mutant proteins L58R and L114R (figure 28 B). From these findings it was concluded that amino acids Leu56, Leu58, Val69 and Leu114 are constituents of the proposed lipid binding pocket, whereof Leu58 and Leu114 are of prime importance for the binding of PA by protein PA3911.

A similar modeling approach as employed in this study was performed to model the three-dimensional structure of the SCP-2 protein from the Oriental leafworm moth *Spodoptera litura* (251). Docking simulations were carried out using the structure model to identify putative amino acids involved in ligand binding. Subsequently, site-directed mutant proteins were tested for their binding activity to CS and palmitic acid. A complete loss of binding to CS and palmitic acid was observed for mutant protein F53W, whereas variant F53A was still able to bind to palmitic acid with a reduced activity. Besides this, mutant I115M showed enhanced CS binding activity, but could no longer bind to palmitic acid. These two amino acids of the SCP-2 protein from *S. litura* were, among others, identified as important for CS and/or palmitic acid binding and sequence comparison revealed that they are related to amino acids Leu58 and Leu114 of PA3911 which were identified as key residues for PA binding in this study.

Only recently the three-dimensional structure of the SCP-2 protein from cotton bollworm was elucidated (252). The CS binding activity of this protein was analyzed using docking simulations and subsequent mutagenesis experiments. Amino acids Tyr51 and Phe53 were identified, *inter alia*, as key residues for the binding of CS. Sequence comparison (figure 26) and superposition of the PA3911 model clearly relates these SCP-2 residues to the lipid binding residues Leu56 and Leu58 of PA3911 which were identified in this study.

To some extent, the differing specificity of PA3911 and SCP-2 proteins might be mediated *via* spatially conserved C_α positions (e.g. Leu56/Tyr51, Leu58/Phe53 and Leu114/Ile115) in combination with varying hydrophobic side chains.

3.18 Comparative lipid analyses

It was demonstrated that protein PA3911 is able to bind the lipid PA on Membrane Lipid Strips™ (3.16). Therefore, PA3911 function might be related to the phospholipid metabolism of *P. aeruginosa* with PA serving as a central hub metabolite. Accordingly, the cellular lipid composition of strain PW7609 was analyzed using well-established two-dimensional TLC according to Tindall (1990) (171) in combination with molybdatophosphoric acid, molybdenum blue and ninhydrin staining (2.8.2). The analyses were performed with cells cultivated under neutral conditions (pH 7.3) or under acidic conditions (pH 5.3) which allow for A-PG formation in *P. aeruginosa*. However, no differences in the cellular concentration of PE, PG, DPG and A-PG between the parental and the mutant strain were observed.

Furthermore, alternative solvent systems for the specific PA separation from the major lipid classes using TLC techniques in combination with molybdenum blue staining were employed (2.8.2). In the one-dimensional TLC approach according to Vaden *et al.* (2005) (172) lipid separation was not sufficient to clearly identify PA in the respective *P. aeruginosa* sample. The two-dimensional TLC method described by Abramson and Blecher (1964) (173) allowed for significantly enhanced lipid separation. After molybdenum blue staining a PA spot was assigned by comparison to the migration characteristics of a reference sample. However, detected PA amounts were extremely low so that the reliable comparison of the wild type and the mutant strain was not possible.

3.19 Phosphatidic acid quantification assay

For the cellular PA content a relative ratio of 0.2-2% compared to the overall lipid content has been described in the literature (253, 254). Therefore, a more sophisticated methodology than lipid analyses by TLC and subsequent staining (3.18) was required to quantify the PA content in the parental and the mutant strain. A commercially available coupled enzymatic quantification assay (Cell Biolabs, San Diego, CA, USA) was used which allowed for the fluorometric determination of micromolar PA amounts.

For analyses, cells of the *P. aeruginosa* strains MPAO1 and PW7609 were cultivated aerobically and anaerobically in AB minimal medium pH 7.3 (supplemented with KNO_3 for anaerobic growth) to the mid-logarithmic phase.

Identical amounts of the respective cells were harvested, washed and stored at -20 °C. The lipids were extracted and the PA quantification assay was performed according to the manufacturer's instructions (2.8.3). PA that is present in the particular sample is initially hydrolyzed by a lipase yielding G3P and the respective fatty acids. Afterwards G3P is oxidized by a G3P oxidase resulting in the stoichiometric formation of dihydroxyacetone phosphate and hydrogen peroxide. The subsequent reaction of a fluorometric probe with hydrogen peroxide in the presence of a peroxidase results in a detectable fluorescence signal. To calculate the PA content of a particular sample the measured fluorescence value is compared to a PA calibration curve as depicted in figure 29.

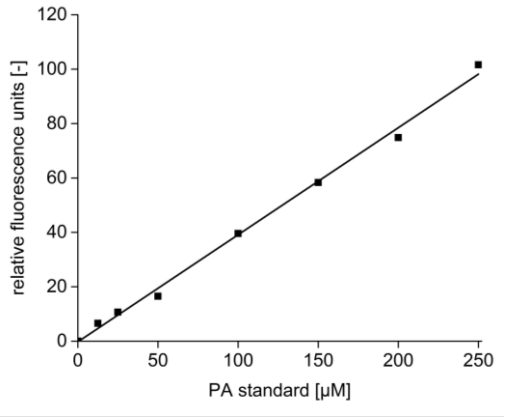

Figure 29: PA calibration curve
To quantify the PA amount in the respective samples a PA calibration curve was prepared. Therefore, the PA standard (provided by the manufacturer) was diluted to defined concentrations in the range of 0-250 µM. These PA standard solutions were subsequently employed for the Total Phosphatidic Acid Assay according to the manufacturer's instructions. A new calibration curve was prepared each time the assay was performed. For the coefficient of determination values of $R^2 > 0.995$ were obtained for all prepared calibration curves.

For aerobically grown *P. aeruginosa* MPAO1 cells a PA content of 4.2 ± 0.3 pmol per OD_{578} was determined. Compared to that, a decreased value of 2.6 ± 1.0 pmol per OD_{578} was obtained for the PA3911 mutant strain PW7609. Based on the findings of Magnowska (2010) (113) that PA3911 is the second-most significantly upregulated protein under anaerobic culture conditions, the cellular PA concentrations of anaerobically grown MPAO1 or PW7609 cultures with NO_3^- as an alternative electron acceptor were quantified. For both strains a significantly decreased PA content compared to the aerobically grown cells was determined: 1.3 ± 0.4 or 1.5 ± 0.3 pmol per OD_{578}

for the parental or mutant strain, respectively.
These results show that there is no direct correlation between the PA3911 content and the overall cellular PA amounts. Complex regulatory circuits for the lipid homeostasis of *P. aeruginosa* might be related to varying PA3911 protein concentrations, resulting in variations of the cellular PA status. With respect to this, PA3911 might be responsible for the short-term storage and/or the subsequent channeling of the lipophilic PA molecule within the framework of glycerophospholipid homeostasis.

In the present study it was demonstrated that PA3911 is a specific PA binding protein (key residues Leu58 and Leu114) (3.16, 3.17), which can influence the overall PA content of the cell (3.19). In comparison to other polar glycerophospholipids the low-abundant PA is carrying a characteristically small, highly negatively charged head group (255). The cellular PA concentration might thus alter the charge characteristics, the fluidity and/or the permeability of the bacterial membrane (255–257). Biophysical studies could show that PA molecules favor a negative membrane curvature and tend to form microdomains (255). The local arrangement of specific glycerophospholipids was described to be essential for many membrane-associated processes, e.g. the localization of membrane proteins, the regulation of protein channels and/or the direct microdomain-antimicrobial interaction (258, 31).
Such indirect effects might be also related to the increased twitching motility and impaired biofilm formation of the PA3911 mutant strain (3.13.4). In the literature analogous phenotypical effects were also described for *P. aeruginosa* in response to compounds from hosts, e.g. lactoferrin (259, 260), serum (261) or mucin (262), or due to the treatment with antimicrobial compounds like small cationic peptides (263, 264). However, the underlying molecular mechanisms are complex and not yet fully understood.
PA serves as a key intermediate for the synthesis of neutral lipids (di- and triacylglycerols) and glycerophospholipids including *inter alia* PG, PE, PC, DPG and A-PG (265, 266). Sustaining the cellular PA concentration at low levels of ~0.2-2% (253, 254) might be essential for the coordinated synthesis of phospholipids. At that point, the soluble PA binding protein PA3911 might contribute to PA homeostasis by its potential function as a short-term storage

and/or carrier of PA molecules. Figure 30 summarizes the main metabolic phospholipid pathways in *P. aeruginosa* and highlights the diverse physiological processes for which PA3911 function was demonstrated to be relevant. This includes for instance the antimicrobial susceptibility, resistance to acidic pH conditions, twitching motility and biofilm formation. Further work is required for the molecular understanding of PA3911-dependent physiological processes.

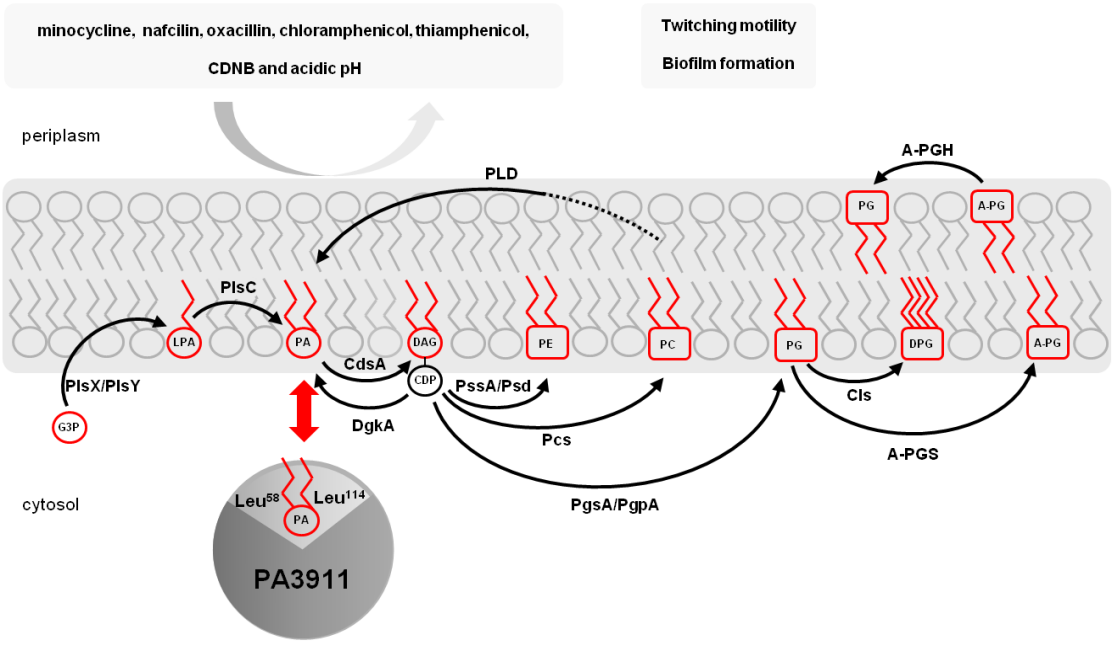

Figure 30: Model of PA3911-dependent lipid homeostasis and the related physiological processes in *P. aeruginosa*
Schematic representation of the biosynthetic pathway for glycerophospholipids starting from water soluble glycerol-3-phosphate (G3P) (6). The *sn*1-position of G3P is acylated by the glycerol-3-phosphate acyltransferase (PlsX/PlsY). The resulting phospholipid lysophosphatidic acid (LPA) is further acylated at the *sn*2-position by a LPA acyltransferase (PlsC) to produce phosphatidic acid (PA), a central hub metabolite of glycerophospholipid biosynthesis. PA is activated with cytidine triphosphate (CTP) to form cytidine diphosphate-diacylglycerol (CDP-DAG) by the enzyme CdsA. Multiple glycerophospholipids are produced from CDP-DAG: *inter alia* phosphatidylethanolamine (PE, by phosphatidylserine synthase/phosphatidylserine decarboxylase (PssA/Psd)), phosphatidylcholine (PC, by PC synthase (Pcs)) and phosphatidylglycerol (PG, by phosphatidylglycerol-phosphate synthase/ phosphatidylglycerol-phosphate phosphatase (PgsA/PgpA)). Condensation of two PG molecules allows for the formation of diphosphatidylglycerol (DPG) by the enzyme cardiolipin synthase (Cls). PG can be modified by aminoacylation. Alanyl-phosphatidylglycerol synthase (A-PGS) catalyzes the synthesis of A-PG (43). Cellular A-PG levels are tightly controlled by the alanyl-phosphatidylglycerol hydrolase (A-PGH) (49). PA can be recovered by virtue of phospholipase D (PLD). PA acts as a key precursor which specifically binds to the water soluble PA3911 protein (key residues Leu58 and Leu114 are highlighted). Sustaining a low cellular PA level might be essential for cellular lipid homeostasis. PA3911 function is relevant for *P. aeruginosa* antimicrobial susceptibility, resistance to acidic pH conditions, twitching motility and biofilm formation. CDNB, 1-chloro-2,4-dinitrobenzene.

4. Summary

Adaptation of the bacterial membrane composition to changing environmental conditions represents an essential survival strategy. One mechanism is the modification of existing glycerophospholipids. Aminoacylation of phosphatidylglycerol (PG) with e.g. alanine or lysine is catalyzed in a transfer RNA (tRNA)-dependent reaction by aminoacyl-phosphatidylglycerol synthases (aaPGS) and results in increased resistance against several antimicrobial compounds. Accordingly, aaPGS inhibition was proposed as a promising strategy to restore bacterial susceptibility. In this context the interaction of the alanyl-phosphatidylglycerol synthase (A-PGS) from *P. aeruginosa* with the tRNA acceptor stem was analyzed and the key residues Lys676, Arg684 and Arg687 were identified.

The protein alanyl-phosphatidylglycerol hydrolase (A-PGH) represents the A-PGS counterpart which contributes to the fine-tuning of the cellular alanyl-phosphatidylglycerol (A-PG) content in *P. aeruginosa*. To understand the molecular principles of A-PG hydrolysis, A-PGH protein crystals were analyzed by X-ray crystallography. The three-dimensional A-PGH structure of the N-terminal part (containing amino acids 34-215) was solved at a resolution of 1.64 Å *via* single-wavelength anomalous dispersion phasing. Structure-based alignments related the N-terminal part of unknown function to hydrolases and esterases possessing an α/β fold. Alternatively, the sole C-terminal part of the A-PGH enzyme or mutants generated based on the Surface Entropy Reduction approach were employed for initial crystallization experiments. The A-PGH low-resolution structure was obtained by small-angle X-ray scattering.

The operon encoding for A-PGS and A-PGH homologs is conserved in several Gram-negatives. For *A. tumefaciens* the respective related proteins LpiA or AcvB and VirJ were identified. An altered membrane lipid composition was detected in *A. tumefaciens* strains Δ*lpiA* or Δ*acvB* which is characterized by either the complete lack of lysyl-phosphatidylglycerol (L-PG) or elevated L-PG amounts. Accordingly, the L-PG hydrolyzing activity of the recombinantly produced and purified proteins AcvB and VirJ was demonstrated *in vitro*. Based on site-directed AcvB mutant proteins the catalytically relevant active site residues Ser336 and His433 were identified. Furthermore, a periplasmic localization of AcvB and VirJ in *A. tumefaciens* was shown. It was demonstrated

that functional AcvB protein is crucial for the translocation of transfer-DNA (T-DNA) during tumorigenesis and it is proposed that a fine-tuned cellular L-PG amount in the *A. tumefaciens* membrane might be important for T-DNA transfer *via* the type IV secretion system.

Adaptation of *P. aeruginosa* to anaerobic biofilm conditions of the cystic fibrosis lung was analyzed in a recent proteomics study which identified the conserved uncharacterized protein PA3911 as the second-most significantly upregulated one. A *P. aeruginosa* PA3911 transposon mutant exhibited a growth phenotype under acidic conditions, an increased susceptibility to specific antimicrobial compounds, enhanced twitching motility and impaired biofilm formation when related to the wild type. A localization study identified PA3911 in the cytoplasm of *P. aeruginosa*. The PA3911 protein and mutant variants were recombinantly produced in *E. coli*, purified and subjected to *in vitro* studies. Under the employed conditions PA3911 was demonstrated to be a specific phosphatidic acid (PA) binding protein and key residues Leu58 and Leu114 for PA binding were identified. It is proposed that protein PA3911 might contribute to PA homeostasis in *P. aeruginosa*.

5. Outlook

The following investigations are suggested for future experiments:

- Elucidation of the three-dimensional structure of full-length A-PGH or alternatively the sole C-terminal part in the presence of a substrate molecule

- Investigation of the detailed role of L-PG in T-DNA transfer of *A. tumefaciens*
- Elucidation of the three-dimensional structure of AcvB and VirJ in the presence of a substrate molecule
- Characterization of AcvB and VirJ substrate specificity
- Identification of the catalytically relevant active site residues of VirJ

- *In vitro* lipid binding assays for protein PA3911 in the presence of liposomes
- Comparative MS-based lipidome analyses for the *P. aeruginosa* PA3911 transposon mutant and the wild type strain

6. References

1. Munk, K., Ed. (2008) Mikrobiologie, Georg Thieme Verlag, Stuttgart, New York
2. Glauert, A. M., and Thornley, M. J. (1969) The topography of the bacterial cell wall. *Annu Rev Microbiol* **23**, 159–198
3. Smit, J., Kamio, Y., and Nikaido, H. (1975) Outer membrane of *Salmonella typhimurium*: Chemical analysis and freeze-fracture studies with lipopolysaccharide mutants. *J Bacteriol* **124**, 942–958
4. Kamio, Y., and Nikaido, H. (1976) Outer membrane of *Salmonella typhimurium*: Accessibility of phospholipid head groups to phospholipase C and cyanogen bromide activated dextran in the external medium. *Biochemistry* **15**, 2561–2570
5. Hobot, J. A., Carlemalm, E., Villiger, W., and Kellenberger, E. (1984) Periplasmic gel: New concept resulting from the reinvestigation of bacterial cell envelope ultrastructure by new methods. *J Bacteriol* **160**, 143–152
6. Zhang, Y.-M., and Rock, C. O. (2008) Membrane lipid homeostasis in bacteria. *Nat Rev Microbiol* **6**, 222–233
7. Cronan, J. E. (2003) Bacterial membrane lipids: Where do we stand? *Annu Rev Microbiol* **57**, 203–224
8. Bell, R. M., Cronan, J. E. (1975) Mutants of *Escherichia coli* defective in membrane phospholipid synthesis. Properties of wild type and K_m defective *sn*-glycerol-3-phosphate acyltransferase activities. *J Biol Chem* **250**, 7147–7152
9. Lu, Y.-J., Zhang, Y.-M., Grimes, K. D., Qi, J., Lee, R. E., and Rock, C. O. (2006) Acyl-phosphates initiate membrane phospholipid synthesis in Gram-positive pathogens. *Mol Cell* **23**, 765–772
10. Rock, C. O., Goelz, S. E., and Cronan, J. E., JR (1981) Phospholipid synthesis in *Escherichia coli*. Characteristics of fatty acid transfer from acyl-acyl carrier protein to *sn*-glycerol 3-phosphate. *J Biol Chem* **256**, 736–742
11. Pieringer, R. A., and Kunnes, R. S. (1965) The Biosynthesis of Phosphatidic Acid and Lysophosphatidic Acid by Glyceride Phosphokinase Pathways in *Escherichia coli*. *J Biol Chem* **240**, 2833–2838
12. Jerga, A., Lu, Y.-J., Schujman, G. E., de Mendoza, D., and Rock, C. O. (2007) Identification of a soluble diacylglycerol kinase required for lipoteichoic acid production in *Bacillus subtilis*. *J Biol Chem* **282**, 21738–21745
13. Selvy, P. E., Lavieri, R. R., Lindsley, C. W., and Brown, H. A. (2011) Phospholipase D: Enzymology, functionality, and chemical modulation. *Chem Rev* **111**, 6064–6119
14. Carter, J. R. (1968) Cytidine triphosphate: Phosphatidic acid cytidyltransferase in *Escherichia coli*. *J Lipid Res* **9**, 748–754
15. Parsons, J. B., and Rock, C. O. (2013) Bacterial lipids: Metabolism and membrane homeostasis. *Prog Lipid Res* **52**, 249–276
16. Dowhan, W. (1992) Phosphatidylserine synthase from *Escherichia coli*. *Methods Enzymol* **209**, 287–298
17. Kanfer, J., and Kennedy, E. P. (1964) Metabolism and function of bacterial lipids. II. Biosynthesis of phospholipids in *Escherichia coli*. *J Biol Chem* **239**, 1720–1726
18. Kaneshiro, T., and Law, J. H. (1964) Phosphatidylcholine synthesis in *Agrobacterium tumefaciens*. I. Purification and properties of a phosphatidylethanolamine N-methyltransferase. *J Biol Chem* **239**, 1705–1713
19. de Rudder, K., Sohlenkamp, C., and Geiger, O. (1999) Plant-exuded Choline Is Used for Rhizobial Membrane Lipid Biosynthesis by Phosphatidylcholine Synthase. *J Biol Chem* **274**, 20011–20016
20. Geiger, O., Lopez-Lara, I. M., and Sohlenkamp, C. (2013) Phosphatidylcholine biosynthesis and function in bacteria. *Biochim Biophys Acta* **1831**, 503–513
21. Jackson, M., Crick, D. C., and Brennan, P. J. (2000) Phosphatidylinositol is an essential phospholipid of mycobacteria. *J Biol Chem* **275**, 30092–30099

22. Geiger, O., Gonzalez-Silva, N., Lopez-Lara, I. M., and Sohlenkamp, C. (2010) Amino acid-containing membrane lipids in bacteria. *Prog Lipid Res* **49**, 46–60
23. Chang, Y. Y., and Kennedy, E. P. (1967) Biosynthesis of phosphatidyl glycerophosphate in *Escherichia coli*. *J Lipid Res* **8**, 447–455
24. de Siervo, A., and Salton, M. (1971) Biosynthesis of cardiolipin in the membranes of *Micrococcus lysodeikticus*. *Biochim Biophys Acta* **239**, 280–292
25. Roy, H., and Ibba, M. (2009) Broad range amino acid specificity of RNA-dependent lipid remodeling by multiple peptide resistance factors. *J Biol Chem* **284**, 29677–29683
26. Huijbregts, R. P., de Kroon, A. I., and de Kruijff, B. (2000) Topology and transport of membrane lipids in bacteria. *Biochim Biophys Acta* **1469**, 43–61
27. Malek, A. A., Wargo, M. J., and Hogan, D. A. (2012) Absence of membrane phosphatidylcholine does not affect virulence and stress tolerance phenotypes in the opportunistic pathogen *Pseudomonas aeruginosa*. *PLoS One* **7**, e30829
28. Aktas, M., Danne, L., Moller, P., and Narberhaus, F. (2014) Membrane lipids in *Agrobacterium tumefaciens*: biosynthetic pathways and importance for pathogenesis. *Front Plant Sci* **5**, 109
29. Alberts, B. (2002) Molecular biology of the cell, 4th Ed., Garland Science, New York, NY
30. Mileykovskaya, E., and Dowhan, W. (2000) Visualization of Phospholipid Domains in *Escherichia coli* by Using the Cardiolipin-Specific Fluorescent Dye 10-*N*-Nonyl Acridine Orange. *J Bacteriol* **182**, 1172–1175
31. Matsumoto, K., Kusaka, J., Nishibori, A., and Hara, H. (2006) Lipid domains in bacterial membranes. *Mol Microbiol* **61**, 1110–1117
32. Castuma, C. E., Crooke, E., and Kornberg, A. (1993) Fluid membranes with acidic domains activate DnaA, the initiator protein of replication in *Escherichia coli*. *J Biol Chem* **268**, 24665–24668
33. Kusters, R., Dowhan, W., and de Kruijff, B. (1991) Negatively charged phospholipids restore prePhoE translocation across phosphatidylglycerol-depleted *Escherichia coli* inner membranes. *J Biol Chem* **266**, 8659–8662
34. Kozloff, L. M., Turner, M. A., Arellano, F., and Lute, M. (1991) Phosphatidylinositol, a phospholipid of ice-nucleating bacteria. *J Bacteriol* **173**, 2053–2060
35. Dowhan, W. (1997) Molecular basis for membrane phospholipid diversity: Why are there so many lipids? *Annu Rev Biochem* **66**, 199–232
36. Wang, X., Bogdanov, M., and Dowhan, W. (2002) Topology of polytopic membrane protein subdomains is dictated by membrane phospholipid composition. *EMBO J* **21**, 5673–5681
37. Minder, A. C., de Rudder, K. E., Narberhaus, F., Fischer, H. M., Hennecke, H., and Geiger, O. (2001) Phosphatidylcholine levels in *Bradyrhizobium japonicum* membranes are critical for an efficient symbiosis with the soybean host plant. *Mol Microbiol* **39**, 1186–1198
38. Wessel, M., Klusener, S., Godeke, J., Fritz, C., Hacker, S., and Narberhaus, F. (2006) Virulence of *Agrobacterium tumefaciens* requires phosphatidylcholine in the bacterial membrane. *Mol Microbiol* **62**, 906–915
39. MacFarlane, M. G. (1962) Characterization of Lipoamino-Acids as *O*-Amino-Acid Esters of Phosphatidyl-Glycerol. *Nature* **196**, 136–138
40. Houtsmuller, U. M., and van Deenen, L. L. (1965) On the amino acid esters of phosphatidyl glycerol from bacteria. *Biochim Biophys Acta* **106**, 564–576
41. den Kamp, J. A., Redai, I., and van Deenen, L. L. (1969) Phospholipid composition of *Bacillus subtilis*. *J Bacteriol* **99**, 298–303
42. Roy, H. (2009) Tuning the properties of the bacterial membrane with aminoacylated phosphatidylglycerol. *IUBMB Life* **61**, 940–953
43. Klein, S., Lorenzo, C., Hoffmann, S., Walther, J. M., Storbeck, S., Piekarski, T., Tindall, B. J., Wray, V., Nimtz, M., and Moser, J. (2009) Adaptation of *Pseudomonas aeruginosa* to various conditions includes tRNA-dependent formation of alanyl-phosphatidylglycerol. *Mol Microbiol* **71**, 551–565

44. Dare, K., and Ibba, M. (2012) Roles of tRNA in cell wall biosynthesis. *Wiley Interdiscip Rev RNA* **3**, 247–264
45. Sacre, M. M., El Mashak, E. M., and Tocanne, J. F. (1977) A monolayer (pi,deltaV) study of the ionic properties of alanylphosphatidylglycerol: Effects of pH and ions. *Chem Phys Lipids* **20**, 305–318
46. Jones, T., Yeaman, M. R., Sakoulas, G., Yang, S.-J., Proctor, R. A., Sahl, H.-G., Schrenzel, J., Xiong, Y. Q., and Bayer, A. S. (2008) Failures in clinical treatment of *Staphylococcus aureus* Infection with daptomycin are associated with alterations in surface charge, membrane phospholipid asymmetry, and drug binding. *Antimicrob Agents Chemother* **52**, 269–278
47. Hebecker, S., Arendt, W., Heinemann, I. U., Tiefenau, J. H. J., Nimtz, M., Rohde, M., Soll, D., and Moser, J. (2011) Alanyl-phosphatidylglycerol synthase: mechanism of substrate recognition during tRNA-dependent lipid modification in *Pseudomonas aeruginosa*. *Mol Microbiol* **80**, 935–950
48. Arendt, W., Hebecker, S., Jager, S., Nimtz, M., and Moser, J. (2012) Resistance phenotypes mediated by aminoacyl-phosphatidylglycerol synthases. *J Bacteriol* **194**, 1401–1416
49. Arendt, W., Groenewold, M. K., Hebecker, S., Dickschat, J. S., and Moser, J. (2013) Identification and characterization of a periplasmic aminoacyl-phosphatidylglycerol hydrolase responsible for *Pseudomonas aeruginosa* lipid homeostasis. *J Biol Chem* **288**, 24717–24730
50. Ernst, C. M., Staubitz, P., Mishra, N. N., Yang, S.-J., Hornig, G., Kalbacher, H., Bayer, A. S., Kraus, D., and Peschel, A. (2009) The bacterial defensin resistance protein MprF consists of separable domains for lipid lysinylation and antimicrobial peptide repulsion. *PLoS Pathog* **5**, e1000660
51. Slavetinsky, C. J., Peschel, A., and Ernst, C. M. (2012) Alanyl-phosphatidylglycerol and lysyl-phosphatidylglycerol are translocated by the same MprF flippases and have similar capacities to protect against the antibiotic daptomycin in *Staphylococcus aureus*. *Antimicrob Agents Chemother* **56**, 3492–3497
52. Vinuesa, P., Neumann-Silkow, F., Pacios-Bras, C., Spaink, H. P., Martinez-Romero, E., and Werner, D. (2003) Genetic analysis of a pH-regulated operon from *Rhizobium tropici* CIAT899 involved in acid tolerance and nodulation competitiveness. *Mol Plant Microbe Interact* **16**, 159–168
53. Lewenza, S., Gardy, J. L., Brinkman, F. S. L., and Hancock, R. E. W. (2005) Genome-wide identification of *Pseudomonas aeruginosa* exported proteins using a consensus computational strategy combined with a laboratory-based PhoA fusion screen. *Genome Res* **15**, 321–329
54. Peschel, A., Jack, R. W., Otto, M., Collins, L. V., Staubitz, P., Nicholson, G., Kalbacher, H., Nieuwenhuizen, W. F., Jung, G., Tarkowski, A., van Kessel, K. P., and van Strijp, J. A. (2001) *Staphylococcus aureus* resistance to human defensins and evasion of neutrophil killing via the novel virulence factor MprF is based on modification of membrane lipids with L-lysine. *J Exp Med* **193**, 1067–1076
55. Bao, Y., Sakinc, T., Laverde, D., Wobser, D., Benachour, A., Theilacker, C., Hartke, A., and Huebner, J. (2012) Role of *mprF*1 and *mprF*2 in the pathogenicity of *Enterococcus faecalis*. *PLoS One* **7**, e38458
56. Staubitz, P., Neumann, H., Schneider, T., Wiedemann, I., and Peschel, A. (2004) MprF-mediated biosynthesis of lysylphosphatidylglycerol, an important determinant in staphylococcal defensin resistance. *FEMS Microbiol Lett* **231**, 67–71
57. Hebecker, S., Krausze, J., Hasenkampf, T., Schneider, J., Groenewold, M., Reichelt, J., Jahn, D., Heinz, D. W., and Moser, J. (2015) Structures of two bacterial resistance factors mediating tRNA-dependent aminoacylation of phosphatidylglycerol with lysine or alanine. *Proc Natl Acad Sci U S A* **112**, 10691–10696
58. Arendt, W. (2013) Alanyl-phosphatidylglycerol-dependent lipid homeostasis in *Pseudomonas aeruginosa*. PhD thesis, Technische Universität Braunschweig, Braunschweig, Germany

59. Sohlenkamp, C., Galindo-Lagunas, K. A., Guan, Z., Vinuesa, P., Robinson, S., Thomas-Oates, J., Raetz, C. R. H., and Geiger, O. (2007) The lipid lysyl-phosphatidylglycerol is present in membranes of *Rhizobium tropici* CIAT899 and confers increased resistance to polymyxin B under acidic growth conditions. *Mol Plant Microbe Interact* **20**, 1421–1430
60. Wirawan, I. G., Kang, H. W., and Kojima, M. (1993) Isolation and characterization of a new chromosomal virulence gene of *Agrobacterium tumefaciens*. *J Bacteriol* **175**, 3208–3212
61. Kalogeraki, V. S., and Winans, S. C. (1995) The octopine-type Ti plasmid pTiA6 of *Agrobacterium tumefaciens* contains a gene homologous to the chromosomal virulence gene *acvB*. *J Bacteriol* **177**, 892–897
62. Kang, H. W., Wirawan, I. G., and Kojima, M. (1994) Cellular localization and functional analysis of the protein encoded by the chromosomal virulence gene(*acvB*) of *Agrobacterium tumefaciens*. *Biosci Biotechnol Biochem* **58**, 2024–2032
63. Pan, S. Q., Jin, S., Boulton, M. I., Hawes, M., Gordon, M. P., and Nester, E. W. (1995) An *Agrobacterium* virulence factor encoded by a Ti plasmid gene or a chromosomal gene is required for T-DNA transfer into plants. *Mol Microbiol* **17**, 259–269
64. Pantoja, M., Chen, L., Chen, Y., and Nester, E. W. (2002) *Agrobacterium* type IV secretion is a two-step process in which export substrates associate with the virulence protein VirJ in the periplasm. *Mol Microbiol* **45**, 1325–1335
65. Cascales, E., and Christie, P. J. (2003) The versatile bacterial type IV secretion systems. *Nat Rev Microbiol* **1**, 137–149
66. Escobar, M. A., and Dandekar, A. M. (2003) *Agrobacterium tumefaciens* as an agent of disease. *Trends Plant Sci* **8**, 380–386
67. Gelvin, S. B. (2003) *Agrobacterium*-Mediated Plant Transformation: The Biology behind the "Gene-Jockeying" Tool. *Microbiol Mol Biol Rev* **67**, 16–37
68. de Cleene, M., and de Ley, J. (1976) The host range of crown gall. *Bot Rev* **42**, 389–466
69. Fabre, E., and Dunal, M. F. (1853) Observations sur les maladies régnantes de la vigne. *Bull Soc Cent Agric Dep Herault* **40**, 46
70. Smith, E. F., and Townsend, C. O. (1907) A plant-tumor of bacterial origin. *Science* **25**, 671–673
71. Braun, A. C. (1947) Thermal Studies on the Factors Responsible for Tumor Initiation in Crown Gall. *Am J Bot* **34**, 234
72. Chilton, M.-D., Drummond, M. H., Merlo, D. J., Sciaky, D., Montoya, A. L., Gordon, M. P., and Nester, E. W. (1977) Stable incorporation of plasmid DNA into higher plant cells: The molecular basis of crown gall tumorigenesis. *Cell* **11**, 263–271
73. Winans, S. C. (1992) Two-way chemical signaling in *Agrobacterium*-plant interactions. *Microbiol Rev* **56**, 12–31
74. Stachel, S. E., and Zambryski, P. C. (1986) *virA* and *virG* control the plant-induced activation of the T-DNA transfer process of *A. tumefaciens*. *Cell* **46**, 325–333
75. Howard, E., and Citovsky, V. (1990) The emerging structure of the *Agrobacterium* T-DNA transfer complex. *BioEssays* **12**, 103–108
76. Gelvin, S. B. (2010) Plant proteins involved in *Agrobacterium*-mediated genetic transformation. *Annu Rev Phytopathol* **48**, 45–68
77. Morris, R. O. (1986) Genes Specifying Auxin and Cytokinin Biosynthesis in Phytopathogens. *Annu Rev Plant Physiol* **37**, 509–538
78. Guyon, P., Chilton, M. D., Petit, A., and Tempe, J. (1980) Agropine in "null-type" crown gall tumors: Evidence for generality of the opine concept. *Proc Natl Acad Sci U S A* **77**, 2693–2697
79. Stover, C. K., Pham, X. Q., Erwin, A. L., Mizoguchi, S. D., Warrener, P., Hickey, M. J., Brinkman, F. S., Hufnagle, W. O., Kowalik, D. J., Lagrou, M., Garber, R. L., Goltry, L., Tolentino, E., Westbrock-Wadman, S., Yuan, Y., Brody, L. L., Coulter, S. N., Folger, K. R., Kas, A., Larbig, K., Lim, R., Smith, K., Spencer, D., Wong, G. K.,

Wu, Z., Paulsen, I. T., Reizer, J., Saier, M. H., Hancock, R. E., Lory, S., and Olson, M. V. (2000) Complete genome sequence of *Pseudomonas aeruginosa* PAO1, an opportunistic pathogen. *Nature* **406**, 959–964
80. Schobert, M., and Jahn, D. (2010) Anaerobic physiology of *Pseudomonas aeruginosa* in the cystic fibrosis lung. *Int J Med Microbiol* **300**, 549–556
81. Young, L. S. (1984) The clinical challenge of infections due to *Pseudomonas aeruginosa*. *Rev Infect Dis* **6 Suppl 3**, S603-7
82. Carmeli, Y., Troillet, N., Karchmer, A. W., and Samore, M. H. (1999) Health and Economic Outcomes of Antibiotic Resistance in *Pseudomonas aeruginosa*. *Arch Intern Med* **159**, 1127
83. Strateva, T., and Yordanov, D. (2009) *Pseudomonas aeruginosa* - a phenomenon of bacterial resistance. *J Med Microbiol* **58**, 1133–1148
84. Mesaros, N., Nordmann, P., Plesiat, P., Roussel-Delvallez, M., van Eldere, J., Glupczynski, Y., van Laethem, Y., Jacobs, F., Lebecque, P., Malfroot, A., Tulkens, P. M., and van Bambeke, F. (2007) *Pseudomonas aeruginosa*: Resistance and therapeutic options at the turn of the new millennium. *Clin Microbiol Infect* **13**, 560–578
85. Khoury, A. E., Lam, K., Ellis, B., and Costerton, J. W. (1992) Prevention and control of bacterial infections associated with medical devices. *ASAIO J* **38**, M174-8
86. O'Toole, G. A., and Kolter, R. (1998) Flagellar and twitching motility are necessary for *Pseudomonas aeruginosa* biofilm development. *Mol Microbiol* **30**, 295–304
87. Simm, R., Morr, M., Kader, A., Nimtz, M., and Romling, U. (2004) GGDEF and EAL domains inversely regulate cyclic di-GMP levels and transition from sessility to motility. *Mol Microbiol* **53**, 1123–1134
88. Davies, D. G. (1998) The Involvement of Cell-to-Cell Signals in the Development of a Bacterial Biofilm. *Science* **280**, 295–298
89. Colvin, K. M., Irie, Y., Tart, C. S., Urbano, R., Whitney, J. C., Ryder, C., Howell, P. L., Wozniak, D. J., and Parsek, M. R. (2012) The Pel and Psl polysaccharides provide *Pseudomonas aeruginosa* structural redundancy within the biofilm matrix. *Environ Microbiol* **14**, 1913–1928
90. Stewart, P. S., and Franklin, M. J. (2008) Physiological heterogeneity in biofilms. *Nat Rev Microbiol* **6**, 199–210
91. Williamson, K. S., Richards, L. A., Perez-Osorio, A. C., Pitts, B., McInnerney, K., Stewart, P. S., and Franklin, M. J. (2012) Heterogeneity in *Pseudomonas aeruginosa* biofilms includes expression of ribosome hibernation factors in the antibiotic-tolerant subpopulation and hypoxia-induced stress response in the metabolically active population. *J Bacteriol* **194**, 2062–2073
92. Hoyle, B. D., and Costerton, J. W. (1991) Bacterial resistance to antibiotics: The role of biofilms. *Prog Drug Res* **37**, 91–105
93. Drenkard, E. (2003) Antimicrobial resistance of *Pseudomonas aeruginosa* biofilms. *Microbes Infect* **5**, 1213–1219
94. Costerton, J. W., Stewart, P. S., and Greenberg, E. P. (1999) Bacterial biofilms: A common cause of persistent infections. *Science* **284**, 1318–1322
95. Ratjen, F., and Döring, G. (2003) Cystic fibrosis. *The Lancet* **361**, 681–689
96. Gaspar, M. C., Couet, W., Olivier, J.-C., Pais, A. A. C. C., and Sousa, J. J. S. (2013) *Pseudomonas aeruginosa* infection in cystic fibrosis lung disease and new perspectives of treatment: A review. *Eur J Clin Microbiol Infect Dis* **32**, 1231–1252
97. George, A. M., Jones, P. M., and Middleton, P. G. (2009) Cystic fibrosis infections: Treatment strategies and prospects. *FEMS Microbiol Lett* **300**, 153–164
98. Boucher, R. C. (2007) Airway surface dehydration in cystic fibrosis: Pathogenesis and therapy. *Annu Rev Med* **58**, 157–170
99. Worlitzsch, D., Tarran, R., Ulrich, M., Schwab, U., Cekici, A., Meyer, K. C., Birrer, P., Bellon, G., Berger, J., Weiss, T., Botzenhart, K., Yankaskas, J. R., Randell, S., Boucher, R. C., and Döring, G. (2002) Effects of reduced mucus oxygen concentration in airway *Pseudomonas* infections of cystic fibrosis patients. *J Clin Invest* **109**, 317–325

100. Rogers, G. B., Carroll, M. P., Serisier, D. J., Hockey, P. M., Jones, G., and Bruce, K. D. (2004) Characterization of bacterial community diversity in cystic fibrosis lung infections by use of 16S ribosomal DNA terminal restriction fragment length polymorphism profiling. *J Clin Microbiol* **42**, 5176–5183
101. Geller, D. E. (2009) Aerosol antibiotics in cystic fibrosis. *Respir Care* **54**, 658–670
102. Smith, E. E., Buckley, D. G., Wu, Z., Saenphimmachak, C., Hoffman, L. R., D'Argenio, D. A., Miller, S. I., Ramsey, B. W., Speert, D. P., Moskowitz, S. M., Burns, J. L., Kaul, R., and Olson, M. V. (2006) Genetic adaptation by *Pseudomonas aeruginosa* to the airways of cystic fibrosis patients. *Proc Natl Acad Sci U S A* **103**, 8487–8492
103. Oliver, A., Canton, R., Campo, P., Baquero, F., and Blazquez, J. (2000) High frequency of hypermutable *Pseudomonas aeruginosa* in cystic fibrosis lung infection. *Science* **288**, 1251–1254
104. Hogardt, M., and Heesemann, J. (2013) Microevolution of *Pseudomonas aeruginosa* to a chronic pathogen of the cystic fibrosis lung. *Curr Top Microbiol Immunol* **358**, 91–118
105. Poetsch, A., and Wolters, D. (2008) Bacterial membrane proteomics. *Proteomics* **8**, 4100–4122
106. Krogh, A., Larsson, B., von Heijne, G., and Sonnhammer, E. L. (2001) Predicting transmembrane protein topology with a hidden Markov model: application to complete genomes. *J Mol Biol* **305**, 567–580
107. Wilson, J. W., Schurr, M., LeBlanc, C., Ramamurthy, R., Buchanan, K., and Nickerson, C. (2002) Mechanisms of bacterial pathogenicity. *Postgrad Med J* **78**, 216–224
108. Thein, M., Sauer, G., Paramasivam, N., Grin, I., and Linke, D. (2010) Efficient Subfractionation of Gram-negative Bacteria for Proteomics Studies. *J Proteome Res* **9**, 6135–6147
109. Klose, J. (1975) Protein mapping by combined isoelectric focusing and electrophoresis of mouse tissues. A novel approach to testing for induced point mutations in mammals. *Humangenetik* **26**, 231–243
110. O'Farrell, P. H. (1975) High resolution two-dimensional electrophoresis of proteins. *J Biol Chem* **250**, 4007–4021
111. Blonder, J., Goshe, M. B., Xiao, W., Camp, D. G., Wingerd, M., Davis, R. W., and Smith, R. D. (2004) Global Analysis of the Membrane Subproteome of *Pseudomonas aeruginosa* Using Liquid Chromatography-Tandem Mass Spectrometry. *J Proteome Res* **3**, 434–444
112. Wu, C. C., and Yates, J. R. 3. (2003) The application of mass spectrometry to membrane proteomics. *Nat Biotechnol* **21**, 262–267
113. Magnowska, Z. (2010) Membranes provide new insight into the pathogenicity of *Pseudomonas aeruginosa* in cystic fibrosis. PhD thesis, Medizinische Hochschule Hannover, Hannover, Germany
114. Ross, P. L., Huang, Y. N., Marchese, J. N., Williamson, B., Parker, K., Hattan, S., Khainovski, N., Pillai, S., Dey, S., Daniels, S., Purkayastha, S., Juhasz, P., Martin, S., Bartlet-Jones, M., He, F., Jacobson, A., and Pappin, D. J. (2004) Multiplexed protein quantitation in *Saccharomyces cerevisiae* using amine-reactive isobaric tagging reagents. *Mol Cell Proteomics* **3**, 1154–1169
115. Zieske, L. R. (2006) A perspective on the use of iTRAQ reagent technology for protein complex and profiling studies. *J Exp Bot* **57**, 1501–1508
116. Hundertmark, C., Fischer, R., Reinl, T., May, S., Klawonn, F., and Jansch, L. (2009) MS-specific noise model reveals the potential of iTRAQ in quantitative proteomics. *Bioinformatics* **25**, 1004–1011
117. Filiatrault, M. J., Picardo, K. F., Ngai, H., Passador, L., and Iglewski, B. H. (2006) Identification of *Pseudomonas aeruginosa* genes involved in virulence and anaerobic growth. *Infect Immun* **74**, 4237–4245

118. Alvarez-Ortega, C., and Harwood, C. S. (2007) Responses of *Pseudomonas aeruginosa* to low oxygen indicate that growth in the cystic fibrosis lung is by aerobic respiration. *Mol Microbiol* **65**, 153–165
119. Trunk, K. (2005) Definition des regulatorischen Netzwerkes von *Pseudomonas aeruginosa* zur Anpassung an anaerobe Lebensbedingungen. PhD thesis, Technische Universität Braunschweig, Braunschweig, Germany
120. Benkert, B. (2009) Regulatory and metabolic adaptation of *Pseudomonas aeruginosa* to changes in oxygen tension and growth phase. PhD thesis, Technische Universität Braunschweig, Braunschweig, Germany
121. Wu, M., Guina, T., Brittnacher, M., Nguyen, H., Eng, J., and Miller, S. I. (2005) The *Pseudomonas aeruginosa* proteome during anaerobic growth. *J Bacteriol* **187**, 8185–8190
122. Palmer, G. C. (2012) Investigations into the Role of Aromatic Amino Acids in Quorum Sensing-mediated Virulence in *Pseudomonas aeruginosa*. PhD thesis, University of Texas at Austin, Austin, TX, USA
123. Overhage, J., Lewenza, S., Marr, A. K., and Hancock, R. E. W. (2007) Identification of genes involved in swarming motility using a *Pseudomonas aeruginosa* PAO1 mini-Tn*5*-*lux* mutant library. *J Bacteriol* **189**, 2164–2169
124. Ockner, R. K., Manning, J. A., Poppenhausen, R. B., and Ho, W. K. (1972) A binding protein for fatty acids in cytosol of intestinal mucosa, liver, myocardium, and other tissues. *Science* **177**, 56–58
125. Burgardt, N. I., Gianotti, A. R., Ferreyra, R. G., and Ermacora, M. R. (2017) A structural appraisal of sterol carrier protein 2. *Biochim Biophys Acta* **1865**, 565–577
126. Choinowski, T., Hauser, H., and Piontek, K. (2000) Structure of Sterol Carrier Protein 2 at 1.8 Å Resolution Reveals a Hydrophobic Tunnel Suitable for Lipid Binding. *Biochemistry* **39**, 1897–1902
127. Gallegos, A. M., Atshaves, B. P., Storey, S. M., Starodub, O., Petrescu, A. D., Huang, H., McIntosh, A. L., Martin, G. G., Chao, H., Kier, A. B., and Schroeder, F. (2001) Gene structure, intracellular localization, and functional roles of sterol carrier protein-2. *Prog Lipid Res* **40**, 498–563
128. Seedorf, U., Brysch, P., Engel, T., Schrage, K., and Assmann, G. (1994) Sterol carrier protein X is peroxisomal 3-oxoacyl coenzyme A thiolase with intrinsic sterol carrier and lipid transfer activity. *J Biol Chem* **269**, 21277–21283
129. Haapalainen, A. M., van Aalten, D. M., Merilainen, G., Jalonen, J. E., Pirila, P., Wierenga, R. K., Hiltunen, J. K., and Glumoff, T. (2001) Crystal structure of the liganded SCP-2-like domain of human peroxisomal multifunctional enzyme type 2 at 1.75 A resolution. *J Mol Biol* **313**, 1127–1138
130. Dyer, D. H., Lovell, S., Thoden, J. B., Holden, H. M., Rayment, I., and Lan, Q. (2003) The structural determination of an insect sterol carrier protein-2 with a ligand-bound C16 fatty acid at 1.35-A resolution. *J Biol Chem* **278**, 39085–39091
131. Studier, F. W., Rosenberg, A. H., Dunn, J. J., and Dubendorff, J. W. (1990) Use of T7 RNA polymerase to direct expression of cloned genes. *Methods Enzymol* **185**, 60–89
132. Grant, S. G., Jessee, J., Bloom, F. R., and Hanahan, D. (1990) Differential plasmid rescue from transgenic mouse DNAs into *Escherichia coli* methylation-restriction mutants. *Proc Natl Acad Sci U S A* **87**, 4645–4649
133. Thoma, S., and Schobert, M. (2009) An improved *Escherichia coli* donor strain for diparental mating. *FEMS Microbiol Lett* **294**, 127–132
134. Jacobs, M. A., Alwood, A., Thaipisuttikul, I., Spencer, D., Haugen, E., Ernst, S., Will, O., Kaul, R., Raymond, C., Levy, R., Chun-Rong, L., Guenthner, D., Bovee, D., Olson, M. V., and Manoil, C. (2003) Comprehensive transposon mutant library of *Pseudomonas aeruginosa*. *Proc Natl Acad Sci U S A* **100**, 14339–14344
135. Arnold, M. E. (2016) Towards the structure of the aminoacyl-phosphatidylglycerol hydrolase from *Pseudomonas aeruginosa*. Master thesis, Technische Universität Braunschweig, Braunschweig, Germany

136. Wiesselmann, M. J. (2014) In-Fusion HD Cloning als neuartige Klonierungsstrategie und Charakterisierung einer Lysyl-Phosphatidylglycerol Hydrolase aus *Agrobacterium tumefaciens*. Bachelor thesis, Technische Universität Braunschweig, Braunschweig, Germany
137. Wendtland, A. (2015) Lysyl-Phosphatidylglycerol-Hydrolase aus *Agrobacterium tumefaciens*. Bachelor thesis, Technische Universität Braunschweig, Braunschweig, Germany
138. Wolf, A.-K. (2013) Untersuchungen zum potentiellen Lipid-Carrier PA3911 aus *Pseudomonas aeruginosa*. Master thesis, Technische Universität Braunschweig, Braunschweig, Germany
139. Massmig, M. (2014) Reinigen und Charakterisierung des potentiellen Lipid-Carrier-Proteins PA3911 aus *Pseudomonas aeruginosa*. Bachelor thesis, Technische Universität Braunschweig, Braunschweig, Germany
140. Hoang, T. T., Karkhoff-Schweizer, R. R., Kutchma, A. J., and Schweizer, H. P. (1998) A broad-host-range Flp-FRT recombination system for site-specific excision of chromosomally-located DNA sequences: application for isolation of unmarked *Pseudomonas aeruginosa* mutants. *Gene* **212**, 77–86
141. Uliczka, F., Pisano, F., Kochut, A., Opitz, W., Herbst, K., Stolz, T., and Dersch, P. (2011) Monitoring of gene expression in bacteria during infections using an adaptable set of bioluminescent, fluorescent and colorigenic fusion vectors. *PLoS One* **6**, e20425
142. Pusch, I. (2015) Untersuchungen zur Lokalisierung der Lysyl-Phosphatidylglycerol Hydrolasen AcvB und VirJ aus *Agrobacterium tumefaciens*. Bachelor thesis, Technische Universität Braunschweig, Braunschweig, Germany
143. Schmidt-Eisenlohr, H., Domke, N., and Baron, C. (1999) TraC of IncN plasmid pKM101 associates with membranes and extracellular high-molecular-weight structures in *Escherichia coli*. *J Bacteriol* **181**, 5563–5571
144. West, S., Schweizer, H. P., Dall, C., Sample, A. K., and Runyen-Janecky, L. J. (1994) Construction of improved *Escherichia-Pseudomonas* shuttle vectors derived from pUC18/19 and sequence of the region required for their replication in *Pseudomonas aeruginosa*. *Gene* **148**, 81–86
145. Müller, C. (2016) Charakterisierung der Lysyl-Phosphatidylglycerol Hydrolase AcvB aus *Agrobacterium tumefaciens*. Bachelor thesis, Technische Universität Braunschweig, Braunschweig, Germany
146. Sambrook, J., and Russell, D. W. (2001) Molecular cloning: A laboratory manual, 3rd Ed., Cold Spring Harbor Laboratory Press, Cold Spring Harbor, N.Y
147. Heydorn, A., Nielsen, A. T., Hentzer, M., Sternberg, C., Givskov, M., Ersboll, B. K., and Molin, S. (2000) Quantification of biofilm structures by the novel computer program COMSTAT. *Microbiology* **146 (Pt 10)**, 2395–2407
148. Schmidt-Eisenlohr, H., Domke, N., Angerer, C., Wanner, G., Zambryski, P. C., and Baron, C. (1999) Vir proteins stabilize VirB5 and mediate its association with the T pilus of *Agrobacterium tumefaciens*. *J Bacteriol* **181**, 7485–7492
149. Wu, H. Y., Liu, K. H., Wang, Y. C., Wu, J. F., Chiu, W. L., Chen, C. Y., Wu, S. H., Sheen, J., and Lai, E. M. (2014) AGROBEST: an efficient *Agrobacterium*-mediated transient expression method for versatile gene function analyses in *Arabidopsis* seedlings. *Plant methods* **10:19**
150. Heidler, T. V. (2015) Structural investigation of the *Yersinia pseudotuberculosis* AB-toxin CNF_Y. PhD thesis, Technische Universität Braunschweig, Braunschweig, Germany
151. Engler, C., Kandzia, R., and Marillonnet, S. (2008) A one pot, one step, precision cloning method with high throughput capability. *PLoS One* **3**, e3647
152. Xu, R., and Li, Q. Q. (2008) Protocol: Streamline cloning of genes into binary vectors in *Agrobacterium* via the Gateway® TOPO vector system. *Plant methods* **4**, 4

153. Mullis, K., Faloona, F., Scharf, S., Saiki, R., Horn, G., and Erlich, H. (1986) Specific enzymatic amplification of DNA in vitro: the polymerase chain reaction. *Cold Spring Harb Symp Quant Biol* **51 Pt 1**, 263–273
154. Zhu, B., Cai, G., Hall, E. O., and Freeman, G. J. (2007) In-Fusion™ assembly: seamless engineering of multidomain fusion proteins, modular vectors, and mutations. *Biotechniques* **43**, 354–359
155. Schmidt, T. G. M., and Skerra, A. (2007) The Strep-tag system for one-step purification and high-affinity detection or capturing of proteins. *Nat Protoc* **2**, 1528–1535
156. Derewenda, Z. S. (2004) Rational protein crystallization by mutational surface engineering. *Structure* **12**, 529–535
157. Hoffman, C. S., and Wright, A. (1985) Fusions of secreted proteins to alkaline phosphatase: an approach for studying protein secretion. *Proc Natl Acad Sci U S A* **82**, 5107–5111
158. Sanger, F., Nicklen, S., and Coulson, A. R. (1977) DNA sequencing with chain-terminating inhibitors. *Proc Natl Acad Sci U S A* **74**, 5463–5467
159. Quan, S., Hiniker, A., Collet, J.-F., and Bardwell, J. C. A. (2013) Isolation of bacteria envelope proteins. *Methods Mol Biol* **966**, 359–366
160. Bradford, M. M. (1976) A rapid and sensitive method for the quantitation of microgram quantities of protein utilizing the principle of protein-dye binding. *Anal Biochem* **72**, 248–254
161. Laemmli, U. K. (1970) Cleavage of Structural Proteins during the Assembly of the Head of Bacteriophage T4. *Nature* **227**, 680–685
162. Righetti, P. G. (1990) Recent developments in electrophoretic methods. *J Chromatogr* **516**, 3–22
163. Edman, P., Högfeldt, E., Sillén, L. G., and Kinell, P.-O. (1950) Method for Determination of the Amino Acid Sequence in Peptides. *Acta Chem Scand* **4**, 283–293
164. Niesen, F. H., Berglund, H., and Vedadi, M. (2007) The use of differential scanning fluorimetry to detect ligand interactions that promote protein stability. *Nat Protoc* **2**, 2212–2221
165. Mertens, H. D. T., and Svergun, D. I. (2010) Structural characterization of proteins and complexes using small-angle X-ray solution scattering. *J Struct Biol* **172**, 128–141
166. Skou, S., Gillilan, R. E., and Ando, N. (2014) Synchrotron-based small-angle X-ray scattering of proteins in solution. *Nat Protoc* **9**, 1727–1739
167. Pernot, P., Round, A., Barrett, R., de Maria Antolinos, A., Gobbo, A., Gordon, E., Huet, J., Kieffer, J., Lentini, M., Mattenet, M., Morawe, C., Mueller-Dieckmann, C., Ohlsson, S., Schmid, W., Surr, J., Theveneau, P., Zerrad, L., and McSweeney, S. (2013) Upgraded ESRF BM29 beamline for SAXS on macromolecules in solution. *J Synchrotron Radiat* **20**, 660–664
168. Petoukhov, M. V., Franke, D., Shkumatov, A. V., Tria, G., Kikhney, A. G., Gajda, M., Gorba, C., Mertens, H. D. T., Konarev, P. V., and Svergun, D. I. (2012) New developments in the ATSAS program package for small-angle scattering data analysis. *J Appl Crystallogr* **45**, 342–350
169. Bligh, E. G., and Dyer, W. J. (1959) A rapid method of total lipid extraction and purification. *Can J Biochem Physiol* **37**, 911–917
170. Czolkoss, S., Fritz, C., Holzl, G., and Aktas, M. (2016) Two Distinct Cardiolipin Synthases Operate in *Agrobacterium tumefaciens*. *PLoS One* **11**, e0160373
171. Tindall, B. J. (1990) Lipid composition of *Halobacterium lacusprofundi*. *FEMS Microbiol Lett* **66**, 199–202
172. Vaden, D. L., Gohil, V. M., Gu, Z., and Greenberg, M. L. (2005) Separation of yeast phospholipids using one-dimensional thin-layer chromatography. *Anal Biochem* **338**, 162–164
173. Abramson, D., and Blecher, M. (1964) Quantitative two-dimensional thin-layer chromatography of naturally occurring phospholipids. *J Lipid Res* **5**, 628–631

174. Cazes, J., Ed. (2001) Encyclopedia of chromatography, Dekker, New York
175. Filloux, A., and Ramos, J.-L., Eds. (2014) Pseudomonas Methods and Protocols, Humana Press Springer, New York
176. Smejkal, G. B., and Kaul, C. A. (2001) Stability of nitroblue tetrazolium-based alkaline phosphatase substrates. *J Histochem Cytochem* **49**, 1189–1190
177. De Maagd, R. A., and Lugtenberg, B. (1986) Fractionation of *Rhizobium leguminosarum* cells into outer membrane, cytoplasmic membrane, periplasmic, and cytoplasmic components. *J Bacteriol* **167**, 1083–1085
178. Wu, H.-Y., Chung, P.-C., Shih, H.-W., Wen, S.-R., and Lai, E.-M. (2008) Secretome analysis uncovers an Hcp-family protein secreted via a type VI secretion system in *Agrobacterium tumefaciens*. *J Bacteriol* **190**, 2841–2850
179. Forsythe, E. L., Maxwell, D. L., and Pusey, M. (2002) Vapor diffusion, nucleation rates and the reservoir to crystallization volume ratio. *Acta Crystallogr D Biol Crystallogr* **58**, 1601–1605
180. Bergfors, T. M., Ed. (2009) Protein crystallization, 2nd Ed., International University Line, La Jolla, CA
181. Burkhardt, A., Pakendorf, T., Reime, B., Meyer, J., Fischer, P., Stübe, N., Panneerselvam, S., Lorbeer, O., Stachnik, K., Warmer, M., Rödig, P., Göries, D., and Meents, A. (2016) Status of the crystallography beamlines at PETRA III. *Eur Phys J Plus* **131**
182. Kabsch, W. (2010) XDS. *Acta Crystallogr D Biol Crystallogr* **66**, 125–132
183. Kabsch, W. (2010) Integration, scaling, space-group assignment and post-refinement. *Acta Crystallogr D Biol Crystallogr* **66**, 133–144
184. Sheldrick, G. M. (2010) Experimental phasing with *SHELXC/D/E*: Combining chain tracing with density modification. *Acta Crystallogr D Biol Crystallogr* **66**, 479–485
185. Emsley, P., and Cowtan, K. (2004) Coot: model-building tools for molecular graphics. *Acta Crystallogr D Biol Crystallogr* **60**, 2126–2132
186. Adams, P. D., Afonine, P. V., Bunkoczi, G., Chen, V. B., Davis, I. W., Echols, N., Headd, J. J., Hung, L.-W., Kapral, G. J., Grosse-Kunstleve, R. W., McCoy, A. J., Moriarty, N. W., Oeffner, R., Read, R. J., Richardson, D. C., Richardson, J. S., Terwilliger, T. C., and Zwart, P. H. (2010) PHENIX: a comprehensive Python-based system for macromolecular structure solution. *Acta Crystallogr D Biol Crystallogr* **66**, 213–221
187. Goldschmidt, L., Cooper, D. R., Derewenda, Z. S., and Eisenberg, D. (2007) Toward rational protein crystallization: A Web server for the design of crystallizable protein variants. *Protein Sci* **16**, 1569–1576
188. Chen, V. B., Arendall, W. B., Headd, J. J., Keedy, D. A., Immormino, R. M., Kapral, G. J., Murray, L. W., Richardson, J. S., and Richardson, D. C. (2010) MolProbity: all-atom structure validation for macromolecular crystallography. *Acta Crystallogr D Biol Crystallogr* **66**, 12–21
189. Kantardjieff, K. A., and Rupp, B. (2003) Matthews coefficient probabilities: Improved estimates for unit cell contents of proteins, DNA, and protein-nucleic acid complex crystals. *Protein Sci* **12**, 1865–1871
190. Collaborative Computational Project, Number 4 (1994) The CCP4 suite: programs for protein crystallography. *Acta Crystallogr D Biol Crystallogr* **50**, 760–763
191. Potterton, E., Briggs, P., Turkenburg, M., and Dodson, E. (2003) A graphical user interface to the CCP4 program suite. *Acta Crystallogr D Biol Crystallogr* **59**, 1131–1137
192. Baker, N. A., Sept, D., Joseph, S., Holst, M. J., and McCammon, J. A. (2001) Electrostatics of nanosystems: application to microtubules and the ribosome. *Proc Natl Acad Sci U S A* **98**, 10037–10041
193. Holm, L., Kaariainen, S., Rosenstrom, P., and Schenkel, A. (2008) Searching protein structure databases with DaliLite v.3. *Bioinformatics* **24**, 2780–2781

194. Holm, L., and Sander, C. (1993) Protein structure comparison by alignment of distance matrices. *J Mol Biol* **233**, 123–138
195. Altschul, S. F., Gish, W., Miller, W., Myers, E. W., and Lipman, D. J. (1990) Basic local alignment search tool. *J Mol Biol* **215**, 403–410
196. Sievers, F., Wilm, A., Dineen, D., Gibson, T. J., Karplus, K., Li, W., Lopez, R., McWilliam, H., Remmert, M., Soding, J., Thompson, J. D., and Higgins, D. G. (2011) Fast, scalable generation of high-quality protein multiple sequence alignments using Clustal Omega. *Mol Syst Biol* **7**, 539
197. Mao, X., Ma, Q., Zhou, C., Chen, X., Zhang, H., Yang, J., Mao, F., Lai, W., and Xu, Y. (2014) DOOR 2.0: presenting operons and their functions through dynamic and integrated views. *Nucleic Acids Res* **42**, 9
198. Juncker, A. S., Willenbrock, H., von Heijne, G., Brunak, S., Nielsen, H., and Krogh, A. (2003) Prediction of lipoprotein signal peptides in Gram-negative bacteria. *Protein Sci* **12**, 1652–1662
199. Goldberg, T., Hecht, M., Hamp, T., Karl, T., Yachdav, G., Ahmed, N., Altermann, U., Angerer, P., Ansorge, S., Balasz, K., Bernhofer, M., Betz, A., Cizmadija, L., Do, K. T., Gerke, J., Greil, R., Joerdens, V., Hastreiter, M., Hembach, K., Herzog, M., Kalemanov, M., Kluge, M., Meier, A., Nasir, H., Neumaier, U., Prade, V., Reeb, J., Sorokoumov, A., Troshani, I., Vorberg, S., Waldraff, S., Zierer, J., Nielsen, H., and Rost, B. (2014) LocTree3 prediction of localization. *Nucleic Acids Res* **42**, 5
200. Käll, L., Krogh, A., and Sonnhammer, E. L. L. (2004) A combined transmembrane topology and signal peptide prediction method. *J Mol Biol* **338**, 1027–1036
201. Hiller, K., Grote, A., Scheer, M., Munch, R., and Jahn, D. (2004) PrediSi: prediction of signal peptides and their cleavage positions. *Nucleic Acids Res* **32**, 9
202. Yu, N. Y., Wagner, J. R., Laird, M. R., Melli, G., Rey, S., Lo, R., Dao, P., Sahinalp, S. C., Ester, M., Foster, L. J., and Brinkman, F. S. L. (2010) PSORTb 3.0: improved protein subcellular localization prediction with refined localization subcategories and predictive capabilities for all prokaryotes. *Bioinformatics* **26**, 1608–1615
203. Petersen, T. N., Brunak, S., von Heijne, G., and Nielsen, H. (2011) SignalP 4.0: discriminating signal peptides from transmembrane regions. *Nat Methods* **8**, 785–786
204. Biasini, M., Bienert, S., Waterhouse, A., Arnold, K., Studer, G., Schmidt, T., Kiefer, F., Gallo Cassarino, T., Bertoni, M., Bordoli, L., and Schwede, T. (2014) SWISS-MODEL: modelling protein tertiary and quaternary structure using evolutionary information. *Nucleic Acids Res* **42**, 8
205. Schrödinger, L. (2010) The PyMOL Molecular Graphics System (Schrödinger, LLC, New York), Version 1.5.0.4
206. Walden, H. (2010) Selenium incorporation using recombinant techniques. *Acta Crystallogr D Biol Crystallogr* **66**, 352–357
207. Barton, W. A., Tzvetkova-Robev, D., Erdjument-Bromage, H., Tempst, P., and Nikolov, D. B. (2006) Highly efficient selenomethionine labeling of recombinant proteins produced in mammalian cells. *Protein Sci* **15**, 2008–2013
208. Matthews, B. W. (1968) Solvent content of protein crystals. *J Mol Biol* **33**, 491–497
209. Karplus, P. A., and Diederichs, K. (2012) Linking crystallographic model and data quality. *Science* **336**, 1030–1033
210. Brünger, A. T. (1992) Free R value: a novel statistical quantity for assessing the accuracy of crystal structures. *Nature* **355**, 472–475
211. Debye, P. (1913) Interferenz von Röntgenstrahlen und Wärmebewegung. *Ann Phys* **348**, 49–92
212. Waller, I. (1923) Zur Frage der Einwirkung der Wärmebewegung auf die Interferenz von Röntgenstrahlen. *Z Phys* **17**, 398–408

213. Ramachandran, G. N., Ramakrishnan, C., and Sasisekharan, V. (1963) Stereochemistry of polypeptide chain configurations. *J Mol Biol* **7**, 95–99
214. Holm, L., and Rosenström, P. (2010) Dali server: conservation mapping in 3D. *Nucleic Acids Res* **38**, 9
215. Gehret, J. J., Gu, L., Gerwick, W. H., Wipf, P., Sherman, D. H., and Smith, J. L. (2011) Terminal alkene formation by the thioesterase of curacin A biosynthesis: structure of a decarboxylating thioesterase. *J Biol Chem* **286**, 14445–14454
216. Jensen, M.-B. V., Horsfall, L. E., Wardrope, C., Togneri, P. D., Marles-Wright, J., and Rosser, S. J. (2016) Characterisation of a New Family of Carboxyl Esterases with an OsmC Domain. *PLoS One* **11**, e0166128
217. McCulloch, K. M., Mukherjee, T., Begley, T. P., and Ealick, S. E. (2010) Structure determination and characterization of the vitamin B6 degradative enzyme (E)-2-(acetamidomethylene)succinate hydrolase. *Biochemistry* **49**, 1226–1235
218. Lai, K.-K., Stogios, P. J., Vu, C., Xu, X., Cui, H., Molloy, S., Savchenko, A., Yakunin, A., and Gonzalez, C. F. (2011) An inserted alpha/beta subdomain shapes the catalytic pocket of *Lactobacillus johnsonii* cinnamoyl esterase. *PLoS One* **6**, e23269
219. Fu, J., Leiros, H.-K. S., de Pascale, D., Johnson, K. A., Blencke, H.-M., and Landfald, B. (2013) Functional and structural studies of a novel cold-adapted esterase from an Arctic intertidal metagenomic library. *Appl Microbiol Biotechnol* **97**, 3965–3978
220. Ollis, D. L., Cheah, E., Cygler, M., Dijkstra, B., Frolow, F., Franken, S. M., Harel, M., Remington, S. J., Silman, I., and Schrag, J. (1992) The alpha/beta hydrolase fold. *Protein Eng* **5**, 197–211
221. Carr, P. D., and Ollis, D. L. (2009) Alpha/beta hydrolase fold: An update. *Protein Pept Lett* **16**, 1137–1148
222. Putnam, C. D., Hammel, M., Hura, G. L., and Tainer, J. A. (2007) X-ray solution scattering (SAXS) combined with crystallography and computation: Defining accurate macromolecular structures, conformations and assemblies in solution. *Q Rev Biophys* **40**, 191–285
223. Breisch, J. (2015) Charakterisierung der Lysyl-Phosphatidylglycerol Hydrolasen AcvB und VirJ. Bachelor thesis, Technische Universität Braunschweig, Braunschweig, Germany
224. Uhlig, C. (2011) Säureinduzierte Lipidmodifikation in unterschiedlichen Mikroorganismen. Bachelor thesis, Technische Universität Braunschweig, Braunschweig, Germany
225. Aktas, M., and Narberhaus, F. (2009) *In vitro* characterization of the enzyme properties of the phospholipid N-methyltransferase PmtA from *Agrobacterium tumefaciens*. *J Bacteriol* **191**, 2033–2041
226. Smith, R. J. (1995) Calcium and bacteria. *Adv Microb Physiol* **37**, 83–133
227. Groenewold, M. (2013) Aminoacyl-Phosphatidylglycerol Hydrolase aus *Pseudomonas aeruginosa* PAO1. Master thesis, Technische Universität Braunschweig, Braunschweig, Germany
228. Derman, A. I., and Beckwith, J. (1991) *Escherichia coli* alkaline phosphatase fails to acquire disulfide bonds when retained in the cytoplasm. *J Bacteriol* **173**, 7719–7722
229. Salmond, G. P. C. (1994) Secretion of Extracellular Virulence Factors by Plant Pathogenic Bacteria. *Annu Rev Phytopathol* **32**, 181–200
230. Link, G. K. K., and Eggers, V. (1941) Hyperauxiny in Crown Gall of Tomato. *Bot Gaz* **103**, 87–106
231. Braun, A. C. (1958) A Physiological Basis for Autonomous Growth of the Crown-Gall Tumor Cell. *Proc Natl Acad Sci U S A* **44**, 344–349
232. Christie, P. J. (1997) *Agrobacterium tumefaciens* T-complex transport apparatus: a paradigm for a new family of multifunctional transporters in eubacteria. *J Bacteriol* **179**, 3085–3094

233. Zambryski, P., Holsters, M., Kruger, K., Depicker, A., Schell, J., van Montagu, M., and Goodman, H. (1980) Tumor DNA structure in plant cells transformed by *A. tumefaciens*. *Science* **209**, 1385–1391
234. Narasimhulu, S. B., Deng, X. B., Sarria, R., and Gelvin, S. B. (1996) Early Transcription of *Agrobacterium* T-DNA Genes in Tobacco and Maize. *Plant Cell* **8**, 873–886
235. Jefferson, R. A., Kavanagh, T. A., and Bevan, M. W. (1987) GUS fusions: beta-glucuronidase as a sensitive and versatile gene fusion marker in higher plants. *EMBO J* **6**, 3901–3907
236. Vences-Guzmán, M. A., Guan, Z., Bermúdez-Barrientos, J. R., Geiger, O., and Sohlenkamp, C. (2013) Agrobacteria lacking ornithine lipids induce more rapid tumour formation. *Environ Microbiol* **15**, 895–906
237. Chumakov, M. I. (2013) Protein apparatus for horizontal transfer of agrobacterial T-DNA to eukaryotic cells. *Biochemistry (Mosc)* **78**, 1321–1332
238. Wirawan, I. G., and Kojima, M. (1996) A Chromosomal Virulence Gene (*acvB*) Product of *Agrobacterium tumefaciens* That Binds to a T-Strand to Mediate Its Transfer to Host Plant Cells. *Biosci Biotechnol Biochem* **60**, 44–49
239. Yoshioka, Y., Takahashi, Y., Matsuoka, K., Nakamura, K., Koizumi, J., Kojima, M., and Machida, Y. (1996) Transient Gene Expression in Plant Cells Mediated by *Agrobacterium tumefaciens*: Application for the Analysis of Virulence Loci. *Plant Cell Physiol* **37**, 782–789
240. Stolowich, N. J., Petrescu, A. D., Huang, H., Martin, G. G., Scott, A. I., and Schroeder, F. (2002) Sterol carrier protein-2: Structure reveals function. *Cell Mol Life Sci* **59**, 193–212
241. Li, N. C., Fan, J., and Papadopoulos, V. (2016) Sterol Carrier Protein-2, a Nonspecific Lipid-Transfer Protein, in Intracellular Cholesterol Trafficking in Testicular Leydig Cells. *PLoS One* **11**, e0149728
242. Finn, R. D., Coggill, P., Eberhardt, R. Y., Eddy, S. R., Mistry, J., Mitchell, A. L., Potter, S. C., Punta, M., Qureshi, M., Sangrador-Vegas, A., Salazar, G. A., Tate, J., and Bateman, A. (2016) The Pfam protein families database: Towards a more sustainable future. *Nucleic Acids Res* **44**, D279-85
243. Habig, W. H., Pabst, M. J., and Jakoby, W. B. (1974) Glutathione S-transferases. The first enzymatic step in mercapturic acid formation. *J Biol Chem* **249**, 7130–7139
244. Kazmierczak, B. I., Schniederberend, M., and Jain, R. (2015) Cross-regulation of *Pseudomonas* motility systems: The intimate relationship between flagella, pili and virulence. *Curr Opin Microbiol* **28**, 78–82
245. Persat, A., Inclan, Y. F., Engel, J. N., Stone, H. A., and Gitai, Z. (2015) Type IV pili mechanochemically regulate virulence factors in *Pseudomonas aeruginosa*. *Proc Natl Acad Sci U S A* **112**, 7563–7568
246. Turnbull, L., and Whitchurch, C. B. (2014) Motility assay: Twitching motility. *Methods Mol Biol* **1149**, 73–86
247. Klausen, M., Aaes-Jørgensen, A., Molin, S., and Tolker-Nielsen, T. (2003) Involvement of bacterial migration in the development of complex multicellular structures in *Pseudomonas aeruginosa* biofilms. *Mol Microbiol* **50**, 61–68
248. Shrout, J. D., Tolker-Nielsen, T., Givskov, M., and Parsek, M. R. (2011) The contribution of cell-cell signaling and motility to bacterial biofilm formation. *MRS bulletin* **36**, 367–373
249. Burrows, L. L. (2012) *Pseudomonas aeruginosa* twitching motility: Type IV pili in action. *Annu Rev Microbiol* **66**, 493–520
250. Sharp, P. M., and Li, W. H. (1987) The codon Adaptation Index--a measure of directional synonymous codon usage bias, and its potential applications. *Nucleic Acids Res* **15**, 1281–1295
251. Zhang, L., Li, D., Xu, R., Zheng, S., He, H., Wan, J., and Feng, Q. (2014) Structural and functional analyses of a sterol carrier protein in *Spodoptera litura*. *PLoS One* **9**, e81542

252. Ma, H., Ma, Y., Liu, X., Dyer, D. H., Xu, P., Liu, K., Lan, Q., Hong, H., Peng, J., and Peng, R. (2015) NMR structure and function of *Helicoverpa armigera* sterol carrier protein-2, an important insecticidal target from the cotton bollworm. *Sci Rep* **5**, 18186
253. Ganong, B. R., Leonard, J. M., and Raetz, C. R. (1980) Phosphatidic acid accumulation in the membranes of *Escherichia coli* mutants defective in CDP-diglyceride synthetase. *J Biol Chem* **255**, 1623–1629
254. Vance, J. E., and Steenbergen, R. (2005) Metabolism and functions of phosphatidylserine. *Prog Lipid Res* **44**, 207–234
255. Kooijman, E. E., Chupin, V., de Kruijff, B., and Burger, K. N. J. (2003) Modulation of membrane curvature by phosphatidic acid and lysophosphatidic acid. *Traffic* **4**, 162–174
256. Kooijman, E. E., and Burger, K. N. J. (2009) Biophysics and function of phosphatidic acid: A molecular perspective. *Biochim Biophys Acta* **1791**, 881–888
257. Sutterlin, H. A., Zhang, S., and Silhavy, T. J. (2014) Accumulation of phosphatidic acid increases vancomycin resistance in *Escherichia coli*. *J Bacteriol* **196**, 3214–3220
258. Lopez, D., and Kolter, R. (2010) Functional microdomains in bacterial membranes. *Genes Dev* **24**, 1893–1902
259. Singh, P. K., Parsek, M. R., Greenberg, E. P., and Welsh, M. J. (2002) A component of innate immunity prevents bacterial biofilm development. *Nature* **417**, 552–555
260. Singh, P. K. (2004) Iron sequestration by human lactoferrin stimulates *P. aeruginosa* surface motility and blocks biofilm formation. *Biometals* **17**, 267–270
261. Hammond, A., Dertien, J., Colmer-Hamood, J. A., Griswold, J. A., and Hamood, A. N. (2010) Serum inhibits *P. aeruginosa* biofilm formation on plastic surfaces and intravenous catheters. *J Surg Res* **159**, 735–746
262. Haley, C. L., Kruczek, C., Qaisar, U., Colmer-Hamood, J. A., and Hamood, A. N. (2014) Mucin inhibits *Pseudomonas aeruginosa* biofilm formation by significantly enhancing twitching motility. *Can J Microbiol* **60**, 155–166
263. Overhage, J., Campisano, A., Bains, M., Torfs, E. C. W., Rehm, B. H. A., and Hancock, R. E. W. (2008) Human host defense peptide LL-37 prevents bacterial biofilm formation. *Infect Immun* **76**, 4176–4182
264. De la Fuente-Núnez, C., Korolik, V., Bains, M., Nguyen, U., Breidenstein, E. B. M., Horsman, S., Lewenza, S., Burrows, L., and Hancock, R. E. W. (2012) Inhibition of bacterial biofilm formation and swarming motility by a small synthetic cationic peptide. *Antimicrob Agents Chemother* **56**, 2696–2704
265. Athenstaedt, K., and Daum, G. (1999) Phosphatidic acid, a key intermediate in lipid metabolism. *Eur J Biochem* **266**, 1–16
266. Yao, J., and Rock, C. O. (2013) Phosphatidic acid synthesis in bacteria. *Biochim Biophys Acta* **1831**, 495–502

7. Appendix

7.1 GPC analysis of protein A-PGH$_{trunc}$

The relative molecular mass and oligomeric state of protein A-PGH$_{trunc}$ were analyzed by analytical GPC as described in chapter 2.7.6 (135). The respective chromatogram indicating a monomeric protein with a relative molecular mass of 28’000 is presented in figure 31.

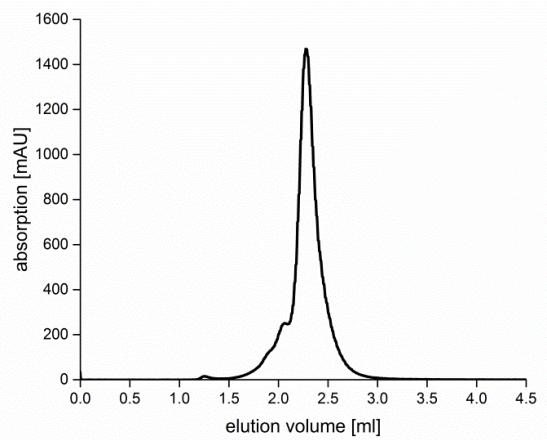

Figure 31: A-PGH$_{trunc}$ elution profile of GPC analysis
50 µl of a 9.8 mg/ml A-PGH$_{trunc}$ sample was loaded onto a Superdex™ 200 Increase 5/150 GL chromatography column. Protein elution was performed at a flow rate of 0.45 ml/min with washing buffer A, simultaneously monitoring the absorption at 280 nm. Employed standard proteins for calibration (data not shown): cytochrome c (M_r = 12’400), carbonic anhydrase (M_r = 29’000), BSA (M_r = 66’000), yeast alcohol dehydrogenase (M_r = 150’000) and β-amylase (M_r = 200’000).

7.2 Localization of AcvB and VirJ in *A. tumefaciens* – malate dehydrogenase activity assay

Impurities of the periplasmic fractions with cytoplasmic proteins were detected *via* the MD activity assay performed as described in chapter 2.12.1.5 (142). A representative activity measurement with the isolated periplasmic and cytoplasmic fractions, indicating almost no impurities of cytoplasmic proteins in the periplasmic fractions, is shown in figure 32.

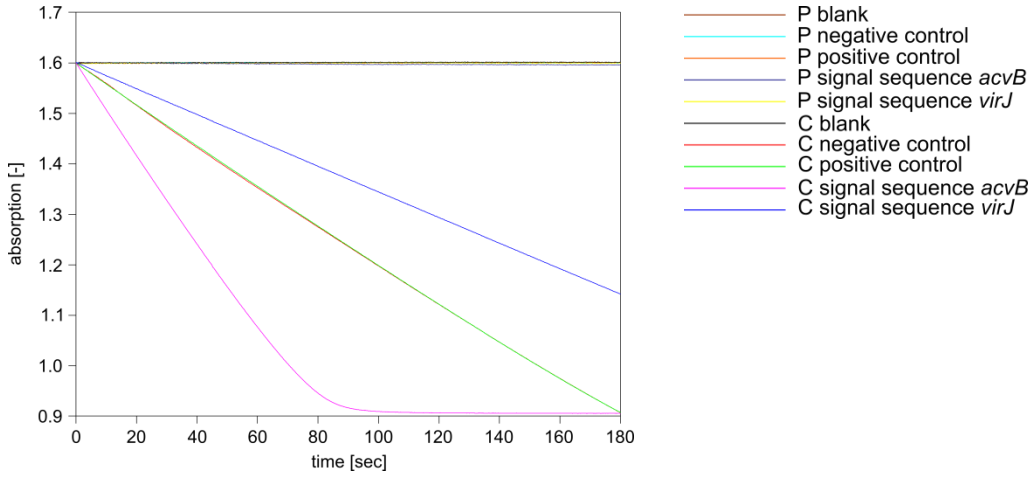

Figure 32: MD activity assay using the isolated periplasmic and cytoplasmic fractions of the different localization strains.
To determine the MD activity 50 µl of the respective periplasmic or cytoplasmic fraction was mixed with 500 µl of the test solution MD (50 mM HEPES-NaOH pH 7.2, 0.3 mM NADH). 25 µl of a 10 mM oxaloacetate solution were added and the absorption at a wavelength of 340 nm, corresponding to $NADH+H^+$, was monitored (2.12.1.5). In the diagram the determined absorption at 340 nm was plotted against the time and it clearly shows a decrease of $NADH+H^+$ in the cytoplasmic fractions of all localization strains, whereas no change in the $NADH+H^+$ content is visible for the periplasmic fractions. In the adjacent legend the abbreviations P and C stand for the periplasmic and cytoplasmic fraction, respectively.

7.3 Sequence alignment of homologous proteins A-PGH, AcvB and VirJ

The sequences of proteins A-PGH, AcvB and VirJ were aligned using Clustal Omega (2.15) and the alignment is presented in figure 33.

```
A-PGH   MSVVKRHWRRFLVAALVLIVGAALLLWSRPAAQAKLEALDLDDGGHATLAEPGEKPRSRV  60
AcvB    --MMKRNLIGAFIAASTLLSSSVAFSQDKPAYETGMIPA-----DH--IMVPDGDIQASI  51
VirJ    ------------------------------------------------------------  0

A-PGH   VVIAAPEQQ--LNDAQMLNLAHDSA-------ARVIQYFPPENGDCRAQQSRLEAV---I  108
AcvB    FLISDANGWTEADETRAKALVEKGAAVVGIDFKEYLKALEADDDECIYMISDIESLSQQI  111
VirJ    ------------------------------------------------------------  0

A-PGH   ARLG----GKPNLVAGIGPGSTTAWRWLASQDDDKAK---ALSVGFDIALAERDCDAPLP  161
AcvB    QRTAGTGSYRLPIVTGIGKGGTLALAMIAQSPVSTVREAVAVDPKAGLPLEKILCTPA-T  170
VirJ    ------------------------------------------------------------  0

A-PGH   HQASHGQWLLAWNDN--PDDDTAVFV---------------RKQSSA--ETSISDYDTPL  202
AcvB    KDKVDGETVYGLTDGALPAPVSVIFTPDADQKGRDHVNALVKLHSDIEVTDVTDKADEVL  230
VirJ    ------------------------------------MAIKLVLI-LVFTLFLAADAAY  21
                                                :             *

A-PGH   SDVLAHQL-RLQLQGNAEALPVLEVPAAQPSDIVTLFYSGDGGWRDLDKDSAEHMASMGY  261
AcvB    TQTLSDKVDAAGDSGNPLGLPITVLEAKPVMDTMAVIYSGDGGWRDLDEEVGSALQKQGV  290
VirJ    ANDRANGVMWSNGGEAGVRLPLRVFNAKPAKNTVAIIYSGDAGWQNIDEVIGTYLQTEGI  81
        ::  :. :           **:  . *    : :::*****.**:::*:  .  : . *

A-PGH   PVVGIDTLRYYWQHKSPEQSAADLSKLMQHYREKWGAKRFVLAGYSFGADILPAIYNRLP  321
AcvB    PVIGVDALRYFWKEKDPKEVAGDLARIIDTYRKEWKVKNVVLIGYSFGADIIPATYNLLP  350
VirJ    PVIGVSSLRYFWSERSPSETAKDLGHIIDVYTKHFGVQNVLLIGYSFGADVMPASFNRLT  141
        **:*:.:***:*..:.*.: * **.:::: * :.: .:..:* *******::** :* *

A-PGH   GKDQQQVKAMLLLALARTGSFEIEVEGWLGKAGEEAATG--PEMARLPAAKVFCIYGAEE  379
AcvB    DRVKSSVAQLSLLGLSNEVDFEISVQGWLGVAGEGKGGKTVDDIAKIDPKLVQCVYGTEE  410
VirJ    LEQKNRVKQISLLALSHQVDYVVSFRGWLQLETEGKGGNPLDDLRFIDPAIVQCMYGRED  201
         . :. *  : **.*:.  .: :...***    *  .     ::  :    * *:** *:

A-PGH   KDESGCTQSQAVG-EKLELPGGHHFDEDYLSLAKKMLQAIRDRENAPDA------       427
AcvB    EDEDPCPGLKAKGVETIGIEGGHHFDEDYEALAKRIVTSLKTRLAK---------       456
VirJ    -RNNACPSLRQTGAEVIGFSGGHHFGNDFKKLSTRVVSGLVARLSHQYSSGPAPL      255
          :. *   :  * * : : *****.:*:  *:.::: .:  *
```

Figure 33: Sequence alignment of proteins A-PGH, AcvB and VirJ
The alignment was generated with Clustal Omega using the protein sequences A-PGH from *P. aeruginosa* PAO1, AcvB from *A. tumefaciens* C58 and VirJ from the octopine-type Ti-plasmid pTiA6 (2.15). The key catalytic serine and histidine residues are depicted in bold letters and amino acids mutated by site-directed mutagenesis are highlighted with a grey background. Conservation degrees are indicated: semi-conserved (.), conserved (:), identical (*).

Danksagung

Mein Dank gilt zuerst meinem Doktorvater Herrn Prof. Dr. Dirk W. Heinz für die Möglichkeit, diese Arbeit anfertigen zu können.

Bei Herrn Prof. Dr. Dieter Jahn möchte ich mich für die Übernahme des Zweitgutachtens sowie für die Möglichkeit die praktische Arbeit in seinem Arbeitskreis durchführen zu können bedanken.

Frau PD Dr. Simone Bergmann danke ich für die Übernahme des Prüfungsvorsitzes.

Ich bedanke mich bei Herrn Prof. Dr. Wulf Blankenfeldt für die Aufnahme in seine Arbeitsgruppe, die fachliche Unterstützung und die Mitgliedschaft in meinem Thesis Committee.

Ganz besonderer Dank gilt Herrn Dr. Jürgen Moser für die hervorragende Betreuung, die gute Zusammenarbeit und die fortwährende Unterstützung in den letzten Jahren.

Ich danke Herrn Dr. Jörn Krauße für die Aufnahme der A-PGH-Datensätze und die Lösung der N-terminalen A-PGH-Struktur. Vielen Dank für die praktische Durchführung der SAXS-Messungen und die daraus resultierende Lösungsstruktur der A-PGH.
Des Weiteren möchte ich mich bei den Herren Prof. Dr. Lothar Jänsch und Dr. Manfred Nimtz für die gute Kooperation im Rahmen des PA3911-Projektes bedanken. Herrn Dr. Manfred Nimtz sei hierbei insbesondere für die MALDI-TOF- und ESI-MS-Analysen gedankt. Ich bedanke mich bei Frau Beate Jaschok-Kentner für die Durchführung von N-terminalen Sequenzierungen und bei Frau Claudia Hanko für die reibungslose Abwicklung der Bestellungen.
Der Arbeitsgruppe Schomburg und insbesondere Frau Elisabeth Majer danke ich für die Möglichkeit Biolog-Experimente bei ihnen durchführen zu können.

Besonders bedanken möchte ich mich bei Herrn Prof. Dr. Franz Narberhaus und Frau Dr. Meriyem Aktas für die hervorragende Kooperation im Rahmen des AcvB-Projektes und das sie mir ermöglicht haben, Studien zur *A. tumefaciens* Tumorgenese und zum T-DNA Transfer in ihrem Labor an der Ruhr-Universität Bochum durchführen zu können. Für die praktische Anleitung zu den Versuchen gilt mein Dank Frau Christiane Fritz.

Sehr herzlich möchte ich mich bei den derzeitigen und ehemaligen Mitgliedern der AG Moser, namentlich Dr. Stefanie Hebecker, Dr. Wiebke Arendt, Dr. Svenja Kiesel, Dr. Christiane Lange, Janis Füller, Simone Virus, Jan Jasper, Marco Massmig und Milan Wiesselmann, für die angenehme Laboratmosphäre

und die ständige Hilfsbereitschaft bedanken. Gedankt sei insbesondere Frau Dr. Stefanie Hebecker für die Bereitstellung der gereinigten A-PGS$_{543-881}$ Proteinvarianten für die *in vitro* Aktivitätsanalysen.

Ein großer Dank geht an meine Arbeitskolleginnen und Freundinnen Janis Füller und Miriam Becker für eine tolle Zeit im Labor und außerhalb des Labors und dafür, dass ihr immer ein offenes Ohr für mich hattet.

Zudem danke ich Marco Massmig, Ilka Pusch, Meike Arnold, Carolin Müller, Milan Wiesselmann, Arne Wendtland und Jennifer Breisch, die im Rahmen ihrer Bachelor- und Masterarbeiten meine Arbeit maßgeblich unterstützt haben.

Bei allen Mitarbeitern des Instituts für Mikrobiologie möchte ich mich für die nette Arbeitsatmosphäre, die gute Zusammenarbeit, den Wissenstransfer und die große Hilfsbereitschaft bedanken.

Besonders Christina Nitzsche, Gunhild Voß, Daniela Schnobel, Bernd Hoppe, Angelika Arnscheidt, Ute Grumer, Lisa Spanier, Barbara Cwiklinski und Dagmar Rose danke ich für die fortwährende Unterstützung in allen bürokratischen Angelegenheiten und im Laboralltag.

Abschließend möchte ich mich ganz herzlich bei meiner Familie und meinen Freunden bedanken, die mich in jeder Lebenslage voll und ganz unterstützt haben und auf die ich mich immer verlassen konnte und kann.